INFILTRATION AND CONTAMINANT TRANSPORT MODELING REPORT WHITE MESA MILL SITE BLANDING, UTAH

DENISON MINES (USA) CORP

November 2007

Prepared for:

Denison Mines (USA) Corp.
1050 17th Street, Suite 950
Denver, Colorado
80265

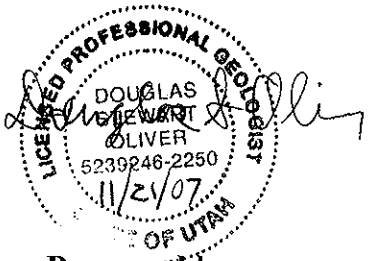

Prepared by:

MWH Americas, Inc.
10619 South Jordan Gateway, Suite 100
Salt Lake City, Utah
84095

TABLE OF CONTENTS

TABLE OF CONTENTS
(continued)

LIST OF APPENDICES

TABLE OF CONTENTS
(continued)

LIST OF TABLES
(Tables at end of respective section)

TABLE OF CONTENTS
(continued)

LIST OF FIGURES
(Figures at end of respective section)

LIST OF ACRONYMS

µg/l	micrograms per liter
ADE	advection dispersion equation
amsl	above mean sea level
bgs	below ground surface
cm/sec	centimeters per second
DoD	Department of Defense
DRC	Division of Radiation Control
ET	evapotranspiration
FML	flexible membrane liner
ft/ft	foot per feet
GMS	Groundwater Modeling System
GWCL	Ground Water Compliance Limits
GWQS	Ground Water Quality Standards
HDPE	high-density polyethylene
HFO	hydrous ferric oxide
L	length
mg/l	milligrams per liter
MWH	MWH Americas, Inc.
PE	potential soil evaporation
PET	potential evapotranspiration
PT	potential transpiration
PVC	poly vinyl chloride
RMSE	root mean squared errors
TDS	total dissolved solids
U.S. EPA	United States Environmental Protection Agency
USGS	United States Geologic Survey

EXECUTIVE SUMMARY

This document presents the results of infiltration and contaminant transport modeling to support Denison's Groundwater Discharge Permit (Ground Water Quality Discharge Permit No. UGW370004) (the "Permit") for its White Mesa uranium milling and tailings disposal facility. The White Mesa Mill (the "Mill") is located in southeastern Utah, approximately six miles south of Blanding, Utah. As described in Part I.H.11 of the Permit, Denison is required to prepare an infiltration and contaminant transport model. The primary objective of the infiltration and contaminant transport model is to demonstrate the long-term ability of the tailings cells cover system to adequately contain and control tailings contaminants and protect nearby groundwater quality of the uppermost aquifer.

The computer code HYDRUS-1D was used to model potential infiltration and contaminant transport through the cover system, tailings, tailings cell liner system, and through the underlying bedrock vadose zone. HYDRUS-1D is one of the few commercially available, frequently tested models that can simulate both unsaturated flow and contaminant transport in the vadose zone (including layered stratigraphy) with a variety of initial and boundary conditions.

The computer codes MODFLOW and MT3DMS were used to model groundwater flow and potential contaminant transport in the perched aquifer. These models were selected because they can adequately represent and simulate the hydrogeologic conditions and contaminant-transport processes that could potentially occur in the perched aquifer beneath White Mesa. Furthermore, these models are well-documented, frequently used, and versatile programs that are widely accepted by the scientific and regulatory communities. MODFLOW was also used to evaluate dewatering in Cells 2 and 3.

The Mill includes a mill facility and tailings cells located south of the Mill. The tailings cells comprise the following:

- Cell 1 – 55 acres, used for the evaporation of process solutions
- Cell 2 – 65 acres, used for storage of barren tailings sands
- Cell 3 – 70 acres, used for storage of barren tailings sands and evaporation of process solutions
- Cell 4A – 40 acres, currently unused, but is planned to be used for storage of barren tailings sands and evaporation of process solutions
- Cell 4B – yet to be constructed (approximately 40 acres), but is planned to be used for storage of barren tailings sands and evaporation of process solutions.

The tailings cells generally were excavated into the underlying Dakota Sandstone and are separated by dikes composed of compacted earthen materials covered with a liner. In the vicinity of the tailings cells, the perched water table is approximately 75 to 115 ft below ground surface, which is 40 to 90 ft below the bottom of the tailings cells.

Based on improvements to cover design technology since the original design was proposed, the cover design for the tailings cells can be modified slightly for improved performance. These modifications are:

- Replacing the cobble layer with 6 inches of topsoil with gravel and vegetation consisting primarily of grasses (the cobble layer will be retained for side slopes)
- Increasing the frost barrier/water storage layer from 2 to 3 ft.

This cover was tested with the vadose zone infiltration model and significantly improved performance over the original design (average model-predicted long-term infiltration rates were reduced from 1.0×10^{-2} cm/day for the original cover design to 1.0×10^{-4} cm/day for the modified cover design, a reduction of two orders-of-magnitude). The vegetation is expected to enhance evapotranspiration and to significantly reduce infiltration of water into the tailings. As specified in Part I.H.11 of the Permit, the Permittee may include supplemental information to justify modification of certain Permit

requirements, including tailings cell cover system engineering design and construction specifications. Upon Executive Secretary approval of the final infiltration and contaminant transport report, the Reclamation Plan may be modified to accommodate necessary changes to protect public health and the environment. In the modeling performed and presented in this report, we have assumed that the cover design for the tailings cells has been modified as described above.

The contaminants modeled included natural uranium, chloride, and sulfate. These compounds are the most dependable indicators of site water quality and of potential cell failure due to their predominance (uranium) and predominance and mobility (chloride and sulfate). In particular, because sorption of chloride is minimal, it will migrate unretarded and act as a conservative tracer and thus would be expected to be detected before all other contaminants, particularly uranium, which will sorb onto mineral surfaces in the vadose zone.

Modeling of the tailings dewatering system with MODFLOW suggests that it is not practical to fully dewater the tailings in Cells 2 and 3. Modeling predicted that dewatering rates would decline to approximately 2 gpm after 10 and 14 additional years of pumping from Cells 2 and 3, respectively, leaving 4 ft of saturated tailings on average. The reduction in pumping rates is caused by the reduction in saturated thickness of tailings. Cells 4A and 4B have a more extensive slimes drain network and were assumed to be dewatered after approximately five years given the more extensive drain network.

Following dewatering activities, modeling of potential flow from the tailings through the liner and underlying bedrock vadose zone was performed with HYDRUS-1D. The model-predicted flux rate through the liner varies as a function of the head (saturated thickness) above the liner. On average, model-predicted flux rates through the liner exceed infiltration rates through the cover. For short periods, potential infiltration rates through the cover are predicted to exceed potential flux rates through the liner, during which times water levels temporarily increase in the tailings. However, the pressure head (saturated thickness of tailings) is not predicted to exceed the initial water level in Cells 2 and 3 (122 cm [4 ft]) or Cells 4A and 4B (30 cm [1 ft]). Thus the model predicts that

water will not overtop the maximum liner elevation (pressure head equal to approximately 914 cm [30 ft]), even without active dewatering.

Modeling of potential flow from the tailings through the liner and underlying bedrock vadose zone was performed with HYDRUS-1D. It should be noted that in performing this modeling, we have assumed potential defects in the liner and have made other assumptions that may overestimate any potential fluxes from the tailings cells. In reality, the actual flux rates may be lower than model-predicted values or there may be no flux at all. Model-predicted potential flux rates through the bedrock vadose zone beneath Cells 2 and 3 decline rapidly from an initial rate of 9.0×10^{-4} cm/day, then gradually decline to 2.5×10^{-4} cm/day at 200 years. For Cells 4A and 4B, model-predicted flux rates through the bedrock vadose zone decline rapidly from an initial rate of 5.2×10^{-4} cm/day, then gradually decline to a steady-state rate of 1.4×10^{-4} cm/day by approximately 175 years, after the tailings are predicted to have become unsaturated.

Modeling of potential chloride and sulfate transport from the tailings through the tailings cell liner and bedrock vadose zone, using these assumptions, was also performed with HYDRUS-1D. Beneath Cells 2 and 3, chloride and sulfate concentrations in porewater at the bottom of the bedrock vadose zone are predicted, using these assumptions, to increase to concentrations of 0.39 and 0.09 mg/l, respectively, at 200 years. Beneath Cells 4A and 4B, chloride and sulfate concentrations in porewater at the bottom of the vadose zone are predicted to increase to concentrations of 0.011 and 3.2×10^{-4} mg/l, respectively, at 200 years. Chloride was assumed to migrate unretarded (i.e., no sorption) through the vadose zone. Sulfate was assumed to have a maximum retardation factor of 1.07, such that it is considered highly mobile, but it is slightly retarded relative to chloride. These are the model-predicted chloride and sulfate concentrations in vadose zone porewater that could potentially reach the perched aquifer, based on the assumptions used in the model; however, these are not the predicted concentrations in groundwater.

Modeling of chloride and sulfate transport in the perched aquifer was performed with MODFLOW and MT3DMS. The Permit stipulates that concentrations of contaminants in groundwater monitoring wells shall not exceed specified Ground Water Compliance

Limits (GWCLs). Downgradient monitoring wells with GWCLs specified in the Permit include MW-5, MW-11, and MW-12, located on the berm immediately south (downgradient) of Cell 3, and MW-14 and MW-15, located on the berm immediately south (downgradient) of Cell 4A. Due to the low mass flux rates predicted to reach the aquifer, model-predicted chloride and sulfate concentration increases at these wells due to the tailings cells are insignificant, and fall far below laboratory detection limits. At 200 years, the modeled fluxes from the tailings cells are predicted to increase chloride by less than 0.03 % of the proposed GWCLs in all monitoring wells. The modeled fluxes from the tailings cells are predicted to increase sulfate by less than 0.0002 % of the proposed GWCLs.

Retardation rates for uranium (VI) were calculated based on equilibrium soil-water partition coefficients (K_d) using the mass of hydrous-ferric oxide (HFO) present in the bedrock and the equilibrated solution compositions predicted with the geochemical code PHREEQC. Neutralization of the infiltrating tailings-pore waters and sorption of solutes was determined with PHREEQC. The masses of HFO and calcite were determined for samples collected from the vadose zone for core samples from the Dakota Sandstone. Through this method, a sorption value for the Dakota Sandstone immediately beneath the tailings cells was estimated to be 8.47 kilograms per liter. Assuming a volumetric moisture content of 7%, a retardation factor of 251 was calculated.

Modeling of potential uranium transport from the tailings through the tailings cell liner and into the vadose zone was performed with HYDRUS-1D. Due to the strong sorption and the resulting high-retardation coefficients, uranium is not predicted to migrate much beyond 20 cm (8 inches) below the liner system in 200 years beneath Cells 2 and 3 and Cells 4A and 4B. At 30 cm (1 ft) below the liner at 200 years, dissolved-phase uranium concentrations are predicted to be 3.0×10^{-4} mg/l beneath Cells 2 and 3 and 2.0×10^{-8} mg/l beneath Cells 4A and 4B. No uranium is predicted to reach the perched aquifer within 200 years. While there is some naturally-occurring uranium in the vadose zone initially, the modeling assumed no initial uranium for simplicity, and because there is a lack of data concerning background uranium and distribution of uranium in the vadose zone. Dissolved uranium concentrations were assumed to remain at a concentration of

94 mg/l in the tailings. Because uranium was predicted to migrate such a short distance in the bedrock vadose zone, there appears to be no threat to groundwater posed by uranium.

Sorption coefficients and retardation factors were calculated for contaminants of potential concern to assess their potential transport through the bedrock vadose zone. Solutes predicted to have high K_d values resulting in high retardation factors and low mobility include arsenic, beryllium, chromium, copper, lead, uranium, vanadium, and zinc. Similarly to uranium, these contaminants are not predicted to migrate through the vadose zone to the perched water table in 200 years, given their high retardation factors. Solutes predicted to have intermediate K_d values include cadmium, cobalt, manganese, molybdenum, and nickel. These contaminants also are not predicted to migrate through the vadose zone to the perched water table in 200 years. Solutes predicted to have low K_d values include selenium and sulfate; while iron, fluoride, mercury, silver and thallium were predicted to migrate unretarded, like chloride. This assumes that there is no sorption or any other loss mechanisms such as degradation, precipitation, or other transformations. Based on K_d values reported in Sheppard and Thibault (1990), U.S. EPA (1996), and U.S. EPA (1999), sorption and retardation of cadmium, cobalt, iron, manganese, mercury, nickel, selenium, silver, and thallium are likely to be significantly larger than model-predicted values. As a result only chloride, sulfate, and fluoride are predicted to migrate with little or no sorption.

Given the magnitude of model-predicted impacts to groundwater for chloride and sulfate (minimal), the impact caused by the other mobile contaminant (fluoride) was estimated. Using dilution/attenuation of chloride from tailings fluids to groundwater as a proxy, the concentration of fluoride was estimated. Because the monitoring well predicted to be impacted the most by potential releases from the tailings cells is monitoring well MW-12, the fluoride concentration was estimated for this location. Assuming a dilution factor of 768,000, a fluoride concentration of 0.002 mg/l was estimated for MW-12. The proposed GWCL for fluoride in MW-12 is 2 mg/l. As a result, the predicted concentrations of fluoride as well as other contaminants of concern are not predicted to exceed proposed GWCLs at 200 years.

Under Part I.D.6 (Closed Cell Performance Requirements) of the Permit:

"before reclamation and closure of any tailings disposal cell, the Permittee shall ensure that the final design, construction, and operation of the cover system at each tailings cell will comply with all requirements of an approved Reclamation Plan, and will for a period of not less than 200 years meet the following minimum performance requirements:

a) Minimize infiltration of precipitation or other surface water into the tailings, including, but not limited to the radon barrier, and

b) Prevent the accumulation of leachate head within the tailings waste layer that could rise above or over-top the maximum FML liner elevation internal to any disposal cell, i.e. create a "bathtub" effect.

c) Ensure that groundwater quality at the compliance monitoring wells does not exceed the Ground Water Quality Standards or Ground Water Compliance Limits specified in Part I.C.1 and Table 2 of this Permit."

Based on the model results presented in this report, all three requirements are met by the modified cover design.

1.0 INTRODUCTION

This document presents the results of infiltration and contaminant transport modeling to support Denison Mines (USA) Corp.'s (formerly International Uranium (USA) Corporation's) Groundwater Discharge Permit (Ground Water Quality Discharge Permit No. UGW370004) (the "Permit") for its White Mesa uranium milling and tailings disposal facility (the "Mill"). As described in Part I.H.11 of the Permit, Denison is required to prepare an infiltration and contaminant transport model.

Denison has engaged MWH Americas, Inc. (MWH) to work with Denison personnel to develop the assumptions and data for the infiltration and contaminant transport model and interpret the model results.

1.1 OBJECTIVES OF INFILTRATION AND CONTAMINANT TRANSPORT MODEL

The primary objective of the infiltration and contaminant transport model is to demonstrate the long-term ability of the tailings cells cover system to adequately contain and control tailings contaminants and protect nearby groundwater quality of the uppermost aquifer.

1.2 PERMIT REQUIREMENTS

Part I.H.11 (Infiltration and Contaminant Transport Modeling Work Plan and Report) of Denison's Permit presents the requirements for infiltration and contaminant transport modeling, as summarized below.

An infiltration and contaminant transport modeling report that demonstrates the long-term ability of the tailings cells cover system to adequately contain and control tailings contaminants and protect nearby groundwater quality of the uppermost aquifer must be submitted. This report shall demonstrate how the tailings cell engineering design and specifications will comply with the minimum performance requirements of Part I.D.6 of the Permit. The original permit specified that a work plan also must be submitted for the

infiltration and contaminant transport modeling. Denison submitted a work plan to the Utah Division of Radiation Control (DRC) in September 2005. However, the DRC did not review this work plan and removed this requirement from the permit as stated in a letter from DRC Executive Secretary to Denison dated 3 November 2006. This letter also specified that all modeling must be completed and a final report must be submitted for Executive Secretary approval by 1 June 2007. Subsequently, Denison requested and received approval for an extension of this submittal to 1 September 2007 and subsequently extended this to 23 November 2007.

The infiltration and transport modeling report must describe:

- Applicable and pertinent historic studies and modeling reports relevant to the tailings cell cover design and tailings cell system performance.
- Information necessary for infiltration and contaminant transport modeling, including representative input values for vadose zone and aquifer soil-water partitioning (K_d) coefficients, tailings source term concentrations, vadose zone and aquifer dispersivity, contaminant half-life or other rates of decay, etc. If any required information is not currently available, conservative assumptions can be used for the model input.
- Computer models that will be used to simulate long-term performance of the tailings cells cover system. Specific information on model design, including governing equations and their applicability to site conditions, grid design, duration of simulation, and selection of time steps must be described.
- The conceptual model used and justify why it is representative or conservative of actual field conditions at the site. The conceptual model will identify the physical domain and geometries simulated including the tailings cell design and construction, all boundary and initial conditions assigned in the models.
- How the infiltration and contaminant transport problem has been conceptualized, planned, and executed to demonstrate compliance with the requirements of Part I.D.6 of the Permit.

- Model results, model calibration, steady state conditions, sensitivity analyses, post-model audit plan.

Additionally, Part I.D.6 (Closed Cell Performance Requirements) of the Permit presents requirements regarding performance requirements for closed cells at the facility, which impacts both actual infiltration at the site as well as how this infiltration will be modeled, as follows:

- Before reclamation and closure of any tailings disposal cell, the Permittee shall ensure that the final design, construction, and operation of the cover system at each tailings cell will comply with all requirements of an approved Reclamation Plan, and will for a period of not less than 200 years meet the following minimum performance requirements:

  - Minimize infiltration of precipitation or other surface water into the tailings, including, but not limited to the radon barrier, and

  - Prevent the accumulation of leachate head within the tailings waste layer that could rise above or over-top the maximum flexible membrane liner (FML) elevation internal to any disposal cell, i.e., create a "bathtub effect".

  - Ensure the groundwater quality at the compliance monitoring wells does not exceed the Ground Water Quality Standards (GWQS) or Ground Water Compliance Limits (GWCL) specified in Part I.C.1 and Table 2 of the Permit.

Further, Part I.C.1 (Permit Limits) of the Permit includes the following:

- The Permittee shall comply with the following GWCLs – contaminant concentrations measured in each monitoring well shall not exceed the GWCLs defined in Table 2 of the permit. Groundwater quality at the site must at all times meet all the applicable GWQS and the ad hoc GWQS defined in R317-6

even though this permit does not require monitoring for each specific contaminant.

Part I.H.11 also states that "Upon Executive Secretary approval of the final infiltration and contaminant transport report, the Reclamation Plan may be modified to accommodate necessary changes to protect public health and the environment."

This report has been prepared to comply with the Permit as described above.

1.3 DOCUMENT ORGANIZATION

The remainder of this report includes the following sections:

- Section 2.0 – Site Background; descriptions of the site including tailings cell cover and liner design, as well as tailings chemical and physical characteristics, site geology and hydrogeology, conceptual model of water flow and potential contaminant transport through the vadose zone.
- Section 3.0 – Methodology; descriptions of the vadose zone and groundwater flow and contaminant transport models, input parameters and boundary conditions, and modeling assumptions.
- Section 4.0 – Results; descriptions of the results of the vadose zone and groundwater flow and contaminant transport modeling and sensitivity analysis.
- Section 5.0 – Conclusions; provides a summary with the conclusions of the vadose zone and groundwater flow and contaminant transport modeling along with recommendations for a post-audit monitoring plan.
- Section 6.0 – References.
- Appendix A – Laboratory report with unsaturated hydraulic properties for cores from White Mesa.

- Appendix B – Speciation and surface-complexation modeling of tailings porewater.
- Appendix C – HYDRUS-1D modeling files (electronic files on DVD).
- Appendix D – PHREEQC modeling files (electronic files on DVD).
- Appendix E – MODFLOW and MT3DMS modeling files (electronic files on DVD).

2.0 BACKGROUND

This section provides information on the:

- Site background including descriptions of the White Mesa Mill facility, tailings cell cover design, and tailings cell liner systems;
- Site characteristics including geology, hydrogeology, and vadose zone characteristics; and
- Conceptual model of flow and contaminant transport in the vadose zone.

Site-specific studies and reports reviewed to prepare this modeling report included:

- Construction Report, Initial Phase – Tailings Management System, White Mesa Uranium Project, Blanding, Utah (D'Appolonia Consulting Engineers, Inc., 1982)
- Revised Construction Drawings, DMC White Mesa Mill, Cell 4A Lining System (Geosyntec Consultants, 2007a)
- Analysis of Slimes Drains for White Mesa Mill - Cell 4A Computations (Geosyntec Consultants, 2007b)
- Stockpile Evaluation Tailings Cell 4A, White Mesa Mill - Technical Memo submitted to International Uranium (USA) Corporation (Geosyntec Consultants, 2006)
- Hydraulic Testing at the White Mesa Uranium Mill Site, near Blanding, Utah During July 2002 (Hydro Geo Chem, Inc., 2002)
- Site Hydrogeology and Estimation of Groundwater Travel Times in the Perched Zone, White Mesa Uranium Mill Site, near Blanding, Utah. (Hydro Geo Chem, Inc., 2003)

- Revised Background Groundwater Quality Report: Existing Wells for Denison Mines (USA) Corp.'s White Mesa Uranium Mill Site, San Juan County, Utah (INTERA, 2007)
- Reclamation Plan, White Mesa Mill, Blanding, Utah (International Uranium (USA) Corporation, 2000)
- Environmental Report (International Uranium (USA) Corporation, 2003)
- Evaluation for Potential for Tailing Cell Discharge – White Mesa Mill. Attachment 5, Groundwater Information Report, (Knight-Piesold, 1998)
- Hydrogeological Evaluation of White Mesa Uranium Mill (TITAN Environmental Corporation, 1994)
- Tailings Cover Design, White Mesa Mill, Blanding Utah (TITAN Environmental Corporation, 1996)
- Draft Ground Water Discharge Permit, Statement of Basis for a Uranium Milling Facility at White Mesa, South of Blanding (Utah Division of Radiation Control, 2004)

Complete citations for these and other sources cited throughout this document are provided in the References Section.

2.1 SITE OVERVIEW

2.1.1 Facility Description

The White Mesa Mill is located in southeastern Utah, approximately six miles south of Blanding, Utah. The Mill includes a mill facility and four tailings cells located south of the Mill (see Figure 2-1). The focus of this report is the tailings cells; for information concerning site history or milling operations, see the *Reclamation Plan, Revision 3.0* (International Uranium (USA) Corporation, 2000).

The tailings cells comprise the following:

- Cell 1 – 55 acres, used for the evaporation of process solutions
- Cell 2 – 65 acres, used for storage of barren tailings sands
- Cell 3 – 70 acres, used for storage of barren tailings sands and evaporation of process solutions
- Cell 4A – 40 acres, currently unused, but is planned to be used for storage of barren tailings sands and evaporation of process solutions
- Cell 4B – yet to be constructed (approximately 40 acres), but is planned to be used for storage of barren tailings sands and evaporation of process solutions.

The tailings cells generally were excavated into the underlying Dakota Sandstone and are separated by dikes composed of compacted earthen materials covered with a liner. In the vicinity of the tailings cells, the perched water table is approximately 75 to 115 ft below ground surface, which is 40 to 90 ft below the bottom of the tailings cells.

The White Mesa Mill is a zero discharge facility; thus all liquids must be eliminated through evaporation. Currently, Denison is actively evaporating process waters from Cell 1 and Cell 3 only. Cell 1 is currently used as an evaporation pond only and will not be used to hold solid tailings. Water removed from Cells 2 and 3 by the dewatering system will be discharged to Cell 1 and subsequently evaporated. As part of the closure plan, sediment and evaporite crystals in Cell 1 will be removed and placed in Cells 2 and/or 3 prior to closure. Cells 2 and 3 will be filled with tailings and covered. Cells 4A and 4B also are expected to be filled with tailings and covered. Descriptions of the tailings cover and liner systems are provided in the sections below.

2.1.2 Tailings Cover Design

An engineered multi-layered cover will be installed over a portion of Cell 1 (i.e., Cell 1-I, where approximately 10 acres will be filled with contaminated materials from the Mill site decommissioning) and the entirety of Cells 2, 3, 4A, and 4B. The multilayered cover

as presented in the *Tailings Cover Design* (TITAN Environmental Corporation, 1996) and the *Reclamation Plan, Revision 3.0* (International Uranium (USA) Corporation, 2000) consists of a 3-ft thick (minimum thickness; expected to be much greater in some areas) platform (e.g., support or grading) fill layer composed of random fill, primarily silty sand and sandy silt, the top 1 ft of which will meet compaction standards. The purpose of this layer is twofold: to raise the base of the cover to the desired subgrade elevation and to attenuate radon flux. Above the platform fill will be a 1-ft thick layer of compacted clay. The purpose of this layer is to inhibit vertical infiltration and to attenuate the upward flux of radon. The design also includes a 2-ft frost barrier composed of sandy silt and silty sand overlying the clay layer and a layer of riprap on top of the frost barrier layer (8 inches on the side-slopes). For additional information concerning the currently approved tailings cells and cover design, see the *Tailings Cover Design* (TITAN Environmental Corporation, 1996) and the *Reclamation Plan, Revision 3.0* (International Uranium (USA) Corporation, 2000).

Based on improvements to cover design technology since the original design was proposed, the currently approved cover design will be modified slightly for improved performance (see Figure 2-2). These modifications are:

- Replacing the cobble layer with 6 inches of topsoil with gravel and vegetation consisting primarily of grasses (the cobble layer will be retained for side slopes)
- Increasing the frost barrier/water storage layer from 2 to 3 ft.

This cover was tested with the vadose zone infiltration model (described in Section 3.0) and significantly improved performance over the original design (average long-term model-predicted infiltration rates were reduced from 1.0×10^{-2} cm/day for the original cover design to 1.0×10^{-4} cm/day for the modified cover design, a reduction of two orders-of-magnitude). The vegetation is expected to enhance evapotranspiration and to significantly reduce the potential for infiltration of water into the tailings. Gravel is included in the topsoil layer to improve durability and longevity. The increase in thickness of the frost barrier/water storage layer is to allow additional temporary water

storage for uptake by vegetation. The thickness of the frost/barrier water storage layer was based on the amount of water storage required during winter months when evapotranspiration is minimal, and the expected rooting depth of grasses, which is typically less than 3 ft (Kurc and Small, 2004; Currie and Hammer, 1979; Foxx and Tierney, 1987; Schuster, 1964; Lee and Lauenroth, 1994). Bolen et al. (2001) used a 3-ft water storage layer in an ET cover tested in Monticello, Utah.

Numerous studies of vegetated "evapotranspiration (ET)" covers have illustrated the effectiveness of vegetation at reducing deep drainage (through the cover system), particularly in arid and semi-arid regions (Albright et al., 2004; Bolen et al., 2001; Fayer and Gee, 2006; Gee et al 1994; Scanlon et al., 2005). Albright et al. (2004) measured infiltration rates of less than 4.1×10^{-4} cm/day for seven of 10 vegetated covers tested in semi-arid regions over a four-year period. The cover tested at Monticello, Utah as part of this study had no measurable infiltration (reported as 0.0 mm/year; implying less than 3×10^{-5} cm/day) during this test. Fayer and Gee (2006) measured less than 1.4×10^{-4} cm/day for weighing lysimeters with vegetated covers at the Hanford, Washington site. With vadose zone modeling, Khire et al. (2000) predicted total annual percolation rates of less than 2.7×10^{-4} cm/day for covers in a variety of climatic settings, assuming the water storage layer is at least 60 cm (2 ft) thick.

2.1.3 Tailings Cell Liner System

The tailings cell liner systems consist of a minimum of 0.5 ft of crushed sandstone underlay, a 0.030 inch (30-mil) poly vinyl chloride (PVC) flexible membrane liner (FML) (Cells 2 and 3), a 1-ft thick liner protective blanket of silty sand soil, and a slimes drain collection system of perforated PVC pipe (see Figure 2-2) in a 1-ft layer of clean sand. Rather than a single 30-mil PVC FML, Cells 4A and 4B will have a geosynthetic clay liner overlain by two 60-mil high-density polyethylene (HDPE) geomembrane layers separated by a geonet (woven geotextile) layer. Slimes drain systems are installed in Cells 2, 3, 4A, and 4B. The slimes drains in Cells 2 and 3 include both 1.5-inch and 3-inch diameter slotted PVC pipe, installed in a 1-ft thick clean sand layer above the protective blanket. These lateral drains are installed on 50-ft centers parallel to the

southern edge of the tailings cells and cover an area that is approximately 400 ft (north-south) by 600 ft (east-west). The slimes drains in Cells 4A and 4B are on 50-ft centers and are located beneath the entirety of the cells. Leak detection systems are installed under the cells and are monitored weekly to ensure that leakage does not occur. Details of the liner systems are provided in D'Appolonia Consulting Engineers (1982) for Cells 2 and 3, and in Geosyntec Consultants (2007a) for Cell 4A (Cell 4B liner design is anticipated to follow same specifications as Cell 4A).

Using methods developed by Giroud and Bonaparte (1989) and Giroud et al. (1992), Knight-Piesold (1998) estimated potential fluxes from Tailings Cell 3 at White Mesa Mill. Theoretically, a geomembrane liner consists of an impermeable material that should preclude leakage into the underlying vadose zone. However, the occurrence of a limited number of manufacturing and installation defects is generally anticipated and incorporated during assessment of environmental impacts (Giroud and Bonaparte, 1989). Knight-Piesold considered potential flux through the liner due to:

- Assumed vapor diffusion
- Assumed pinholes due to manufacturing flaws
- Assumed larger defects resulting from seaming errors, abrasion, and punctures during installation.

Using a combination of empirical and analytical equations, and assuming a certain number of potential defects and defect sizes taken from the literature (Giroud and Bonaparte, 1989) and a head of 4 ft above the liner of the cell, Knight-Piesold (1989) calculated a potential flux rate of 4.6×10^{-4} cm/day. It should be noted that in performing this modeling, we have assumed potential defects in the liner and have made other assumptions that may overestimate any potential fluxes from the tailings cells. In reality, the actual flux rates may be lower than model-predicted values or there may be no flux at all.

Long-term compatibility of liner materials with the acidic tailings fluids is unknown; however, short-term testing provides evidence that mechanical and hydraulic properties

of PVC and HDPE liners are not affected by acidic fluids (Mitchell, 1985; Gulec et al., 2004; Gulec et al., 2007). Tests performed by Mitchell (1985) used a simulated leachate from uranium mill tailings with a pH between 1.5 and 2.5. Both one-sided and two-sided (immersion) tests were performed on HDPE and PVC liners with contact times of four months. Mitchell (1985) reported that mechanical properties were impacted minimally. Tests performed by Gulec et al. (2007) used acidic solutions with pH 2 and involved two-sided immersion tests of HDPE liners with contact times of 22 months. Gulec et al. (2007) reported no statistically significant changes to mechanical or hydraulic properties of liner materials tested.

Long-term performance of the liner system on the order of hundreds of years is unknown, but there is strong evidence that there has been no leakage from Cells 2 and 3 over the past 25 years indicating the effectiveness of the existing PVC liner system. Evidence that the cells are not leaking includes:

- No leakage indicated by the leak detection systems
- No significant leakage indicated by the perched aquifer water table elevations
- No significant leakage indicated by water levels in the tailings cells
- No tailings contaminants detected in groundwater at levels above natural background levels (see INTERA, 2007).

Given that Cells 2 and 3 have held tailings and fluids since 1983, the above lines of evidence support the hypothesis that there has not been leakage.

2.1.4 Characteristics of Tailings

The tailings are generally silty sand but heterogeneous due to the placement process. Based on grain-size analyses performed on the tailings, sand-sized particles are dominant (55 percent on average) with the remainder being silt and clay sized particles (Colorado School of Mines Research Institute, 1978). Based on grain-size analysis of tailings at the Moab UMTRA site, clay content is likely on the order of 1 to 10 percent. Specifically,

tailings described as sand, slimy sand, sand-slimes, and slimes had average clay contents of 1, 4, 12, and 17 percent, respectively (U.S. Department of Energy, 2003).

The tailings are initially saturated when placed but are dewatered through evaporation and pumping from the slimes drains system.

The tailings chemistry is a function of the feedstock materials processed and the mill process reagents used in the extraction process. Tailings wastewater chemistry is based on data collected between September 1980 and March 2003, as presented in the Statement of Basis (Utah Division of Radiation Control, 2004). The tailings fluids are high in ammonia (average concentration of 3,131 milligrams per liter [mg/l] as N), chloride (average concentration of 4,608 mg/l), fluoride (average concentration of 1,695 mg/l), sulfate (average concentration of 64,914 mg/l), and total dissolved solids (TDS; average concentration of 85,960 mg/l). Metals concentrations in the tailings wastewater that exceed Utah GWQSs include arsenic, beryllium, cadmium, chromium, cobalt, copper, iron, lead, manganese, mercury, molybdenum, nickel, thallium, uranium, vanadium, and zinc. The average concentration of natural uranium was calculated to be 94 mg/l.

2.2 SITE CHARACTERISTICS

2.2.1 Climate

The climate of the Blanding area is considered semi-arid with normal annual precipitation of 13.3 inches (Utah Climate Center, 2007). Most precipitation falls in the form of rain, with about one-quarter of the precipitation falling as snow. There are two separate rainfall seasons in the area: a late summer season when monsoonal moisture from the Gulf of Mexico leads to thunderstorms and a winter season related to fronts from the Pacific. The average annual Class A pan evaporation rate is 68 inches.

Climatological data are available for the weather station near Blanding, Utah (420738), located approximately six miles north of the White Mesa Mill at an elevation of 6,040 ft above mean sea level (amsl). Data are available for the period December 1904 through

December 2006; however, large gaps in the dataset (i.e., missing precipitation and/or air-temperature measurements) occurred during 1905, 1910 to 1912, 1915, 1916, 1917, 1927, 1929, 1931, 1989, and 2005. Data for the period between 1932 and 1988 are nearly continuous.

The long-term average annual precipitation at the Blanding weather station was 13.3 inches with a standard deviation of 3.9 inches. Annual precipitation for the period 1905 through 2005 is presented in Figure 2-3. The largest annual event occurred in 1909 (24.5 inches), but other years that exceeded 20 inches include 1906 (23.6 inches), 1957 (22.4 inches), 1941 (21.5 inches), 1908 (20.2 inches), 1997 (20.2 inches), and 1965 (20.1 inches). Daily precipitation for the period 1905 through 2005 is presented in Figure 2-4. The largest daily precipitation event was 4.48 inches, which occurred on 1 August 1968.

The mean annual temperature for Blanding, Utah is 52°F, based on the period 1971-2000. January is typically the coldest month, with a mean monthly temperature of about 30°F. July is generally the warmest month, with a mean monthly temperature of 76°F. Daily ranges in temperatures are typically large.

Winds are generally light to moderate (less than 15 miles per hour) at the site during all seasons, with winds prevailing from the south. Strong winds are associated with summer thunderstorms and frontal activity during the late winter and spring.

2.2.2 Summary of Site Geology

The White Mesa Mill is located within the Blanding Basin of the Colorado Plateau physiographic province. The average elevation at the site is 5,600 ft amsl. The site is underlain by unconsolidated alluvium overlying consolidated sedimentary rocks consisting primarily of sandstone and shale. The unconsolidated deposits are primarily aeolian silt and sand and range from 1 to 30 ft thick (these deposits have been removed where the tailings cells are located). The consolidated bedrock underlying the site is relatively undeformed and horizontal (generally dips are less than 3 degrees). The first units encountered are the Cretaceous-aged Dakota Sandstone and Burro Canyon

Formation, both sandstone units having a combined thickness of 100 to 140 ft beneath the site. Beneath the Burro Canyon Formation is the Morrison Formation, which is primarily shale. The Brushy Basin Member is the uppermost member of the Morrison Formation and is composed primarily of bentonitic mudstones, siltstones, and claystones. The contact between the Burro Canyon Formation and Brushy Basin Member dips gently to the south. Beneath the Brushy Basin Member are the Westwater Canyon, Recapture, and Salt Wash members of the Morrison Formation. Beneath the Morrison Formation are the Summerville Formation, Entrada Sandstone, and Navajo Sandstone. For more detailed descriptions of the geologic setting see the *Reclamation Plan, Revision 3.0* (International Uranium (USA) Corporation, 2000).

2.2.3 Site Hydrogeology

Groundwater beneath the site is first encountered as a perched zone within the Burro Canyon Formation. The low permeability Brushy Basin Member acts as an aquitard and forms the base of the perched aquifer. Monitoring wells at the site are screened across the saturated portion of the Burro Canyon Formation and generally extend down to the contact with the Brushy Basin Member. The saturated thickness of the perched zone ranges from less than 5 to 82 ft beneath the site, assuming the base of the Burro Canyon Formation is the base of the perched aquifer. The water table of the perched aquifer was encountered at 13 to 116 ft below ground surface (bgs) at the facility in 2007 (57 to 116 ft bgs beneath Cells 2, 3, and 4A). The perched water table is shallowest near the wildlife ponds (13 ft in piezometer P-2), east of the Mill and tailings cells. Groundwater within the perched zone generally flows south to southwest beneath the site (see Figure 2-5). Recharge to the perched aquifer is primarily from areal recharge due to infiltration of precipitation and seepage from the wildlife ponds on the eastern margin of the site. Discharge from the perched aquifer is believed to be to springs and seeps along Westwater Creek Canyon and Cottonwood Wash to the west-southwest and along Corral Canyon to the east of the site. The discharge point located most directly downgradient of the tailings cells is believed to be Ruin Spring in Westwater Creek Canyon, a tributary to Cottonwood Wash, approximately two miles from the tailings cells.

The horizontal hydraulic gradient in the perched aquifer ranges from approximately 0.01 to 0.04 feet per foot (ft/ft) and is generally to the south and southwest with local variations in magnitude and direction (see Figure 2-5). Recharge from the wildlife ponds causes localized mounding of the water table.

The hydraulic conductivity of the perched aquifer has been characterized through aquifer pumping tests, slug tests, packer tests, and laboratory analysis of core samples. The results of aquifer pumping tests performed in 12 monitoring wells and packer tests performed in 30 borings in the perched aquifer are presented in the *Reclamation Plan, Revision 3.0* (International Uranium (USA) Corporation, 2000). The geometric mean horizontal hydraulic conductivity of the perched aquifer is 0.03 ft/day (1.0×10^{-5} centimeters per second [cm/sec]), based on the average of values estimated from 12 aquifer pumping tests and from 30 packer tests. The horizontal hydraulic conductivity from these tests ranged from 5.4×10^{-4} to 4.5 ft/day (1.9×10^{-7} to 1.6×10^{-3} cm/sec) (TITAN Environmental Corporation, 1994).

Additional hydraulic testing was performed in 2002, which focused on wells to the south of Cell 3. In this effort, one monitoring well was pump tested and seven monitoring wells were slug tested, the results of which are presented in *Hydraulic Testing at the White Mesa Uranium Mill near Blanding, Utah during July 2002* (Hydro Geo Chem, Inc., 2002). Hydraulic conductivity values from these tests ranged from 0.0022 to 1.5 ft/day (7.7×10^{-7} to 5.3×10^{-4} cm/sec). The geometric mean hydraulic conductivity for wells south of Cell 3 (MW-3, MW-5, MW-11, MW-12, MW-14, MW-15, MW-17, MW-20, and MW-22) ranged from 0.054 to 0.12 ft/day (1.9×10^{-5} to 4.1×10^{-5} cm/sec), depending on the slug test analysis method used (Hydro Geo Chem, Inc., 2003).

Using the geometric mean values for horizontal hydraulic conductivity, horizontal hydraulic gradient, and assuming a porosity of 18.3 percent (the average from samples collected while drilling MW-16, which also corresponds closely with the average of values from cores analyzed from MW-23 and MW-30 discussed below in Section 2.2.5), the average linear velocity of groundwater is estimated to be 0.002 ft/day. Using hydraulic properties for the perched zone downgradient of the tailings cells, average

linear velocities of groundwater were calculated to range from 0.0035 to 0.0076 ft/day (Hydro Geo Chem, Inc., 2003). For further details concerning hydrogeology see *Site Hydrogeology and Estimation of Groundwater Travel Times in the Perched Zone, White Mesa Uranium Mill Site, near Blanding, Utah* (Hydro Geo Chem, Inc., 2003), *Hydraulic Testing at the White Mesa Uranium Mill Site, near Blanding, Utah During July 2002* (Hydro Geo Chem, Inc., 2002), *Hydrogeological Evaluation of White Mesa Uranium Mill* (TITAN Environmental Corporation, 1994), and the *Reclamation Plan, Revision 3.0* (International Uranium (USA) Corporation, 2000).

2.2.4 Groundwater Quality

The groundwater quality of the perched aquifer is highly variable with TDS concentrations that range from 600 to over 5,300 mg/l. Based on historical data from 33 wells, 16 appear to have Class II or drinking water quality groundwater and the other 17 have Class III or limited use quality groundwater. Manganese, selenium, and uranium have been found to exceed their respective State Ground Water Quality Standards at several monitoring wells.

Average chloride concentrations in the perched groundwater south of Cell 4A for the period 2006-2007 ranged from 18 to 63 mg/l. Chloride concentrations in monitoring wells MW-14 and MW-15 located along the south side of Cell 4A had average concentrations for 2006-2007 of 18 and 39 mg/l, respectively. Average sulfate concentrations in the perched groundwater south of Cell 4A for the period 2006-2007 ranged from 2,180 to 3,320 mg/l. Sulfate concentrations in monitoring wells MW-14 and MW-15 had average concentrations for 2006-2007 of 2,180 and 2,380 mg/l, respectively. Average uranium concentrations in the perched groundwater south of Cell 4A for the period 2006-2007 ranged from 28.9 to 59.8 micrograms per liter (µg/l). Uranium concentrations in monitoring wells MW-14 and MW-15 had average concentrations for 2006-2007 of 59.8 and 49.3 µg/l, respectively.

For additional detail regarding groundwater quality see the *Revised Background Groundwater Quality Report* (INTERA, 2007).

2.2.5 Vadose Zone Characteristics

The vadose zone beneath White Mesa is the zone between the ground surface and the perched water table. The vadose zone is within the unconsolidated deposits (removed during construction of the tailings cells), the Dakota Sandstone, and Burro Canyon Formation. The vadose zone is 13 to 116 ft thick, based on the depth to groundwater in 2007 (between 57 and 116 ft thick based on water levels in monitoring wells in the vicinity of Cells 2, 3, and 4A).

Although no site specific data are available, water contents in the vadose zone are believed to be very low due to the semi-arid environment. Water contents beneath the wildlife ponds are likely to be high due to artificial recharge caused by pond leakage.

Select core samples collected while drilling monitoring wells MW-23 and MW-30 were analyzed for unsaturated hydraulic properties by the laboratory at Daniel B. Stephens & Associates (2007). These samples are from the Dakota Sandstone and Burro Canyon Formation and were selected by MWH to represent the vadose zone beneath the tailings cells. Samples were analyzed for porosity, saturated hydraulic conductivity, and unsaturated soil water retention properties. Vertical hydraulic conductivity values were determined for the cores with falling head tests performed with flexible wall permeameter. Soil-water retention values were determined with a combination of hanging columns (0 to -200 cm pressure), pressure plates (-500 cm pressure), water activity meters (-15,000 to -44,000 cm pressure), and relative humidity box (-851,000 cm pressure). From these data, van Genuchten parameters (see Section 2.3) were estimated for soil water retention curves and unsaturated hydraulic conductivities. Hydraulic properties determined with these tests are summarized in Table 2-1; for complete results including graphical representations of the soil-water retention curves and unsaturated hydraulic conductivity functions, see Appendix A. Saturated vertical hydraulic conductivities ranged from 2.9×10^{-5} to 3.0×10^{-3} cm/sec with a geometric mean of 2.7×10^{-4} cm/sec for the samples analyzed. Generally, unsaturated hydraulic conductivity decreases dramatically as moisture contents decline. Under relatively dry conditions, the unsaturated hydraulic conductivity of sand is lower than that of silt and clay for a given

soil-water pressure (pressure is negative and commonly referred to as tension). This is because the volumetric water content of a sand under relatively dry conditions is lower than that of silt and clay for a given soil-water pressure.

The vertical hydraulic conductivity of the underlying Brushy Basin Member is significantly lower demonstrating why it acts as a perching layer. Cores from the Brushy Basin Member had vertical hydraulic conductivities of 7.28×10^{-11} to 5.95×10^{-4} cm/sec with a geometric mean of 1.23×10^{-8} cm/sec (International Uranium (USA) Corporation, 2000).

2.3 VADOSE ZONE FLOW AND TRANSPORT CONCEPTUAL MODEL

This section presents the conceptual model for flow and potential contaminant transport in the vadose zone. Details of the implementation of the conceptual model into the numerical model as well as parameter values, boundary conditions, and initial conditions used in the modeling are described in detail in Section 3.0.

2.3.1 Unsaturated Flow

Unsaturated Flow Governing Equation. Unsaturated flow through the vadose zone can be described with a modified Richards' Equation. The Richards' equation is derived by combining the Darcy-Buckingham equation with the mass continuity equation. For one-dimensional vertical flow the governing flow equation is given by the following modified form of the Richards' equation (Simunek et al., 2005):

$$\frac{\partial \theta}{\partial t} = \frac{\partial}{\partial z}[K(\frac{\partial h}{\partial z} + 1)] - S$$

where:

θ = volumetric water content [L^3L^{-3}]

h = water pressure head [L]

S = sink term = volume of water removed from a unit volume of soil per unit time (e.g., uptake by plants) [$L^3L^{-3}T^{-1}$]

z = spatial coordinate in the vertical direction [L]

t = time [T]

K = unsaturated hydraulic conductivity [LT^{-1}].

The unsaturated hydraulic conductivity is a function of the volumetric water content and pressure head and as a result can vary in both space and time.

Unsaturated Hydraulic Conductivity. To solve the above equations, it is necessary to specify the relationships of unsaturated hydraulic conductivity versus water saturation (S_w), and of pressure head (h) versus water saturation (θ). The relationship of pressure head (h) to water saturation (θ) is described by the following equation (van Genuchten, 1980; Mualum, 1976).

$$\theta(h) = \begin{cases} \theta_r + \dfrac{\theta_s - \theta_r}{[1 + |\alpha h|^n]^m} & h < 0 \\ \theta_s & h \geq 0 \end{cases}$$

where:

θ_r = the residual water content [L^3L^{-3}]

θ_s = the saturated water content [L^3L^{-3}]

h = the pressure head [L]

α = the inverse of the air-entry value (or bubbling pressure) [L^{-1}]

n = the pore size distribution index [dimensionless]

$m = 1 - 1/n \quad , \quad n > 1$

The relationship of unsaturated hydraulic conductivity versus water saturation is described by the following equation (van Genuchten, 1980):

$$K(h) = K_s S_e^l \left[1 - (1 - S_e^{1/m})^m\right]^2$$

where:

K(h,z) = unsaturated hydraulic conductivity function [LT^{-1}]

K_s = saturated hydraulic conductivity [LT^{-1}]

S_e = the effective saturation [dimensionless fraction].

L = the pore connectivity parameter [dimensionless]

m = 1 – 1/n, where n>1

For unsaturated porous media, the pressure head of soil porewater is negative (i.e., less than atmospheric pressure) and is commonly referred to as matric potential or soil-water tension (negative). The unsaturated hydraulic conductivity is a function of the saturated hydraulic conductivity, pressure head, and moisture content. As a result, the unsaturated hydraulic conductivity in the vadose zone can vary through time. See Table 2-1 for properties K_s, α, n, θ_r, and θ_s from the six cores tested as described in Section 2.2.5.

Plant-Water Uptake. The sink term in the Richards' Equation is defined as the volume of water removed from a unit volume of soil per unit time. This accounts for plant-water uptake and can be defined in terms of soil-water pressure head as described by the following equation (Feddes et al., 1978):

$$S(h) = \alpha(h) S_p$$

where:

$\alpha(h)$ = root water uptake water stress response function [dimensionless]

S_p = potential water uptake rate [T^{-1}]

The value of $\alpha(h)$ ranges between 0 and 1. Below a certain head, when conditions are extremely dry, plants cease to uptake water. A plant-root-distribution function can also be used to account for variable plant-water uptake with depth. For grasses, roots are usually most dense near the ground surface and decrease with depth (Kurc and Small, 2003; Foxx and Tierney, 1987; Schuster, 1964; Lee and Lauenroth, 1994).

2.3.2 Contaminant Transport in the Unsaturated Zone

Transport through the vadose zone is affected by advection, dispersion (both mechanical dispersion and molecular diffusion), sorption, and degradation or other transformations (e.g., biotransformations, radioactive decay, precipitation and loss from aqueous solution/sorption). Advective velocities are largely controlled by soil moisture content because the unsaturated hydraulic conductivity and effective porosity varies through time as moisture content varies.

Contaminant Transport Governing Equation. Contaminant transport can be described by the advection-dispersion equation (ADE). The governing equation for unsaturated zone contaminant transport with advection, dispersion, sorption (retardation) of contaminants, as well as production and transformations (losses) of contaminants is (Simunek et al., 2005):

$$D_z \frac{\partial^2 C}{\partial z^2} - V_z \frac{\partial C}{\partial z} = R \frac{\partial C}{\partial t} + R \lambda C + R \frac{qC}{\theta}$$

where:

z = spatial coordinates in the vertical direction [L]

C = dissolved concentration of chemical [ML^{-3}]

D_z = dispersion coefficient in the z direction [L^2T^{-1}]

V_z = one dimensional, uniform seepage velocity in the z direction [LT^{-1}]

R = retardation factor [dimensionless]

t = elapsed time [T]

λ = effective first-order decay coefficient [T^{-1}]

q = net recharge [LT^{-1}]

θ = volumetric water content [L^3L^{-3}].

Dispersion. The process of hydrodynamic dispersion acts to dilute and spread contamination as it is transported by advection. Hydrodynamic dispersion is the combination of mechanical dispersion and molecular diffusion. Mechanical dispersion is generally dominant unless flow velocities are extremely slow, as may be the case under very dry conditions with extremely low unsaturated hydraulic conductivities. There are three basic factors contributing to mechanical dispersion:

- velocity differences in an individual pore and between pores of different sizes
- transverse diffusion into pores of stagnant water or slower velocity relative to faster flow paths
- molecular diffusion ahead of the wetting front.

These processes occur in all porous media. Longitudinal dispersion spreads the contaminant along the direction of flow whereas transverse or lateral dispersion spreads the contaminant perpendicular to flow. Both have the effect of spreading of contaminants, and increasing the plume area, while decreasing contaminant concentrations through dilution. At the field scale, aquifer heterogeneities also will cause dispersion. Flow perpendicular to layered heterogeneities (as in the vadose zone at White Mesa where bedding is flat lying) leads to relatively less dispersion than flow parallel to bedding planes (Khaleel et al., 2002).

The hydrodynamic dispersion coefficient in the liquid phase is defined as (Simunek et al., 2005):

$$D = D_L q + \theta D_w \tau_w$$

where:

D = hydrodynamic dispersion coefficient [L^2T^{-1}]

D_L = longitudinal dispersivity [L]

q = Darcian fluid velocity [LT^{-1}]

θ = volumetric water content [L^3L^{-3}]

D_w = molecular diffusion coefficient in free water [L^2T^{-1}]

τ_w = tortuosity factor in the liquid phase [dimensionless].

Sorption and Retardation. Chemical reactions between dissolved constituents in groundwater (e.g., metals and radionuclides) and the aquifer matrix often dictate spatial and temporal variations in contaminant-plume transport and mobility in the subsurface by controlling the degree of adsorption-desorption of aqueous complexes to surface assemblages. Surface-complexation models apply principles of chemical equilibrium to reactions between dissolved species and potential sorption sites. A series of heterogeneous mass-action equations, mass-balance equations for surface sites, and charge-potential relations for each surface are coupled with aqueous-speciation equilibria to determine sorbate-sorbent interactions, commonly using a geochemical-computer code (e.g., Parkhurst and Appelo, 1999). In the geochemical model PHREEQC, surface-complexation reactions are reproduced after the Dzombak and Morel (1990) double-layer model with the option to include effects from electrostatic potentials (Parkhurst and Appelo, 1999). The generalized, two-layer model quantifies the adsorption of speciated-aqueous complexes onto hydrous-ferric oxide (HFO) surface sites (Dzombak and Morel, 1990).

For a specific contaminant that exhibits linear sorption, a retardation factor can be calculated with the distribution coefficient (Freeze and Cherry, 1979):

$$R = 1 + \rho_b K_d/\theta$$

where:

R	=	retardation factor of contaminant [dimensionless]
ρ_b	=	dry soil bulk density of the porous media [ML^{-3}]
K_d	=	sorption coefficient of contaminant [L^3M^{-1}]
θ	=	volumetric water content [L^3L^{-3}].

A retardation factor of 1.0 indicates that the contaminant plume migrates at the same rate as the advective velocity, as is typically the case for chloride. Retardation values used in the modeling are presented in Section 3.0, and described in detail in Appendix B. Sorption and retardation values for other site contaminants are presented in Section 4.3 and Table 4-1, and described in detail in Appendix B.

TABLE 2-1

UNSATURATED HYDRAULIC PROPERTIES FOR CORES FROM WHITE MESA

Location ID	Sample Depth (feet below ground surface)	Inverse Air-Entry Pressure α (cm^{-1})[1]	Pore-Size Dsitribution Index n (dimensionless)[1]	Residual soil water content θ_r (% vol)	Saturated soil water content θ_s (% vol)[2]	Dry Bulk Density (grams/cm^3)	Saturated Hydraulic Conductivity K_{sat} (cm/sec)
MW-30	35.5-36.0	0.0266	1.348	0.00	19.86	1.98	8.1E-04
MW-30	44.0-44.5[3]	0.0074	1.202	0.00	27.59	2.23	8.2E-06
MW-30	44.0-44.5[3] volume adjusted	0.0081	1.201	0.00	26.43	2.12	--[3]
MW-23	55.5-56.0	0.0103	1.386	0.00	18.38	2.03	1.1E-04
MW-23	74.3-74.6	0.0003	1.354	0.00	12.16	2.33	2.9E-05
MW-23	82.7-82.9	0.0069	1.336	0.00	16.01	2.10	1.7E-04
MW-23	103.3-103.5	0.0287	1.349	0.00	20.51	1.84	3.0E-03

Notes: All testing performed by Daniel B. Stephens & Associates, Inc. Laboratory / Testing Facility. For full results see Appendix A.

1. Parameter in van Genuchten soil water retention function
2. Equivalent to total porosity
3. Sample MW-30 44.0-44.5 experienced swelling and water gain during and after the initial saturation process. This sample also cracked horizontally during moisture retention testing

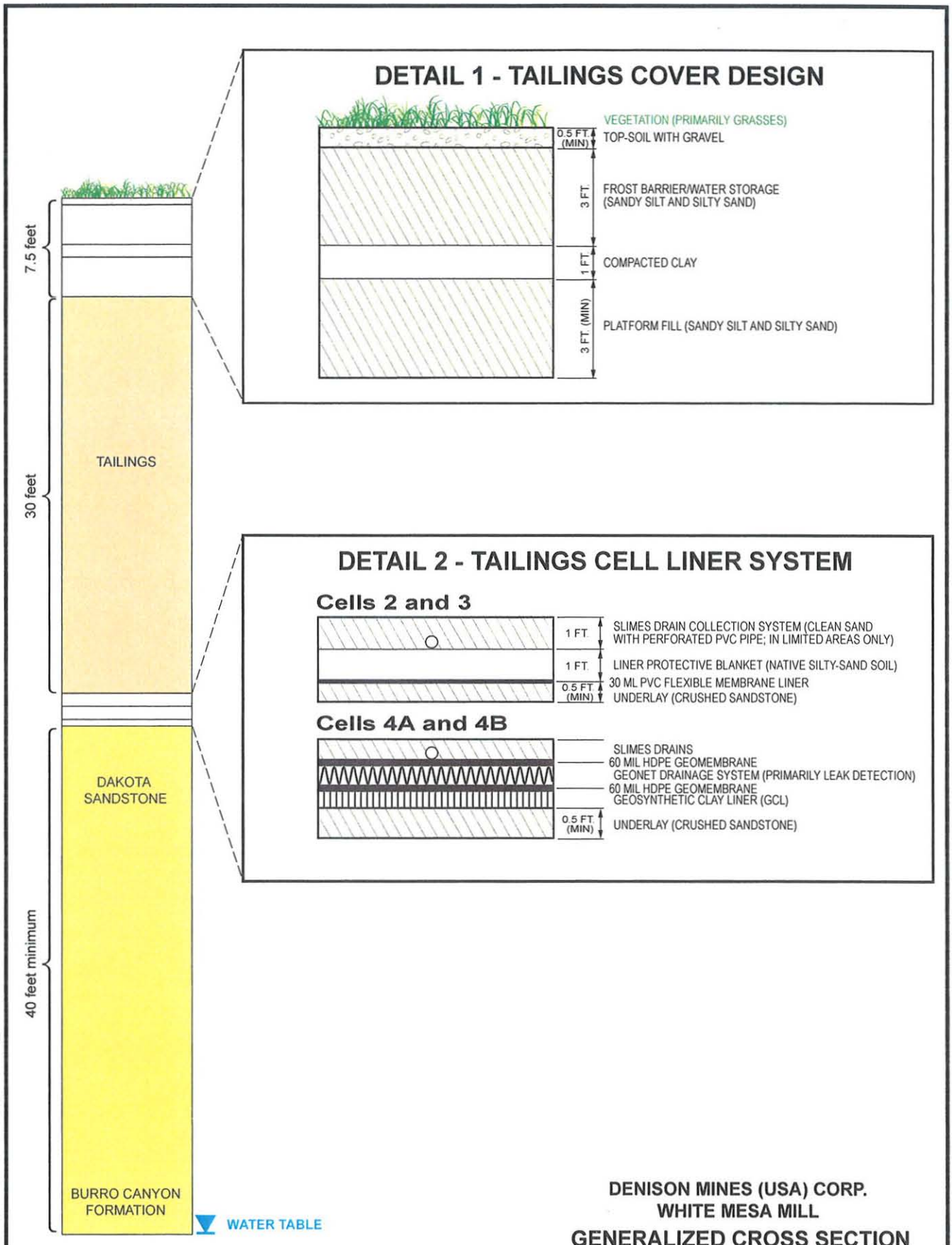

Note: Cross section represents minimum separation distance between tailings and water table based on data from monitoring wells.

DENISON MINES (USA) CORP.
WHITE MESA MILL

GENERALIZED CROSS SECTION WITH MODIFIED COVER DESIGN

FIGURE 2-2

FILE *Fig 2-2 Generalized modified Cross Section_1107.ai 11/21/07 SLC*

FILE *Fig 2-3 Denison Annual precip_Chart_807.ai 08/30/07 SLC*

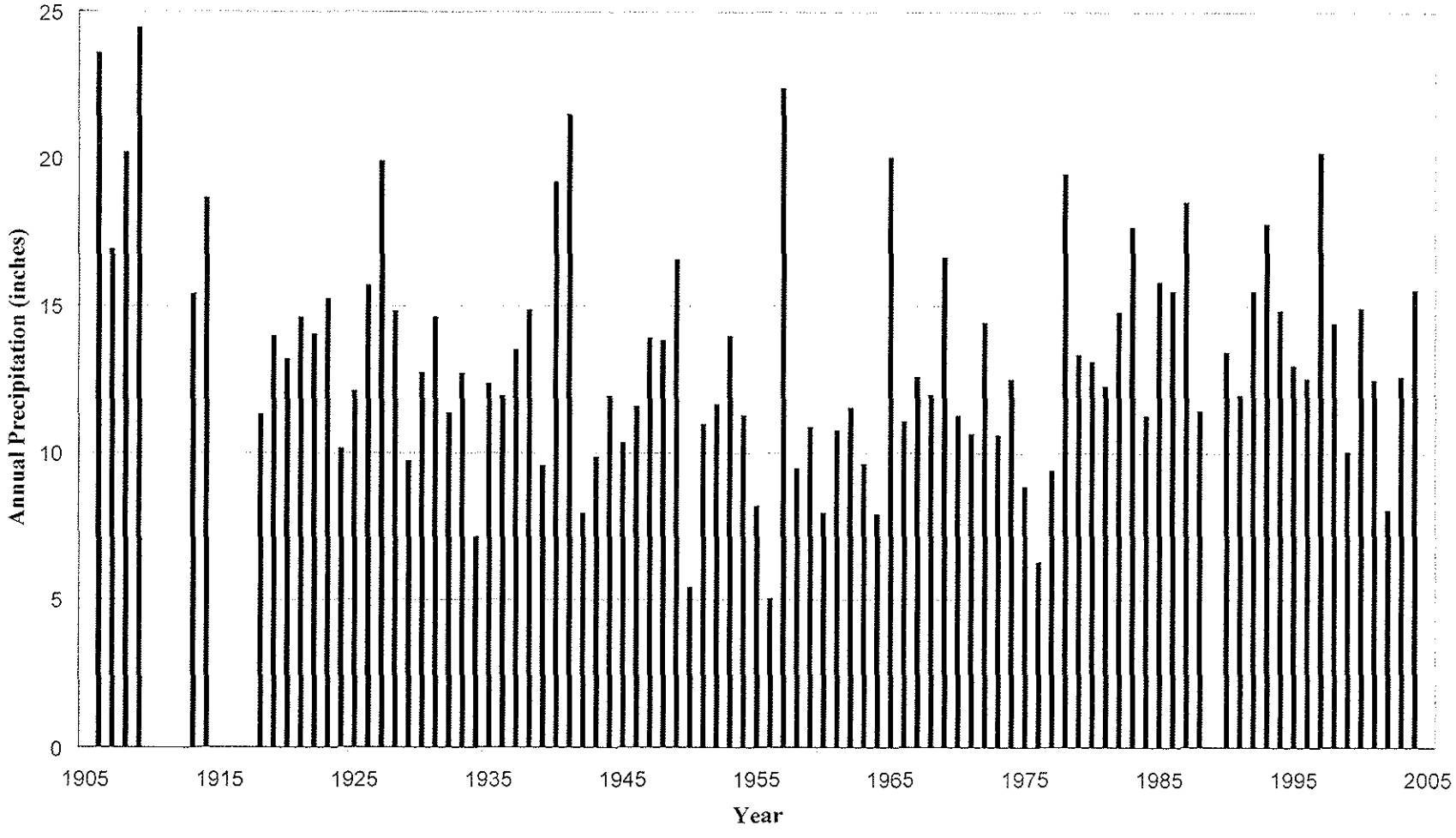

DENISON MINES (USA) CORP.
WHITE MESA MILL

ANNUAL PRECIPITATION AT BLANDING, UTAH (1905 TO 2005)

FIGURE 2-3

Note: years with incomplete data not shown.

FILE *Fig 2-4 Denison Daily precip_Chart_807.ai 08/30/07 SLC*

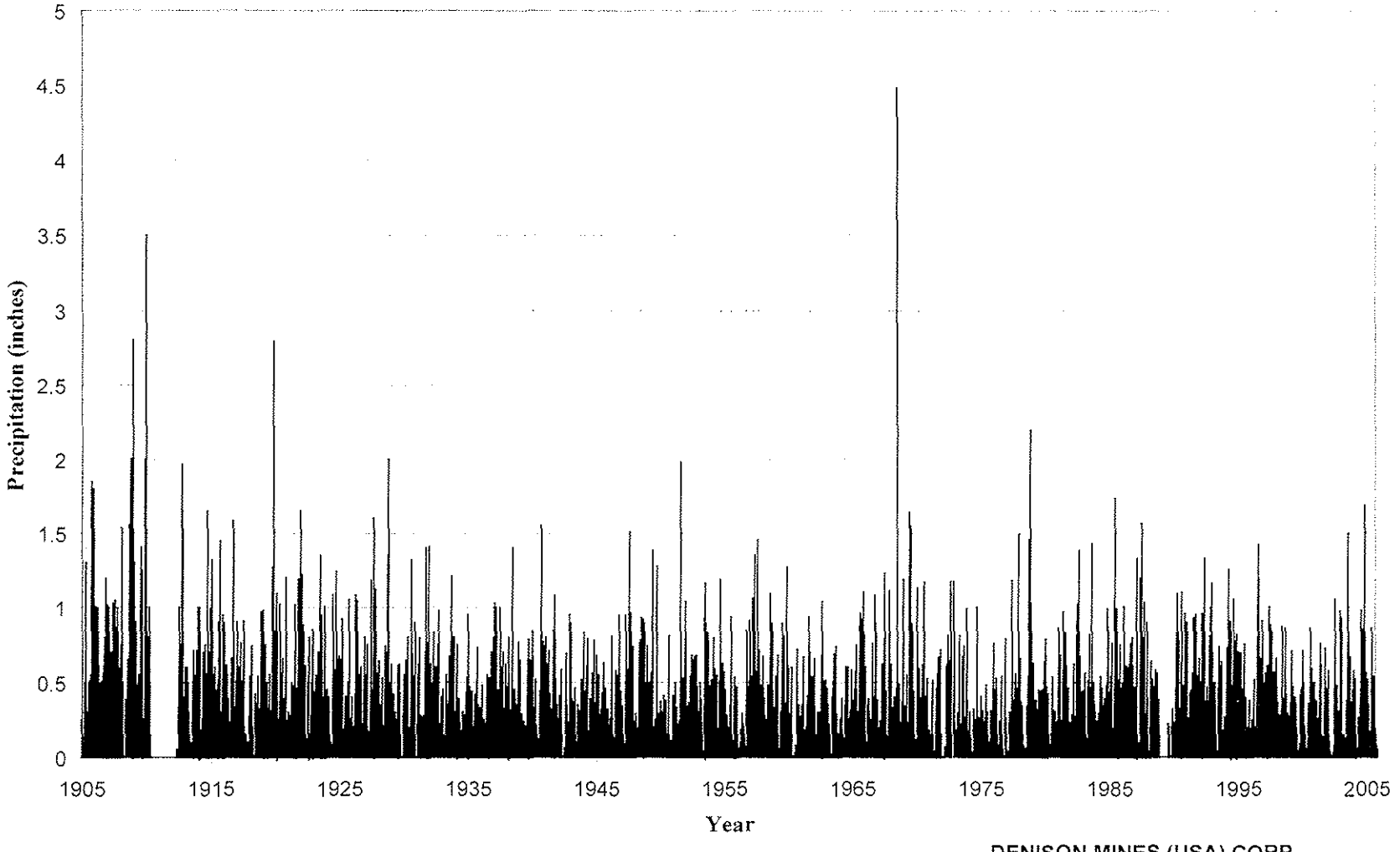

DENISON MINES (USA) CORP.
WHITE MESA MILL

DAILY PRECIPITATION AT BLANDING, UTAH (1905 TO 2005)

FIGURE 2-4

File: *Fig 2-1_Denison site map_1007.mxd SLC 10/16/07*

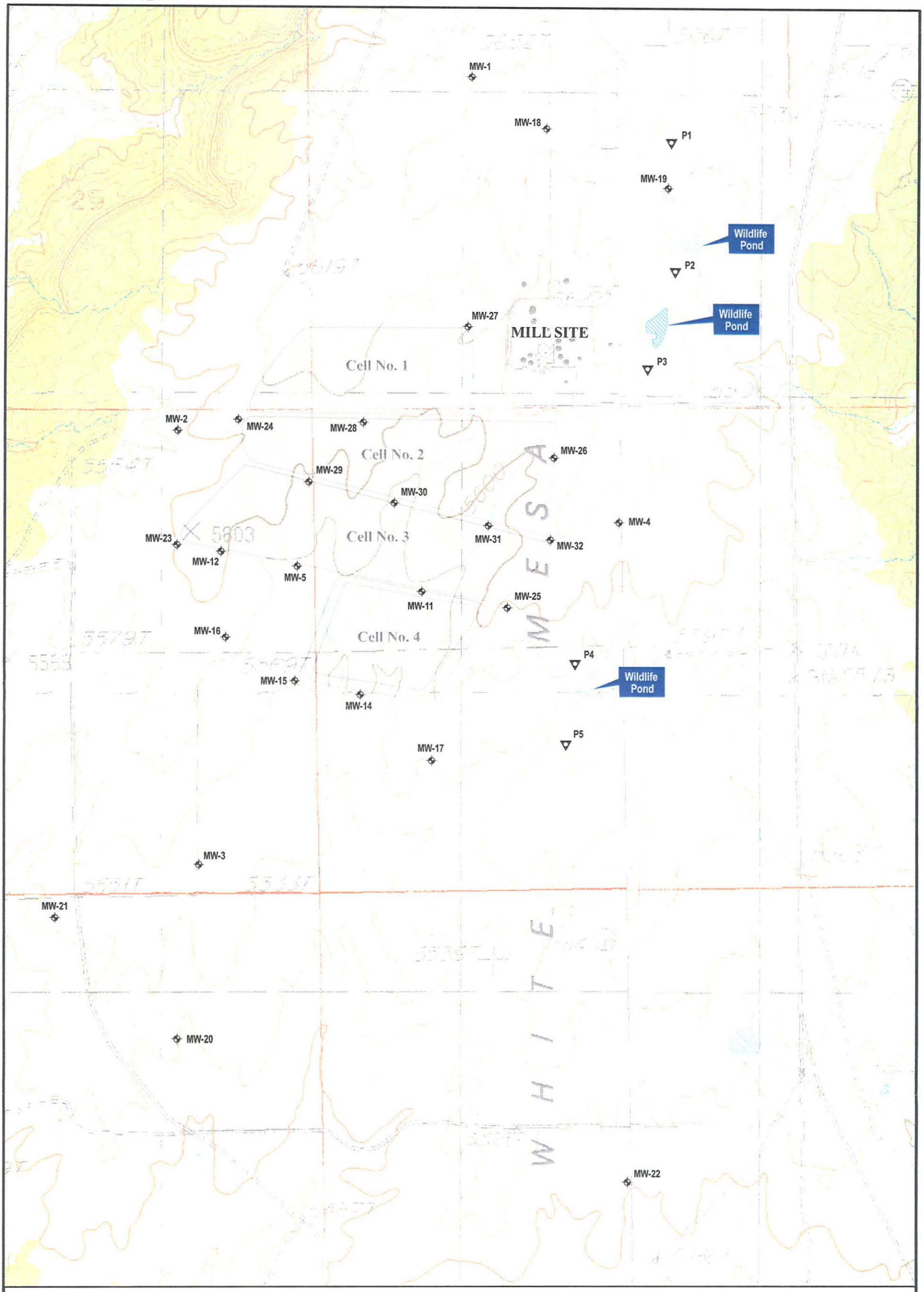

N
W E
S

0 1000
Feet

Base map adapted from USGS 7.5 Minute Topographic maps of Black Mesa Butte, Blanding South, No-Mans Island, and Big Bench, Utah Quadrangles.

Coordinates are UTM Zone 12, NAD 1927 meters.

EXPLANATION

Monitoring well

Piezometer

DENISON MINES (USA) CORP.
WHITE MESA MILL

SITE MAP

FIGURE 2-1

File: *Fig 2-5 Piezo surface contours_1107.mxd SLC 11/20/07*

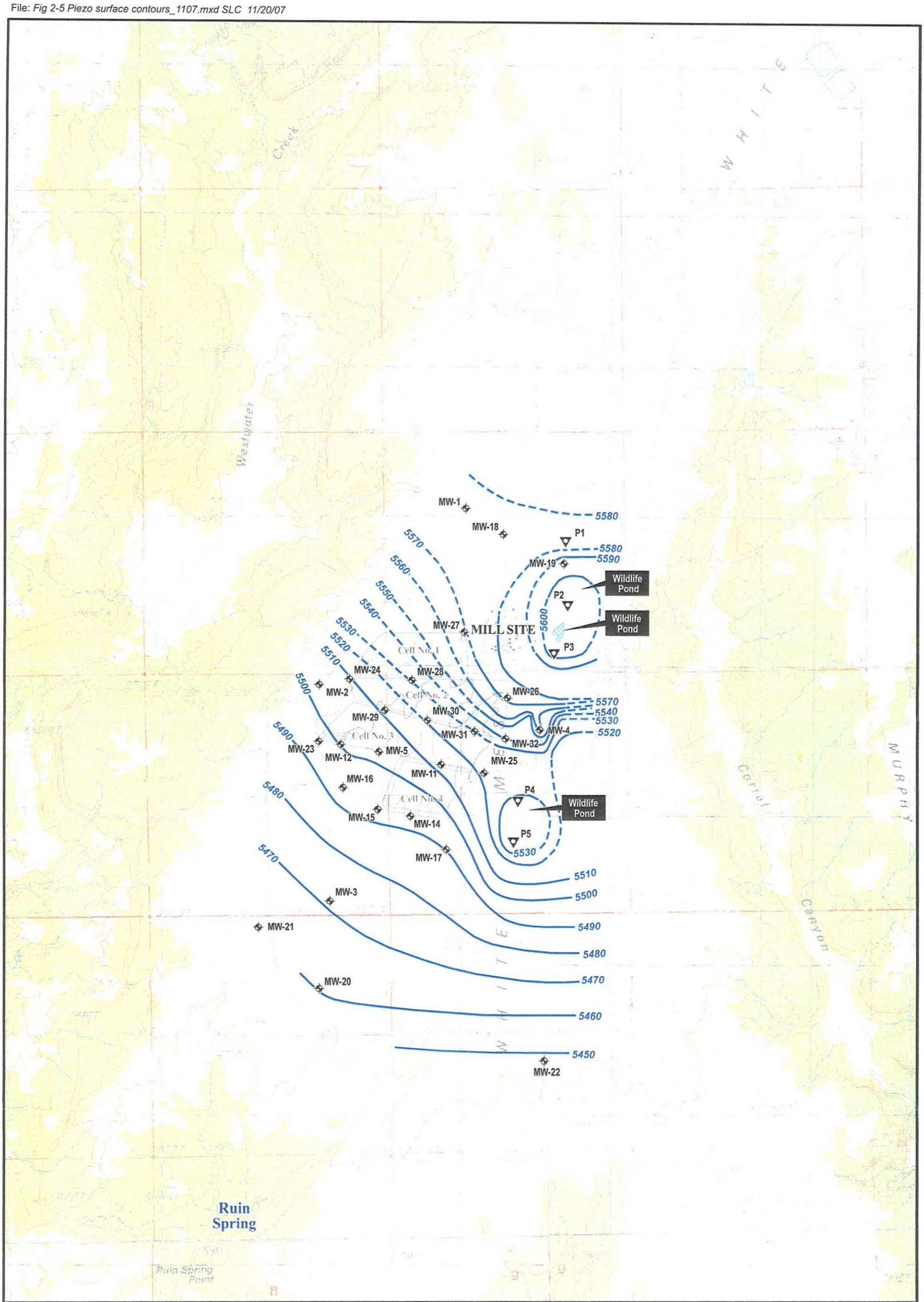

N
W E
S
0 2000
Feet

Note: Water level contours from Hydro Geo Chem, Inc. (2003) Wells MW-23 to MW-32.

Base map adapted from USGS 7.5 Minute Topographic maps of Black Mesa Butte, Blanding South, No-Mans Island, and Big Bench, Utah Quadrangles.

Coordinates are UTM Zone 12, NAD 1927 meters.

EXPLANATION

- Water level contour line, dashed where uncertain
- Monitoring well
- Piezometer

DENISON MINES (USA) CORP.
WHITE MESA MILL

PIEZOMETRIC SURFACE CONTOURS PERCHED AQUIFER (SEPTEMBER 2002)

FIGURE 2-5

3.0 METHODOLOGY

3.1 OVERALL MODELING APPROACH

This section provides information regarding the conceptual and mathematical models used in:

- Predicting potential infiltration rates through the tailings cell cover;
- Predicting potential flow and contaminant transport from the tailings (Cells 2, 3, 4A, and 4B) through the tailings cell liner system and underlying vadose zone to the water table; and
- Predicting potential contaminant transport in the perched aquifer and subsequent impacts to groundwater quality.

Following conceptual-model development, numerical modeling was completed sequentially according to the numbered list detailed below (see Figure 3-1):

1. Vadose zone flow modeling with HYDRUS-1D of the tailings cell cover with daily precipitation and evapotranspiration to estimate potential infiltration rates to the tailings.
2. Groundwater flow modeling with MODFLOW of Cells 2 and 3 to estimate tailings-dewatering rates through time and average water levels (saturated thickness) that will remain in the tailings (water-yield properties of tailings predicted with HYDRUS-1D in step 1 above). The predicted saturated thickness of the tailings after active dewatering is used as an initial condition in the HYDRUS-1D model of the tailings and vadose zone in steps 3, 4 and 5 below for Cells 2 and 3 (dewatering predictions for Cells 4A and 4B were from Geosyntec Consultants [2007b]).
3. Vadose zone flow modeling with HYDRUS-1D of tailings to get initial conditions for moisture content and pressure head in tailings above the

saturated layer (potential infiltration through cover predicted by HYDRUS-1D in step 1; saturated thickness of tailings predicted with MODFLOW in step 2).

4. Vadose zone flow modeling with HYDRUS-1D of tailings, tailings cell liner system, and underlying vadose zone to calibrate for liner properties and obtain quasi-steady-state water content and pressure head throughout the vadose zone (potential infiltration rate through the cover from HYDRUS-1D modeling in step 1; saturated thickness of tailings predicted with MODFLOW in step 2; initial water contents and pressure head in tailings above saturated tailings from HYDRUS-1D in step 3).

5. Vadose zone flow and potential contaminant transport modeling with HYDRUS-1D of tailings, tailings cell liner system, and underlying vadose zone (potential infiltration rate through the cover from HYDRUS-1D modeling in step 1; initial saturated thickness from MODFLOW modeling in step 2; initial water content and pressure head in tailings above saturated tailings from HYDRUS-1D in step 3; initial water content and pressure head in vadose zone from HYDRUS-1D in step 4).

6. Groundwater flow and potential contaminant transport modeling of perched aquifer simulated with MODFLOW and MT3DMS (potential contaminant-source loading, contaminant concentrations, and groundwater-recharge rates beneath the tailings cells predicted with HYDRUS-1D modeling in step 5).

Detailed descriptions of the modeling effort are provided in the remainder of this section. Vadose-zone modeling is described in Section 3.2; groundwater modeling of the tailings cell dewatering, in addition to groundwater flow and potential contaminant transport in the perched aquifer, is described in Section 3.3. For ease of comparison to model files, wherever possible, units of measure used in the models have been retained in the text (i.e., feet and days for MODFLOW, centimeters and days for HYDRUS-1D, and mg/l for both MT3DMS and HYDRUS-1D).

3.2 VADOSE ZONE FLOW AND TRANSPORT MODEL

3.2.1 Computer Code

The computer code HYDRUS-1D was used for the infiltration and contaminant transport modeling. HYDRUS is a finite-element model that simulates water flow and solute transport in variably-saturated media, and was developed by the U.S. Salinity Laboratory in collaboration with the Department of Environmental Sciences at the University of California at Riverside (Simunek et al., 1998; Simunek et al., 2005). The program can be used to analyze water and solute movement in unsaturated, partially-saturated, or saturated porous media. HYDRUS allows for spatial and temporal variation in soil properties, allowing for simulation of a heterogeneous soil profile under variably-saturated, unsteady-flow conditions. HYDRUS can simulate one-dimensional advection, dispersion, retardation (sorption), and degradation of contaminants. HYDRUS was selected because it is capable of simulating the dominant processes affecting infiltration and contaminant transport given the semi-arid conditions and multiple layers (cover layer, tailings, and vadose zone) that must be simulated at the site.

HYDRUS-1D is one of the few, commercially available, frequently tested models that can simulate both unsaturated flow and contaminant transport in the vadose zone (including layered stratigraphy) with a variety of initial and boundary conditions. Consideration of discontinuities in capillary and unsaturated hydraulic conductivity is very important for layered systems because travel times and storage of water and contaminants in the vadose zone is complex (due to potential capillary-barrier effects). The model provides accurate results when appropriate spatial discretization for the finite-element domain is established.

HYDRUS has been used to simulate deep percolation beneath final-closure designs for radioactive-waste management at the Nevada Test Site, flow around nuclear-subsidence craters at the Nevada Test Site, and influences of a capillary barrier at the Texas low-level radioactive waste disposal site. A comparison of HYDRUS to other codes (CHAIN, MULTIMED-DP, FECTUZ, and CHAIN 2D) was prepared by the U.S. Environmental Protection Agency in order to evaluate each code's ability to predict

radionuclide fate and transport in the unsaturated zone (Chen et al., 2002). Of the codes evaluated by Chen et al. (2002), HYDRUS was the most comprehensive, containing the greatest number of physical processes. Scanlon et al. (2002) performed a comparison of codes for simulation of landfill covers in semi-arid environments. In addition to HYDRUS, the evaluation by Scanlon et al. (2002) included the codes HELP, Soil-Cover, SHAW, SWIM, UNSAT-H, and VS2DT1. This evaluation indicated that Richards'-Equation-based codes such as HYDRUS-1D are more appropriate for simulating near surface water balance than those using a water-balance approach such as HELP. Only HYDRUS-1D, SWIM, and VS2DT1 could simulate a seepage face. Of these VS2DT1, did not simulate the upper atmospheric boundary conditions as well as HYDRUS-1D.

The HYDRUS-1D program numerically solves the Richards' equation for saturated/unsaturated water flow and the Fickian-based advection-dispersion equation for heat-and-solute transport. HYDRUS-1D incorporates unsaturated soil-hydraulic properties using the van Genuchten (1980), Brooks and Corey (1964), or modified van Genuchten-type (Vogel and Cislerova, 1988) analytical functions. The water flow portion of the model can incorporate (constant or time-varying) prescribed head and flux boundaries, as well as boundaries controlled by atmospheric conditions. Soil surface boundary conditions may change during the simulation from prescribed flux to prescribed head-type conditions. The code also allows for internal sinks such as plant-water uptake.

The HYDRUS-1D program numerically solves the advective-dispersive equation for solute transport. The transport equations include provisions for nonlinear and/or nonequilibrium reactions between the solid and liquid phases, linear equilibrium reactions between the liquid and gaseous phases, zero-order production, and two first-order degradation reactions (one independent of other solutes and one which provides coupling between solutes involved in sequential first-order decay reactions). The code supports both (constant and time-varying) prescribed concentration and concentration flux boundaries. The dispersion tensor includes a term reflecting the effects of molecular diffusion and tortuosity.

3.2.2 Domain

The vadose-zone-model domain consisted of a one-dimensional conceptual representation of the planned cover design, tailings, liner system, and underlying site stratigraphy. That is, the model domain is a one-dimensional vertical column extending from the land surface at the top surface of the tailings cell cover to the perched water table in the Burro Canyon Formation (see Figure 3-1). The vadose zone beneath Cells 2 and 3 was assumed to be 42-ft thick, representing the minimum distance from the base of the tailings to the perched water table, based on the average 2007 water level in monitoring well MW-30 and the base of Cell 3. The vadose zone beneath Cells 4A and 4B was assumed to be 40-ft thick, representing the minimum distance from the base of the tailings to the perched water table, based on the average 2007 water level in monitoring well MW-25 and the base of Cell 4A. The top of the domain corresponds to the top of the tailings cell cover layer. The base of the domain corresponds to the perched water table in the Burro Canyon Formation. To reduce simulation times, the domain was subdivided into two sub-domains for the different modeling steps as described in Section 3.1 above. As illustrated in Figure 3-1, the first sub-domain represented the cover system only (simulated in step 1), while the second sub-domain represented the tailings, tailings cell liner system, and underlying vadose zone (simulated in steps 3-5). Furthermore, there were two separate models of the second sub-domain representing the tailings, tailings cell liner system, and underlying bedrock vadose zone: one model representing Cells 2 and 3 and a second model representing Cells 4A and 4B.

3.2.3 Finite Element Node Spacing

The finite-element nodes were discretized in the vertical direction to simulate layers in the tailings cell cover, tailings, tailings cell liner system, and vadose zone. Construction of the finite-element mesh is dependent on surface and bottom boundary conditions and represented lithologic heterogeneities due to stratigraphic layering (Simunek et al., 2005). As a result, node spacing was finer than the geologic layers and tailings-cover layers in order to simulate steep hydraulic gradients which result from transient wetting (precipitation and infiltration) and drying (evapotranspiration) fronts. Fine-grid spacing

is necessary to accurately simulate water flow through the unsaturated zone since hydraulic properties vary significantly as a function of moisture content and pressure head. Because hydraulic properties vary much faster and on a finer scale near the land surface due to rapid changes in atmospheric conditions (daily variations in precipitation and evapotranspiration were modeled), the node spacing varied between 0.1 and 1 cm near the top of the domain representing the tailings-cover system. Whereas deeper in the vadose zone (i.e., in the Dakota Sandstone), the node spacing varied between 1 and 10 cm since moisture contents and pressure heads (i.e., hydraulic properties) vary at a much slower rate. Due to the extremely low hydraulic conductivity in the tailings cell liner system, the node spacing varied between 0.5 and 1 cm. In order to reduce errors due to numerical dispersion, the ratio between neighboring elements did not exceed 1.5 (Simunek et al., 2005).

3.2.4 Boundary Conditions for the Vadose Zone Flow Model

As discussed above, the domain was subdivided to perform simulations for different purposes; as a result, additional intermediate boundary conditions were required for each separate sub-domain. For the fist sub-domain, an atmospheric upper boundary condition was applied across the top of the model representing the tailings cell cover to simulate meteorological conditions and was a function of precipitation and potential evapotranspiration, as described in the paragraphs that follow. Free drainage (i.e., unit gradient) was assumed for the lower boundary condition of the model representing the tailings cell cover, which is conservative in that it probably overestimated potential flow from the base of the cover. For the second sub-domain, which simulated potential flow and transport from the tailings through the vadose zone to the water table, specified fluxes were applied to the upper boundary at the top of the tailings. Values for these specified fluxes were determined using the results from the tailings cell cover model. The lower boundary at the base of the domain was assumed to be fully saturated (i.e., water table conditions with a constant pressure head equal to atmospheric pressure), representing the water-table surface of the perched aquifer. Because of the one-dimensional nature of the model, the sides of the domain are implicitly assumed to be zero-flux boundaries.

Atmospheric Boundary Condition. Daily precipitation and air-temperature measurements were obtained for the Blanding weather station and used in the model (Utah Climate Center, 2007). Given the flat nature of the cover (0.2 percent slope), no runon- or runoff-based processes were assumed to occur and a surface layer with a maximum pressure head of zero was defined for the upper boundary condition applied across the top of the model. As a result, precipitation applied to the upper boundary was either removed through evaporation or transpiration, retained in the soil profile as storage, or transmitted downward as infiltration (potential recharge to the tailings). The 57-year period between 1932 and 1988 was selected for use in the vadose zone model because it contained:

- a nearly continuous time series
- a mixture of the largest annual and daily precipitation events
- consecutive-wet years.

The third and fourth wettest years on record (1957 and 1941; 22.4 and 21.5 inches, respectively) are within the time series selected, and are approximately 9% and 14% less than the maximum annual precipitation of 24.5 inches recorded during 1909. The largest daily precipitation event of 4.48 inches, which occurred on 1 August 1968, is represented in the time series selected.

Some interpolation was necessary to construct a continuous time series between 1932 and 1988. Missing precipitation measurements were left blank but accounted for only a small subset of the population (10 days out of 20,820 days). Air-temperature measurements were interpolated between missing data points, but overall accounted for a small subset (55 days out of 20,820 days) of the time series.

A combination temperature-based and solar-radiation-based approach was used to estimate daily evapotranspirative fluxes. Potential evapotranspiration (PET) was calculated for each day from measured maximum and minimum air temperatures in addition to estimated radiative fluxes following the methodology outlined in the work of Allen et al. (1998). The average annual PET between 1932 and 1988 was 47.9 inches.

Since actual evapotranspirative fluxes are a function of atmospheric, hydrogeologic, and ecologic conditions, PET was partitioned into potential soil evaporation (PE) and potential transpiration (PT) components. HYDRUS then calculates transpiration and evaporation depending on soil-water contents (e.g., saturation status) and water-stress properties intrinsic to the prescribed vegetation type. The minimum pressure head allowed at the surface was fixed at -15,000 cm, which controls how evapotranspiration is computed (J. Simunek, electronic communication, 2006). The fraction of radiation intercepted by the canopy and transmitted to the soil surface (Campbell and Norman, 1998) was used to partition PET between PE and PT assuming a grassland-cover leaf-area-index equal to 1.2 (Dwyer, 2003) and a canopy-extinction coefficient equal to 0.67 (Campbell and Norman 1998). As a result, the fraction of radiation intercepted by the canopy equaled 55%.

The 57-year climate record comprised of measured precipitation and calculated potential evaporation and transpiration was repeated to establish a synthetic atmospheric record for greater durations (e.g., 200 years). Generation of a concatenated atmospheric record assumes that historic meteorological conditions are considered representative for the future.

Plant-Water Uptake. The maximum rooting depth was specified as 100 cm based on average rooting depths reported for grasses (Kurc and Small, 2004; Currie and Hammer, 1979; Foxx and Tierney, 1987; Schuster, 1964; Lee and Lauenroth, 1994). For grasses, roots are usually denser near the ground surface and decrease with depth. A linear decrease with depth was assumed for the root-water-uptake function (i.e., assumes vegetation removes more water near the ground surface and less with depth). The root-water-uptake function is a dimensionless number proportional to the root distribution or root density. The Feddes et al. (1978) water-uptake model with water-response functions for grass was selected in HYDRUS.

3.2.5 Input Parameters for the Vadose Zone Flow Model

Hydraulic properties required for the vadose zone flow model include vertical saturated and unsaturated hydraulic conductivity, residual soil-water content, saturated soil-water

content (porosity), and the soil-water-retention curve-fitting parameters. Wherever possible, site-specific data obtained from previous investigations at the site were used to construct the vadose zone flow model. As presented in Table 2-1 and Appendix A, the saturated and unsaturated hydraulic properties were measured for cores from the Dakota Sandstone and Burro Canyon Formation. Unsaturated hydraulic properties for the tailings cell cover materials, as well as for the tailings, were estimated using grain-size data for these materials and the soil-properties database in HYDRUS. Hydraulic properties used in the model are presented in Table 3-1. The van Genuchten-Mualem single-porosity soil-hydraulic-property model enabling an air-entry value of -2 cm was selected to characterize the soil-hydraulic properties. Lacking site-specific measurements, the vadose zone was assumed to be unaffected by hysteresis.

During initial transient vadose zone flow simulations without a tailings cell liner, the tailings were observed to completely desaturate within an unrealistic timeframe. As a result, the geomembrane liner was represented as a low-permeability layer in HYDRUS to more accurately simulate potential water flux and contaminant transport into the underlying vadose zone. Theoretically, a geomembrane liner should consist of an impermeable material that precludes leakage into the underlying vadose zone. However, the occurrence of a limited number of manufacturing and installation defects is generally anticipated and incorporated during assessment of environmental impacts (Giroud and Bonaparte, 1989). The saturated hydraulic conductivity of the liner was selected as a fitting parameter, and was calibrated to match potential flux rates predicted by Knight-Piesold (1998), assuming 122 cm (4 ft) of head above the liner of Cell 3. Using a combination of empirical and analytical equations, and assuming a certain number of defects and defect sizes taken from the literature (Giroud and Bonaparte, 1989), Knight-Piesold (1989) calculated a total potential flux rate of 4.6×10^{-4} cm/day for Cell 3. This flux rate was selected as a calibration target for the potential flux through the geomembrane for Cells 2 and 3.

The saturated hydraulic conductivity of the liner for Cells 4A and 4B was calibrated to a potential flux rate calculated following the approach outlined in the work of Foose et al. (2001), which is very similar to the approach adapted by Knight-Piesold (1989). For

Cells 4A and 4B, the following assumptions were incorporated into the calculations: 30 cm (1 ft) of head above the liner (Geosyntec Consultants, 2007b), a GCL saturated hydraulic conductivity of 2.4 x 10^{-2} cm/day (Kashir and Yanful, 2001; Jo et al., 2005), a GCL thickness of 1 cm, 1-hole defect per acre and 2-seam-tear defects per acre (Giroud and Bonaparte, 1989), a hole radius of 1 mm and a seam-tear width of 1 cm, and good contact between the geomembrane and the GCL. The calculated potential flux rate and calibration target for Cells 4A and 4B was 2.6 x 10^{-4} cm/day.

The saturated tailings were allowed to drain and the saturated hydraulic conductivity of the geomembrane was varied in order to obtain pseudo-steady-state water fluxes (equivalent to the seepage velocity calibration target) through the simulated liner. A saturated hydraulic conductivity of 7.3 x 10^{-5} cm/day was obtained for the geomembrane liner in Cells 2 and 3 at a pressure head (i.e., saturated thickness) of 122 cm (4 ft); while a saturated hydraulic conductivity of 9.2 x 10^{-5} cm/day was obtained for the geomembrane liner in Cells 4A and 4B at a pressure head (i.e., saturated thickness) of 30 cm (1 ft). Slight pressure-head differences above and below the liner between the two scenarios (calculated versus calibrated) resulted from equilibration in HYDRUS-1D during tailings draindown and establishment of pseudo-steady-state water fluxes.

As a comparison, the calibrated saturated hydraulic conductivities used in the model to represent the PVC and HDPE liners are approximately three orders of magnitude lower than a well-compacted clay (Geosyntec Consultants, 2006) and two orders of magnitude higher than a typical value for a PVC geomembrane and four orders of magnitude higher than a typical value for a HDPE geomembrane reported by Giroud and Bonaparte (1989). As part of the sensitivity analysis, high- and low-variant flux rates through the Cells (and different saturated hydraulic conductivities of the liners) were simulated to determine a range of potential water fluxes and contaminant transport in the vadose zone. Increasing the saturated hydraulic conductivity of the liner is equivalent to increasing the number of presumed defects.

3.2.6 Initial Conditions for Vadose Zone Flow Model

In the infiltration model, the tailings were assumed to have a saturated thickness of 122 cm (4 ft) initially for Cells 2 and 3 and 30 cm (1 ft) for Cells 4A and 4B. The value for Cells 2 and 3 is based on the results of the dewatering modeling performed with MODFLOW, assuming dewatering will be discontinued after 10 and 14 years, respectively. The value for Cells 4A and 4B was calculated with analytical equations (Geosyntec Consultants, 2007b). The moisture-content profile in the tailings above this saturated base were calculated with an assumed steady-state infiltration rate through the cover, based on the long-term rate determined with the vadose zone flow model for the tailings cell cover. For all HYDRUS simulations, initial conditions were prescribed as pressure heads (as opposed to water content) in order to facilitate model convergence.

3.2.7 Boundary Conditions for Vadose Zone Transport Model

For the second sub-domain, which simulated potential flow and transport from the tailings through the vadose zone to the water table, specified mass fluxes equal to zero were applied to the upper boundary at the top of the tailings. Free drainage was assumed for the lower boundary condition of the model. Because of the one-dimensional nature of the model, the sides of the domain are implicitly assumed to be zero-flux boundaries.

3.2.8 Input Parameters for the Vadose Zone Transport Model

Contaminants Modeled. The contaminants modeled were natural uranium, chloride, and sulfate. These compounds are the most dependable indicators of site water quality and of potential cell failure due to their predominance (uranium) and predominance and mobility (chloride and sulfate). In particular, because sorption of chloride is minimal, it will migrate unretarded and act as a conservative tracer and thus would be expected to be detected before all other site contaminants. Likewise, sulfate will migrate relatively unretarded and occurs in high concentrations. Uranium was included because it is one of the primary contaminants of concern and is representative of metals and radionuclides. Transport of other site contaminants was not explicitly modeled, but rather was inferred

based on retardation factors calculated for other contaminants relative to chloride, sulfate, and uranium.

Diffusion and Dispersivity. The hydrodynamic-dispersion coefficient for transport in the unsaturated zone is a function of molecular diffusion and mechanical dispersion. Molecular-diffusion coefficients for chloride, sulfate, and uranyl (UO_2^{2+}) in free water assuming infinite dilution were 1.75, 0.92, and 0.37 cm^2/day, respectively (Li and Gregory, 1974). The diffusion coefficient for uranyl is considered to be a conservative estimate since uranium (VI) is expected to complex with dissolved species including sulfate and carbonate (Appendix B), which would tend to decrease the diffusion coefficient. Tortuosity, and its effect on molecular diffusion, was explicitly modeled during contaminant transport modeling by incorporation of a tortuosity factor for the liquid phase (Simunek et al., 2006). Effective diffusion coefficients for chloride near residual saturations are on the order of 0.01 cm^2/day (Schaefer et al., 1995). Estimates of dispersivity were assumed equal to 50 cm for chloride and sulfate, which is comparable to values presented in the work of Khaleel et al. (2002). Given the extremely low advective velocity of uranium as a result of sorption, mechanical dispersion was assumed to be negligible relative to molecular diffusion. Sensitivity of contaminant transport to variations in dispersivity was also evaluated.

Porosity and Dry-Bulk Density. Porosity and dry-bulk density are required for the transport model to calculate advective velocities and retardation factors. Porosity (saturated-water content) and dry-bulk density of the underlying Dakota Sandstone and Burro Canyon Formation were measured for core samples collected while drilling monitoring wells MW-23 and MW-30. Porosity and dry-bulk density values used in the vadose zone transport model are presented in Table 3-2.

Sorption and Retardation. Retardation rates were calculated based on equilibrium soil-water partition coefficients (K_d). Chloride was assumed to migrate unretarded (i.e., $R = 1$, no sorption). Similar to chloride, sorption of sulfate is relatively low. K_d values for uranium were calculated using the mass of HFO present in the bedrock and the equilibrated solution compositions predicted with the geochemical code PHREEQC

(Parkhurst and Appelo, 1999). Uranium chemistry is fairly complicated and is highly variable depending on the solution pH, carbonate concentration, and oxidation-reduction potential of the water. Neutralization of the infiltrating tailings porewaters and sorption of solutes was determined with PHREEQC. The mass of HFO and calcite was determined for samples collected from the vadose zone from the Dakota Sandstone and Burro Canyon Formation from cores collected while drilling monitoring wells MW-23 and MW-30. For details of the methodology, laboratory-analytical results, and geochemical-modeling results, refer to Appendix B. K_d and resulting retardation factor values used in the vadose zone transport model are presented in Table 3-2.

Degradation and Production. No degradation or production of uranium, chloride, or sulfate was assumed. Radioactive decay of uranium is considered to be relatively minor due to the slow processes involved (e.g., the half-life for natural uranium, which is predominantly U-238, is 4.4×10^9 years). Although uranium can be removed from solution through microbial processes, in order to yield more conservative model predictions these processes were not simulated.

3.2.9 Initial Conditions for Vadose Zone Transport Model

Source Concentrations. Source concentrations for natural uranium, chloride, and sulfate were derived from tailings-wastewater samples collected between September 1980 and March 2003 by International Uranium (USA) Corporation and its predecessors and the U.S. Nuclear Regulatory Commission as presented in the Statement of Basis (Utah Division of Radiation Control, 2004). For natural uranium, the average concentration was calculated to be 94 mg/l. For chloride, the average concentration was calculated to be 4,608 mg/l. For sulfate, the average concentration in the tailings was 64,914 mg/l; however, the equilibrium concentration was calculated to be 44,248 mg/l, based on equilibrium with gypsum and barite (see Appendix B) and was used as the initial concentration in the vadose zone transport model. For Cells 2 and 3, pore fluids in the tailings, slime-drain-collection system, and liner-protective blanket, were assumed to have these concentrations initially, in which the total amount of mass released in the profile is equal to the depth-integral of the concentration and volumetric-water contents at

time zero. For Cells 4A and 4B, pore-fluids in the tailings and underlying geonet were assumed to have these concentrations initially. Initially, all water in the tailings was equal to the average concentrations reported above. No source degradation or treatment was assumed: the only process reducing these concentrations was flushing with uncontaminated water that had infiltrated through the tailings cell cover.

3.2.10 Duration of Simulations and Time Steps

Simulations were run to predict 200 years into the future as required by the Permit. As described above, climatological data for the 57-year period 1932 through 1988 were repeated to generate the necessary duration of input data. Climatic data were input on a daily basis for the tailings-cover model. Daily flux rates predicted by the simulations through the tailings cover were used for input to the model of the tailings, liner, and bedrock vadose zone. The minimum and maximum time-step lengths were 1×10^{-6} day (0.086 seconds) and 0.5 days, respectively, enabling an initial time step of 5×10^{-4} day (4.32 seconds) for the HYDRUS-1D models. The maximum number of iterations per time step was 40. In HYDRUS-1D, solution efficiency is maximized by incorporating adaptive-time-step adjustments based on criteria described in Simunek et al. (2005).

3.2.11 Sensitivity Analysis

A sensitivity analysis was performed to quantify the model-prediction uncertainty due to estimating input parameters. Three values were selected for each input parameter, representing three different conditions such as a minimum, expected, and maximum value. The input variables selected for analysis as part of the sensitivity analysis included precipitation, liner saturated hydraulic conductivity, and dispersivity. Saturated thickness of the tailings was not included in the sensitivity analysis because it is a parameter that is controlled rather than an unknown (e.g., future precipitation, liner saturated hydraulic conductivity, and dispersivity). Unsaturated hydraulic conductivity of the vadose zone was not included in the sensitivity analysis because these values vary to match flux rates under a unit hydraulic gradient. Daily predictions of water fluxes exiting the tailings cell cover model were used as an upper boundary condition for the vadose-zone-transport model.

First, the input precipitation was varied. As a worst-case scenario, the three largest precipitation years were inserted into the long-term meteorological time series, replacing years of average precipitation. For a maximum precipitation worst-case scenario, the three largest precipitation years, 1957 (22.4 inches), 1909 (24.5 inches), and 1906 (23.6 inches), were consecutively inserted in the data record replacing precipitation values measured between 1946 and 1948 (which were 11.6, 13.9, and 13.8 inches, respectively, and are close to the long-term average of 13.3 inches). This sequence was included in each 57-year record of the maximum precipitation runs. Inclusion of consecutive-wet years, as recommended by Khire et al. (2000), was used to evaluate if long-term accumulation of water in the water-storage layer is problematic and if the ET cover is likely to perform as designed and to evaluate the effects of increased precipitation on water flow and potential contaminant transport in the vadose zone. Initial simulations suggested some ponding of water on the surface; as a result, a minimum surface pressure of 2 cm was enabled. This ensured that all precipitation was accounted for. Additionally, the three smallest precipitation years were inserted into the long-term meteorological time series, replacing years of average precipitation.

Second, the saturated conductivity of the liner was changed to match different potential fluxes. As a worst-case scenario, the base-case potential flux through the liner of Cells 2 and 3 and Cells 4A and 4B (see Section 3.2.5) were increased by a factor of 2.4 to 1.1×10^{-3} and 6.2×10^{-4} cm/day, respectively. This resulted in liner conductivities of 1.8×10^{-4} and 2.1×10^{-4} cm/day, for Cells 2 and 3 and Cells 4A and 4B, respectively. Increasing the conductivity of the liner is expected to result in increased potential water and solute fluxes to the aquifer, and is conceptually equivalent to increasing the number of assumed liner defects.

Third, because pressure heads are expected to vary within the vadose zone, the dispersivity was changed to quantify associated model uncertainty for this input parameter. Theoretically-based sensitivity analyses presented in the work of Khaleel et al. (2002) suggest that dispersivity is strongly dependent on the mean pressure head in the vadose zone. As a worst-case scenario, the dispersivity was increased by a factor of 2.5 to 125 cm, which is similar to values presented by Khaleel et al. (2002). Increasing the

dispersivity of the vadose zone is expected to decrease the arrival time of potential contaminant breakthrough. Additionally, given the low unsaturated hydraulic conductivities and fluid velocities, the dispersivity was set to zero to simulate diffusive transport of chloride and sulfate.

3.3 GROUNDWATER FLOW AND CONTAMINANT TRANSPORT MODELING

Two groundwater models were constructed: one model represented the water in the tailings cells to evaluate tailings cell dewatering for Cells 2 and 3 and the other model represented the perched aquifer to evaluate potential future impacts to shallow groundwater and contaminant transport. A tailings cell dewatering model was not constructed for Cells 4A (or 4B) because analytical solutions presented by Geosyntec Consultants (2007b) were deemed adequate given the uniform distribution of the drain system in this cell.

3.3.1 Model Codes

The computer codes MODFLOW and MT3DMS were used in this modeling effort with the Department of Defense (DoD) Groundwater Modeling System (GMS) pre- and post-processor. MODFLOW is a modular three-dimensional finite-difference flow model developed by the United States Geological Survey (USGS) (McDonald and Harbaugh, 1988; Harbaugh et al., 2000) to calculate hydraulic-head distribution and determine flow within a simulated aquifer. MT3DMS (Zheng and Wang, 1999) is an updated version of the United States Environmental Protection Agency (U.S. EPA)'s model MT3D (Zheng, 1990) and is capable of simulating transport of multiple contaminants simultaneously. Contaminant-transport processes that are simulated by MT3DMS include advection, dispersion, degradation, and sorption. These models were selected because they can adequately represent and simulate the hydrogeologic conditions and potential contaminant-transport processes that could occur in the perched aquifer beneath White Mesa. Furthermore, these models are well-documented, frequently used, and versatile programs that are widely accepted by the scientific and regulatory communities (Anderson and Woessner, 1992; Zheng and Bennett, 1995).

3.3.2 Model Domains, Layering, and Grids

Tailings Cell Model. The domain for the tailings cell model is approximately 3,500 by 1,200 ft, representing the tailings cells (see Figure 3-2). The finite-difference grid employs a constant spacing of 10 ft. The model includes two layers to represent the tailings and slimes drains. The bottom layer was 1-ft thick and represented the tailings-drain layer, and the top layer had a variable thickness that represents the tailings. The water level in the top layer was allowed to vary spatially and temporally. The bottom elevations were set based on information presented in the tailings cell construction report (D'Appolonia Consulting Engineers, 1982).

Perched Aquifer Model. The model domain for the perched aquifer extends 12,000 ft in the north-south direction (extending to Ruin Spring in the south) and 6,900 ft in the east-west direction (see Figure 3-3). The finite-difference grid employs a constant spacing of 50 ft and is a single layer representing the perched aquifer in the Burro Canyon Formation above the Brushy Basin Member. A single layer was deemed sufficient to model groundwater flow and transport at the site, considering the limited thickness of the perched aquifer and given that flow is primarily horizontal due to the extremely low vertical hydraulic conductivity of the Brushy Basin Member.

3.3.3 Boundary Conditions

Boundary conditions define hydraulic constraints at the boundaries of the model domain. There are three general types of boundary conditions:

1. Specified head or Dirichlet (e.g., constant head)
2. Specified flux or Neumann (e.g., constant flow, areal recharge, extraction wells, no flow)
3. Head-dependent flux or Cauchy (e.g., drains, evapotranspiration)

No-flow boundaries are a special case of the specified flux boundary in which the flow is set to zero.

Tailings Cell Model. For the tailings cell model, no-flow boundaries were assumed to surround the domain. A net flux rate from the cell was assumed across the entire domain. This assumed flux rate represents the combination of potential fluxes from the cell through the liner and potential infiltration into the cell through the cover. The net flux rate was calculated using the average infiltration rate through the cover predicted by the HYDRUS-1D tailings cover model and the potential flux rate through the bottom of Cells 2 and 3 calculated by Knight-Piesold (1998). The resulting average net flux rate for Cells 2 and 3 was 6.9×10^{-4} cm/day (2.27×10^{-5} ft/day). This assumed net flux rate was applied uniformly across the domain and was simulated with MODFLOW as a negative recharge rate.

The slimes drains were simulated with the Drain package in MODFLOW. Drains are head-dependent boundary conditions in which flow varies based on the difference in hydraulic head in the aquifer and the drain: as head in the aquifer declines (tailings in this case), so does the dewatering rate. Drain cells were set along nine alignments spaced 50-ft apart. Each drain was 600-ft long. Drains were set in the model as shown on drawings for Cells 2 and 3 (D'Appolonia Consulting Engineers, 1982).

Perched Aquifer Model. For the perched-aquifer model, "artificial" hydraulic boundary conditions were used to surround the domain due to a lack of data outside the White Mesa Mill property boundaries (except at Ruin Spring). Specified head boundaries were assigned along the north, south, and west sides of the perched-aquifer model, while a no-flow boundary was assigned along the east side of the model as it ran perpendicular to groundwater flow (see Figure 3-3). The specified heads were estimated based on perched-water levels measured at the site.

A constant net areal recharge was assigned to the entire model domain, except for areas beneath the tailings cells during transport simulations. The net areal recharge is the combined total of the recharge less evapotranspiration. Evapotranspiration was not simulated explicitly in the model but rather was assumed in the net areal recharge term. Recharge was estimated to be 3×10^{-4} cm/day (9×10^{-6} ft/day), or 0.3 percent of average annual precipitation for Blanding. Average recharge rates in arid to semi-arid regions

generally represent 0.1 to 5% of the long-term average annual precipitation (Scanlon et al., 2006). These percentage-based global-recharge rates are in agreement with values obtained in southwestern Utah through a comprehensive study performed by the U.S. Geological Survey (Heilweil et al., 2006) at a site which has a similar climate (although slightly hotter and drier) and geology as compared to White Mesa. Natural recharge rates through the vadose zone estimated by Heilweil et al. (2006) were calculated to range from 6.6×10^{-4} to 1.6×10^{-2} cm/day based on tritium analyses and 8.2×10^{-5} to 3.6×10^{-3} cm/day based on chloride analyses. Average recharge beneath the tailings cells was assigned based on results of the HYDRUS-1D model of the tailings cells and bedrock vadose zone.

Several small ponds that impact groundwater flow directions exist within the model domain. These ponds were simulated using general head (Cauchy) boundary conditions, for which a head and conductance is assigned and flux into or out of the model is calculated. Heads in these ponds were based on water levels measured nearby and were varied during calibration.

3.3.4 Hydraulic Properties

Tailings Cell Model. Hydraulic properties of the tailings were estimated based on aquifer testing performed in uranium mill tailings at the Canon City Mill (MFG Inc., 2005). The average hydraulic conductivity of the tailings ranged from 2.1 ft/day (7.4×10^{-4} cm/sec) to 8.5 ft/day (3.0×10^{-3} cm/sec) with an average value of 4.8 ft/day (1.7×10^{-3} cm/sec) (MFG Inc., 2005). A hydraulic conductivity of 4.8 ft/day was assumed for the tailings cell model.

Perched Aquifer Model. Hydraulic properties of the perched aquifer were based on field and laboratory measurements. As described in Section 2.2.3, field-measured hydraulic conductivities ranged from 5.4×10^{-4} to 4.5 ft/day. The magnitude and distribution of hydraulic conductivity were varied during calibration. The final hydraulic conductivities ranged between 0.08 and 1 ft/day. A porosity of 18 percent was assumed for the modeling. This value was based on samples collected while drilling monitoring

well MW-16 (Hydro Geo Chem, Inc., 2003), but also is in agreement with values for samples collected while drilling MW-23 (see Table 2-1).

3.3.5 Calibration of Flow Models

The calibration process involved iterating values for model parameters in sequential model simulations to produce estimated heads that better matched field-measured data. After each calibration simulation, the model results were compared to known data targets, which in this case were piezometric-head data from monitoring wells. The initial-parameter values were adjusted through calibration until the model produced results that adequately simulated the known data. As with any groundwater problem, calibration using different combinations of parameter values can lead to the same outcome for a given steady-state problem. However, if adequate data are available to characterize the hydrogeology and constrain the model parameters to a certain range of realistic, site-specific values, a more unique solution will result. The general changes made through the calibration process are described below.

Tailings Cell Model. The tailings cell model was calibrated by varying the drain conductance term until the flow rates approximately matched the 2007 dewatering rates (average rate of 12.5 gpm) and average water levels of 20 ft above the liner.

Perched Aquifer Model. The calibration was evaluated through both qualitative and quantitative methods. Qualitatively, the simulated water table contour map and the actual perched water table contour maps were compared visually to evaluate whether the patterns were similar. Quantitatively, the model results were analyzed statistically using the differences between actual target values and simulated values. The model results were analyzed statistically using the difference between the target head and the modeled head (this difference is known as the residual head). The calibration statistics included (Anderson and Woessner, 1992):

- The mean residual (the mean difference between measured and simulated heads);

- The absolute mean residual (the mean of the absolute value of the differences between measured and simulated heads); and
- The root mean squared error (the mean of the squared differences between measured and simulated heads).

The calibration process seeks to minimize residuals. The calibration statistics for the calibrated model are provided in Section 4.4. The mean residual provides information on the average error for all targets. This should be near zero; otherwise the predicted water levels are biased. However, a mean residual of zero does not indicate that the calibration is acceptable, it simply indicates that the water levels are not biased high or low. The absolute mean residual gives an indication of the total error of the model and should be minimized. The root mean squared error is similar to the absolute mean residual, except that it gives more weight to points with greater error. Again, this should be minimized. Another measure of the calibration is based on the root mean squared error divided by the total head drop across the model domain. For an acceptable calibration, this normalized root mean squared error should be less than 10 percent. Residuals also were examined spatially to assist in adjusting parameters to achieve better correspondence between modeled and actual-head values in subsequent calibration simulations.

Piezometric-head measurements from 26 locations (21 monitoring wells [MW-series] and five piezometers [P-series]) spread across the White Mesa site were used for calibration targets (see Table 3-3). To avoid biasing the calibration to a small area southeast of the Mill Site, the chloroform wells [TW4-series] were not used as calibration targets. Water-level-target values were the average of the four quarterly measurements for the 2007 water year. The range in water levels for the four quarterly measurements was less than 3 feet during the year for all but two wells (MW-23 and MW-31) and less than 1 foot for 15 of the 26 wells used as calibration targets, indicating little variation in water levels.

3.3.6 Contaminant Transport Model

Modeling of potential contaminant transport was performed for the perched-aquifer model only. Vadose-zone modeling with HYDRUS-1D provided inputs to the

groundwater flow-and-contaminant-transport model. These inputs include both a water flux and concentration through time at the water table. These potential fluxes were input as recharge directly beneath the area of Tailings Cells 2 and 3 and Cells 4A and 4B. The steady-state solution of the advective flow field was then used as the basis for the transport simulations. Because the HYDRUS-1D model of the tailings and vadose zone predicted that only chloride and sulfate will potentially reach the water table within 200 years, chloride and sulfate transport was simulated in the perched aquifer. Although there is chloride initially in the groundwater from natural sources, to clearly illustrate the potential chloride from the tailings cells, it was assumed that there was no background chloride in groundwater. The resulting potential chloride plume predicted by the model can be viewed as additional chloride and can be added to the background level. The potential concentrations of chloride were assigned as recharge-concentration sources beneath the tailings cells, and the model was run forward for 200 years to assess impacts to groundwater.

Transport Parameters. Dispersivity, degradation rates, porosity, and sorption (or retardation) are all required as input parameters in the transport model and were estimated from field data, laboratory data, and literature values. Because chloride is considered a conservative tracer, it was assumed to neither adsorb nor degrade. As a result sorption was set to zero, resulting in a retardation coefficient of 1.0. The degradation rate was also set to zero.

Dispersivity. Longitudinal dispersivity of contaminants in groundwater is frequently reported as a function of plume length or transport distance. Gelhar et al. (1992) examined many plumes and related longitudinal dispersivity (α_L) to plume length (L). Xu and Eckstein (1995) fitted a curve to the longitudinal dispersivity data presented by Gelhar et al (1992), which was later corrected by Al-Suwaiyan (1996) and is:

$$\alpha_L = 0.82(\log_{10} L)^{2.446}$$

This equation assumes that the measurements are in meters. Dispersivity transport was estimated based on an assumed transport distance. The HYDRUS-1D modeling

predicted that potential vadose zone porewater chloride concentrations beneath Cells 2 and 3 would be 0.001 mg/l immediately above the water table after 127 years (see Figure 4-5 for chloride breakthrough curve). Because the potential threat to groundwater was being assessed at 200 years, the advective velocity was used to calculate the transport distance for 73 years. This resulted in a transport distance of 420 ft; which was used to calculate the dispersivity. The resulting longitudinal dispersivity was approximately 17 ft. Transverse dispersivity is typically 10 percent of longitudinal dispersivity, thus it was estimated to be of 1.7 ft.

Ground Water Compliance Limit. The model predicted chloride and sulfate concentrations were compared to the proposed GWCLs established for individual compounds at individual wells. Proposed GWCLs are presented in the *Revised Background Groundwater Quality Report* (INTERA, 2007).

TABLE 3-1

SATURATED AND UNSATURATED HYDRAULIC PROPERTIES
OF THE WHITE MESA MILL VADOSE ZONE FLOW MODEL

Hydrostratigraphic Unit	Model-layer Description and Purpose	Model Layer Thickness z (ft)	Model Layer Thickness z (cm)	Residual Water Content θ_r (-)	Saturated Water Content (porosity) θ_s (-)	Inverse Air Entry Pressure α (cm^{-1})	Pore Size Distribution Index n (-)	Saturated Hydraulic Conductivity K_s (cm/d)
Cells 2 and 3								
loam	frost barrier and water storage[b]	3.5	107	0.0425	0.3228	0.0186	1.339	6.3
compacted clay	compacted-clay liner[c]	1	31	0.068	0.407	0.0037	1.068	0.041
loam	platform fill and grading[b]	3	91	0.0425	0.3228	0.0186	1.339	6.3
tailings	tailings[d]	30	914	0.035	0.323	0.0321	1.336	146.3
sandy loam	slimes drain collection system[e]	1	31	0.065	0.410	0.0750	1.890	106.1
loam	liner-protective blanket[b]	1	31	0.0425	0.3228	0.0186	1.339	6.3
geomembrane liner	geosynthetic liner beneath tailings[f]	1	30	0.068	0.407	0.0037	1.068	7.3×10^{-5}
loam	liner underlay and subbase grade[g]	0.5	15	0.078	0.430	0.0360	1.560	24.96
vadose zone top[a]	MW-30 35.5-36.0[h]	13.8	422	0.004	0.199	0.0266	1.348	69.81
vadose zone middle[a]	MW-23 55.5-56.0[h]	14.1	430	0.003	0.184	0.0103	1.386	9.33
vadose zone bottom[a]	MW-23 74.3-74.6[h]	14.1	430	0.016	0.122	0.0003	1.354	2.47
Cells 4A and 4B								
loam	frost barrier and water storage[b]	3.5	107	0.0425	0.3228	0.0186	1.339	6.3
compacted clay	compacted-clay liner[c]	1	31	0.068	0.407	0.0037	1.068	0.041
loam	platform fill and grading[b]	3	91	0.0425	0.3228	0.0186	1.339	6.3
tailings	tailings[d]	30	914	0.035	0.323	0.0321	1.336	146.3
loamy sand	geonet-drainage system[i]	0.1	3	0.057	0.410	0.1240	2.280	350.2
geomembrane liner	geosynthetic liner beneath tailings[j]	1	30	0.068	0.407	0.0037	1.068	9.2×10^{-5}
geosynthetic-clay liner	geosynthetic-clay liner beneath geomembrane[k]	0.03	1	0.068	0.407	0.0037	1.068	0.024
loam	liner underlay and subbase grade[g]	0.5	15	0.078	0.430	0.0360	1.560	24.96
vadose zone top[a]	MW-30 35.5-36.0[h]	13.2	402	0.004	0.199	0.0266	1.348	69.81
vadose zone middle[a]	MW-23 55.5-56.0[h]	13.5	410	0.003	0.184	0.0103	1.386	9.33
vadose zone bottom[a]	MW-23 74.3-74.6[h]	13.3	407	0.016	0.122	0.0003	1.354	2.47

[a] The vadose zone was subdivided into three hydrostratigraphic units based on hydrogeologic properties and the minimum separation distance between the bottom of the tailings cells (Cells 2 and 3 and Cells 4A and 4B) and the water-table surface beneath the tailings cells.

[b] Hydraulic properties predicted using the soil-properties database in HYDRUS assuming an average grain size comprised of 43% sand, 41.5% silt, and 15.5% clay and a dry-bulk density of 1.71 g/cm^3 (TITAN Environmental Corporation, 1996, Appendix D).

[c] Compacted-clay van Genuchten parameters from Tinjum et al. (1997, Table 5, Soil F). Soil-type F selected based on soil classification of borrow-source materials described in the reclamation plan (International Uranium Corporation, 2000). Compacted-clay saturated-hydraulic conductivity (4.7×10^{-7} cm/s) taken from Geosyntec Consultants (2006, Table 1). Residual-water content taken from the HYDRUS soil-properties database for a clay soil texture.

[d] Hydraulic properties predicted using the soil-properties database in HYDRUS assuming an average grain size comprised of 56% sand, 34% silt, and 10% clay (Colorado School of Mines Research Institute, 1978) and tailings bulk-dry density (1.67 g/cm^3) taken from TITAN Environmental Corporation (1996, Appendix D); percent sand measured while percent clay assumed. Saturated hydraulic conductivity taken from MFG, Inc. (2005).

[e] Hydraulic properties predicted using the soil-properties database in HYDRUS assuming a sandy loam soil texture.

[f] Unsaturated hydraulic properties assumed equal to values represented by the compacted clay described above. The saturated hydraulic conductivity was obtained by calibrating nodal fluxes of the geomembrane liner to values determined by Knight-Piesold (1998), as explained in the text.

[g] Hydraulic properties predicted using the soil-properties database in HYDRUS assuming a loam soil texture.

[h] Hydraulic properties of core samples measured by Daniel B. Stephens & Associates (2007). The residual-water content is assumed equal to moisture conditions measured at -851,293 cm. Core-depth intervals measured in feet below land surface.

[i] Hydraulic properties predicted using the soil-properties database in HYDRUS assuming a loamy sand soil texture.

[j] Unsaturated hydraulic properties assumed equal to values represented by the compacted clay described above. The saturated hydraulic conductivity was obtained by calibrating nodal fluxes of the geomembrane liner to values determined using the methodology described in Foose et al. (2001), as explained in the text.

[k] Unsaturated hydraulic properties assumed equal to values represented by the compacted clay described above. The saturated hydraulic conductivity was obtained from the literature (Jo et al., 2005), and reduced one order of magnitude as suggested by Kashir and Yanful (2001).

TABLE 3-2

PHYSICAL AND CHEMICAL PROPERTIES OF THE WHITE MESA MILL
VADOSE ZONE TRANSPORT MODEL

Hydrostratigraphic Unit	Model Layer Description and Purpose	Chloride Dispersivity (cm)	Sulfate Dispersivity (cm)	Uranium Dispersivity (cm)	Dry Bulk Density ρ_b (mg/cm^3)	Volumetric Water Content[c] θ (-)	Sulfate Soil-water Partition Coefficient[d] K_d (mL/mg)	Sulfate Retardation Coefficient R (-)	Uranium Soil-water Partition Coefficient[d] K_d (mL/mg)	Uranium Retardation Coefficient R (-)
vadose zone top[a]	MW-30 35.5-36.0[b]	50	50	0	1980	0.067	2×10^{-6}	1.07	8.47×10^{-3}	251
vadose zone middle[a]	MW-23 55.5-56.0[b]	50	50	0	2030	0.089	3×10^{-6}	1.01	1.04×10^{-2}	239
vadose zone bottom[a]	MW-23 74.3-74.6[b]	50	50	0	2330	0.121	0	1	0	1

[a] The vadose zone was subdivided into three hydrostratigraphic units based on hydrogeologic properties and the minimum groundwater elevation used to represent the perched water table beneath the tailings cells.

[b] Dry-bulk density measured from core samples Daniel B. Stephens & Associates (2007). Core-depth interval measured in ft below ground surface.

[c] Volumetric-water content predicted with HYDRUS-1D for Cells 2 and 3 base-case scenario.

[d] Predicted using the geochemical code PHREEQC (Appendix B). Only adsorption of uranium and sulfate onto hydrous-ferric oxide present in the bedrock was considered.

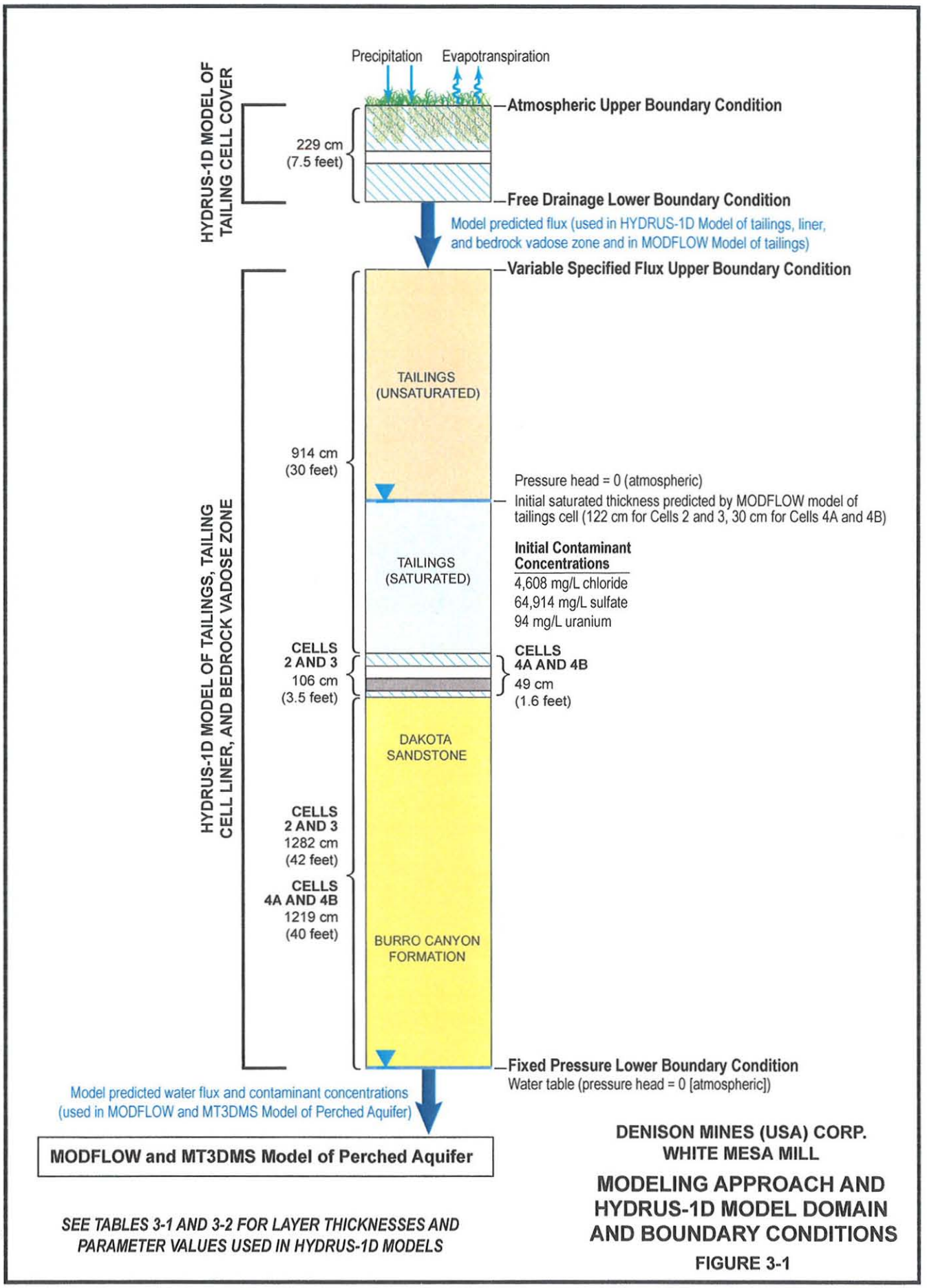

SEE TABLES 3-1 AND 3-2 FOR LAYER THICKNESSES AND PARAMETER VALUES USED IN HYDRUS-1D MODELS

DENISON MINES (USA) CORP.
WHITE MESA MILL

MODELING APPROACH AND HYDRUS-1D MODEL DOMAIN AND BOUNDARY CONDITIONS

FIGURE 3-1

FILE *Fig 3-1 HYDRUS1D Model Domain_1107.ai 11/20/07 SLC*

FILE *Fig 3-2 Dennison tailings Cell Domain_1007.ai 10/16/07 SLC*

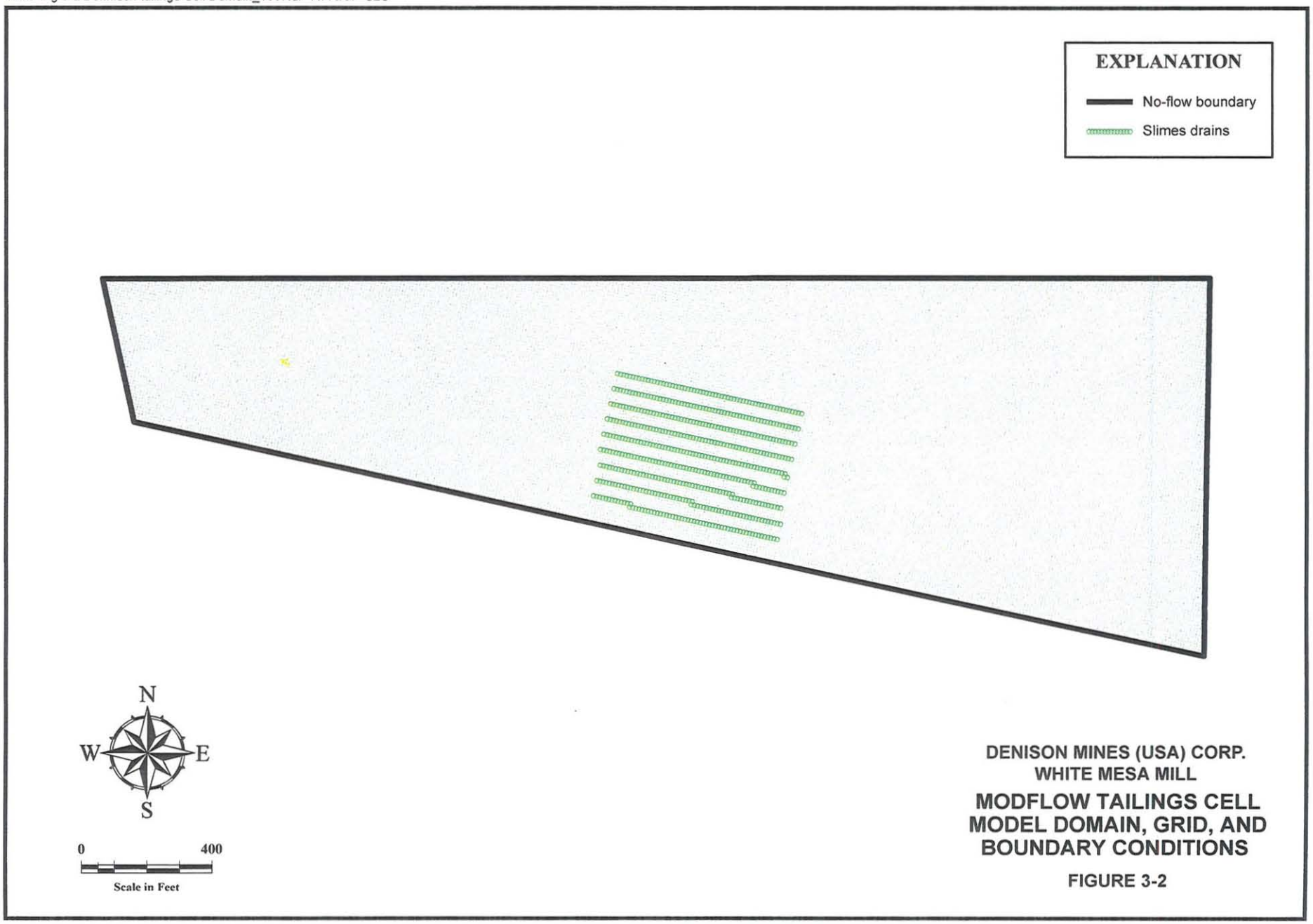

DENISON MINES (USA) CORP.
WHITE MESA MILL

MODFLOW TAILINGS CELL MODEL DOMAIN, GRID, AND BOUNDARY CONDITIONS

FIGURE 3-2

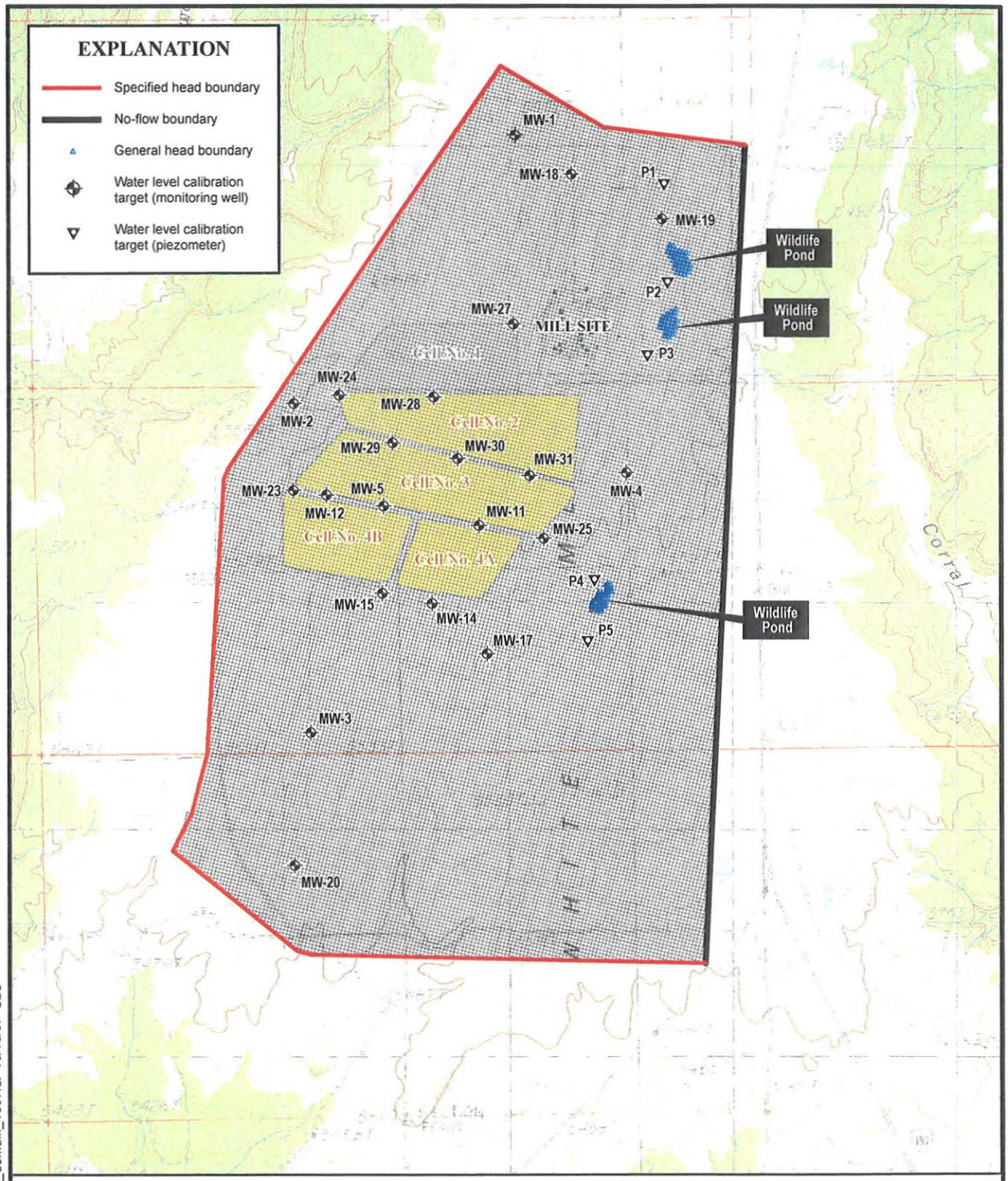

Water level calibration targets are average of 4 water levels measured in 2007 water year

Base map adapted from USGS 7.5 Minute Topographic maps of Black Mesa Butte, Blanding South, No-Mans Island, and Big Bench, Utah Quadrangles.

Coordinates are UTM Zone 12, NAD 1927 meters.

N
W E
S

0 2000

Feet

DENISON MINES (USA) CORP.
WHITE MESA MILL

PERCHED AQUIFER MODEL DOMAIN, GRID AND BOUNDARY CONDITIONS

FIGURE 3-3

FILE Fig 3-3_Denison GWmodel_domain_1007.ai 10/16/07 SLC

4.0 RESULTS

This section presents the results from the vadose zone infiltration and contaminant transport modeling as well as the groundwater flow and contaminant transport modeling. The HYDRUS-1D model was used to predict potential water fluxes through the tailings-cover system (results presented in Section 4.1). The model-predicted flux at the bottom boundary of the cover-system model (potential flux predicted through the cover) was used as input to the MODFLOW model to predict tailings cell dewatering and the HYDRUS-1D model to predict potential flow and transport through the tailings, tailings cell liner system, and bedrock vadose zone to the perched aquifer. The results of the groundwater modeling performed with MODFLOW to predict dewatering of the tailings cells are presented in Section 4.2. Water levels predicted with MODFLOW to remain in the tailings after dewatering were also used as input for the HYDRUS-1D vadose zone flow and contaminant transport model. Results of the vadose zone flow and transport modeling (i.e., model-predicted flow and contaminant transport through the tailings, tailings cell liner system, and underlying bedrock vadose zone to the perched aquifer) are presented in Section 4.3. The potential water flux and contaminant concentrations (combined to get contaminant mass flux rates) predicted at the bottom boundary (perched aquifer water table) of the HYDRUS-1D model were used as input to the perched aquifer groundwater flow and contaminant transport model (MODFLOW and MT3DMS). Results of groundwater flow and contaminant transport modeling of the perched aquifer are presented in Section 4.4. The results of the sensitivity analysis are described in Section 4.5. Key modeling assumptions and model uncertainty are discussed in Section 4.6. For ease of comparison to model files, wherever possible, units of measure used in the models have been retained in the text (i.e., feet and days for MODFLOW, centimeters and days for HYDRUS-1D, and mg/l for both MT3DMS and HYDRUS-1D).

4.1 TAILINGS CELL COVER SYSTEM MODELING

The HYDRUS-1D model was used to predict potential water fluxes through the tailings-cover system assuming atmospheric boundary conditions and a cover design as presented in Figure 3-1. All precipitation was assumed to enter the model domain (infiltrate at least

into layer 1); no runoff was assumed. Water was then removed through evapotranspiration, stored within the cover system, or transported downward through the cover system. The model-predicted flux rate through the cover was used as input to the MODLOW model of the tailings cells and the HYDRUS-1D model of the tailings cells and bedrock vadose zone.

The tailings-cover model was run for 228 years, repeating the 57-year climatic record four times. To reduce the impacts from transient changes in storage and equilibration of initial conditions, water fluxes predicted for the fourth 57-year period were used as input into the other models; however flux rates predicted for the first, second, and third 57-year periods were very similar to the fourth. The model-predicted daily flux rates through the tailings cell cover for one 57-year period are shown on Figure 4-1. The model-predicted water flux rate varies during the 57-year period from a minimum rate of 7.4×10^{-6} cm/day to a maximum rate of 2.0×10^{-3} cm/day, with an average flux rate through the cover system of 1.0×10^{-4} cm/day. The model predicted flux rates through the cover system are in agreement with values reported for similar ET cover systems under similar climatic conditions (Section 2.1.2). The average flux rate was assumed for the recharge rate to the tailings dewatering MODFLOW model. The transient flux rates (daily predictions) were used for input into the HYDRUS-1D model of the tailings, tailings-liner systems, and bedrock vadose zone for Cells 2 and 3 and Cells 4A and 4B.

4.2 TAILINGS CELL DEWATERING MODELING

The tailings cell dewatering simulated with MODFLOW was performed to estimate future dewatering rates and water levels within Cells 2 and 3. The average water level in Cell 2 in 2007 was used for initial conditions. In 2007, the average depth to water measured in Cell 2 was approximately 10 feet, leaving a maximum saturated thickness of approximately 20 feet and an average saturated thickness of approximately 14 feet. Cell 3 was assumed to be fully saturated initially since dewatering operations have yet to begin.

The MODFLOW tailings cell model predicts that as water levels decline in the tailings due to dewatering, pumping rates will decline as well. The average water level (saturated

thickness) in the tailings is predicted to decline to approximately 4 ft after 10 years of pumping for Cell 2 and 14 years for Cell 3 (see Figure 4-2). The model predicts that dewatering rates will decline to approximately 2 gpm after 10 and 14 years of pumping in Cells 2 and 3, respectively. These pumping rates are the maximum sustainable constant pumping rates the system can yield if pumped continuously. While higher short-term pumping rates could be obtained by temporarily discontinuing dewatering operations, allowing water levels to re-equilibrate, and then resuming pumping (i.e., pulsing); the average pumping rate could not exceed the continuous pumping rate. This reduction in pumping rates is caused by the reduction in saturated thickness of tailings. Dewatering rates are also controlled by the saturated hydraulic conductivity of the tailings. If the actual hydraulic conductivity of the tailings is higher than the value assumed in the model, dewatering rates could be higher and water levels could be lowered more rapidly. Conversely, if the actual hydraulic conductivity of the tailings is lower than the value assumed in the model, dewatering rates could be lower and water levels could require more time to dewater.

A dewatering model was not constructed for Cells 4A and 4B because dewatering rates were estimated by Geosyntec Consultants (2007b). Water levels in Cell 4A were estimated to decline to less than 1 foot after 5.5 years of dewatering. Cell 4A is estimated to be dewatered significantly faster than Cells 2 and 3 due to the more extensive slimes drain network. The dewatering system in Cell 4B is assumed to be designed similarly to Cell 4A, thus dewatering rates were assumed to be similar.

4.3 TAILINGS AND VADOSE ZONE FLOW AND TRANSPORT MODELING

The HYDRUS-1D vadose-zone model was used to predict potential flow rates and contaminant transport rates from the tailings, through the tailings cell liner system, and through the bedrock vadose zone to the perched aquifer. The infiltration rate varies through time and is predicted by the HYDRUS-1D model of the tailings cover (infiltration data input to the HYDRUS-1D model of the tailings cell and vadose zone on a daily basis). The average saturated thickness of the tailings was assumed to be 4 ft (122 cm) for Cells 2 and 3 and 1 ft (30 cm) for Cells 4A and 4B at the beginning of these

simulations. Active dewatering was assumed to have been discontinued prior to the start of the vadose zone modeling. Water flux rates will be discussed first followed by contaminant transport.

4.3.1 Saturated Thickness of Tailings and Flux Rates Beneath Tailings Cells

The predicted pressure heads in the tailings (i.e., saturated thickness of tailings) for Cells 2, 3, 4A, and 4B (post-active dewatering) predicted by HYDRUS-1D are shown in Figure 4-3. The water level (i.e., saturated thickness) in the Cells 2 and 3 tailings was predicted to slowly decline through time reaching 39 cm (1.3 ft) at 200 years, primarily as a result of potential flux through defects in the liner. However, this decline is a net decline and is a result of the combined effect of the potential flux out of the cell through the liner and potential input of water from infiltration through the cover. The pressure heads in the tailings of Cells 4A and 4B were predicted to decline through time reaching unsaturated conditions (negative pressures) after 135 years (Figure 4-3).

The model-predicted flux rate through the liner varies as a function of the head (saturated thickness) above the liner. On average, model-predicted flux rates through the liner exceed infiltration rates through the cover. For short periods, potential infiltration rates through the cover are predicted to exceed potential flux rates through the liner, during which times water levels temporarily increase in the tailings (for example, between years 50 and 55 on Figure 4-3). However, the pressure head (saturated thickness of tailings) is not predicted to exceed the initial water level in Cells 2 and 3 (122 cm [4 ft]) or Cells 4A and 4B (30 cm [1 ft]), as shown on Figure 4-3. Thus the model predicts that water will not overtop the maximum liner elevation (pressure head equal to approximately 914 cm [30 ft]), even without active dewatering.

The model-predicted water flux rates through the vadose zone to the perched aquifer for Cells 2 and 3 and Cells 4A and 4B vary through time as shown on Figure 4-4 (time = 0 is assumed when active dewatering is terminated). The flux rate through the bedrock vadose zone for Cells 2 and 3 is predicted to decline rapidly from an initial rate of 9.0×10^{-4} cm/day (see Figure 4-4). After approximately 15 years, when the head in the tailings cells is 109 cm (3.6 ft), the potential flux rate is predicted to be 4.6×10^{-4} cm/day

and then gradually declines to 2.5 x 10^{-4} cm/day at 200 years. For Cells 4A and 4B, the model-predicted flux rate through the bedrock vadose zone is initially 5.2 x 10^{-4} cm/day, but rapidly decreases to 3.0 x 10^{-4} cm/day after seven years, then gradually declines to 1.4 x 10^{-4} cm/day at 200 years.

Once quasi-steady-state conditions have been achieved, the model-predicted flux rate through the liner is generally the same as the model-predicted flux rate to the perched aquifer (with some differences in timing). This is because the flux rate approaches the unsaturated hydraulic conductivity (at steady state) through the bottom of the liner and the water content of the vadose zone adjusts such that the value of unsaturated hydraulic conductivity corresponds to the prescribed flux. As a result, the model results are not sensitive to the unsaturated hydraulic conductivity properties of the vadose zone materials as long as conditions do not approach saturation.

Initially, model-predicted flux rates through the liner exceed the model-predicted steady-state flux through the cover because of the saturated conditions in the tailings cells in addition to potential infiltration through the cover. However, the model-predicted flux rate through the liner and the perched aquifer slowly declines through time as the water levels in the tailings decline. Slight variations caused by variations in fluxes through the tailings cell cover resulted in variations in the decline of the tailings water levels. The saturated tailings attenuated most of the variability associated with infiltration through the cover. If the tailings become unsaturated throughout their entire thickness, then the potential flux through the liner and bedrock vadose zone would be very similar to the rates predicted for flux rates through the tailings cell cover.

4.3.2 Contaminant Concentrations and Mass Flux Rates

Chloride. The model-predicted breakthrough curve for chloride (vadose zone porewater concentration versus time) at the bottom of the vadose zone beneath Cells 2 and 3 is shown on Figure 4-5 and beneath Cells 4A and 4B is shown on Figure 4-6. The breakthrough curve presented represents the model-predicted addition of chloride as a result of flux from the tailings cells. While there is naturally-occurring chloride in the vadose zone initially, the modeling assumed no initial chloride for simplicity, and

because there is a lack of data concerning background chloride and distribution of chloride in the vadose zone. Furthermore, these are the predicted chloride concentrations in vadose zone porewater that will reach the perched aquifer; however these are not the predicted concentrations in groundwater. These vadose zone chloride concentrations for Cells 2 and 3 and Cells 4A and 4B were used as input for mass-loading terms in the perched aquifer model (input to the MODFLOW and MT3DMS model), which was used to predict concentrations in groundwater. Beneath Cells 2 and 3, chloride is predicted to reach the bottom of the bedrock vadose zone at a concentration of 0.001 mg/l at 127 years and at a concentration of 0.1 mg/l at 177 years, as shown on Figure 4-5. Chloride concentrations are predicted to reach the bottom of the vadose zone at a concentration of 0.39 mg/l at 200 years beneath Cells 2 and 3. Beneath Cells 4A and 4B, a chloride concentration of 0.011 mg/l is predicted to reach the bottom of the vadose zone at 200 years, as shown on Figure 4-6.

The mass flux rate is a function of the chloride concentrations predicted to migrate through the vadose zone (Figure 4-5 or 4-6) and the water flux rates predicted through the vadose zone (Figure 4-4). Based on these assumptions, the model-predicted maximum chloride mass flux rate is approximately 9.8×10^{-8} mg/cm^2 per day at 200 years for Cells 2 and 3. The model-predicted chloride mass flux rate at the bottom of the vadose zone beneath Cells 4A and 4B is predicted to be approximately 1.6×10^{-9} mg/cm^2 per day at 200 years.

Sulfate. The model-predicted breakthrough curve for sulfate (vadose zone porewater concentration versus time) at the bottom of the vadose zone beneath Cells 2 and 3 is shown on Figure 4-7. Sulfate beneath Cells 4A and 4B is not shown because it is predicted to be at concentrations of less than 1.0×10^{-3} mg/l at 200 years. The breakthrough curve presented represents the model-predicted addition of sulfate as a result of the potential flux from the tailings cells. While there is naturally-occurring sulfate in the vadose zone initially, the modeling assumed no initial sulfate for simplicity. These vadose zone sulfate concentrations for Cells 2 and 3 and Cells 4A and 4B were used as input for mass-loading terms in the perched aquifer model (input to the MODFLOW and MT3DMS model), which was used to predict sulfate concentrations in

groundwater. Beneath Cells 2 and 3, sulfate is predicted to reach the bottom of the bedrock vadose zone at a concentration of 0.001 mg/l at 152 years, and at a concentration of 0.09 mg/l at 200 years, as shown on Figure 4-7. Sulfate concentrations are predicted to reach the bottom of the vadose zone at a concentration of 3.2×10^{-4} mg/l at 200 years beneath Cells 4A and 4B.

The model-predicted mass flux rate is a function of the sulfate concentrations predicted to migrate through the vadose zone (Figure 4-7) and the water flux rates predicted through the vadose zone (Figure 4-4). Based on these assumptions, the model-predicted maximum sulfate mass flux rate is approximately 2.3×10^{-8} mg/cm^2 per day at 200 years for Cells 2 and 3. The model-predicted sulfate mass flux rate at the bottom of the vadose zone beneath Cells 4A and 4B is predicted to be approximately 4.3×10^{-11} mg/cm^2 per day at 200 years.

Uranium. The model-predicted distribution of uranium in the vadose zone beneath the tailings cell liner at 200 years is shown on Figure 4-8. Due to the strong sorption and the resulting high-retardation coefficients, uranium is not predicted to migrate much beyond 20 cm (8 inches) below the liner system in 200 years beneath Cells 2 and 3 and Cells 4A and 4B. At 30 cm (1 ft) below the liner at 200 years, dissolved-phase uranium concentrations are predicted to be 3.0×10^{-4} mg/l beneath cells 2 and 3 and 2.0×10^{-8} mg/l beneath Cells 4A and 4B. No uranium is predicted to reach the perched aquifer within 200 years. While there is some naturally-occurring uranium in the vadose zone initially, the modeling assumed no initial uranium for simplicity, and because there is a lack of data concerning background uranium and distribution of uranium in the vadose zone. Uranium concentrations presented on Figure 4-8 represent the predicted uranium concentration in vadose zone porewater above background levels. The predicted distribution of uranium beneath the liner assumes the tailings cells are the only source of uranium. Dissolved uranium concentrations were assumed to remain at a concentration of 94 mg/l in the tailings.

4.3.3 Sorption, Retardation, and Potential Migration of Other Contaminants

Sorption coefficients and retardation factors were calculated for contaminants of potential concern to assess their potential transport through the bedrock vadose zone. To calculate sorption coefficients for potential contaminants of concern, two geochemical processes were assumed to control solute-transport mobility in the vadose zone: adsorption of solutes onto HFO and precipitation of minerals. However, other sorption processes may occur, further slowing potential contaminant migration. The calculated K_d values and retardation factors are considered conservative since only one iron-oxyhydroxide phase was considered to participate in surface-complexation reactions (e.g., adsorption of metals onto goethite, montmorillonite, and quartz were not included in the model) and coprecipitation of metals onto the surfaces of precipitating phases (e.g., hydrous-ferric oxide, sulfates, carbonates) was ignored. Details regarding the methodology to predict sorption coefficients and geochemical-modeling results are included in Appendix B.

The distribution coefficients and retardation factors for the potential contaminants of concern are presented in Table 4-1. Solutes predicted to have high K_d values resulting in high retardation factors and low mobility include arsenic, beryllium, chromium, copper, lead, uranium, vanadium, and zinc. Similarly to uranium, these contaminants are not predicted to migrate through the vadose zone to the perched water table in 200 years, given their high retardation factors. Solutes predicted to have intermediate K_d values include cadmium, cobalt, manganese, molybdenum, and nickel. These contaminants also are not predicted to migrate through the vadose zone to the perched water table in 200 years. Solutes predicted to have low K_d values include selenium and sulfate; while iron, fluoride, mercury, silver and thallium were predicted to migrate unretarded, like chloride. This assumes that there is no sorption or any other loss mechanisms such as degradation, precipitation, or other transformations. Based on K_d values reported in Sheppard and Thibault (1990), U.S. EPA (1996), and U.S. EPA (1999), sorption and retardation of cadmium, cobalt, iron, manganese, mercury, nickel, selenium, silver, and thallium are likely to be significantly larger than model-predicted values presented in Table 4-1. As a result only chloride, sulfate, and fluoride are predicted to migrate with

little or no sorption. Potential concentrations of these contaminants are predicted in groundwater and described in Section 4.4.2.

Sorption generally is greatest in the middle vadose zone unit, which contains sufficient buffering minerals capable of neutralizing the low-pH fluids present in the tailings (see Table 4-1). Neutralization of infiltrating tailings porewaters was calculated for each individual bedrock unit, and not with an iterative (pseudo-reactive transport) approach, which also was considered a conservative approach. Specifically, if a more sophisticated approach were used in which water chemistry changes were modeled along with contaminant transport through the vadose zone, then larger retardation factors would result, particularly for the deepest bedrock unit.

4.4 GROUNDWATER MODELING RESULTS

The MODFLOW and MT3DMS perched-aquifer model was used to predict groundwater flow and potential contaminant transport in the perched aquifer. The groundwater flow model results will be discussed first followed by contaminant transport.

4.4.1 Groundwater Flow Model Calibration

Both qualitative and quantitative methods used to evaluate the calibration of the groundwater-flow model indicated that the model adequately represents the actual groundwater-flow conditions in the perched aquifer for the calibration period. The model-simulated piezometric surface contours for the perched aquifer are depicted in Figure 4-9 (compare to Figure 2-5 depicting contours from measured water levels). In general, model-predicted flow directions and water levels reasonably represent observed conditions.

For the groundwater-flow model of the perched aquifer, the mean error, absolute mean error, and root mean squared errors (RMSE) were calculated by comparing simulated water levels to observed water levels for 26 water level targets (water levels in monitoring wells and piezometers) distributed throughout the domain. The mean error was 0.4 ft, indicating that on average the model simulated actual water levels reasonably

well (e.g., the model did not systematically over predict or under predict water levels across the site). The mean absolute error was 4.3 ft and the RSME was 5.1 ft. Given the average total head drop was 185 ft across the perched aquifer model domain, the normalized RSME was 2.8 %, indicating an acceptable calibration (generally anything less than 10 % is considered acceptable [Rumbaugh and Rumbaugh, 2001]).

Volumetric Flow Budget. Water fluxes into the groundwater-flow model include areal recharge from precipitation, fluxes from wildlife ponds, potential fluxes from the tailings cells, and water entering through upgradient specified-head boundaries (groundwater flow from upgradient of model domain). Water leaves the groundwater-flow model through specified-head boundaries, which includes simulation of groundwater flow to the aquifer beyond the model domain and discharge to seeps and springs where the perched aquifer outcrops (e.g., Ruin Spring). The overall mass balance error for the flow model was 0.1 % (2 ft^3/day with a total flow of 2,244 ft^3/day). Areal recharge from precipitation accounted for 26 % of water entering the model, while fluxes from the wildlife ponds and potential fluxes from the tailings cells (Cells 2, 3, 4A and 4B) accounted for 67 % and 6 %, respectively, of the flow entering the model. Specified-head boundaries represented less than 2 % of flow entering the model, but 100 % of the flow leaving the model.

4.4.2 Contaminant Concentrations and Distribution in Groundwater

The groundwater contaminant transport model was used to predict chloride and sulfate transport and concentrations in the perched aquifer resulting from potential fluxes from the tailings cells. As with the vadose zone model, this model was run for a 200-year period and chloride and sulfate concentrations predicted are additional concentrations above background levels. Background levels were set at zero in the model so as not to obscure the impacts to groundwater chloride and sulfate concentrations caused by assumed fluxes from the tailings cells with the spatial and temporal variability of background concentrations.

The Permit stipulates that concentrations of contaminants in groundwater monitoring wells shall not exceed specified GWCLs. Downgradient monitoring wells with GWCLs specified in the Permit include MW-5, MW-11, and MW-12, located on the berm

immediately south (downgradient) of Cell 3, and MW-14 and MW-15, located on the berm immediately south (downgradient) of Cell 4A. The maximum model-predicted chloride and sulfate concentrations in groundwater at monitoring wells MW-5, MW-11, MW-12, MW-14, and MW-15 at 200 years are presented in Table 4-2. GWCLs for chloride and sulfate in these wells were proposed in the *Revised Background Groundwater Quality Report* (INTERA, 2007) and also are presented in Table 4-2. Due to the low mass flux rates predicted to reach the aquifer, chloride and sulfate concentration increases at these wells due to the tailings cells are insignificant, and fall far below laboratory detection limits. At 200 years, the modeled fluxes from the tailings cells are predicted to increase chloride by less than 0.03 % of the proposed GWCLs in all monitoring wells. The modeled fluxes from the tailings cells are predicted to increase sulfate by less than 0.0002 % of the proposed GWCLs.

Most of the other potential contaminants of concern are retarded relative to chloride and sulfate, and as a result, are not predicted to reach the perched water table aquifer at 200 years. Given the magnitude of impacts predicted to groundwater for chloride and sulfate (minimal), the impacts caused by the other mobile contaminant (fluoride) was estimated. Using dilution/attenuation of chloride from tailings fluids to groundwater as a proxy, the concentration of fluoride was estimated. The average chloride and fluoride concentrations in the tailings fluids were 4,608 and 1,694 mg/l, respectively (Utah Division of Radiation Control, 2004). Because the monitoring well predicted to be impacted the most by potential releases from the tailings cells is monitoring well MW-12, the fluoride concentration was estimated for this location. Assuming a dilution factor of 768,000 (chloride concentration in tailings [4,608 mg/l] divided by chloride concentration predicted in groundwater at monitoring well MW-12 from assumed tailings fluxes at 200 years [0.006 mg/l]), a fluoride concentration of 0.002 mg/l was estimated for MW-12. The proposed GWCL for fluoride in MW-12 is 2 mg/l. As a result, the predicted concentrations of fluoride as well as other contaminants of concern are not predicted to exceed proposed GWCLs at 200 years.

4.5 SENSITIVITY ANALYSIS

Vadose Zone Flow and Transport Model. A sensitivity analysis was performed to evaluate the impacts that uncertainty in parameter values have on model results. The input parameters selected as part of the sensitivity analysis included the precipitation record, saturated hydraulic conductivity of the liner, and vadose-zone dispersivity. To compare the model output for the sensitivity-analysis, the chloride concentration at the bottom of the vadose-zone model at 200 years (for each simulation) was compared to the base-case scenario. In addition, the change in chloride concentration from the base-case scenario was also computed. Only chloride in Cells 2 and 3 was simulated in the sensitivity analysis. The base-case scenario was represented by the measured precipitation record, a saturated hydraulic conductivity of the liner equal to 7.3×10^{-5} cm/day (which was obtained during calibration), and a presumed dispersivity of 50 cm. The results of the sensitivity analysis are tabulated in Table 4-3.

As compared to the base-case scenario, the saturated hydraulic conductivity of the liner appeared to more significantly affect chloride transport through the vadose zone than the other parameters that were varied (see Table 4-3). Increasing the liner conductivity by a factor of 2.4, which was equivalent to increasing the assumed number of liner defects by a factor of 2.4, resulted in a chloride concentration of 16.5 mg/l predicted to be migrating through the vadose zone at 200 years, which is approximately 40 times greater than the base case value (see Table 4-3). Increasing the dispersivity by a factor of 2.5 resulted in a chloride concentration of 7.5 mg/l at 200 years, which is approximately 19 times greater than the base case value (see Table 4-3). However, if anything, the base case dispersivity is overestimated. Inserting the three wettest years (1909, 1906, and 1957) into the precipitation time-series record back-to-back in place of 1946-1948 data (see Section 3.2.11 for a detailed description) resulted in a chloride concentration of 3.1 mg/l at 200 years, which is a factor of eight increase in the chloride concentration relative to the base case.

As a worst-case scenario, assuming a wet precipitation record, increased dispersivity, and increased liner conductivity, a chloride concentration of 252 mg/l was predicted to reach

the base of the vadose zone beneath Cells 2 and 3 at 200 years. A similar run was performed for Cells 4A and 4B and resulted in a chloride concentration of 65 mg/l predicted to reach the base of the vadose zone at 200 years.

The worst-case scenario as identified with chloride transport (i.e., high precipitation, increased liner hydraulic conductivity, and increased dispersivity) was run for sulfate transport. A sulfate concentration of 1,257 mg/l was predicted to reach the base of the vadose zone beneath Cells 2 and 3 at 200 years. A similar run was performed for Cells 4A and 4B and resulted in a sulfate concentration of 218 mg/l predicted to reach the base of the vadose zone at 200 years.

The worst-case scenario as identified with chloride transport (i.e., high precipitation, increased liner hydraulic conductivity, and increased dispersivity) was also run for uranium transport. Uranium concentrations in vadose zone porewater were predicted to reach 3.0×10^{-4} mg/l above background concentrations at a depth of 32 cm (1 ft) beneath the liner of Cells 2 and 3 at 200 years, compared to 30 cm for the base case. For Cells 4A and 4B, under these worst-case conditions, uranium at a concentration of 1.5×10^{-4} mg/l was predicted to migrate 31 cm beneath the liner at 200 years. Given the magnitude of the retardation factors, uranium transport is predicted to remain minimal (i.e., on the order of a few feet into the Dakota Sandstone) despite large changes in advective velocities.

The unsaturated hydraulic conductivity of the vadose zone was not evaluated because the moisture content in the vadose zone varies until the unsaturated hydraulic conductivity essentially becomes equal to the flux rate (at steady state), so vadose zone model results are typically relatively insensitive to changes in the unsaturated hydraulic conductivity, except at high water contents, when the unsaturated hydraulic conductivity approaches the saturated hydraulic conductivity.

Groundwater Flow and Transport Model. A full sensitivity analysis of the groundwater model was not performed, but the results of what was considered to be the worst-case scenario identified through the sensitivity analysis for the vadose zone model were input to the groundwater flow and transport model to evaluate the impact to

groundwater quality for this "worst case." The "worst-case" for the vadose zone model included using wet precipitation record, which included insertion of the three maximum precipitation years back-to-back (see Section 3.2.11 for details), increased dispersivity, and increased liner fluxes. Under these worst-case conditions, chloride was predicted to reach a pore-water concentration of 252 mg/l beneath Cells 2 and 3 and 65 mg/l beneath Cells 4A and 4B at the bottom of the vadose zone at 200 years. Sulfate was predicted to reach a pore-water concentration of 1,257 mg/l beneath Cells 2 and 3 and 218 mg/l beneath Cells 4A and 4B at the bottom of the vadose zone at 200 years. Under these worst-case conditions the average water fluxes were predicted to be 7.5×10^{-4} and 5.0×10^{-4} cm/day beneath Cells 2 and 3 and Cells 4A and 4B, respectively. Using this as input to the groundwater model, the maximum chloride and sulfate concentrations (above background) under worst-case conditions were predicted to occur at monitoring well MW-12 at concentrations of 11 and 48 mg/l, respectively. The proposed GWCLs for chloride and sulfate at monitoring well MW-12 are 80.5 and 2,560 mg/l, respectively.

4.6 UNCERTAINTY AND ASSUMPTIONS

The numerical modeling presented in this report was based on fundamental physical assumptions concerning the mechanisms controlling flow and solute transport in the vadose zone and perched aquifer. However, as with all numerical models, the model only replicates the actual physical system to the extent that it is based on an accurate conceptual model that describes the site hydrogeology, boundary conditions, and initial conditions. The goal of the conceptual model is to describe these conditions (e.g., stratigraphy, hydraulic properties, transport mechanisms, and boundary conditions) with a sufficient level of detail to address the objectives of the study. Because the subsurface environment is heterogeneous, the conceptual and numerical models need to make simplifying assumptions so that the physical characteristics of the system can be quantified and incorporated into the numerical model. One of the most basic assumptions for a subsurface fate and transport model is that the subsurface stratigraphy and hydraulic properties are adequately characterized.

The hydraulic properties of the tailings were assumed in the MODFLOW model constructed to predict tailings cell dewatering rates. If the actual hydraulic conductivity of the tailings is higher than the value assumed in the model, dewatering rates could be higher and water levels could be lowered more rapidly. Conversely, if the actual hydraulic conductivity of the tailings is lower than the value assumed in the model, dewatering rates could be lower and water levels could require more time to dewater. Furthermore, the hydraulic conductivity of the tailings could vary spatially which could impact dewatering rates.

Some of the simplifications include assuming the vadose zone is one thickness beneath Cells 2 and 3 and Cells 4A and 4B. In the model, the vadose zone (distance between the liner beneath the cells and the perched aquifer water table) was assumed to be 42 ft for Cells 2 and 3 and 40 ft for Cells 4A and 4B. This vadose-zone thickness is the minimum depth to the water table (measured in nearby monitoring wells), which only occurs in one small area. The depth from the bottom of the cells to the perched aquifer water table is up to 90 ft in some areas. This assumption is conservative as it results in shorter travel times for contamination to reach the water table. Actual travel times are likely to be much greater than predicted, particularly for transport beneath the western half of Cells 2 and 3 where the vadose zone is much greater than 42 ft thick.

There is considerable evidence that the cells are not leaking. However, flux rates through the tailings cell liner system were calculated using standard equations and assumptions to account for potential defects in the flexible-membrane liners. With these estimated flux rates, hydraulic conductivity values for the liner used in HYDRUS-1D to simulate leaks had to be estimated. The resulting hydraulic conductivity values for the PVC and HDPE liners are average values for the entire tailings cell area to account for potential manufacturing defects, punctures, and tears in the liners.

Leakage from the unlined wildlife ponds have resulted in significant impacts to the perched water table surface (see Figure 2-5), which is not evident beneath the tailings cells. Given that these tailings cells have contained tailings at nearly fully-saturated

conditions for close to 25 years, if leakage were significant it is likely that evidence would have appeared at this point.

Hydraulic properties of the vadose zone were based on a limited data set (six cores from two boreholes). However, as previously discussed, if conditions are unsaturated (and not close to saturation) as they likely are in the bedrock vadose zone at White Mesa, the unsaturated hydraulic conductivity essentially becomes the same as the flux rate (at steady state) and the water content of the vadose zone adjusts such that the value of unsaturated hydraulic conductivity corresponds to the prescribed flux. As a result, the model results are not sensitive to the unsaturated hydraulic conductivity properties of the vadose zone materials as long as conditions do not approach saturation. Hydraulic properties of the tailings cover materials were estimated based on grain-size distribution.

The bedrock vadose zone was assumed to not be fractured in the modeling. Under unsaturated conditions, fractures will tend to act as barriers to flow similar to a capillary break, particularly if they are open. Under saturated conditions, fractures can act as preferential pathways to flow. Groundwater-recharge studies at a site which has a similar climate (although slightly hotter and drier) and geology as compared to White Mesa indicates that recharge to the aquifer through the vadose zone is via matric flow through primary porosity rather than through fractures (Heilweil et al., 2006).

The vadose-zone model of the cover assumed that all precipitation infiltrated at least into the top layer of the model (i.e., no precipitation was assumed to runoff). This is considered to be slightly conservative, but given how flat the cover is (0.2 % slope), it is a realistic assumption.

The vadose-zone model assumed no lateral flow, only vertical flow. This ignores the impacts that horizontal heterogeneities may have on migration in the vadose zone. Because there is so little information concerning vadose-zone heterogeneities, a two- or three-dimensional model could not be constructed with a large degree of certainty. However, given that hydraulic gradients in the vadose zone are strongly vertical, flow is primarily vertical, and thus a one-dimensional model is adequate for vadose zone flow and transport.

Vadose zone modeling of the tailings, liner system, and underlying bedrock vadose zone was assumed to begin when active dewatering (i.e., pumping the slimes drains) was assumed to be discontinued. Thus the HYDRUS modeling only included drainage of the tailings through assumed leaks in the liner rather than active pumping. The duration of active pumping (estimated to be 14 years or less) was minimal relative to the overall period of the simulations, and was assumed to be completed before the 200 year period began.

The HYDRUS-1D vadose zone flow model cannot be calibrated because there are no moisture content or pressure head data available for the vadose zone. Quantifying moisture fluxes through desert vadose zones is very difficult due to the small magnitude of fluxes and the very long response times (Walvoord et al., 2002). Furthermore, the transport component cannot be calibrated because there are no contaminant data available for the vadose zone.

The vadose zone modeling assumes a uniform density fluid. Density affects the hydraulic gradient and hydraulic conductivity values. However, the impacts that density has on these is minimal relative to the impacts that moisture contents have on unsaturated hydraulic conductivity. As a result, the impact of ignoring density effects in the vadose zone is likely minimal.

The vadose zone modeling does not account for vapor transport. Under natural conditions, water transport in thick desert vadose zones is dominated by upward vapor transport over very long time periods (Walvoord et al., 2002). Modeling performed by Walvoord et al. (2002) indicates that most thick desert vadose zones are in a slow drying process that is on the order of tens of thousands of years. Upward vapor transport would act to slow downward contaminant migration.

Another key assumption is that future climatic conditions will be similar to past climatic conditions within the historical record. It is unclear what impacts global warming may have on the climate and how these changes will impact tailings cell cover performance. However, speculating on the possible impacts of global warming to climatic conditions is beyond the scope of this report.

TABLE 4-1

DISTRIBUTION (Kd) COEFFICIENTS AND RETARDATION FACTORS (R)
FOR SELECTED CONTAMINANTS PRESENT IN THE TAILINGS PORE FLUIDS WHITE MESA MILL VADOSE ZONE [a,b]

Vadose Zone Hydrostratigraphic Unit	Arsenic K_d (l/kg)	Beryllium K_d (l/kg)	Cadmium K_d (l/kg)	Chromium K_d (l/kg)	Cobalt K_d (l/kg)	Copper K_d (l/kg)	Fluoride[c] K_d (l/kg)	Iron[c] K_d (l/kg)	Lead K_d (l/kg)	Manganese[c] K_d (l/kg)	Mercury K_d (l/kg)	Molybdenum K_d (l/kg)	Nickel K_d (l/kg)	Selenium K_d (l/kg)	Silver K_d (l/kg)	Sulfate[c] K_d (l/kg)	Thallium K_d (l/kg)	Uranium K_d (l/kg)	Vanadium K_d (l/kg)	Zinc K_d (l/kg)
top	7.19	82.1	0.001	0.557	0.000	4.13	0.000	0.000	9.48	0.001	0.000	0.014	0.005	0.015	0.000	0.002	0.000	8.47	0.000	0.009
middle	7094	72140	1.033	4.90	0.115	1220	0.0003	0.000	2197	0.901	0.000	0.663	1.380	0.015	0.000	0.003	0.000	10.4	559	11.3
bottom	0.119	0.000	0.000	0.000	0.000	0.000	0.000	0.000	0.000	0.000	0.000	0.000	0.000	0.001	0.000	0.000	0.000	0.000	0.000	0.000

	R (--)	R (--)	R (--)	R (--)	R (--)	R (--)	R (--)	R (--)	R (--)	R (--)	R (--)	R (--)	R (--)	R (--)	R (--)	R (--)	R (--)	R (--)	R (--)	R (--)
top	213	2428	1.02	17	1.00	123	1.00	1.00	281	1.02	1.00	1.41	1.14	1.46	1.00	1.07	1.00	251	1.00	1.26
middle	161804	1645434	25	113	3.63	27822	1.01	1.00	50105	22	1.00	16	32	1.34	1.00	1.07	1.00	239	12744	260
bottom	3.30	1.00	1.00	1.00	1.00	1.00	1.00	1.00	1.00	1.00	1.00	1.00	1.00	1.01	1.00	1.00	1.00	1.00	1.00	1.00

[a] Methodology and assumptions used to determine sorption coefficients are described in Appendix B.

[b] Average volumetric-water content of the underlying vadose zone units were predicted with the HYDRUS-1D base-case scenario for Cells 2 and 3.

[c] Sorption coefficients for fluoride, manganese, and sulfate were corrected to account for precipitation of fluorite, pyrolusite, and gypsum/barite, respectively.

Note: Based on K_d values reported in Sheppard and Thibault (1990), U.S. EPA (1996), and U.S. EPA (1999), sorption and retardation of cadmium, cobalt, iron, manganese, mercury, nickel, selenium, silver, and thallium are likely to be significantly larger than model-predicted values.

TABLE 4-2

MODEL-PREDICTED CHLORIDE AND SULFATE CONCENTRATIONS
IN GROUNDWATER

Monitoring Well	Model-Predicted Chloride Concentration (mg/l)	Chloride GWCLs (mg/l)	Model-Predicted Sulfate Concentration (mg/l)	Sulfate GWCLs (mg/l)
MW-5	0.005	17.0	0.002	1,518
MW-11	0.003	39.2	0.001	1,309
MW-12	0.006	80.5	0.003	2,560
MW-14	1.30E-05	27.0	0	2,330
MW-15	1.30E-05	57.1	0	2,549

TABLE 4-3

MODEL-PREDICTED CHLORIDE CONCENTRATIONS
AT THE BOTTOM OF THE VADOSE ZONE FOR CELLS 2 AND 3 EVALUATED AS PART OF THE SENSITIVITY ANALYSIS

Model Run[a]	Input Parameter Varied			Response Variable Evaluated	Response Variable Statistic
	Precipitation[b]	Dispersivity[c]	K_{sat} geomembrane	Chloride Concentration at the Bottom of the Vadose Zone at 200 yr (mg/L)	Change in Chloride Concentration at the Bottom of the Vadose Zone at 200 yr (mg/L)
1	Minimum	0 cm	LOW	0	-0.4
2	Minimum	50 cm	LOW	0	-0.4
3	Minimum	125 cm	LOW	0.1	-0.3
4	Minimum	0 cm	BC	0	-0.4
5	Minimum	50 cm	BC	0.4	0.0
6	Minimum	125 cm	BC	7.4	7.0
7	Minimum	0 cm	HIGH	0.1	-0.3
8	Minimum	50 cm	HIGH	16.2	15.8
9	Minimum	125 cm	HIGH	85.2	84.8
10	Average	0 cm	LOW	0	-0.4
11	Average	50 cm	LOW	0	-0.4
12	Average	125 cm	LOW	0.1	-0.3
13	Average	0 cm	BC	0	-0.4
14	**Average**	**50 cm**	**BC**	**0.4**	**0.0**
15	Average	125 cm	BC	7.5	7.1
16	Average	0 cm	HIGH	0.1	-0.3
17	Average	50 cm	HIGH	16.5	16.1
18	Average	125 cm	HIGH	86.0	85.6
19	Maximum	0 cm	LOW	0	-0.4
20	Maximum	50 cm	LOW	0	-0.4
21	Maximum	125 cm	LOW	0.7	0.3
22	Maximum	0 cm	BC	0	-0.4
23	Maximum	50 cm	BC	3.1	2.7
24	Maximum	125 cm	BC	33.3	32.9
25	Maximum	0 cm	HIGH	1.8	1.4
26	Maximum	50 cm	HIGH	77.3	76.9
27	Maximum	125 cm	HIGH	251.8	251.4

[a] Model run 14 was selected as the base-case scenario.

[b] The maximum-precipitation record was obtained by inserting the three wettest years into the average precipitation time-series record, whereas the minimum-precipitation recorded was obtained by inserting the three driest years into the average precipitation time-series record.

[c] A dispersivity of zero indicates only diffusive transport of chloride is considered.

File: Fig 4-1 Water Flux Rate_1107.ai 11/20/07 SLC

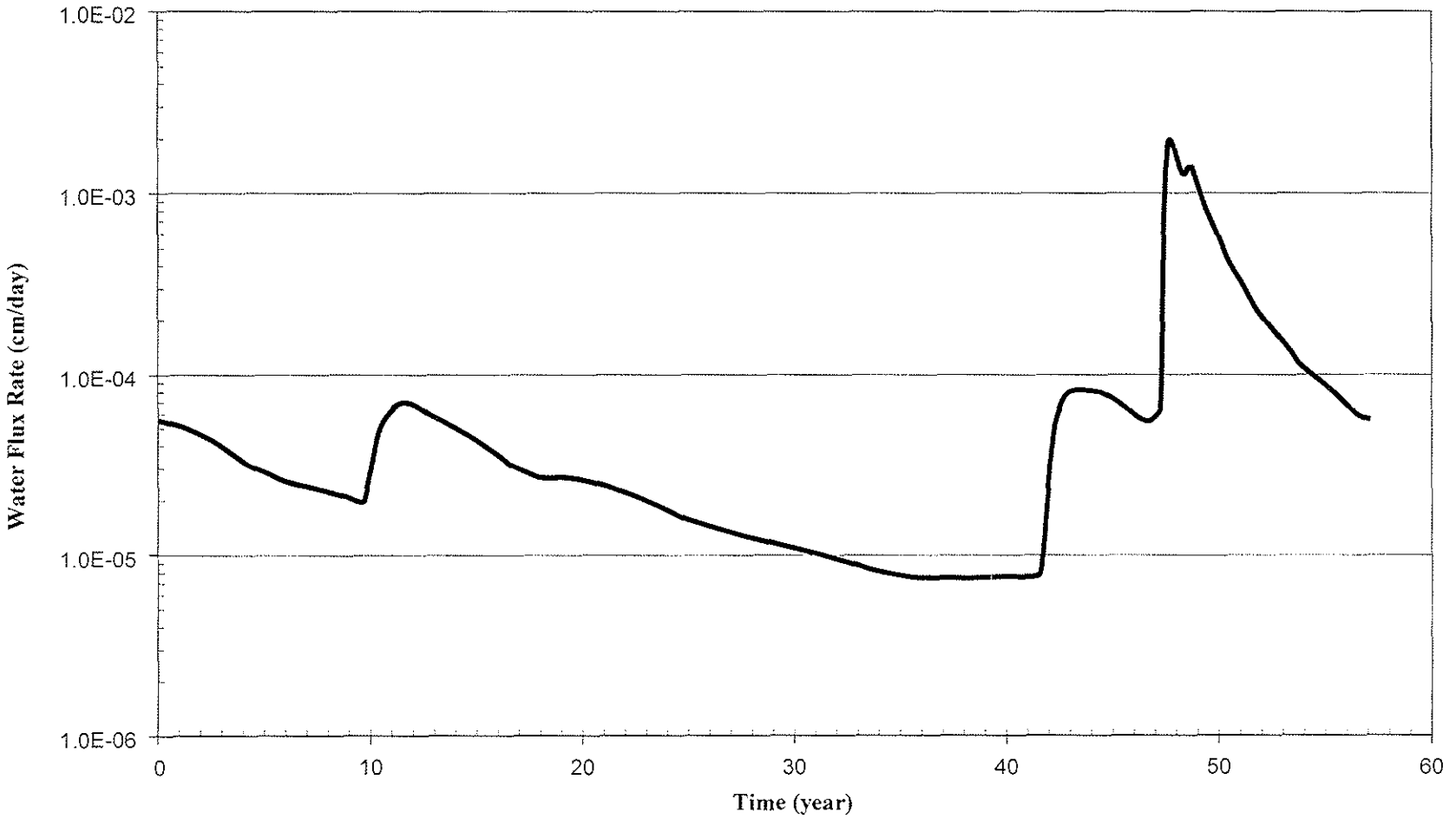

DENISON MINES (USA) CORP.
WHITE MESA MILL

MODEL-PREDICTED WATER FLUX RATE THROUGH TAILINGS CELL COVER (TYPICAL 57-YEAR PERIOD)

FIGURE 4-1

File: Fig 4-2 Saturated Thickness Pumping Rates_1107.ai 11/20/2007 SLC

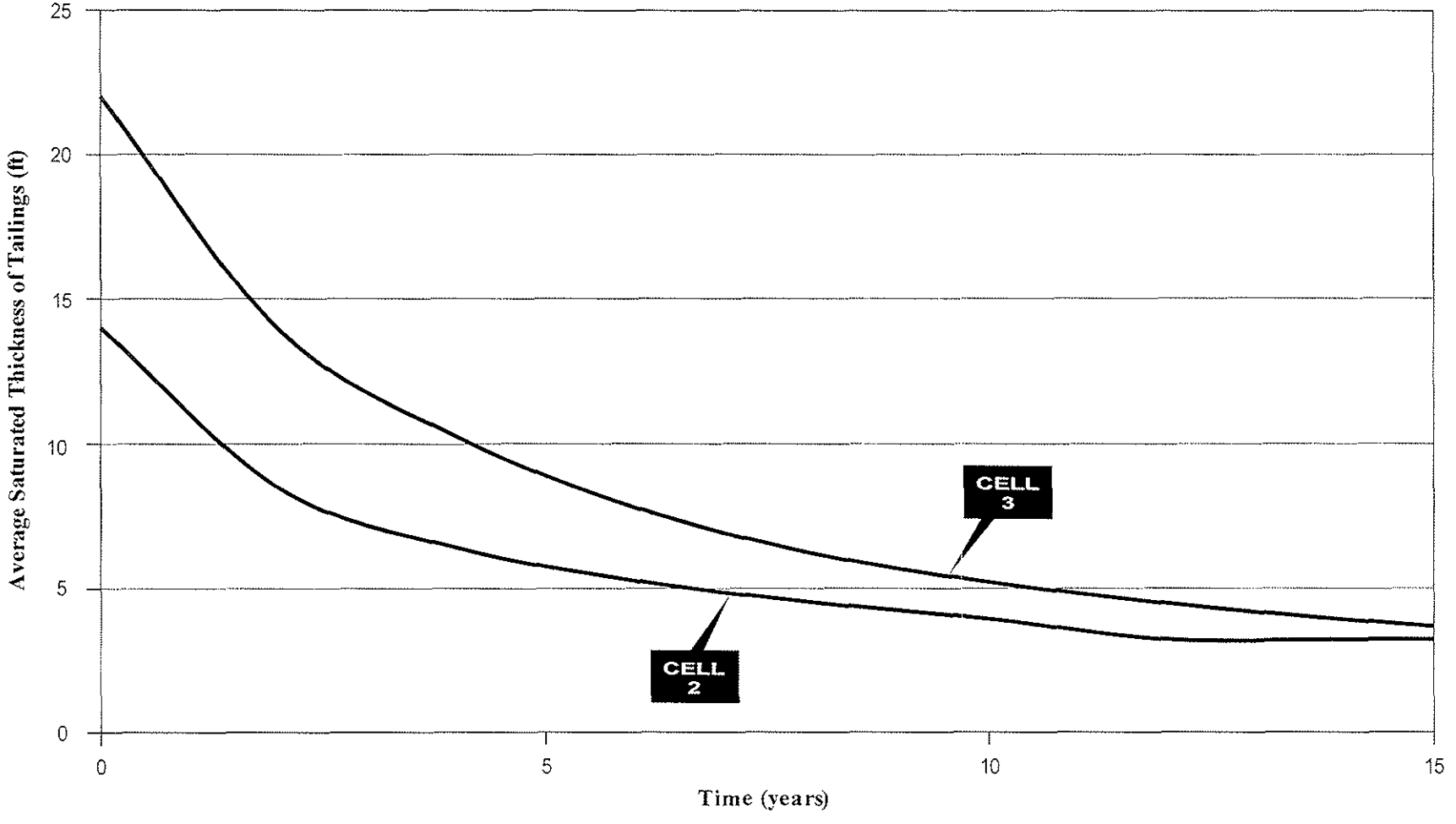

DENISON MINES (USA) CORP.
WHITE MESA MILL

MODFLOW MODEL-PREDICTED SATURATED THICKNESS OF TAILINGS IN CELLS 2 AND 3 ASSUMING CONTINUOUS DEWATERING PUMPING

FIGURE 4-2

File: Fig 4-3 Saturated thickness above liner_1107.ai 11/20/2007 SLC

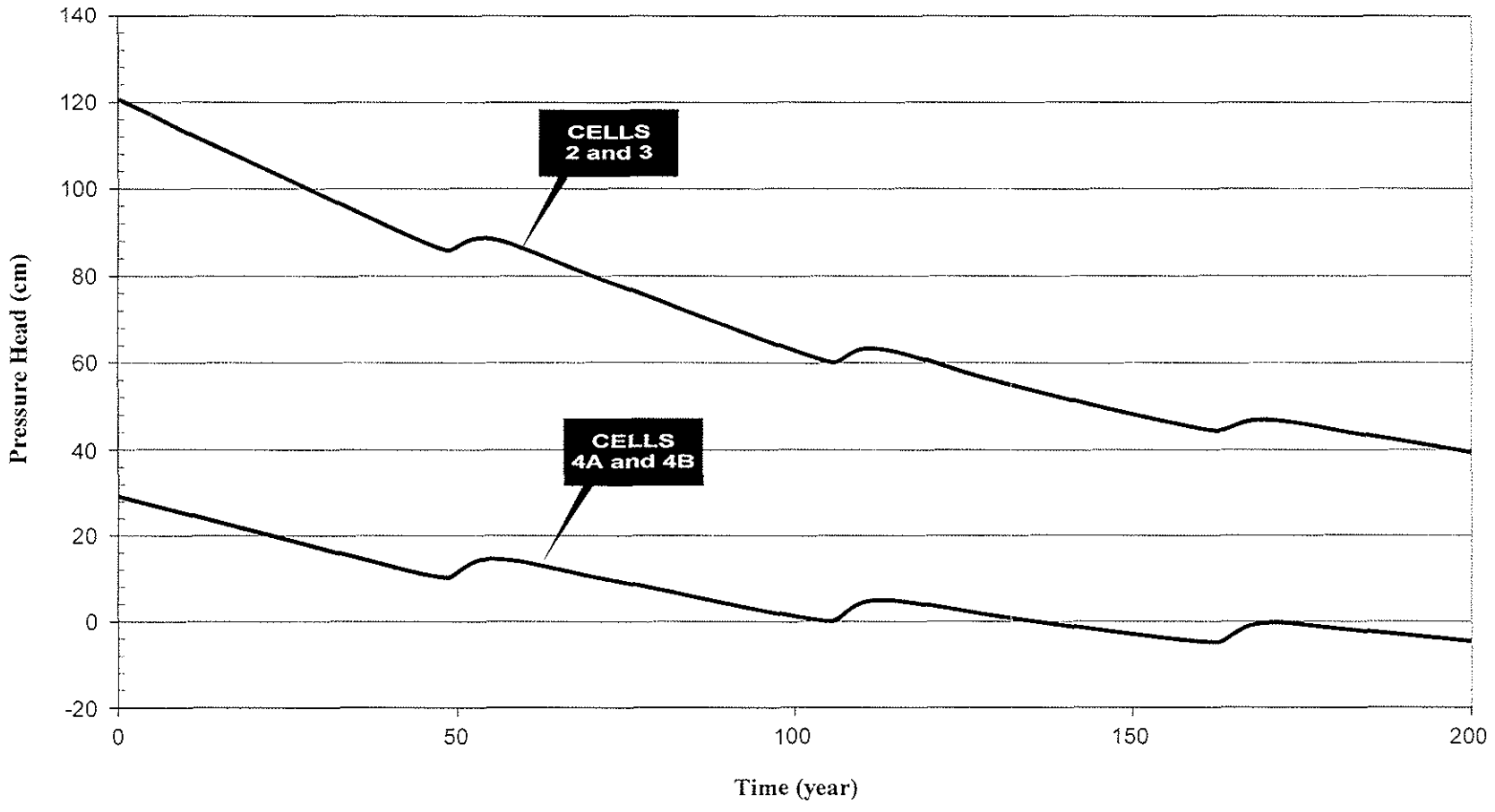

DENISON MINES (USA) CORP.
WHITE MESA MILL

MODEL-PREDICTED SATURATED THICKNESS (PRESSURE HEAD) OF TAILINGS ABOVE THE LINER (POST-DEWATERING)

FIGURE 4-3

File: Fig 4-4 Water Flux to Perched Aquifer_1107.ai 11/20/2007 SLC

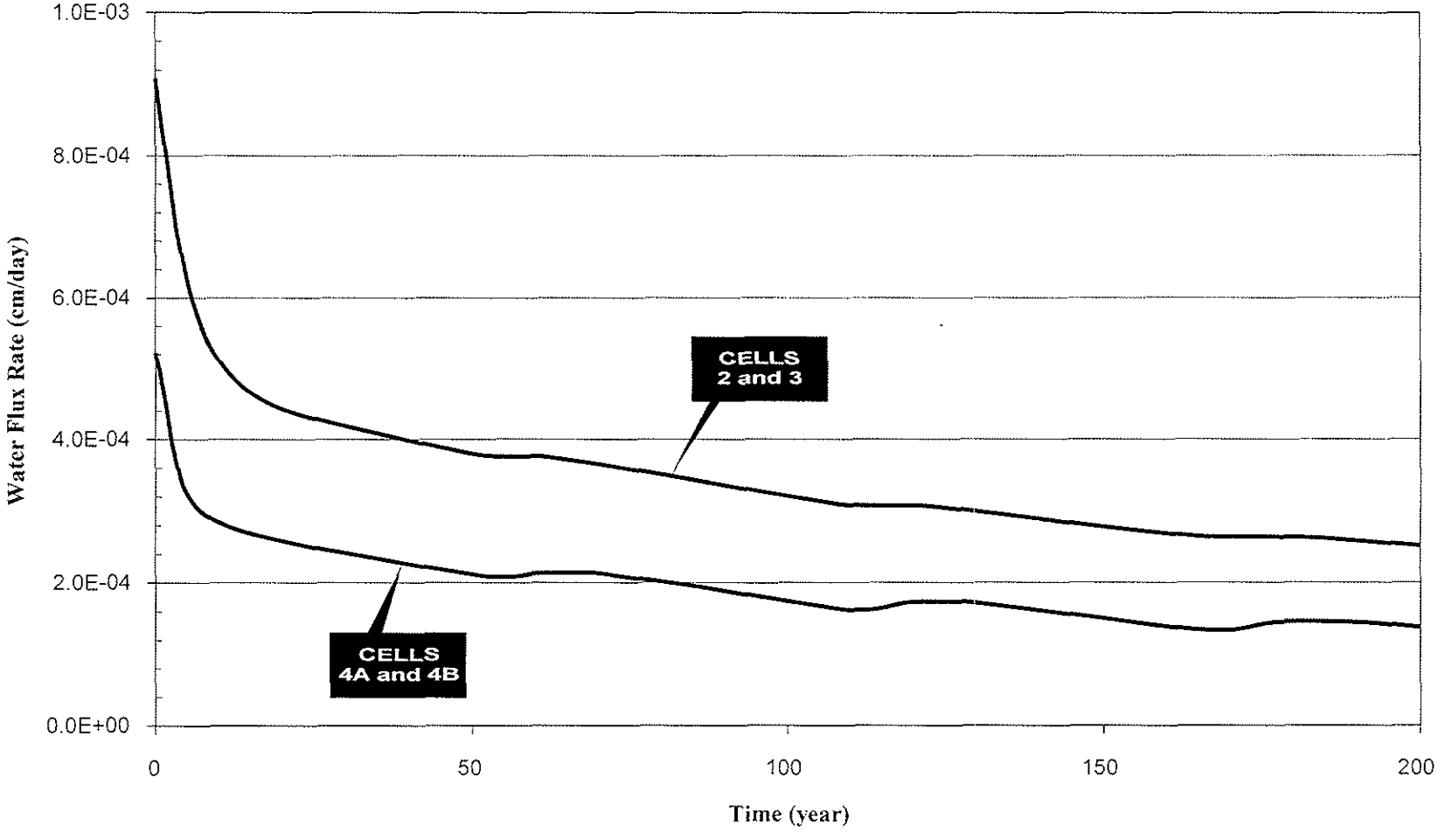

DENISON MINES (USA) CORP.
WHITE MESA MILL

MODEL-PREDICTED WATER FLUX RATES THROUGH THE VADOSE ZONE BENEATH THE TAILINGS CELLS

FIGURE 4-4

File: Fig 4-5 Chloride concentrations_1107.ai 11/20/2007 SLC

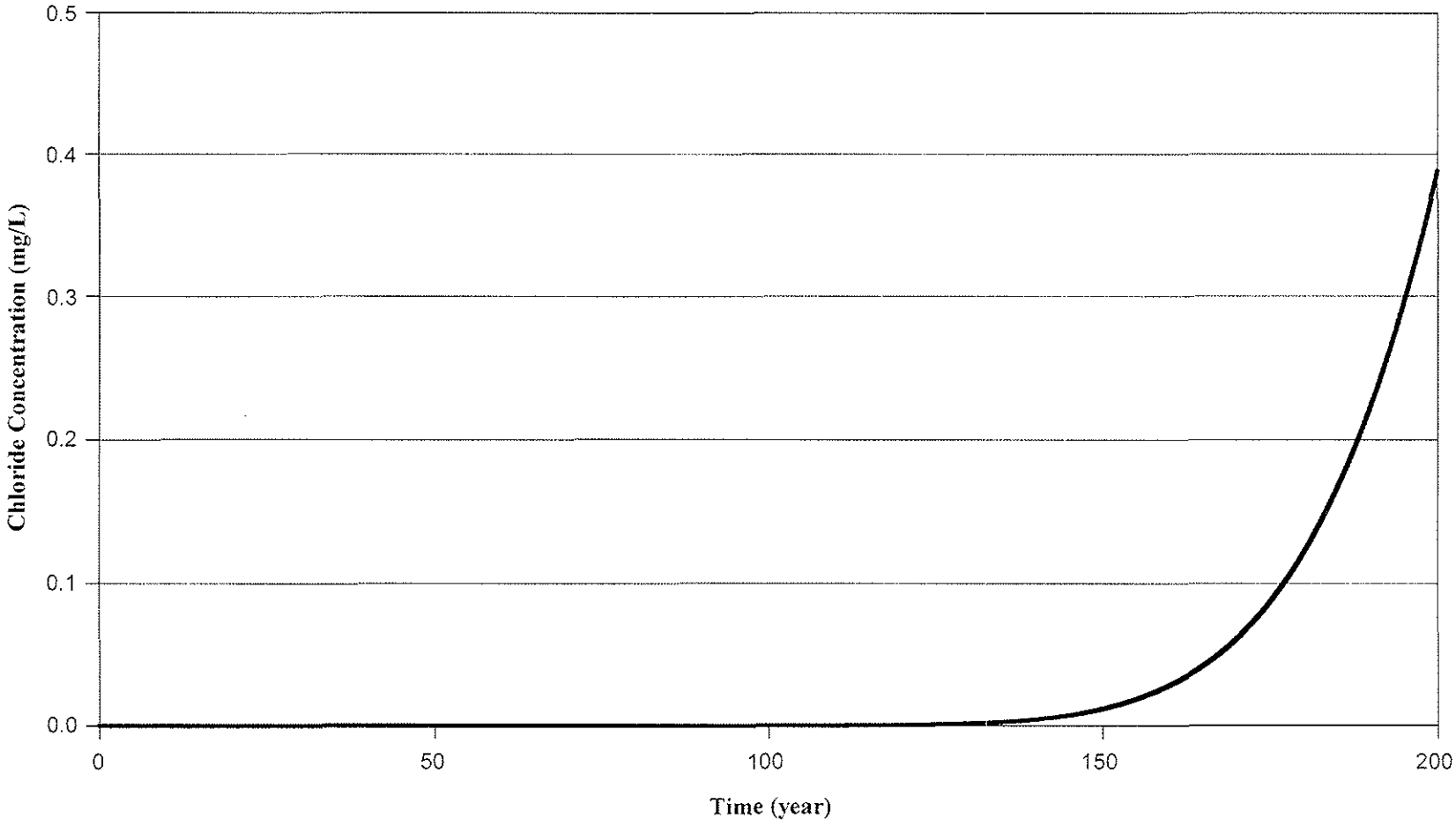

DENISON MINES (USA) CORP.
WHITE MESA MILL

MODEL-PREDICTED CHLORIDE CONCENTRATIONS
IN VADOSE ZONE PORE WATER
IMMEDIATELY ABOVE THE PERCHED AQUIFER
BENEATH CELLS 2 AND 3

FIGURE 4-5

File: Fig 4-6 Chloride concentrations_Cells4A_4B_1107.ai 11/20/2007 SLC

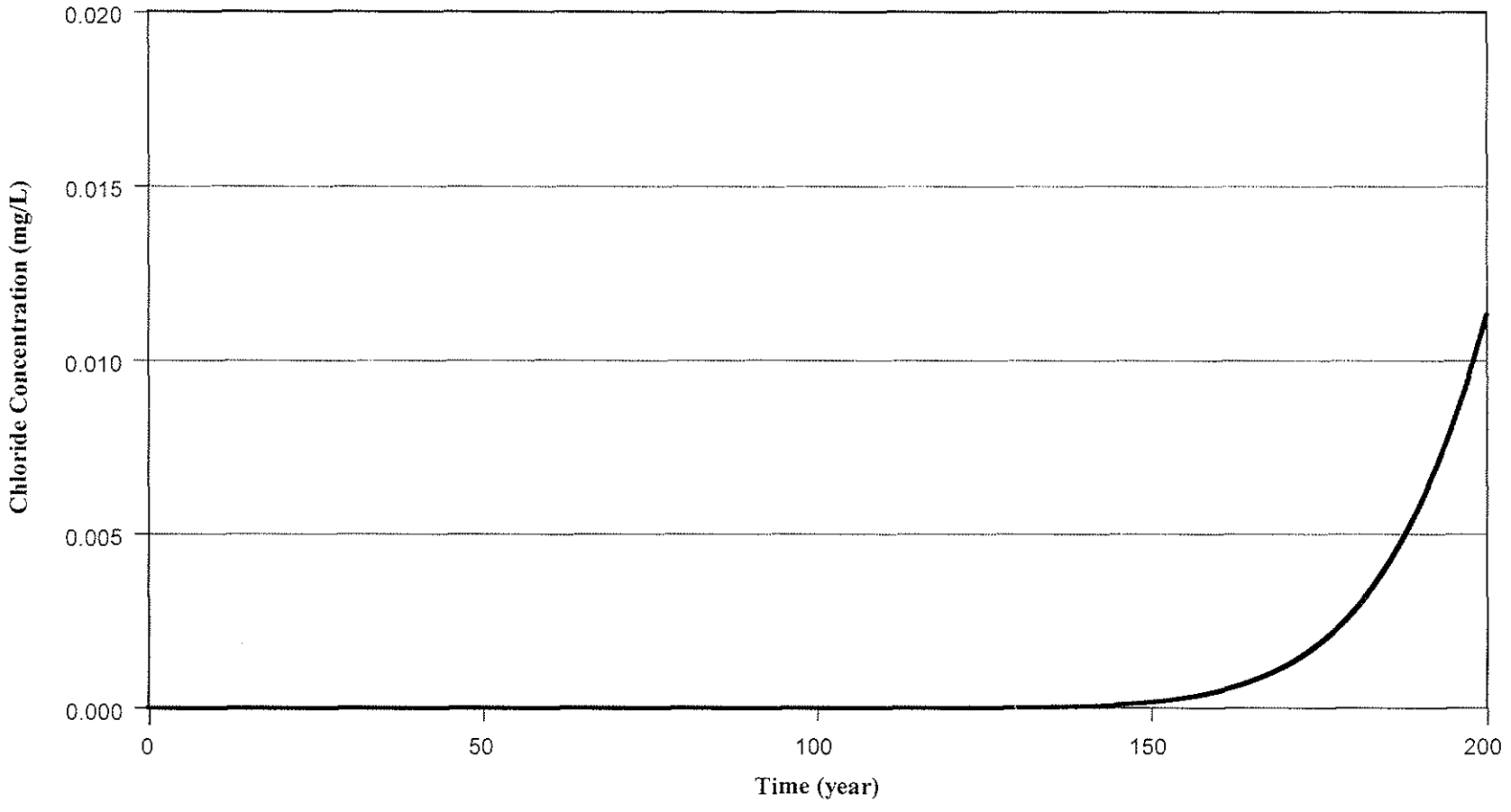

DENISON MINES (USA) CORP.
WHITE MESA MILL

MODEL-PREDICTED CHLORIDE CONCENTRATIONS
IN VADOSE ZONE PORE WATER
IMMEDIATELY ABOVE THE PERCHED AQUIFER
BENEATH CELLS 4A AND 4B

FIGURE 4-6

File: Fig 4-7 Sulfate concentrations_1107.ai 11/20/2007 SLC

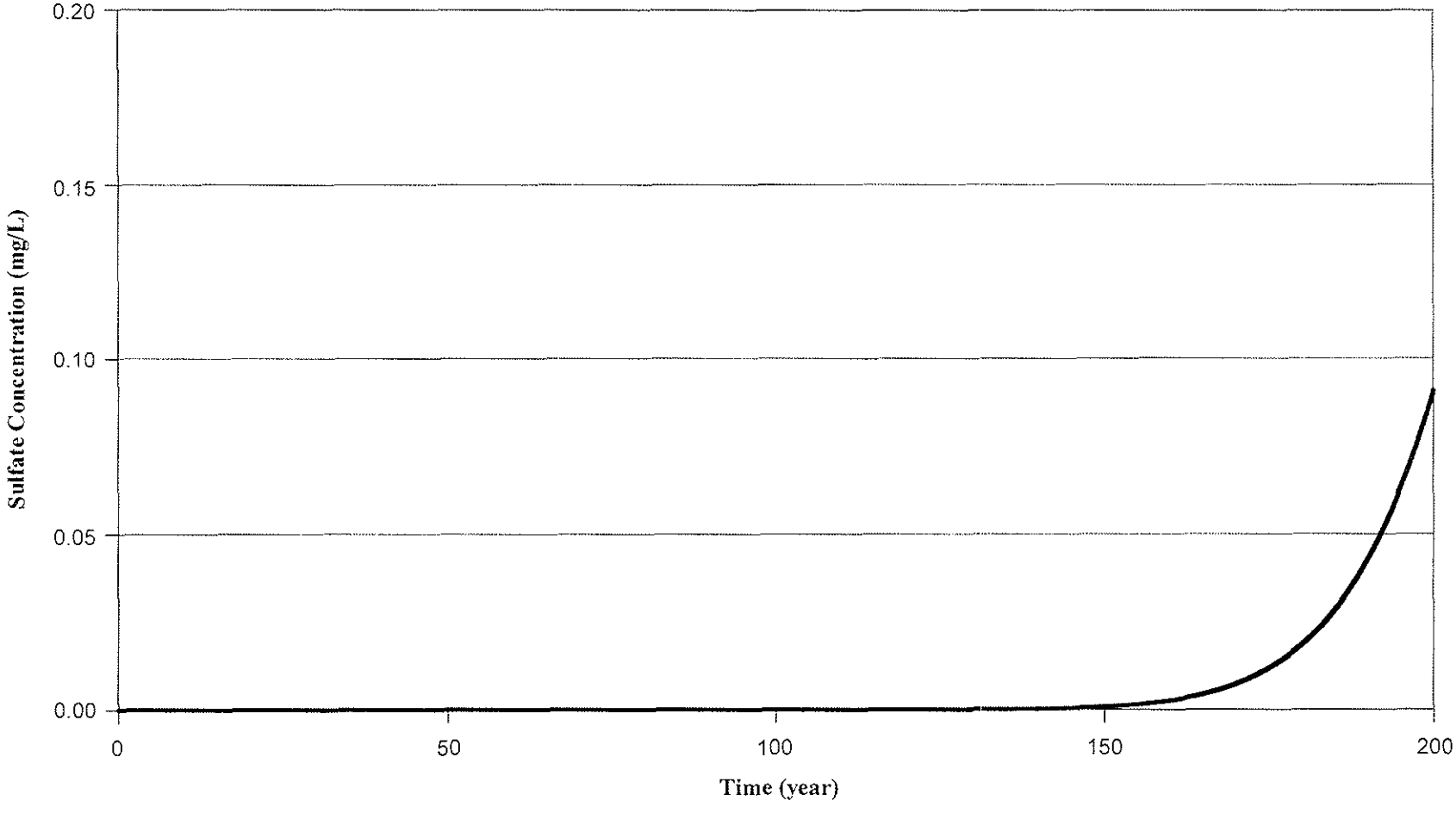

DENISON MINES (USA) CORP.
WHITE MESA MILL

MODEL-PREDICTED SULFATE CONCENTRATIONS
IN VADOSE ZONE PORE WATER
IMMEDIATELY ABOVE THE PERCHED AQUIFER
BENEATH CELLS 2 AND 3

FIGURE 4-7

File: Fig 4-8 Dissolved Uranium in Vadose_200yr_1107.ai 11/20/2007 SLC

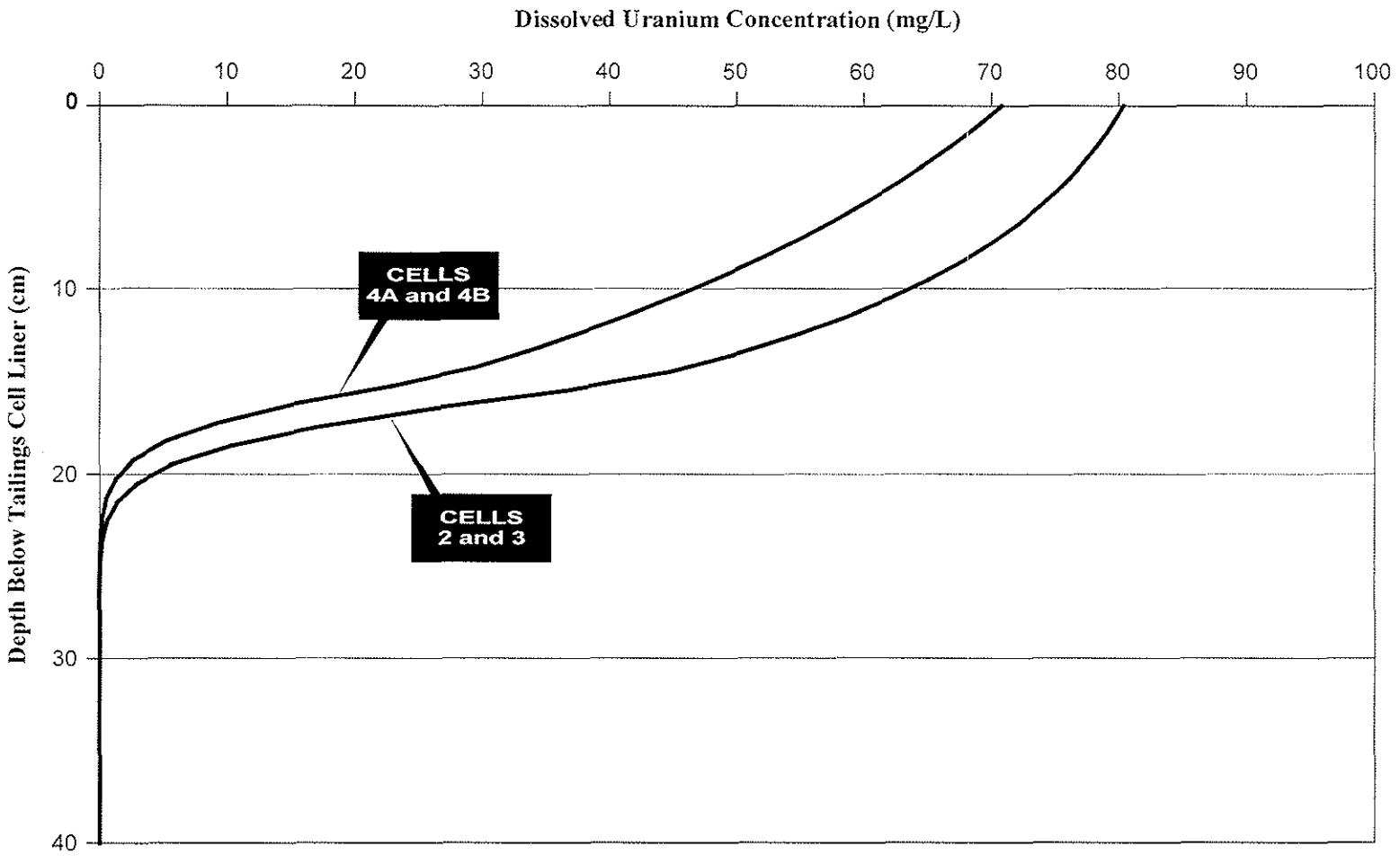

DENISON MINES (USA) CORP.
WHITE MESA MILL

MODEL-PREDICTED DISSOLVED URANIUM CONCENTRATIONS IN VADOSE ZONE PORE WATER AT 200 YEARS

FIGURE 4-8

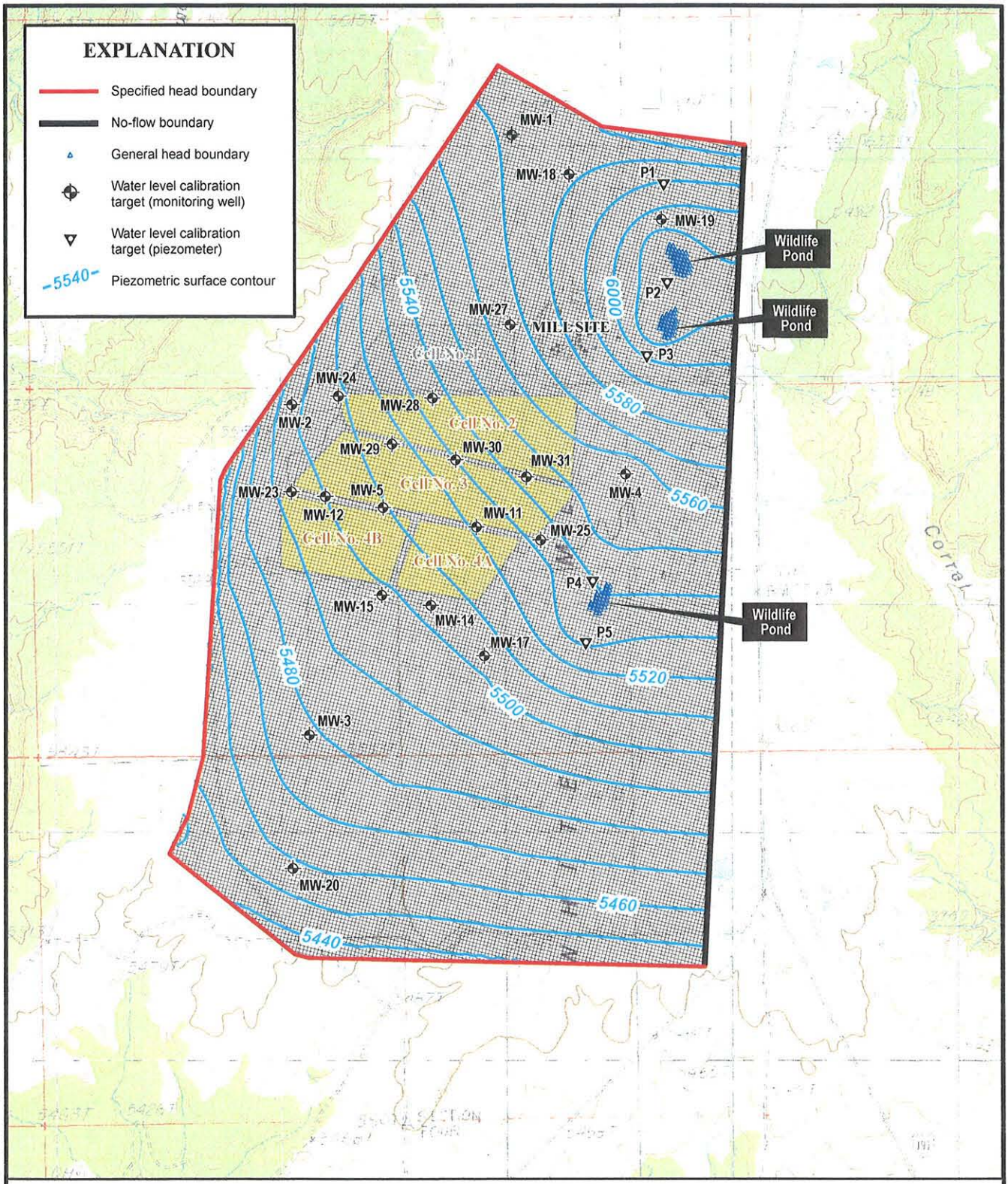

Water level calibration targets are average of 4 water levels measured in 2007 water year

Base map adapted from USGS 7.5 Minute Topographic maps of Black Mesa Butte, Blanding South, No-Mans Island, and Big Bench, Utah Quadrangles.

Coordinates are UTM Zone 12, NAD 1927 meters.

N
W E
S

0 2000
Feet

DENISON MINES (USA) CORP.
WHITE MESA MILL

MODFLOW MODEL-PREDICTED PIEZOMETRIC SURFACE CONTOURS PERCHED AQUIFER

FIGURE 4-9

FILE Fig 4-9 ModPredPiez_1107.ai 11/20/07 SLC

5.0 CONCLUSIONS AND POST-AUDIT MONITORING PLAN

This section summarizes the results of infiltration and contaminant transport modeling to support Denison's Groundwater Discharge Permit for the White Mesa uranium milling and tailings disposal facility and provides recommendations for a post-audit monitoring plan.

5.1 CONCLUSIONS

Modeling of the tailings cell cover with HYDRUS-1D indicated that with slight design modifications to the multilayered cover as presented in the *Tailings Cover Design* (TITAN Environmental Corporation, 1996) and the *Reclamation Plan, Revision 3.0* (International Uranium (USA) Corporation, 2000), infiltration can be reduced significantly (average long-term infiltration rates were reduced from 1.0×10^{-2} cm/day for the original cover design to 1.0×10^{-4} cm/day for the modified cover design, a reduction of two orders-of-magnitude). With a vegetated ET cover, the HYDRUS-1D model predicts that the potential flux rate through the cover could range between 7.4×10^{-6} cm/day and 2.0×10^{-3} cm/day, with an average flux rate through the cover system of 1.0×10^{-4} cm/day. Cover design modifications can include replacing the cobble layer with 6 inches of topsoil with gravel and vegetation, as well as increasing the frost barrier/water storage layer from 2 to 3 ft. As specified in Part I.H.11 of the Permit, the Permittee may include supplemental information to justify modification of certain Permit requirements, including tailings cell cover system engineering design and construction specifications. Upon Executive Secretary approval of the final infiltration and contaminant transport report, the Reclamation Plan may be modified to accommodate necessary changes to protect public health and the environment.

Modeling of the tailings dewatering system with MODFLOW suggests that it is not practical to fully dewater the tailings in Cells 2 and 3. Modeling predicted that dewatering rates would decline to approximately 2 gpm after 10 and 14 additional years of pumping from Cells 2 and 3, respectively, leaving 4 ft of saturated tailings on average. The reduction in pumping rates is caused by the reduction in saturated thickness of

tailings. Cells 4A and 4B have a more extensive slimes drain network and were assumed to be dewatered after approximately five years.

Modeling of potential flow from the tailings through the liner and underlying bedrock vadose zone was performed with HYDRUS-1D. The model-predicted flux rate through the liner varies as a function of the head (saturated thickness) above the liner. On average, model-predicted flux rates through the liner exceed infiltration rates through the cover. For short periods, potential infiltration rates through the cover are predicted to exceed potential flux rates through the liner, during which times water levels temporarily increase in the tailings. However, the pressure head (saturated thickness of tailings) is not predicted to exceed the initial water level in Cells 2 and 3 (122 cm [4 ft]) or Cells 4A and 4B (30 cm [1 ft]), as shown on Figure 4-3. Thus the model predicts that water will not overtop the maximum liner elevation (pressure head equal to approximately 914 cm [30 ft]), even without active dewatering.

Modeling of potential flow from the tailings through the liner and underlying bedrock vadose zone was performed with HYDRUS-1D. Model-predicted flux rates through the bedrock vadose zone beneath Cells 2 and 3 decline rapidly from an initial rate of 9.0×10^{-4} cm/day, then gradually decline to 2.5×10^{-4} cm/day at 200 years. For Cells 4A and 4B, the model-predicted flux rates through the bedrock vadose zone decline rapidly from an initial rate of 5.2×10^{-4} cm/day, then gradually decline to a steady-state rate of 1.4×10^{-4} cm/day by approximately 175 years after the tailings are predicted to have become unsaturated. We have assumed potential defects in the liner and have made other assumptions that may overestimate any potential fluxes from the tailings cells. In reality, the actual flux rates may be lower than model-predicted values or there may be no flux at all.

Modeling of potential chloride and sulfate transport from the tailings through the tailings cell liner and bedrock vadose zone was also performed with HYDRUS-1D. Beneath Cells 2 and 3, chloride and sulfate concentrations in pore water at the bottom of the bedrock vadose zone are predicted to increase to concentrations of 0.39 and 0.09 mg/l, respectively, at 200 years. Beneath Cells 4A and 4B, chloride and sulfate concentrations

in porewater at the bottom of the vadose zone are predicted to increase to concentrations of 0.011 and 3.2 x 10^{-4} mg/l, respectively, at 200 years. Chloride was assumed to migrate unretarded (i.e., no sorption) through the vadose zone. Sulfate was assumed to have a maximum retardation factor of 1.07, such that it is considered highly mobile, but it is slightly retarded relative to chloride. These are the model-predicted chloride and sulfate concentrations in vadose zone porewater that will reach the perched aquifer; however these are not the predicted concentrations in groundwater.

Modeling of chloride and sulfate transport in the perched aquifer was performed with MODFLOW and MT3DMS. The Permit stipulates that concentrations of contaminants in groundwater monitoring wells shall not exceed specified GWCLs. Downgradient monitoring wells with GWCLs specified in the Permit include MW-5, MW-11, and MW-12, located on the berm immediately south (downgradient) of Cell 3, and MW-14 and MW-15, located on the berm immediately south (downgradient) of Cell 4A. Due to the low mass flux rates predicted to reach the aquifer, model-predicted chloride and sulfate concentration increases at these wells due to the tailings cells are insignificant, and fall far below laboratory detection limits. At 200 years, the modeled fluxes from the tailings cells are predicted to increase chloride by less than 0.03 % of the proposed GWCLs in all monitoring wells. The modeled fluxes from the tailings cells are predicted to increase sulfate by less than 0.0002 % of the proposed GWCLs.

Retardation rates for uranium were calculated based on equilibrium soil-water partition coefficients (K_d) using the mass of HFO present in the bedrock and the equilibrated solution compositions predicted with the geochemical code PHREEQC. Neutralization of the infiltrating tailings porewaters and sorption of solutes was determined with PHREEQC. The mass of HFO and calcite were determined for samples collected from the vadose zone for core samples from the Dakota Sandstone and Burro Canyon Formation. Through this method, a sorption value for the Dakota Sandstone immediately beneath the tailings cells was estimated to be 8.47 kg/L. Assuming a volumetric moisture content of 7%, a retardation factor of 251 was calculated.

Modeling of potential uranium transport from the tailings through the tailings cell liner and into the vadose zone was performed with HYDRUS-1D. Due to the strong sorption and the resulting high-retardation coefficients, uranium is not predicted to migrate much beyond 20 cm (8 inches) below the liner system in 200 years beneath Cells 2 and 3 and Cells 4A and 4B. At 30 cm (1 ft) below the liner at 200 years, dissolved-phase uranium concentrations are predicted to be 3.0×10^{-4} mg/l beneath Cells 2 and 3 and 2.0×10^{-8} mg/l beneath Cells 4A and 4B. No uranium is predicted to reach the perched aquifer within 200 years. While there is some naturally-occurring uranium in the vadose zone initially, the modeling assumed no initial uranium for simplicity, and because there is a lack of data concerning background uranium and distribution of uranium in the vadose zone. Dissolved uranium concentrations were assumed to remain at a concentration of 94 mg/l in the tailings. Because uranium was predicted to migrate such a short distance in the bedrock vadose zone, there appears to be no threat to groundwater posed by uranium.

Sorption coefficients and retardation factors were calculated for contaminants of potential concern to assess their potential transport through the bedrock vadose zone. Solutes predicted to have high K_d values resulting in high retardation factors and low mobility include arsenic, beryllium, chromium, copper, lead, uranium, vanadium, and zinc. Similarly to uranium, these contaminants are not predicted to migrate through the vadose zone to the perched water table in 200 years, given their high retardation factors. Solutes predicted to have intermediate K_d values include cadmium, cobalt, manganese, molybdenum, and nickel. These contaminants also are not predicted to migrate through the vadose zone to the perched water table in 200 years. Solutes predicted to have low K_d values include selenium and sulfate; while iron, fluoride, mercury, silver and thallium were predicted to migrate unretarded, like chloride. This assumes that there is no sorption or any other loss mechanisms such as degradation, precipitation, or other transformations. Based on K_d values reported in Sheppard and Thibault (1990), U.S. EPA (1996), and U.S. EPA (1999), sorption and retardation of cadmium, cobalt, iron, manganese, mercury, nickel, selenium, silver, and thallium are likely to be significantly larger than model-predicted values. As a result only chloride, sulfate, and fluoride are predicted to migrate with little or no sorption.

Given the magnitude of model-predicted impacts to groundwater for chloride and sulfate (minimal), the impact caused by the other mobile contaminant (fluoride) was estimated. Using dilution/attenuation of chloride from tailings fluids to groundwater as a proxy, the concentration of fluoride was estimated. Because the monitoring well predicted to be impacted the most by potential releases from the tailings cells is monitoring well MW-12, the fluoride concentration was estimated for this location. Assuming a dilution factor of 768,000, the fluoride concentration of 0.002 mg/l was estimated for MW-12. The proposed GWCL for fluoride in MW-12 is 2 mg/l. As a result, the predicted concentrations of fluoride as well as other contaminants of concern are not predicted to exceed the proposed GWCLs at 200 years.

Under Part I.D.6 (Closed Cell Performance Requirements) of the Permit:

"before reclamation and closure of any tailings disposal cell, the Permittee shall ensure that the final design, construction, and operation of the cover system at each tailings cell will comply with all requirements of an approved Reclamation Plan, and will for a period of not less than 200 years meet the following minimum performance requirements:

a) Minimize infiltration of precipitation or other surface water into the tailings, including, but not limited to the radon barrier, and

b) Prevent the accumulation of leachate head within the tailings waste layer that could rise above or over-top the maximum FML liner elevation internal to any disposal cell, i.e. create a "bathtub" effect.

c) Ensure that groundwater quality at the compliance monitoring wells does not exceed the Ground Water Quality Standards or Ground Water Compliance Limits specified in Part I.C.1 and Table 2 of this Permit."

Based on the model results presented in this report, all three requirements are met by the modified cover design.

5.2 POST-AUDIT MONITORING PLAN

To check the accuracy of the model predictions, a post-audit can be performed, often referred to as model verification. Additional data are collected and after a specified period, the model is rerun with new input data and the results are compared to field-measured data for the same period. Given difficulties associated with data collection and the time-scale on which processes occur in the vadose zone, a post audit of the HYDRUS models is not practical. A post audit of the MODFLOW model for the tailings cell dewatering is described below. Given the time-scale on which the model-predicts contaminants could potentially reach the perched aquifer, post-audit monitoring should include ongoing groundwater level measurements and groundwater sampling, but at a reduced frequency and at a limited set of wells relative to that currently used to establish background levels. Sampling should focus on the closest downgradient monitoring wells.

For post-audit monitoring of the dewatering system, water levels in the tailings and pumping rates and volumes should be measured and recorded monthly, as described above. Weather data should be obtained from the Utah Climate Center for the Blanding weather station. The model predictions should be compared to these data.

If the dewatering rates predicted by the model are considerably different than actual measured rates, the MODFLOW model should be recalibrated by adjusting terms such as areal recharge, hydraulic conductivity of tailings, storage parameters, and/or slimes drain conductance to match dewatering rates and measured water levels. The HYDRUS-1D model for flow and chloride transport through the vadose zone should be rerun with the revised saturated thickness predictions to evaluate changes to mass loading to the perched aquifer. If deemed necessary, the MT3DMS model of the perched aquifer can be rerun for chloride and sulfate transport.

REFERENCES

Albright, W.H., C.H. Benson, G.W. Gee, A.C. Roesler, T. Abichou, P. Apiwantragoon, B.F. Lyles, and S.A. Rock, 2004. Field Water Balance of Landfill Final Covers. Journal of Environmental Quality 33:2317-2332.

Allen, R.G., L.S. Pereira, D. Raes, and M. Smith, 1998. FAO Irrigation and Drainage Paper, No. 56, Crop Evapotranspiration (Guidelines for Computing Crop Water Requirements), pp. 300, FAO - Food and Agriculture Organization of the United Nations, Rome, Italy.

Al-Suwaiyan, M.S., 1996. Discussion of Paper "Use of Weighted Least-Squares Method in Evaluation of the Relationship Between Dispersivity and Field Scale". Ground Water 34 (4): 578.

Anderson, M.P., and W.W. Woessner, 1992. *Applied Groundwater Modeling: Simulation of Flow and Advective Transport.* Academic Press, Inc. Harcourt Brace Jovanovich, Publishers, San Diego, CA. 381p.

Bolen, M.M., A.C. Roesler, C.H. Benson, and W.H. Albright, 2001. Alternative Cover Assessment Program: Phase II Report. Geo Engineering Report 01-10, Department of Civil and Environmental Engineering, University of Wisconsin-Madison.

Brooks, R.H., and A.T. Corey, 1964. *Hydraulic Properties of Porous Media.* Hydrology Paper no. 3. Colorado State University, Fort Collins, CO.

Campbell, G.S., and J.M. Norman, 1998. *An Introduction to Environmental Biophysics*, 2nd ed., pp. 286, Springer, New York, New York.

Chen, J-S., R.L. Drake, X. Lin, and D.G. Jewett, 2002. *Simulating Radionuclide Fate and Transport in the Unsaturated Zone: Evaluation and Sensitivity Analyses of Select Computer Models.* U.S. Environmental Protection Agency EPA/600/R-02/082. July 2002.

Colorado School of Mines Research Institute, 1978. Grinding Study, Appendix A.

Currie, P. O., and F. L. Hammer, 1979. Detecting depth and lateral spread of roots of native range plants using radioactive phosphorus. Journal of Range Management 32:101-103.

Daniel B. Stephens & Associates, 2007. Laboratory Report Prepared for MWH Americas, Inc., April 27, 2007.

D'Appolonia Consulting Engineers, Inc., 1982. Construction Report, Initial Phase – Tailings Management System, White Mesa Uranium Project, Blanding, Utah. Prepared for Energy Fuels Nuclear, Inc.

Davis, J.A., and G.P. Curtis, 2003. Application of Surface Complexation Modeling to Describe Uranium(VI) Adsorption and Retardation at the Uranium Mill Tailings Site at Naturita, Colorado, Report NUREG CR-6820, U. S. Nuclear Regulatory Commission, Rockville, MD., pp. 223.

Davis, J.A., D.E. Meece, M. Kohler, and G.P. Curtis, 2004. Approaches to Surface Complexation Modeling of Uranium(VI) Adsorption on Aquifer Sediments, Geochimica et Cosmochimica Acta, 68:3621-3641.

Dingman, S.L., 2002. *Physical Hydrology*, 2nd ed., Prentice Hall, Upper Saddle River, New Jersey. pp. 646.

Dwyer, S.F., 2003. Water balance measurements and computer simulations of landfill covers, Ph.D. Dissertation, University of New Mexico at Albuquerque, pp. 250.

Dzombak, D.A., and F.M. Morel, 1990. *Surface Complexation Modeling: Hydrous Ferric Oxide*, John Wiley & Sons, New York, NY.

Fayer, M.J., and G.W. Gee, 2006. *Multiple-Year Water Balance of Soil Covers in a Semiarid Setting*. Journal of Environmental Quality 35:366-377.

Feddes, R. A., P. J. Kowalik, and H. Zaradny, 1978. *Simulation of Field Water Use and Crop Yield*, John Wiley & Sons, New York, NY, pp. 188.

Foose, G.J., C.H. Benson, and T.B. Edil, 2001. Predicting leakage through composite landfill liners. Journal of Geotechnical and Geoenvironmental Engineering. 127(6): 510-520.

Foxx, T. S. and G. D. Tierney, 1987. Rooting patterns in the pinyon-juniper woodland, USDA- Forest Service, Intermountain Research Station: 69-79.

Freeze, R.A., and J.A. Cherry, 1979. *Groundwater*, Prentice-Hall, Inc., Englewood Cliffs, N.J.

Gee, G.W., P.J. Wieringa, B.J. Andraski, M.H. Young, M.J. Fayer, and M.L. Rockhold, 1994. *Variations in Water Balance and Recharge Potential at Three Western Desert Sites*. Soil Sci. Soc. Am. J. 58:63-72.

Gelhar, L.W., Welty, C., and Rehfeldt, K.R., 1992. A Critical Review of Data on Field-Scale Dispersion in Aquifers. Water Resources Research 28 (7): 1955-1974.

Geosyntec Consultants, 2006. Stockpile Evaluation Tailings Cell 4A, White Mesa Mill - Technical Memo submitted to International Uranium (USA) Corporation, 23 January 2006.

Geosyntec Consultants, 2007a. Revised Construction Drawings, DMC White Mesa Mill, Cell 4A Lining System. June 2007.

Geosyntec Consultants, 2007b. Analysis of Slimes Drains for White Mesa Mill - Cell 4A, Computations submitted to Denison Mines, 12 May 2007.

Giroud, J.P., and R. Bonaparte, 1989. Leakage through Liners Constructed with Geomembrane Liners, Parts I, II, and Technical Notes, Geotextiles and Geomembranes 8:27-67, 71-111, 337-340.

Giroud, J.P., K.B. Tweneboah, and R. Bonaparte, 1992. Rate of Leakage through a Composite Liner due to Geomembrane Defects, Geotextiles and Geomembranes 11:1-28.

Grenthe, I. et al. 1992. Chemical Thermodynamics of Uranium, Elsevier, Amsterdam, The Netherlands.

Guillaumont, R. et al. 2003. Update on the Chemical Thermodynamics of Uranium, Neptunium, Plutonium, Americium and Technetium, pp. 919, Elsevier, Amsterdam, The Netherlands.

Gulec, S., T. Edil, and C. Benson, 2004. Effect of Acid Mine Drainage on the Polymer Properties of a HDPE Geomembrane. Geosynthetics International 11(2):60-72.

Gulec, S.B., C.H. Benson, and T.B. Edil, 2005. Effect of Acid Mine Drainage (AMD) on the Mechanical and Hydraulic Properties of Three Geosynthetics. Journal of Geotechnical and Geoenvironmental Engineering, Vol. 131, No. 8, pp. 937-950.

Harbaugh, A.W., Banta, E.R., Hill, M.C., and McDonald, M.G., 2000, MODFLOW-2000, the U.S. Geological Survey modular ground-water model -- User guide to modularization concepts and the Ground-Water Flow Process: U.S. Geological Survey Open-File Report 00-92, 121 p.

Heilweil, V.M., D.K. Solomon, and P.M. Gardner, 2006. Borehole Environmental Tracers for Evaluating Net Infiltration and Recharge Through Desert Bedrock, *Vadose Zone Journal* 5:98-120.

Hydro Geo Chem, Inc., 2002. *Hydraulic Testing at the White Mesa Uranium Mill Site, near Blanding, Utah During July 2002.* Prepared for International Uranium (USA) Corporation. August 2002.

Hydro Geo Chem, Inc., 2003. *Site Hydrogeology and Estimation of Groundwater Travel Times in the Perched Zone, White Mesa Uranium Mill Site, near Blanding, Utah.* Prepared for International Uranium Corporation. January 2003.

INTERA, 2007. Revised Background Groundwater Quality Report: Existing Wells for Denison Mines (USA) Corp.'s White Mesa Uranium Mill Site, San Juan County, Utah. Prepared for Denison Mines (USA) Corp. October 2007.

International Uranium (USA) Corporation, 2000. *Reclamation Plan, White Mesa Mill, Blanding, Utah.* Source Material License No. SUA-1358, Docket No. 40-8681 Revision 3.0. July 2000.

International Uranium (USA) Corporation, 2003. *Environmental Report.* June 2003.

Jo, H.Y., C.H. Benson, C.D. Shackelford, J.M., Lee, and T.B. Edil, 2005. Long-Term Hydraulic Conductivity of a Geosynthetic Clay Liner Permeated with Inorganic Salt Solutions. Journal of Geotechnical and Geoenvironmental Engineering. 131: 405-417.

Kashir, M. and E.K. Yanful, 2001. Hydraulic Conductivity of Bentonite Permeated with Acid Mine Drainage. Canadian Geotechnical Journal. 38: 1034-1048.

Khaleel, R., T.-C.J. Yeh, and Z. Lu, 2002. Upscaled Flow and Transport Properties for Heterogeneous Unsaturated Media. Water Resources Research 38:

Khire, M.V., C.H. Benson, and P.J. Bosscher, 2000. Capillary barriers: design variables and water balance, *Journal of Geotechnical and Geoenvironmental Engineering*, 126, 8, 965-708.

Knight-Piesold, 1998. *Evaluation for Potential for Tailing Cell Discharge – White Mesa Mill.* Attachment 5, Groundwater Information Report, White Mesa Uranium Mill, Blanding Utah. Submitted to UDEQ.

Kurc, S.A., and E.E. Small, 2004. Dynamics of Evapotranspiration in Semiarid Grassland and Shrubland Ecosystems During the Summer Monsoon Season, Central New Mexico. Water Resources Research 40:

Langmuir, D., 1997. *Aqueous Environmental Geochemistry*, Prentice-Hall, Inc., Englewood Cliffs, N.J.

Lee, C. A. and W. K. Lauenroth, 1994. Spatial Distributions of Grass and Shrub Root Systems in the Shortgrass Steppe. The American Midland Naturalist 132:117-123.

Li, Y-H., and S. Gregory, 1974. Diffusion of Ions in Sea Water and Deep-Sea Sediments. Geochemica et Cosmochemica Acta 38:703-714.

McDonald, M.G., and A.W. Harbaugh, 1988. *A Modular Three-Dimensional Finite Difference Ground-Water Flow Model.* Techniques of Water Resources Investigations of the U.S. Geological Survey, Book 6, Chapter A1.

MFG, Inc., 2005. Update of the Mill Decommissioning and Tailings Reclamation Plan for the Cotter Corporation Canon City Milling Facility (Appendix A 1999 Tailings Investigation). Prepared for Cotter Corporation. August 2005.

Millington, R. J. and J. M. Quirk, 1961. Permeability of Porous Solids, *Trans. Faraday Soc., 57*, 1200-1207.

Mitchell, D., 1985. Geomembrane Compatibility Tests Using Uranium Acid Leachate. Geotextiles and Geomembranes, 2: 111-127.

Mualem, Y., 1976. A New Model for Prediction the Hydraulic Conductivity of Unsaturated Porous Media, Water Resources Research 12:513-522.

Parkhurst, D.L and C.A.J. Appelo, 1999. User's guide to PHREEQC User's Guide to PHREEQC (Version 2)--A Computer Program for Speciation, Batch-Reaction, One-Dimensional Transport, and Inverse Geochemical Calculations, U.S. Geological Survey Water-Resources Investigations Report 99-4259, pp. 312.

Payne, T.E., 1999. Uranium(VI) Interactions with Mineral Surfaces: Controlling Factors and Surface Complexation Modeling, PhD Dissertation, University of New South Wales, pp. 332.

Pollack, D.W., 1989. *Documentation of Computer Programs to Compute and Display Pathlines Using Results from the U.S. Geological Survey Modular Three-Dimensional Finite-Difference Ground-Water Flow Model.* U.S. Geological Survey Open File Report 89-381.

Rumbaugh, J.O. and D.B. Rumbaugh, 2001. Guide to Using Groundwater Vistas, Version 3, Environmental Simulations Inc., Herndon, Virginia.

Simunek, J., K. Huang, and M. Th. van Genuchten, 1998. *The HYDRUS Code for Simulating the One-Dimensional Movement of Water, Heat, and Multiple Solutes in Variably-Saturated Media.* Research Report No. 144. U.S. Salinity Laboratory, Agricultural Research Service, U.S. Department of Agriculture, Riverside, CA.

Simunek, J., M. Th. van Genuchten, and M. Sejna, 2005. *The HYDRUS-1D Software Package for Simulating the One-Dimensional Movement of Water, Heat, and Multiple Solutes in Variably-Saturated Media, Version 3.0.* Department of Environmental Sciences, University of California – Riverside, Riverside, CA. 240 p.

Scanlon, B.R., K.E. Keese, A.L. Flint, L.E. Flint, C.B. Gaye, M. Edmunds, and I. Simmers, 2006. Global Synthesis of Groundwater Recharge in Semiarid and Arid Regions, *Hydrological Processes*, 20:3335-3370.

Scanlon, B.R., R.C. Reedy, K.E. Keese, and S.F. Dwyer, 2005. *Evaluation of Evapotranspirative Covers for Waste Containment in Arid and Semiarid Regions in the Southwestern USA*. Vadose Zone Journal 4:55-71.

Scanlon, B.R., M. Christman, R.C. Reedy, I. Porro, J. Simunek, and G.N. Flerchinger, 2002. *Intercode Comparisons for Simulating Water Balance of Surficial Sediments in Semiarid Regions*. Water Resources Research 38:1323-1339.

Schaefer, C.E., R.R. Arands, H.A. Van Der Sloot, and D.S. Kosson, 1995. Prediction and Experimental Validation of Liquid-Phase Diffusion Resistance in Unsaturated Soils. Journal of Contaminant Hydrology 20:145-166.

Schuster, J. L., 1964. Root Development of Native Plants Under Three Grazing Intensities. Ecology 45:63-70.

Sheppard, M.I. and D.H. Thibault, 1990. Default soil solid/liquid partition coefficients, K_ds, for four major soil types: a compendium, *Health Physics*, 59(4): 471-482.

Tinjum, J.M., C.H. Benson, and L.R. Blotz, 1997. Soil-Water Characteristic Curves for Compacted Clays. Journal of Geotechnical and Geoenvironmental Engineering 123:1060-1069.

TITAN Environmental Corporation, 1994. *Hydrogeological Evaluation of White Mesa Uranium Mill.* Prepared for Energy Fuels Nuclear, Inc.

TITAN Environmental Corporation, 1996. *Tailings Cover Design, White Mesa Mill, Blanding Utah.* Prepared for Energy Fuels Nuclear, Inc. September 1996.

U.S. Department of Energy, 2003. Moab Ground Water Tailings Seepage Report, U.S. Department of Energy - Grand Junction Office, Document Number X0025700, January 2003.

U.S. EPA, 1996. Soil Screening Guidance: Technical Background Document, Publication 9355.4-17A, 2nd ed., Office of Solid Waste and Emergency Response, U.S. Environmental Protection Agency, May 1996.

U.S. EPA, 1999. Understanding variation in partition coefficient, K_d, values: Review of Geochemistry and Available K_d Values for Cadmium, Cesium, Chromium, Lead, Plutonium, Radon, Strontium, Thorium, Tritium (3H), and Uranium, Volume II, Publication 402-R-99-004B, Office of Air and Radiation, U.S. Environmental Protection Agency, August 1999.

Utah Climate Center, 2007. Daily climate records were extracted from the COOP database from http://climate.usurf.usu.edu/products/data.php for the Blanding, Utah weather station (420738) on 25 January 2007.

Utah Division of Radiation Control, 2004. *Draft Ground Water Discharge Permit, Statement of Basis for a Uranium Milling Facility at White Mesa, South of Blanding.* December 2004.

van Genuchten, M.Th., 1980. *A Closed-Form Equation for Predicting the Hydraulic Conductivity of Unsaturated Soils.* Soil Sci. Am. Jour. 44:892-898.

Vogel, T., and M. Cislerova, 1988. *On the Reliability of Unsaturated Hydraulic Conductivity Calculated from the Moisture Retention Curve.* Transport in Porous Media 3:1-15.

Waite, T.D., J.A. Davis, T.E. Payne, G.A. Waychunas, and N. Xu, 1994. Uranium(VI) Adsorption to Ferrihydrite: Application of a Surface Complexation Model, Geochimica et Cosmochimica Acta, 58:5465-5478.

Walvoord, M.A., M.A. Plummer, and F.M. Phillips, 2002. Deep Arid System Hydrodynamics: 1. Equilibrium States and Response Times in Thick Desert Vadose Zones. Water Resources Research 38.

Wazne, M., G.P. Korfiatis, and X. Meng, 2003. Carbonate Effects on Hexavalent Uranium Adsorption by Iron Oxyhydroxide, Environmental Science & Technology, 37:3619-3624.

Xu, M., and Eckstein, Y., 1995. Use of Weighted Least-Squares Method in Evaluation of the Relationship Between Dispersivity and Field Scale. Ground Water 33 (6): 905-908.

Zheng, C., 1990. *MT3D: A Modular Three-Dimensional Transport Model for Simulation of Advection, Dispersion and Chemical Reactions of Contaminants in Groundwater Systems.* Report to the U.S. Environmental Protection Agency. Ada, OK. 170 p.

Zheng, C., and G.D. Bennett, 1995. Applied Contaminant Transport Modeling: Theory and Practice. Van Nostrand Reinhold (now John Wiley & Sons), New York, 440 pp.

Zheng, C. and P.P. Wang, 1999. MT3DMS: A Modular three-dimensional Multispecies Model for Simulation of Advection, Dispersion and Chemical Reactions of Contaminants in Groundwater Systems; Documentation and User's Guide, Contract Report SERDP-99-1, U.S. Army Engineer Research and Development Center, Vicksburg.

APPENDIX A

UNSATURATED HYDRAULIC PROPERTIES FOR CORES FROM WHITE MESA

Laboratory Report for

MWH Americas, Inc.

(Contract No. 87146-OM)

April 27, 2007

Daniel B. Stephens & Associates, Inc.

6020 Academy NE, Suite 100 • Albuquerque, New Mexico 87109

April 27, 2007

Mr. Doug Oliver
MWH Americas, Inc.
10619 South Jordan Gateway
South Jordan, UT 84095
(810) 617-3200

Re: DBS&A Laboratory Report for MWH Americas, Inc.; Contract No. 87146-OM

Dear Mr. Oliver:

Enclosed is the final report for the MWH Americas, Inc.; contract No. 87146-OM samples. Please review this report and provide any comments as samples will be held for a maximum of 30 days. After 30 days samples will be returned or disposed of in an appropriate manner. All testing results were evaluated subjectively for consistency and reasonableness, and the results appear to be reasonably representative of the material tested. However, DBS&A does not assume any responsibility for interpretations or analyses based on the data enclosed, nor can we guarantee that these data are fully representative of the undisturbed materials at the field site. We recommend that careful evaluation of these laboratory results be made for your particular application.

The testing utilized to generate the enclosed final report employs methods that are standard for the industry. The results do not constitute a professional opinion by DBS&A, nor can the results affect any professional or expert opinions rendered with respect thereto by DBS&A. You have acknowledged that all the testing undertaken by us, and the final report provided, constitutes mere test results using standardized methods, and cannot be used to disqualify DBS&A from rendering any professional or expert opinion, having waived any claim of conflict of interest by DBS&A.

We are pleased to provide this service to MWH Americas, Inc. and look forward to future laboratory testing on other projects. If you have any questions about the enclosed data, please do not hesitate to call.
Sincerely,

DANIEL B. STEPHENS & ASSOCIATES, INC.
LABORATORY / TESTING FACILITY

Joleen Hines
Laboratory Supervising Manager

Enclosure

Daniel B. Stephens & Associates, Inc.
6020 Academy NE, Suite 100 505-822-9400
Albuquerque, NM 87109 FAX 505-822-8877

Summaries

Summary of Tests Performed

Laboratory Sample Number	Initial Soil Properties[1] (θ, ρ_d, ϕ)	Saturated Hydraulic Conductivity[2]		Moisture Characteristics[3]					Unsaturated Hydraulic Conductivity	Particle Size[4]			Effective Porosity	Particle Density	Air Permeability	1/3, 15 Bar Points and Water Holding Capacity	Atterberg Limits	Proctor Compaction
		CH	FH	HC	PP	TH	WP	RH		DS	WS	H						
MW-23 55.5-56.0	X		X	X	X		X	X	X									
MW-23 74.3-74.6	X		X	X	X		X	X	X									
MW-23 82.7-82.9	X		X	X	X		X	X	X									
MW-23 103.3-103.5	X		X	X	X		X	X	X									
MW-30 35.5-36.0	X		X	X	X		X	X	X									
MW-30 44.0-44.5	X		X	X	X		X	X	X									

[1] θ = Initial moisture content, ρ_d = Dry bulk density, ϕ = Calculated porosity

[2] CH = Constant head, FH = falling head

[3] HC = Hanging column, PP = Pressure plate, TH = Thermocouple psychrometer, WP = Water activity meter, RH = Relative humidity box

[4] DS = Dry sieve, WS = Wet sieve, H = Hydrometer

Summary of Sample Volume Changes

	As Received Properties			*Final* Densities*		
Sample Number	Moisture Content (% g/g)	Moisture Content (cm^3/cm^3)	Dry Bulk Density (g/cm^3)	Final Measured Dry Bulk Density (g/cm^3)	Final % Volume Change (%)	Final % of Original Density (%)
MW-23 55.5-56.0	0.3	0.7	2.03	----	----	----
MW-23 74.3-74.6	0.6	1.4	2.33	----	----	----
MW-23 82.7-82.9	0.3	0.7	2.10	----	----	----
MW-23 103.3-103.5	0.8	1.4	1.84	----	----	----
MW-30 35.5-36.0	0.3	0.5	1.98	----	----	----
MW-30 44.0-44.5*	1.7	3.8	2.23	2.12	(+) 5.5%	94.8%

*Final Densities: Volume change measurements were obtained after saturated hydraulic conductivity testing and throughout unsaturated hydraulic conductivity testing. The reported values are the final sample dimensions.

*Sample MW-30 44.0-44.5 experienced swelling and water gain during and after the initial saturation process. This sample also cracked horizontally during moisture retention testing.

Note: (+) denotes observed sample swelling, and (-) denotes observed sample settling.

---- = Not Applicable, no volume change occurred.

Summary of Initial Moisture Content, Dry Bulk Density Wet Bulk Density and Calculated Porosity

Sample Number	Moisture Content				Dry Bulk Density (g/cm^3)	Wet Bulk Density (g/cm^3)	Calculated Porosity (%)
	As Received		Remolded				
	Gravimetric (%, g/g)	Volumetric (%, cm^3/cm^3)	Gravimetric (%, g/g)	Volumetric (%, cm^3/cm^3)			
MW-23 55.5-56.0	0.3	0.7	---	---	2.03	2.03	23.5
MW-23 74.3-74.6	0.6	1.4	---	---	2.33	2.34	12.1
MW-23 82.7-82.9	0.3	0.7	---	---	2.10	2.11	20.7
MW-23 103.3-103.5	0.8	1.4	---	---	1.84	1.85	30.7
MW-30 35.5-36.0	0.3	0.5	---	---	1.98	1.98	25.4
MW-30 44.0-44.5	1.7	3.8	---	---	2.23	2.27	15.8

NA = Not analyzed

--- = This sample was not remolded

Summary of Saturated Hydraulic Conductivity Tests

Sample Number	K_{sat} (cm/sec)	Method of Analysis: Constant Head Flexible Wall	Method of Analysis: Falling Head Flexible Wall
MW-23 55.5-56.0	1.1E-04		X
MW-23 74.3-74.6	2.9E-05		X
MW-23 82.7-82.9	1.7E-04		X
MW-23 103.3-103.5	3.0E-03		X
MW-30 35.5-36.0	8.1E-04		X
MW-30 44.0-44.5	8.2E-06		X

Summary of Moisture Characteristics of the Initial Drainage Curve

Sample Number	Pressure Head (-cm water)	Moisture Content (%, cm^3/cm^3)
MW-23 55.5-56.0	0	18.2
	13	17.7
	35	17.6
	100	15.8
	510	8.5
	15195	3.2
	42832	2.1
	851293	0.3
MW-23 74.3-74.6	0	12.3
	14	12.3
	56	12.2
	155	11.9
	510	11.7
	43851	4.9
	851293	1.6
MW-23 82.7-82.9	0	16.3
	12	15.3
	38	15.3
	97	14.9
	510	9.6
	23557	3.4
	851293	0.3
MW-23 103.3-103.5	0	20.4
	8	19.3
	24	19.2
	85	14.0
	510	6.8
	16827	3.3
	32838	2.5
	851293	0.6

Summary of Moisture Characteristics of the Initial Drainage Curve (Continued)

Sample Number	Pressure Head (-cm water)	Moisture Content (%, cm^3/cm^3)
MW-30 35.5-36.0	0	19.5
	7	19.2
	20	19.0
	74	14.1
	510	7.6
	23251	2.6
	35081	2.1
	851293	0.4
MW-30 44.0-44.5	0	27.9
	35	26.7
	101	24.7
	197	23.6
	510	20.5
	23353	10.9
	851293	3.4
MW-30 44.0-44.5 (Volume Adjusted)	0	26.7
	35	25.6
	101	23.5
	197	22.4
	510	19.4
	23353	10.4
	851293	3.2

Summary of Calculated Unsaturated Hydraulic Properties

Sample Number	α (cm^{-1})	N (dimensionless)	θ_r (% vol)	θ_s (% vol)	Oversize Corrected θ_r (% vol)	Oversize Corrected θ_s (% vol)
MW-23 55.5-56.0	0.0103	1.3860	0.00	18.38	NA	NA
MW-23 74.3-74.6	0.0003	1.3544	0.00	12.16	NA	NA
MW-23 82.7-82.9	0.0069	1.3362	0.00	16.01	NA	NA
MW-23 103.3-103.5	0.0287	1.3494	0.00	20.51	NA	NA
MW-30 35.5-36.0	0.0266	1.3480	0.00	19.86	NA	NA
MW-30 44.0-44.5	0.0074	1.2019	0.00	27.59	NA	NA
MW-30 44.0-44.5 (Volume Adjusted)	0.0081	1.2006	0.00	26.43	NA	NA

— = Oversize correction is unnecessary since coarse fraction < 5% of composite mass

NA = Not analyzed

Laboratory Data and Graphical Plots

Initial Properties

Summary of Initial Moisture Content, Dry Bulk Density Wet Bulk Density and Calculated Porosity

Sample Number	Moisture Content				Dry Bulk Density (g/cm^3)	Wet Bulk Density (g/cm^3)	Calculated Porosity (%)
	As Received		Remolded				
	Gravimetric (%, g/g)	Volumetric (%, cm^3/cm^3)	Gravimetric (%, g/g)	Volumetric (%, cm^3/cm^3)			
MW-23 55.5-56.0	0.3	0.7	---	---	2.03	2.03	23.5
MW-23 74.3-74.6	0.6	1.4	---	---	2.33	2.34	12.1
MW-23 82.7-82.9	0.3	0.7	---	---	2.10	2.11	20.7
MW-23 103.3-103.5	0.8	1.4	---	---	1.84	1.85	30.7
MW-30 35.5-36.0	0.3	0.5	---	---	1.98	1.98	25.4
MW-30 44.0-44.5	1.7	3.8	---	---	2.23	2.27	15.8

NA = Not analyzed

--- = This sample was not remolded

Data for Initial Moisture Content, Bulk Density, Porosity, and Percent Saturation

Job Name: MWH AMERICAS, INC.
Job Number: LB07.0048.00
Sample Number: MW-23 55.5-56.0
Ring Number: NA
Depth: 55.5-56.0

	As Received	Remolded
Test Date:	16-Mar-07	---
Field weight of sample* (g):	172.04	
Tare weight, ring (g):	0.00	
Tare weight, pan/plate (g):	0.00	
Tare weight, other (g):	0.00	
Dry weight of sample (g):	171.46	
Sample volume (cm^3):	84.63	
Assumed particle density (g/cm^3):	2.65	
Gravimetric Moisture Content (% g/g):	0.3	
Volumetric Moisture Content (% vol):	0.7	
Dry bulk density (g/cm^3):	2.03	
Wet bulk density (g/cm^3):	2.03	
Calculated Porosity (% vol):	23.5	
Percent Saturation:	2.9	

Laboratory analysis by: D. O'Dowd
Data entered by: T. Bowekaty
Checked by: J. Hines

Comments:

* Weight including tares
NA = Not analyzed
--- = This sample was not remolded

Data for Initial Moisture Content, Bulk Density, Porosity, and Percent Saturation

Job Name: MWH AMERICAS, INC.
Job Number: LB07.0048.00
Sample Number: MW-23 74.3-74.6
Ring Number: NA
Depth: 74.3-74.6

	As Received	Remolded
Test Date:	16-Mar-07	---
Field weight of sample* (g):	162.07	
Tare weight, ring (g):	0.00	
Tare weight, pan/plate (g):	0.00	
Tare weight, other (g):	0.00	
Dry weight of sample (g):	161.11	
Sample volume (cm^3):	69.19	
Assumed particle density (g/cm^3):	2.65	

Gravimetric Moisture Content (% g/g):	0.6
Volumetric Moisture Content (% vol):	1.4
Dry bulk density (g/cm^3):	2.33
Wet bulk density (g/cm^3):	2.34
Calculated Porosity (% vol):	12.1
Percent Saturation:	11.4

Laboratory analysis by: D. O'Dowd
Data entered by: T. Bowekaty
Checked by: J. Hines

Comments:

* Weight including tares
NA = Not analyzed
--- = This sample was not remolded

Data for Initial Moisture Content, Bulk Density, Porosity, and Percent Saturation

Job Name: MWH AMERICAS, INC.
Job Number: LB07.0048.00
Sample Number: MW-23 82.7-82.9
Ring Number: NA
Depth: 82.7-82.9

	As Received	Remolded
Test Date:	16-Mar-07	---
Field weight of sample* (g):	152.51	
Tare weight, ring (g):	0.00	
Tare weight, pan/plate (g):	0.00	
Tare weight, other (g):	0.00	
Dry weight of sample (g):	151.98	
Sample volume (cm^3):	72.35	
Assumed particle density (g/cm^3):	2.65	
Gravimetric Moisture Content (% g/g):	0.3	
Volumetric Moisture Content (% vol):	0.7	
Dry bulk density (g/cm^3):	2.10	
Wet bulk density (g/cm^3):	2.11	
Calculated Porosity (% vol):	20.7	
Percent Saturation:	3.5	

Laboratory analysis by: D. O'Dowd
Data entered by: T. Bowekaty
Checked by: J. Hines

Comments:

* Weight including tares
NA = Not analyzed
--- = This sample was not remolded

Daniel B. Stephens & Associates, Inc.

Data for Initial Moisture Content, Bulk Density, Porosity, and Percent Saturation

Job Name: MWH AMERICAS, INC.
Job Number: LB07.0048.00
Sample Number: MW-23 103.3-103.5
Ring Number: NA
Depth: 103.3-103.5

	As Received	Remolded
Test Date:	16-Mar-07	---
Field weight of sample* (g):	127.13	
Tare weight, ring (g):	0.00	
Tare weight, pan/plate (g):	0.00	
Tare weight, other (g):	0.00	
Dry weight of sample (g):	126.16	
Sample volume (cm^3):	68.67	
Assumed particle density (g/cm^3):	2.65	

Gravimetric Moisture Content (% g/g):	0.8
Volumetric Moisture Content (% vol):	1.4
Dry bulk density (g/cm^3):	1.84
Wet bulk density (g/cm^3):	1.85
Calculated Porosity (% vol):	30.7
Percent Saturation:	4.6

Laboratory analysis by: D. O'Dowd
Data entered by: T. Bowekaty
Checked by: J. Hines

Comments:

* Weight including tares
NA = Not analyzed
--- = This sample was not remolded

Daniel B. Stephens & Associates, Inc.

Data for Initial Moisture Content, Bulk Density, Porosity, and Percent Saturation

Job Name: MWH AMERICAS, INC.
Job Number: LB07.0048.00
Sample Number: MW-30 35.5-36.0
Ring Number: NA
Depth: 35.5'-36.0'

	As Received	Remolded
Test Date:	16-Mar-07	---
Field weight of sample* (g):	170.24	
Tare weight, ring (g):	0.00	
Tare weight, pan/plate (g):	0.00	
Tare weight, other (g):	0.00	
Dry weight of sample (g):	169.77	
Sample volume (cm^3):	85.85	
Assumed particle density (g/cm^3):	2.65	

Gravimetric Moisture Content (% g/g):	0.3
Volumetric Moisture Content (% vol):	0.5
Dry bulk density (g/cm^3):	1.98
Wet bulk density (g/cm^3):	1.98
Calculated Porosity (% vol):	25.4
Percent Saturation:	2.2

Laboratory analysis by: D. O'Dowd
Data entered by: T. Bowekaty
Checked by: J. Hines

Comments:

* Weight including tares
NA = Not analyzed
--- = This sample was not remolded

Daniel B. Stephens & Associates, Inc.

Data for Initial Moisture Content, Bulk Density, Porosity, and Percent Saturation

Job Name: MWH AMERICAS, INC.
Job Number: LB07.0048.00
Sample Number: MW-30 44.0-44.5
Ring Number: NA
Depth: 44.0-44.5

	As Received	Remolded
Test Date:	16-Mar-07	—
Field weight of sample* (g):	197.08	
Tare weight, ring (g):	0.00	
Tare weight, pan/plate (g):	0.00	
Tare weight, other (g):	0.00	
Dry weight of sample (g):	193.77	
Sample volume (cm^3):	86.88	
Assumed particle density (g/cm^3):	2.65	
Gravimetric Moisture Content (% g/g):	1.7	
Volumetric Moisture Content (% vol):	3.8	
Dry bulk density (g/cm^3):	2.23	
Wet bulk density (g/cm^3):	2.27	
Calculated Porosity (% vol):	15.8	
Percent Saturation:	24.1	

Laboratory analysis by: D. O'Dowd
Data entered by: T. Bowekaty
Checked by: J. Hines

Comments:

* Weight including tares
NA = Not analyzed
--- = This sample was not remolded

Saturated Hydraulic Conductivity

Summary of Saturated Hydraulic Conductivity Tests

Sample Number	K_{sat} (cm/sec)	Method of Analysis: Constant Head Flexible Wall	Method of Analysis: Falling Head Flexible Wall
MW-23 55.5-56.0	1.1E-04		X
MW-23 74.3-74.6	2.9E-05		X
MW-23 82.7-82.9	1.7E-04		X
MW-23 103.3-103.5	3.0E-03		X
MW-30 35.5-36.0	8.1E-04		X
MW-30 44.0-44.5	8.2E-06		X

Saturated Hydraulic Conductivity
Flexible Wall Falling Head-Rising Tail Method

Job name: MWH AMERICAS, INC.
Job number: LB07.0048.00
Sample number: MW-23 55.5-56.0
Date/Time sampled: NA
Depth: 55.5-56.0

Remolded or Initial Sample Properties		Final (Post Test) Sample Properties		Test and Sample Conditions	
Initial Mass (g):	172.04	*Saturated Mass (g):*	186.87	*Permeant liquid used:*	Water
Diameter (cm):	5.369	*Dry Mass (g):*	171.46	*Sample Preparation:*	☑ In situ sample, extruded
Length (cm):	3.738	*Diameter (cm):*	5.369		☐ Remolded Sample
Area (cm^2):	22.64	*Length (cm):*	3.738	*Number of Lifts:*	NA
Volume (cm^3):	84.63	*Area (cm^2):*	22.64	*Split:*	NA
Dry Density (g/cm^3):	2.03	*Volume (cm^3):*	84.63	*Percent Coarse Material (%):*	NA
Dry Density (pcf):	126.48	*Dry Density (g/cm^3):*	2.03	*Particle Density(g/cm^3):*	2.65 ☑ Assumed ☐ Measured
Water Content (%, g/g):	0.3	*Dry Density (pcf):*	126.48	*Cell pressure (PSI):*	32.0
Water Content (%, vol):	0.7	*Water Content (%, g/g):*	9.0	*Influent pressure (PSI):*	30.0
Porosity (%, vol):	23.5	*Water Content (%, vol):*	18.2	*Effluent pressure (PSI):*	30.0
Saturation (%):	2.9	*Porosity (%, vol):*	23.5	*Panel Used:*	☑ A ☐ B ☐ C
		Saturation (%):*	77.3	*Reading:*	☐ Annulus ☑ Pipette
				B-Value (% saturation) prior to test*:	0.95
				Date/Time:	3/20/07 1503

* Per ASTM D5084 percent saturation is ensured (B-Value ≥ 95%) prior to testing, as post test saturation values may be exaggerated or skewed during depressurizing and sample removal.

Laboratory analysis by: D. O'Dowd
Data entered by: D. O'Dowd
Checked by: J. Hines

Daniel B. Stephens & Associates, Inc.

Saturated Hydraulic Conductivity
Flexible Wall Falling Head-Rising Tail Method

Job name: MWH AMERICAS, INC.
Job number: LB07.0048.00
Sample number: MW-23 55.5-56.0
Date/Time sampled: NA
Depth: 55.5-56.0

Date	Time	Temp (°C)	Influent Pipette Reading	Effluent Pipette Reading	Gradient (ΔH/ΔL)	Average Flow (cm^3)	Elapsed Time (s)	Ratio (outflow to inflow)	Change in Head (Not to exceed 25%)	k_{sat} T°C (cm/s)	k_{sat} Corrected (cm/s)
Test # 1:											
20-Mar-07	14:19:06	24.0	15.00	19.40	1.36	0.17	59	1.00	9%	1.15E-04	1.05E-04
20-Mar-07	14:20:05	24.0	15.20	19.20	1.24						
Test # 2:											
20-Mar-07	14:20:05	24.0	15.20	19.20	1.24	0.17	56	1.00	10%	1.35E-04	1.22E-04
20-Mar-07	14:21:01	24.0	15.40	19.00	1.11						
Test # 3:											
20-Mar-07	14:21:01	24.0	15.40	19.00	1.11	0.17	79	1.00	11%	1.07E-04	9.68E-05
20-Mar-07	14:22:20	24.2	15.60	18.80	0.99						
Test # 4:											
20-Mar-07	14:22:20	24.2	15.60	18.80	0.99	0.17	79	1.00	13%	1.21E-04	1.09E-04
20-Mar-07	14:23:39	24.2	15.80	18.60	0.86						

***Average Ksat* (cm/sec):** **1.08E-04**
Calculated Gravel Corrected Average Ksat (cm/sec): ---

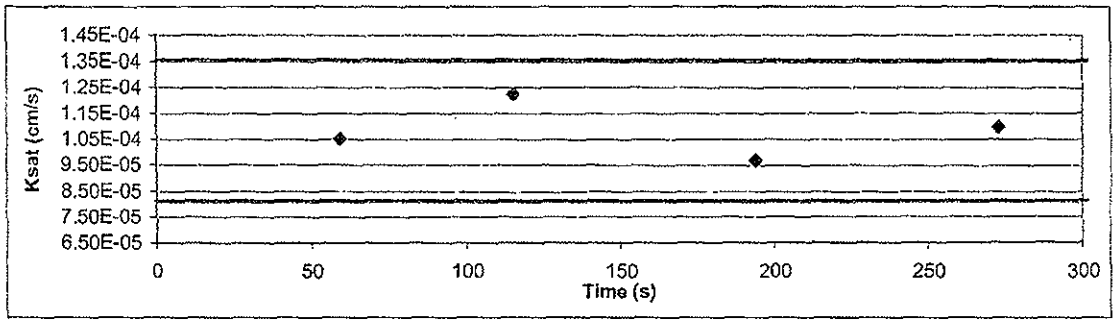

ASTM Required Range (+/- 25%)

Ksat (-25%) (cm/s): 8.13E-05

Ksat (+25%) (cm/s): 1.36E-04

Daniel B. Stephens & Associates, Inc.

Saturated Hydraulic Conductivity
Flexible Wall Falling Head-Rising Tail Method

Job name: MWH AMERICAS, INC.
Job number: LB07.0048.00
Sample number: MW-23 74.3-74.6
Date/Time sampled: NA
Depth: 74.3-74.6

Remolded or Initial Sample Properties		Final (Post Test) Sample Properties		Test and Sample Conditions	
Initial Mass (g):	162.07	*Saturated Mass (g):*	169.61	*Permeant liquid used:*	Water
Diameter (cm):	5.376	*Dry Mass (g):*	161.11	*Sample Preparation:*	☑ In situ sample, extruded
Length (cm):	3.048	*Diameter (cm):*	5.376		☐ Remolded Sample
Area (cm^2):	22.70	*Length (cm):*	3.048	*Number of Lifts:*	NA
Volume (cm^3):	69.19	*Area (cm^2):*	22.70	*Split:*	NA
Dry Density (g/cm^3):	2.33	*Volume (cm^3):*	69.19	*Percent Coarse Material (%):*	NA
Dry Density (pcf):	145.37	*Dry Density (g/cm^3):*	2.33	*Particle Density(g/cm^3):*	2.65 ☑ Assumed ☐ Measured
Water Content (%, g/g):	0.6	*Dry Density (pcf):*	145.37	*Cell pressure (PSI):*	32.0
Water Content (%, vol):	1.4	*Water Content (%, g/g):*	5.3	*Influent pressure (PSI):*	30.1
Porosity (%, vol):	12.1	*Water Content (%, vol):*	12.3	*Effluent pressure (PSI):*	30.0
Saturation (%):	11.4	*Porosity (%, vol):*	12.1	*Panel Used:*	☑ D ☐ E ☐ F
		Saturation (%):*	101.3	*Reading:*	☐ Annulus ☑ Pipette
				B-Value (% saturation) prior to test*:	1.00
				Date/Time:	3/20/07 1500

* Per ASTM D5084 percent saturation is ensured (B-Value ≥ 95%) prior to testing, as post test saturation values may be exaggerated during depressurizing and sample removal.

Laboratory analysis by: D. O'Dowd
Data entered by: D. O'Dowd
Checked by: J. Hines

Daniel B. Stephens & Associates, Inc.

Saturated Hydraulic Conductivity
Flexible Wall Falling Head-Rising Tail Method

Job name: MWH AMERICAS, INC.
Job number: LB07.0048.00
Sample number: MW-23 74.3-74.6
Date/Time sampled: NA
Depth: 74.3-74.6

Date	Time	Temp (°C)	Influent Pipette Reading	Effluent Pipette Reading	Gradient (ΔH/ΔL)	Average Flow (cm^3)	Elapsed Time (s)	Ratio (outflow to inflow)	Change in Head (Not to exceed 25%)	k_{sat} T°C (cm/s)	k_{sat} Corrected (cm/s)
Test # 1:											
20-Mar-07	14:30:19	24.2	15.40	19.85	3.99	0.17	69	1.00	4%	3.27E-05	2.96E-05
20-Mar-07	14:31:28	24.2	15.60	19.65	3.84						
Test # 2:											
20-Mar-07	14:31:28	24.2	15.60	19.65	3.84	0.17	79	1.00	4%	2.97E-05	2.69E-05
20-Mar-07	14:32:47	24.2	15.80	19.45	3.69						
Test # 3:											
20-Mar-07	14:32:47	24.2	15.80	19.45	3.69	0.17	72	1.00	4%	3.40E-05	3.08E-05
20-Mar-07	14:33:59	24.2	16.00	19.25	3.54						
Test # 4:											
20-Mar-07	14:33:59	24.2	16.00	19.25	3.54	0.17	85	1.00	4%	3.00E-05	2.72E-05
20-Mar-07	14:35:24	24.2	16.20	19.05	3.39						

***Average Ksat* (cm/sec):** **2.86E-05**

Calculated Gravel Corrected Average Ksat (cm/sec):

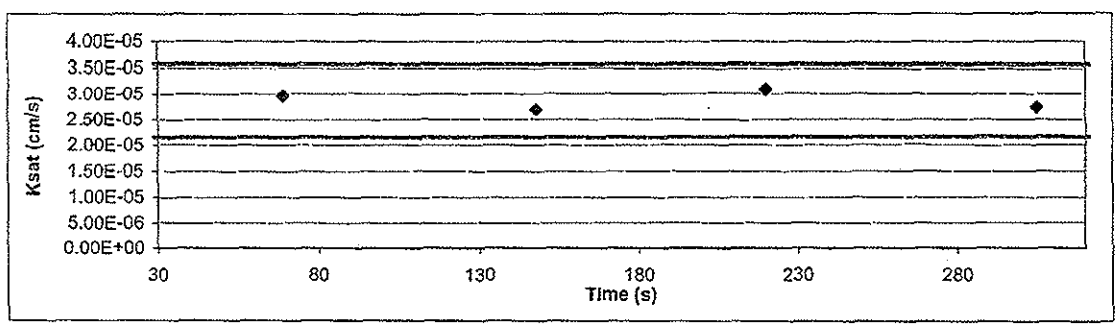

ASTM Required Range (+/- 25%)

Ksat (-25%) (cm/s): 2.15E-05

Ksat (+25%) (cm/s): 3.58E-05

Daniel B. Stephens & Associates, Inc.

Saturated Hydraulic Conductivity
Flexible Wall Falling Head-Rising Tail Method

Job name: MWH AMERICAS, INC.
Job number: LB07.0048.00
Sample number: MW-23 82.7-82.9
Date/Time sampled: NA
Depth: 82.7-82.9

Remolded or Initial Sample Properties		Final (Post Test) Sample Properties		Test and Sample Conditions	
Initial Mass (g):	152.51	*Saturated Mass (g):*	163.8	*Permeant liquid used:*	Water
Diameter (cm):	5.373	*Dry Mass (g):*	151.98	*Sample Preparation:*	☑ In situ sample, extruded
Length (cm):	3.191	*Diameter (cm):*	5.373		☐ Remolded Sample
Area (cm^2):	22.67	*Length (cm):*	3.191	*Number of Lifts:*	NA
Volume (cm^3):	72.35	*Area (cm^2):*	22.67	*Split:*	NA
Dry Density (g/cm^3):	2.10	*Volume (cm^3):*	72.35	*Percent Coarse Material (%):*	NA
Dry Density (pcf):	131.13	*Dry Density (g/cm^3):*	2.10	*Particle Density(g/cm^3):*	2.65 ☑ Assumed ☐ Measured
Water Content (%, g/g):	0.3	*Dry Density (pcf):*	131.13	*Cell pressure (PSI):*	32.0
Water Content (%, vol):	0.7	*Water Content (%, g/g):*	7.8	*Influent pressure (PSI):*	30.0
Porosity (%, vol):	20.7	*Water Content (%, vol):*	16.3	*Effluent pressure (PSI):*	30.0
Saturation (%):	3.5	*Porosity (%, vol):*	20.7	*Panel Used:*	☐ D ☑ E ☐ F
		Saturation (%):*	78.8	*Reading:*	☐ Annulus ☑ Pipette
				B-Value (% saturation) prior to test*:	0.95
				Date/Time:	3/19/07 1305

* Per ASTM D5084 percent saturation is ensured (B-Value ≥ 95%) prior to testing, as post test saturation values may be exaggerated during depressurizing and sample removal.

Laboratory analysis by: D. O'Dowd
Data entered by: D. O'Dowd
Checked by: J. Hines

Daniel B. Stephens & Associates, Inc.

Saturated Hydraulic Conductivity
Flexible Wall Falling Head-Rising Tail Method

Job name: MWH AMERICAS, INC.
Job number: LB07.0048.00
Sample number: MW-23 82.7-82.9
Date/Time sampled: NA
Depth: 82.7-82.9

Date	Time	Temp (°C)	Influent Pipette Reading	Effluent Pipette Reading	Gradient (ΔH/ΔL)	Average Flow (cm^3)	Elapsed Time (s)	Ratio (outflow to inflow)	Change in Head (Not to exceed 25%)	k_{sat} T°C (cm/s)	k_{sat} Corrected (cm/s)
Test # 1:											
19-Mar-07	13:32:09	23.6	13.20	18.00	1.74	0.26	41	1.00	13%	1.99E-04	1.83E-04
19-Mar-07	13:32:50	23.6	13.50	17.70	1.52						
Test # 2:											
19-Mar-07	13:32:50	23.6	13.50	17.70	1.52	0.26	43	1.00	14%	2.19E-04	2.01E-04
19-Mar-07	13:33:33	23.6	13.80	17.40	1.30						
Test # 3:											
19-Mar-07	13:33:33	23.6	13.80	17.40	1.30	0.26	64	1.00	17%	1.74E-04	1.60E-04
19-Mar-07	13:34:37	23.6	14.10	17.10	1.09						
Test # 4:											
19-Mar-07	13:34:37	23.6	14.10	17.10	1.09	0.26	85	1.00	20%	1.61E-04	1.47E-04
19-Mar-07	13:36:02	23.6	14.40	16.80	0.87						

***Average Ksat* (cm/sec):** **1.73E-04**

Calculated Gravel Corrected Average Ksat (cm/sec):

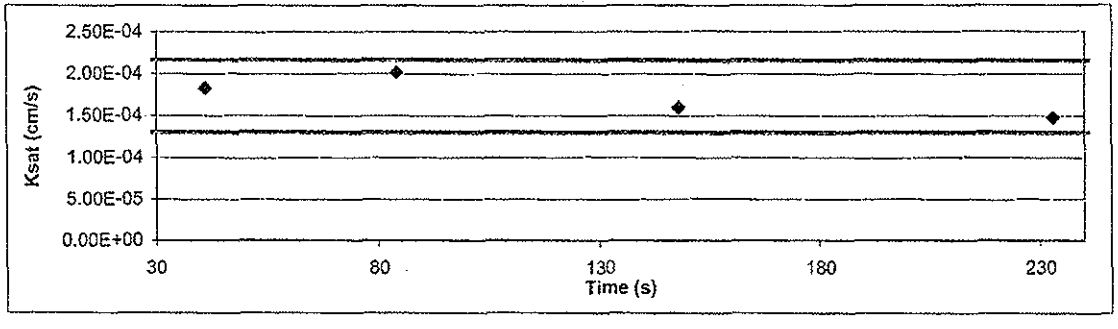

ASTM Required Range (+/- 25%)

Ksat (-25%) (cm/s): 1.30E-04

Ksat (+25%) (cm/s): 2.16E-04

Saturated Hydraulic Conductivity
Flexible Wall Falling Head-Rising Tail Method

Job name: MWH AMERICAS, INC.
Job number: LB07.0048.00
Sample number: MW-23 103.3-103.5
Date/Time sampled: NA
Depth: 103.3-103.5

Remolded or Initial Sample Properties		Final (Post Test) Sample Properties		Test and Sample Conditions	
Initial Mass (g):	127.13	*Saturated Mass (g):*	140.16	*Permeant liquid used:*	Water
Diameter (cm):	5.362	*Dry Mass (g):*	126.16	*Sample Preparation:*	☑ In situ sample, extruded
Length (cm):	3.041	*Diameter (cm):*	5.362		☐ Remolded Sample
Area (cm^2):	22.58	*Length (cm):*	3.041	*Number of Lifts:*	NA
Volume (cm^3):	68.67	*Area (cm^2):*	22.58	*Split:*	NA
Dry Density (g/cm^3):	1.84	*Volume (cm^3):*	68.67	*Percent Coarse Material (%):*	NA
Dry Density (pcf):	114.69	*Dry Density (g/cm^3):*	1.84	*Particle Density(g/cm^3):*	2.65 ☑ Assumed ☐ Measured
Water Content (%, g/g):	0.8	*Dry Density (pcf):*	114.69	*Cell pressure (PSI):*	32.0
Water Content (%, vol):	1.4	*Water Content (%, g/g):*	11.1	*Influent pressure (PSI):*	30.0
Porosity (%, vol):	30.7	*Water Content (%, vol):*	20.4	*Effluent pressure (PSI):*	30.0
Saturation (%):	4.6	*Porosity (%, vol):*	30.7	*Panel Used:*	☐ D ☐ E ☑ F
		Saturation (%):*	66.5	*Reading:*	☑ Annulus ☐ Pipette
				B-Value (% saturation) prior to test*:	0.95
				Date/Time:	3/19/07 1306

* Per ASTM D5084 percent saturation is ensured (B-Value ≥ 95%) prior to testing, as post test saturation values may be exaggerated during depressurizing and sample removal.

Laboratory analysis by: D. O'Dowd
Data entered by: D. O'Dowd
Checked by: J. Hines

Daniel B. Stephens & Associates, Inc.

Saturated Hydraulic Conductivity
Flexible Wall Falling Head-Rising Tail Method

Job name: MWH AMERICAS, INC.
Job number: LB07.0048.00
Sample number: MW-23 103.3-103.5
Date/Time sampled: NA
Depth: 103.3-103.5

Date	Time	Temp (°C)	Influent Pipette Reading	Effluent Pipette Reading	Gradient (ΔH/ΔL)	Average Flow (cm^3)	Elapsed Time (s)	Ratio (outflow to inflow)	Change in Head (Not to exceed 25%)	k_{sat} T°C (cm/s)	k_{sat} Corrected (cm/s)
Test # 1:											
19-Mar-07	13:52:17	23.8	15.90	20.35	1.69	1.17	11	1.00	13%	3.46E-03	3.16E-03
19-Mar-07	13:52:28	23.8	16.20	20.05	1.46						
Test # 2:											
19-Mar-07	13:52:28	23.8	16.20	20.05	1.46	1.17	15	1.00	16%	2.97E-03	2.71E-03
19-Mar-07	13:52:43	23.8	16.50	19.75	1.23						
Test # 3:											
19-Mar-07	13:52:43	23.8	16.50	19.75	1.23	1.17	16	1.00	18%	3.35E-03	3.06E-03
19-Mar-07	13:52:59	23.8	16.80	19.45	1.01						
Test # 4:											
19-Mar-07	13:52:59	23.8	16.80	19.45	1.01	1.17	19	1.00	23%	3.55E-03	3.24E-03
19-Mar-07	13:53:18	23.8	17.10	19.15	0.78						

***Average Ksat* (cm/sec):** **3.04E-03**

Calculated Gravel Corrected Average Ksat (cm/sec):

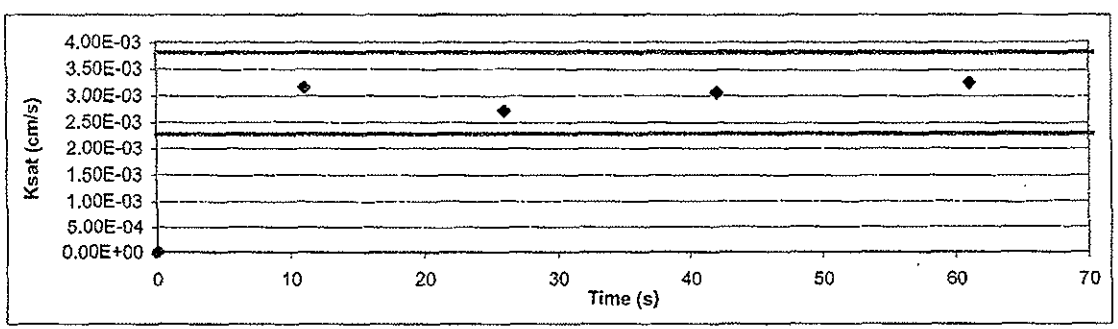

ASTM Required Range (+/- 25%)

Ksat (-25%) (cm/s): 2.28E-03

Ksat (+25%) (cm/s): 3.81E-03

Daniel B. Stephens & Associates, Inc.

Saturated Hydraulic Conductivity
Flexible Wall Falling Head-Rising Tail Method

Job name: MWH AMERICAS, INC.
Job number: LB07.0048.00
Sample number: MW-30 35.5-36.0
Date/Time sampled: NA
Depth: 35.5-36.0

Remolded or Initial Sample Properties		Final (Post Test) Sample Properties		Test and Sample Conditions	
Initial Mass (g):	170.24	*Saturated Mass (g):*	186.53	*Permeant liquid used:*	Water
Diameter (cm):	5.381	*Dry Mass (g):*	169.77	*Sample Preparation:*	☑ In situ sample, extruded
Length (cm):	3.775	*Diameter (cm):*	5.381		☐ Remolded Sample
Area (cm^2):	22.74	*Length (cm):*	3.775	*Number of Lifts:*	NA
Volume (cm^3):	85.85	*Area (cm^2):*	22.74	*Split:*	NA
Dry Density (g/cm^3):	1.98	*Volume (cm^3):*	85.85	*Percent Coarse Material (%):*	NA
Dry Density (pcf):	123.45	*Dry Density (g/cm^3):*	1.98	*Particle Density(g/cm^3):*	2.65 ☑ Assumed ☐ Measured
Water Content (%, g/g):	0.3	*Dry Density (pcf):*	123.45	*Cell pressure (PSI):*	32.0
Water Content (%, vol):	0.5	*Water Content (%, g/g):*	9.9	*Influent pressure (PSI):*	30.0
Porosity (%, vol):	25.4	*Water Content (%, vol):*	19.5	*Effluent pressure (PSI):*	30.0
Saturation (%):	2.2	*Porosity (%, vol):*	25.4	*Panel Used:*	☐ A ☑ B ☐ C
		Saturation (%):*	76.9	*Reading:*	☐ Annulus ☑ Pipette
				B-Value (% saturation) prior to test*:	0.95
				Date/Time:	3/20/07 1510

* Per ASTM D5084 percent saturation is ensured (B-Value ≥ 95%) prior to testing, as post test saturation values may be exaggerated or skewed during depressurizing and sample removal.

Laboratory analysis by: D. O'Dowd
Data entered by: D. O'Dowd
Checked by: J. Hines

Daniel B. Stephens & Associates, Inc.

Saturated Hydraulic Conductivity
Flexible Wall Falling Head-Rising Tail Method

Job name: MWH AMERICAS, INC.
Job number: LB07.0048.00
Sample number: MW-30 35.5-36.0
Date/Time sampled: NA
Depth: 35.5-36.0

Date	Time	Temp (°C)	Influent Pipette Reading	Effluent Pipette Reading	Gradient (ΔH/ΔL)	Average Flow (cm^3)	Elapsed Time (s)	Ratio (outflow to inflow)	Change in Head (Not to exceed 25%)	k_{sat} T°C (cm/s)	k_{sat} Corrected (cm/s)
Test # 1:											
20-Mar-07	14:14:19	24.0	15.70	18.60	0.89	0.17	13	1.00	14%	8.21E-04	7.47E-04
20-Mar-07	14:14:32	24.0	15.90	18.40	0.76						
Test # 2:											
20-Mar-07	14:14:32	24.0	15.90	18.40	0.76	0.17	13	1.00	16%	9.64E-04	8.77E-04
20-Mar-07	14:14:45	24.0	16.10	18.20	0.64						
Test # 3:											
20-Mar-07	14:14:45	24.0	16.10	18.20	0.64	0.17	17	1.00	19%	8.93E-04	8.13E-04
20-Mar-07	14:15:02	24.0	16.30	18.00	0.52						
Test # 4:											
20-Mar-07	14:15:02	24.0	16.30	18.00	0.52	0.17	22	1.00	24%	8.76E-04	7.97E-04
20-Mar-07	14:15:24	24.0	16.50	17.80	0.40						

***Average Ksat* (cm/sec):** **8.08E-04**
Calculated Gravel Corrected Average Ksat (cm/sec): ---

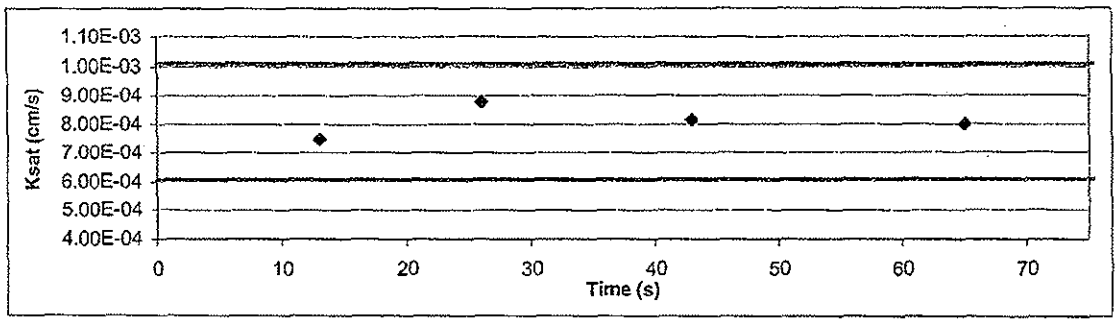

ASTM Required Range (+/- 25%)

Ksat (-25%) (cm/s): 6.06E-04

Ksat (+25%) (cm/s): 1.01E-03

Daniel B. Stephens & Associates, Inc.

Saturated Hydraulic Conductivity
Flexible Wall Falling Head-Rising Tail Method

Job name: MWH AMERICAS, INC.
Job number: LB07.0048.00
Sample number: MW-30 44.0-44.5
Date/Time sampled: NA
Depth: 44.0-44.5

Remolded or Initial Sample Properties	
Initial Mass (g):	197.08
Diameter (cm):	5.361
Length (cm):	3.849
Area (cm^2):	22.57
Volume (cm^3):	86.88
Dry Density (g/cm^3):	2.23
Dry Density (pcf):	139.23
Water Content (%, g/g):	1.7
Water Content (%, vol):	3.8
Porosity (%, vol):	15.8
Saturation (%):	24.1

Final (Post Test) Sample Properties	
Saturated Mass (g):	214.34
Dry Mass (g):	193.77
Diameter (cm):	5.361
Length (cm):	3.849
Area (cm^2):	22.57
Volume (cm^3):	86.88
Dry Density (g/cm^3):	2.23
Dry Density (pcf):	139.23
Water Content (%, g/g):	10.6
Water Content (%, vol):	23.7
Porosity (%, vol):	15.8
Saturation (%):*	149.5

Test and Sample Conditions	
Permeant liquid used:	Water
Sample Preparation:	☑ In situ sample, extruded
	☐ Remolded Sample
Number of Lifts:	NA
Split:	NA
Percent Coarse Material (%):	NA
Particle Density(g/cm^3):	2.65 ☑ Assumed ☐ Measured
Cell pressure (PSI):	32.0
Influent pressure (PSI):	30.2
Effluent pressure (PSI):	30.0
Panel Used:	☐ A ☐ B ☑ C
Reading:	☐ Annulus ☑ Pipette
B-Value (% saturation) prior to test*:	0.95
Date/Time:	3/20/07 1505

* Per ASTM D5084 percent saturation is ensured (B-Value ≥ 95%) prior to testing, as post test saturation values may be exaggerated or skewed during depressurizing and sample removal.

Laboratory analysis by: D. O'Dowd
Data entered by: D. O'Dowd
Checked by: J. Hines

Daniel B. Stephens & Associates, Inc.

Saturated Hydraulic Conductivity
Flexible Wall Falling Head-Rising Tail Method

Job name: MWH AMERICAS, INC.
Job number: LB07.0048.00
Sample number: MW-30 44.0-44.5
Date/Time sampled: NA
Depth: 44.0-44.5

Date	Time	Temp (°C)	Influent Pipette Reading	Effluent Pipette Reading	Gradient (ΔH/ΔL)	Average Flow (cm^3)	Elapsed Time (s)	Ratio (outflow to inflow)	Change in Head (Not to exceed 25%)	k_{sat} T°C (cm/s)	k_{sat} Corrected (cm/s)
Test # 1:											
20-Mar-07	14:23:21	24.2	1.20	19.60	9.18	0.30	197	1.00	2%	8.68E-06	7.86E-06
20-Mar-07	14:26:38	24.2	1.55	19.25	8.97						
Test # 2:											
20-Mar-07	14:26:38	24.2	1.55	19.25	8.97	0.39	237	1.00	3%	9.53E-06	8.63E-06
20-Mar-07	14:30:35	24.2	2.00	18.80	8.70						
Test # 3:											
20-Mar-07	14:30:35	24.2	2.00	18.80	8.70	0.22	146	1.00	2%	8.80E-06	7.97E-06
20-Mar-07	14:33:01	24.2	2.25	18.55	8.55						
Test # 4:											
20-Mar-07	14:33:01	24.2	2.25	18.55	8.55	0.35	230	1.00	3%	9.15E-06	8.28E-06
20-Mar-07	14:36:51	24.2	2.65	18.15	8.31						

***Average Ksat* (cm/sec):** **8.19E-06**
Calculated Gravel Corrected Average Ksat (cm/sec): ---

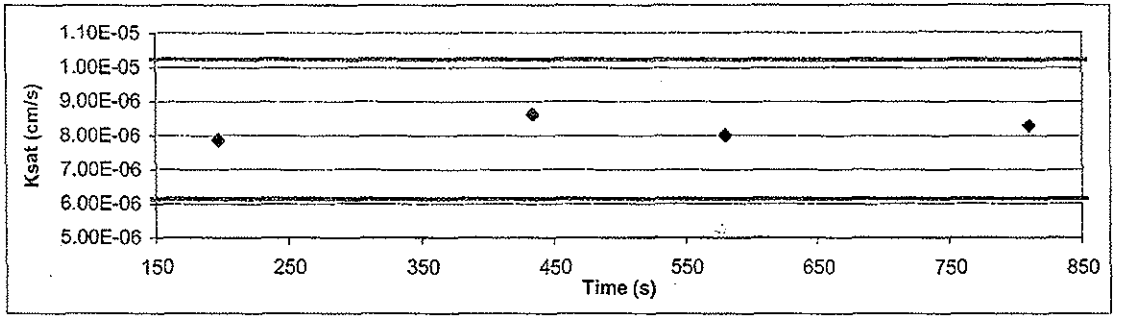

ASTM Required Range (+/- 25%)

Ksat (-25%) (cm/s): 6.14E-06

Ksat (+25%) (cm/s): 1.02E-05

Moisture Retention Characteristics

Summary of Moisture Characteristics of the Initial Drainage Curve

Sample Number	Pressure Head (-cm water)	Moisture Content (%, cm^3/cm^3)
MW-23 55.5-56.0	0	18.2
	13	17.7
	35	17.6
	100	15.8
	510	8.5
	15195	3.2
	42832	2.1
	851293	0.3
MW-23 74.3-74.6	0	12.3
	14	12.3
	56	12.2
	155	11.9
	510	11.7
	43851	4.9
	851293	1.6
MW-23 82.7-82.9	0	16.3
	12	15.3
	38	15.3
	97	14.9
	510	9.6
	23557	3.4
	851293	0.3
MW-23 103.3-103.5	0	20.4
	8	19.3
	24	19.2
	85	14.0
	510	6.8
	16827	3.3
	32838	2.5
	851293	0.6

Summary of Moisture Characteristics of the Initial Drainage Curve (Continued)

Sample Number	Pressure Head (-cm water)	Moisture Content (%, cm^3/cm^3)
MW-30 35.5-36.0	0	19.5
	7	19.2
	20	19.0
	74	14.1
	510	7.6
	23251	2.6
	35081	2.1
	851293	0.4
MW-30 44.0-44.5	0	27.9
	35	26.7
	101	24.7
	197	23.6
	510	20.5
	23353	10.9
	851293	3.4
MW-30 44.0-44.5 (Volume Adjusted)	0	26.7
	35	25.6
	101	23.5
	197	22.4
	510	19.4
	23353	10.4
	851293	3.2

Summary of Calculated Unsaturated Hydraulic Properties

Sample Number	α (cm^{-1})	N (dimensionless)	θ_r (% vol)	θ_s (% vol)	Oversize Corrected θ_r (% vol)	Oversize Corrected θ_s (% vol)
MW-23 55.5-56.0	0.0103	1.3860	0.00	18.38	NA	NA
MW-23 74.3-74.6	0.0003	1.3544	0.00	12.16	NA	NA
MW-23 82.7-82.9	0.0069	1.3362	0.00	16.01	NA	NA
MW-23 103.3-103.5	0.0287	1.3494	0.00	20.51	NA	NA
MW-30 35.5-36.0	0.0266	1.3480	0.00	19.86	NA	NA
MW-30 44.0-44.5	0.0074	1.2019	0.00	27.59	NA	NA
MW-30 44.0-44.5 (Volume Adjusted)	0.0081	1.2006	0.00	26.43	NA	NA

--- = Oversize correction is unnecessary since coarse fraction < 5% of composite mass

NA = Not analyzed

Moisture Retention Data

Hanging Column/Pressure Plate/Thermocouple

Job Name: MWH AMERICAS, INC.
Job Number: LB07.0048.00
Sample Number: MW-23 55.5-56.0
Ring Number: NA
Depth: 55.5-56.0

Dry wt. of sample (g): 171.46
Tare wt., ring (g): 0.00
Tare wt., screen & clamp (g): 0.00
Sample volume (cm^3): 84.63

Saturated weight at 0 cm tension* (g): 186.87
Volume of water† in saturated sample (cm^3): 15.41
Saturated moisture content (% vol): 18.21
Sample bulk density (g/cm^3): 2.03

	Date/Time	Weight* (g)	Matric Potential (-cm water)	Moisture Content† (% vol)
Hanging column:	21-Mar-07 / 10:45	186.87	0.00	18.21
	27-Mar-07 / 10:10	186.47	12.50	17.74
	02-Apr-07 / 08:47	186.38	34.50	17.63
	10-Apr-07 / 13:05	184.81	99.80	15.77
Pressure plate:	19-Apr-07 / 08:35	178.62	509.90	8.46

Comments:

* Weight including tares

† Assumed density of water is 1.0 g/cm^3

Laboratory analysis by: D. O'Dowd
Data entered by: T. Bowekaty
Checked by: J. Hines

Moisture Retention Data

Water Activity Meter/Relative Humidity Box

Job Name: MWH AMERICAS, INC.
Job Number: LB07.0048.00
Sample Number: MW-23 55.5-56.0
Ring Number: NA
Depth: 55.5-56.0

Dry weight of water activity meter sample* (g): 246.44
Tare weight, jar (g): 199.21
Sample bulk density (g/cm^3): 2.03

	Date/Time	Weight* (g)	Matric Potential (-cm water)	Moisture Content† (% vol)
Water Activity Meter:	16-Apr-07 / 11:03	247.19	15195.0	3.22
	13-Apr-07 / 14:45	246.94	42831.6	2.14

Dry weight of relative humidity box sample* (g): 82.32
Tare weight (g): 39.51
Sample bulk density (g/cm^3): 2.03

	Date/Time	Weight* (g)	Matric Potential (-cm water)	Moisture Content† (% vol)
Relative humidity box:	21-Mar-07 / 12:00	82.39	851293	0.32

Comments:

* Weight including tares
† Assumed density of water is 1.0 g/cm^3

Laboratory analysis by: C. Krous/D. O'Dowd
Data entered by: T. Bowekaty
Checked by: J. Hines

Water Retention Data Points

Sample Number: MW-23 55.5-56.0

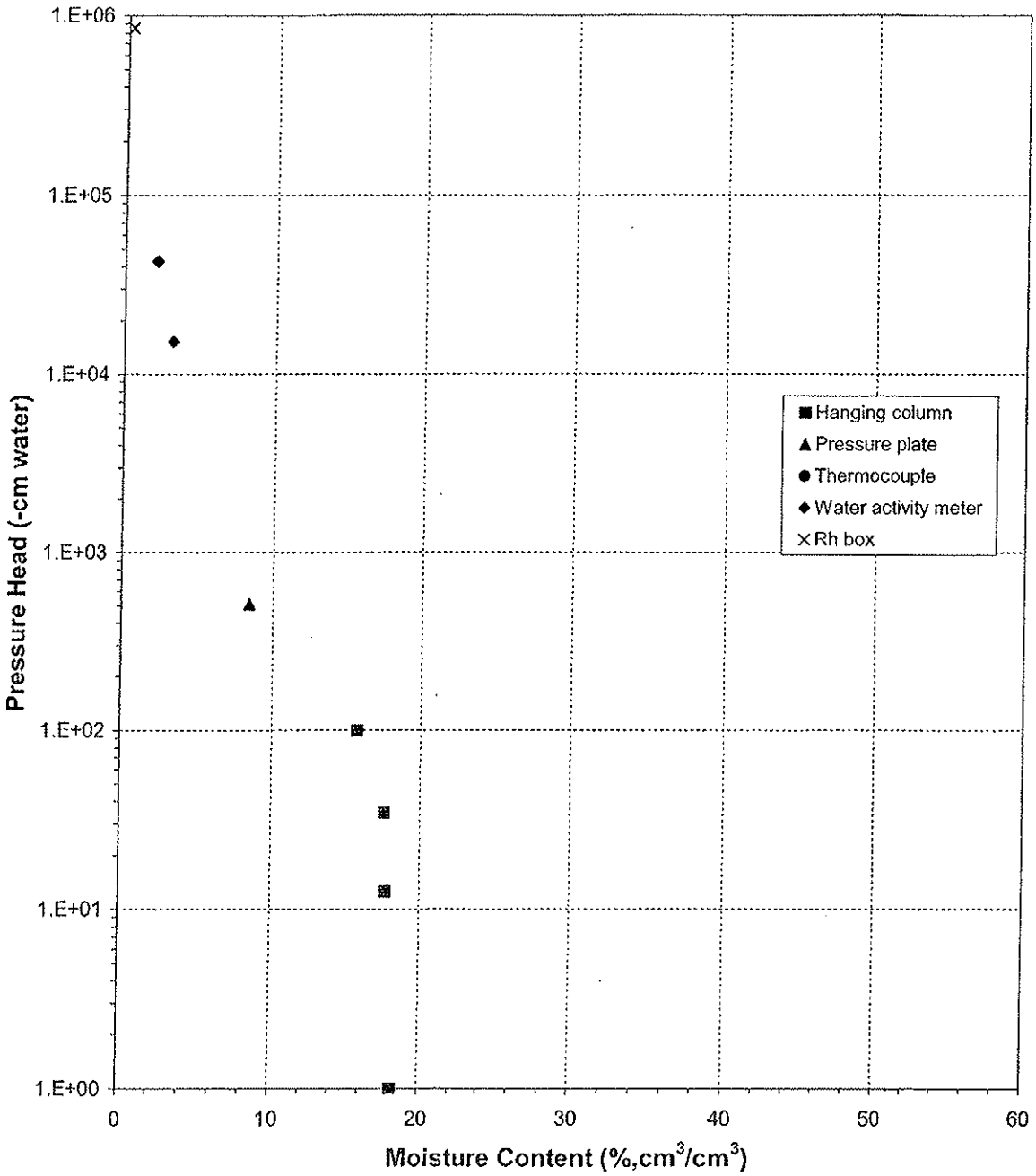

Predicted Water Retention Curve and Data Points

Sample Number: MW-23 55.5-56.0

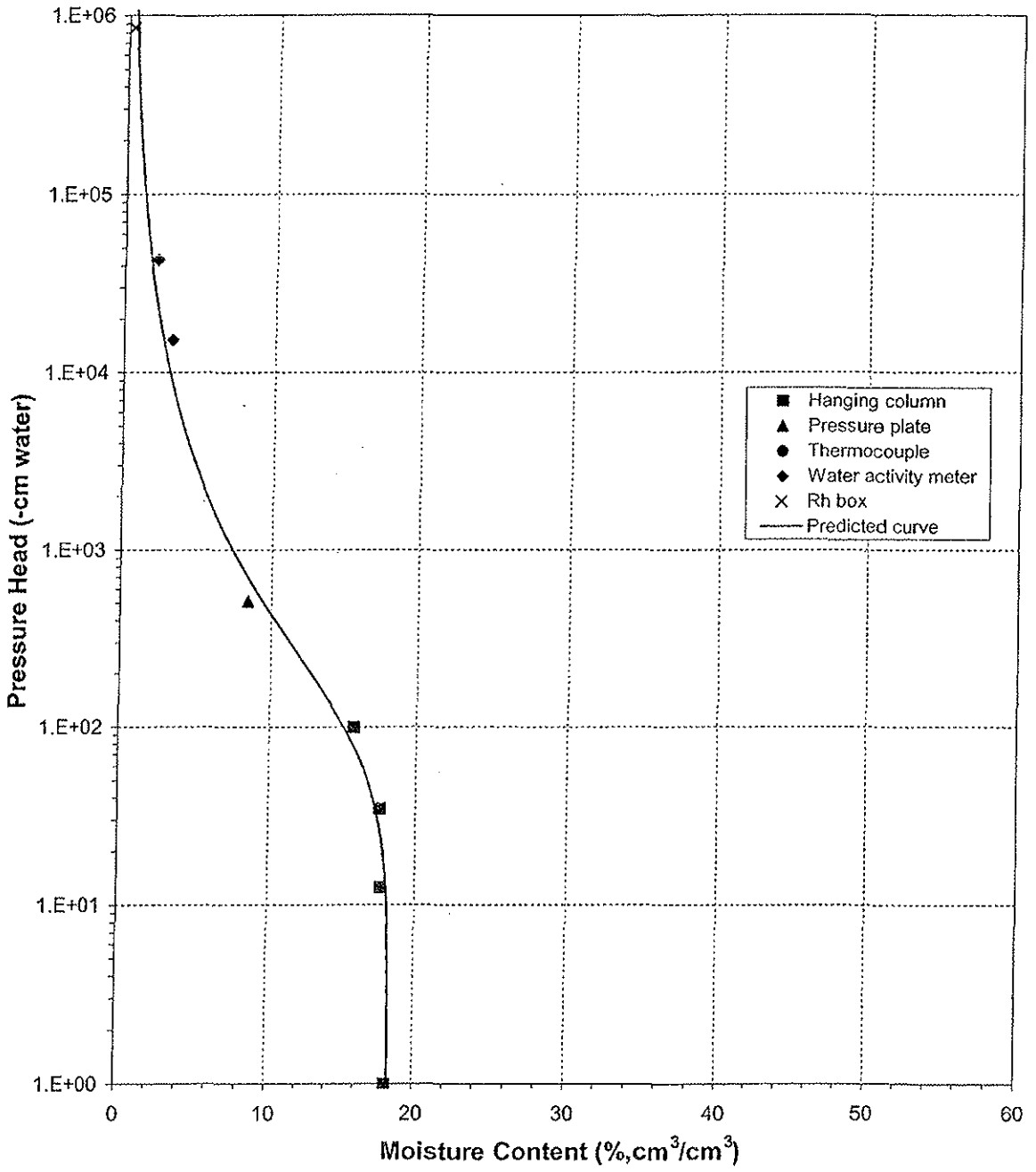

Plot of Relative Hydraulic Conductivity vs Moisture Content

Sample Number: MW-23 55.5-56.0

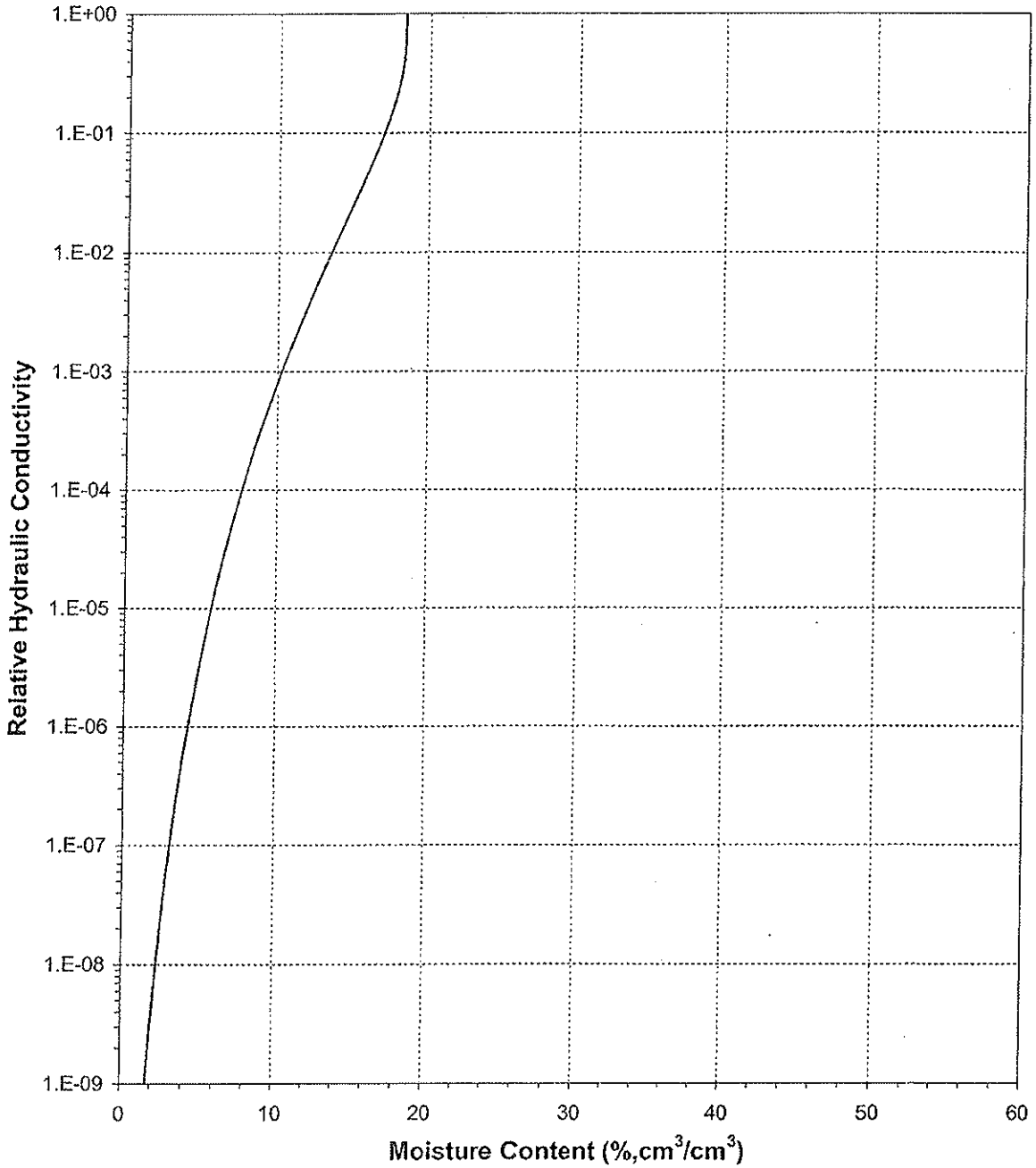

Plot of Hydraulic Conductivity vs Moisture Content

Sample Number: MW-23 55.5-56.0

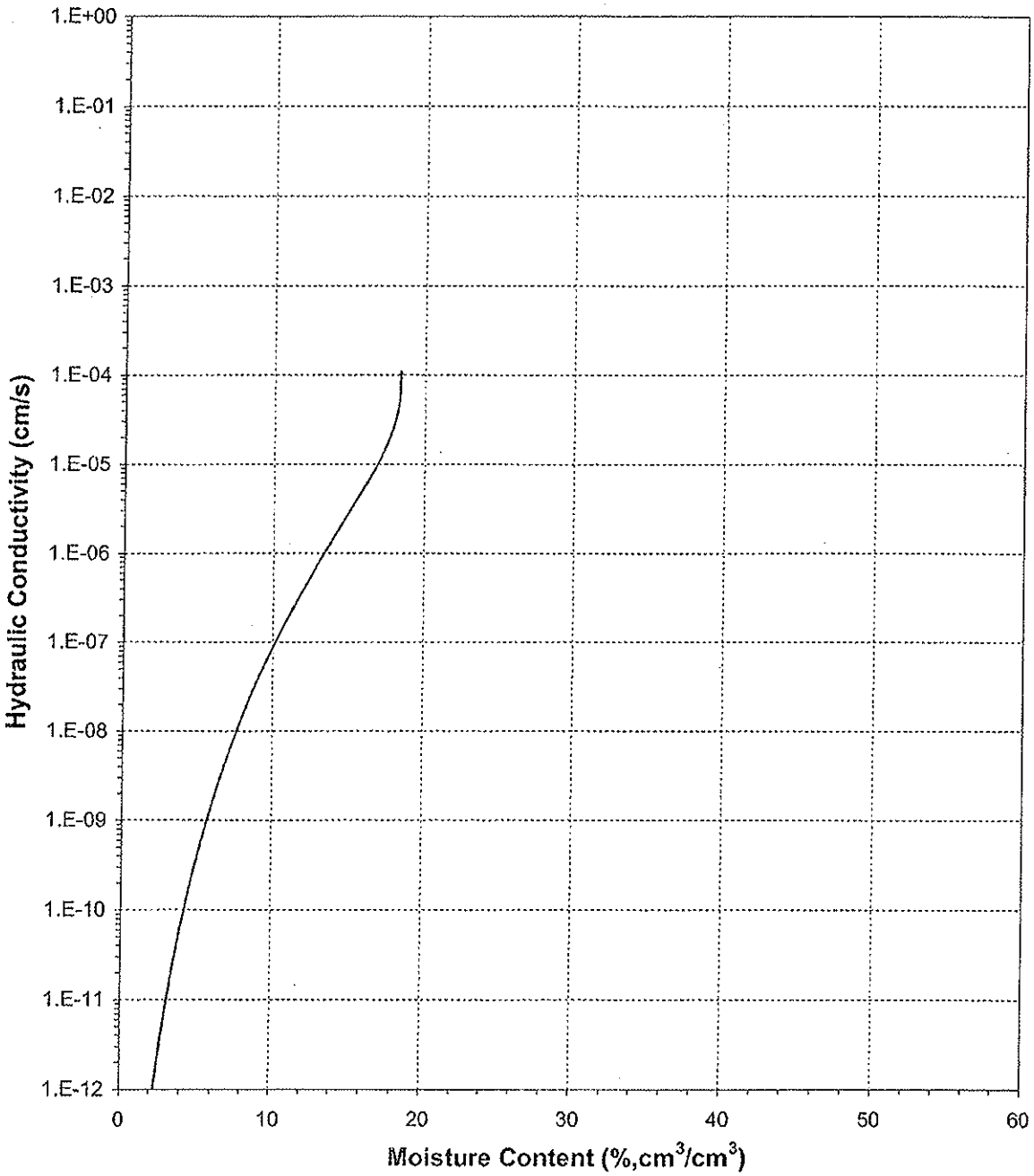

Plot of Relative Hydraulic Conductivity vs Pressure Head

Sample Number: MW-23 55.5-56.0

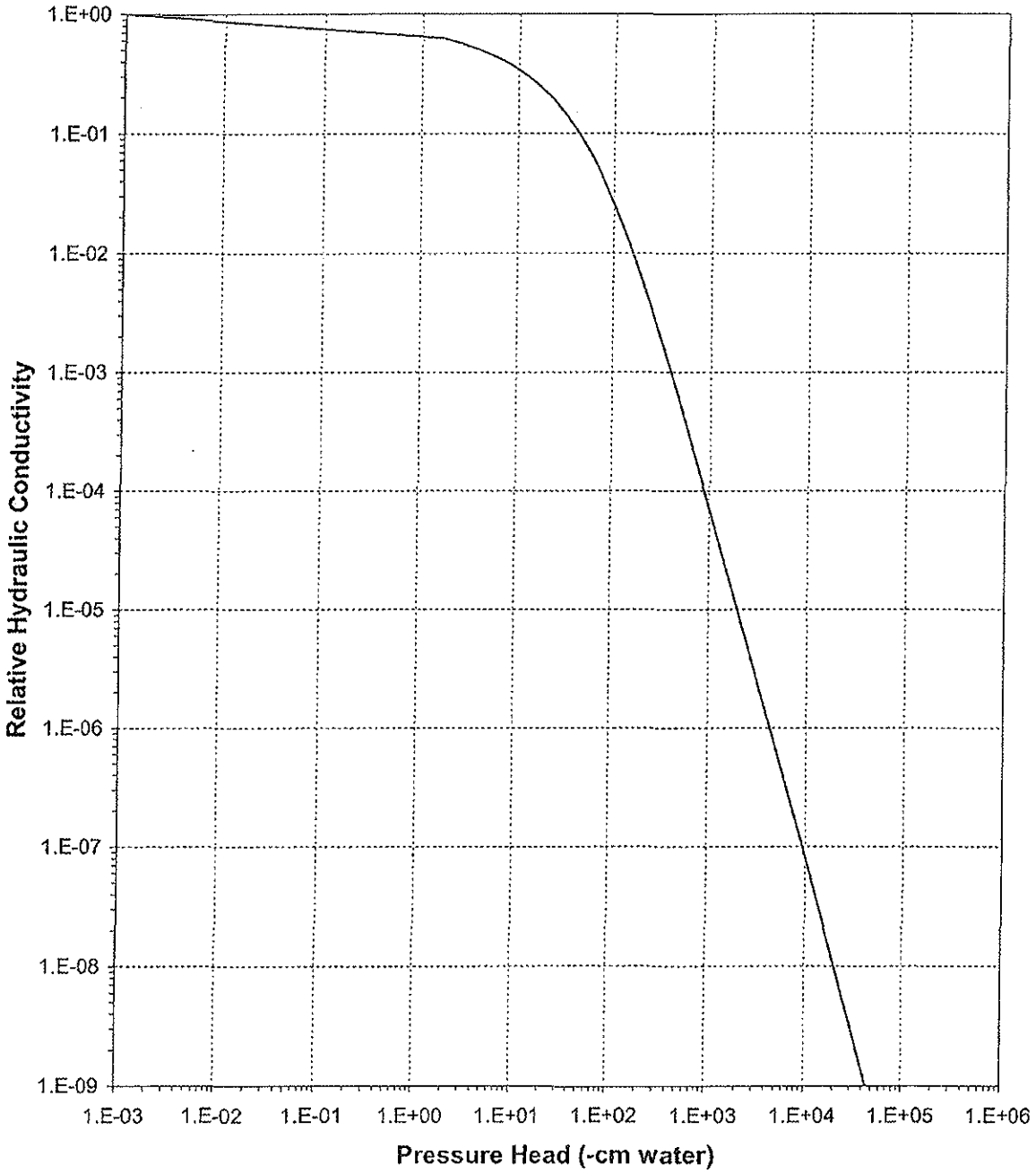

Plot of Hydraulic Conductivity vs Pressure Head

Sample Number: MW-23 55.5-56.0

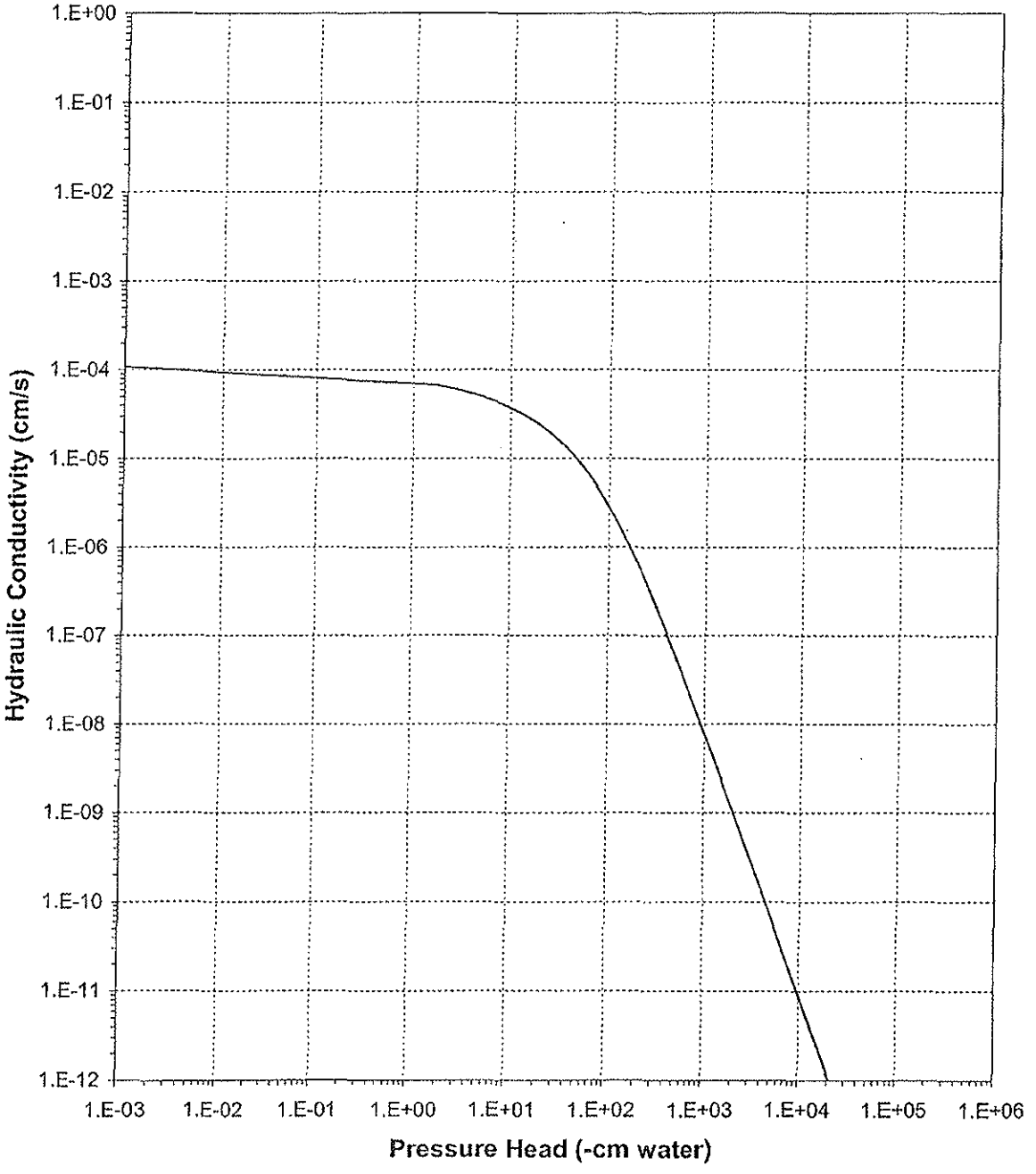

Daniel B. Stephens & Associates, Inc.

Moisture Retention Data

Hanging Column/Pressure Plate/Thermocouple

Job Name: MWH AMERICAS, INC.
Job Number: LB07.0048.00
Sample Number: MW-23 74.3-74.6
Ring Number: NA
Depth: 74.3-74.6

Dry wt. of sample (g): 161.11
Tare wt., ring (g): 0.00
Tare wt., screen & clamp (g): 0.00
Sample volume (cm^3): 69.19

Saturated weight at 0 cm tension* (g): 169.61
Volume of water† in saturated sample (cm^3): 8.50
Saturated moisture content (% vol): 12.29
Sample bulk density (g/cm^3): 2.33

	Date/Time	Weight* (g)	Matric Potential (-cm water)	Moisture Content† (% vol)
Hanging column:	21-Mar-07 / 10:45	169.61	0.00	12.29
	27-Mar-07 / 10:20	169.60	14.10	12.27
	02-Apr-07 / 08:50	169.58	56.40	12.24
	10-Apr-07 / 13:40	169.35	155.00	11.91
Pressure plate:	19-Apr-07 / 08:30	169.23	509.90	11.74

Comments:

* Weight including tares

† Assumed density of water is 1.0 g/cm^3

Laboratory analysis by: D. O'Dowd
Data entered by: T. Bowekaty
Checked by: J. Hines

Moisture Retention Data

Water Activity Meter/Relative Humidity Box

Job Name: MWH AMERICAS, INC.
Job Number: LB07.0048.00
Sample Number: MW-23 74.3-74.6
Ring Number: NA
Depth: 74.3-74.6

Dry weight of water activity meter sample* (g): 246.06
Tare weight, jar (g): 197.61
Sample bulk density (g/cm^3): 2.33

	Date/Time	Weight* (g)	Matric Potential (-cm water)	Moisture Content† (% vol)
Water Activity Meter:	13-Apr-07 / 16:14	247.08	43851.4	4.90

Dry weight of relative humidity box sample* (g): 94.13
Tare weight (g): 41.67
Sample bulk density (g/cm^3): 2.33

	Date/Time	Weight* (g)	Matric Potential (-cm water)	Moisture Content† (% vol)
Relative humidity box:	21-Mar-07 / 12:00	94.49	851293	1.60

Comments:

* Weight including tares
† Assumed density of water is 1.0 g/cm^3

Laboratory analysis by: C. Krous/D. O'Dowd
Data entered by: T. Bowekaty
Checked by: J. Hines

Water Retention Data Points

Sample Number: MW-23 74.3-74.6

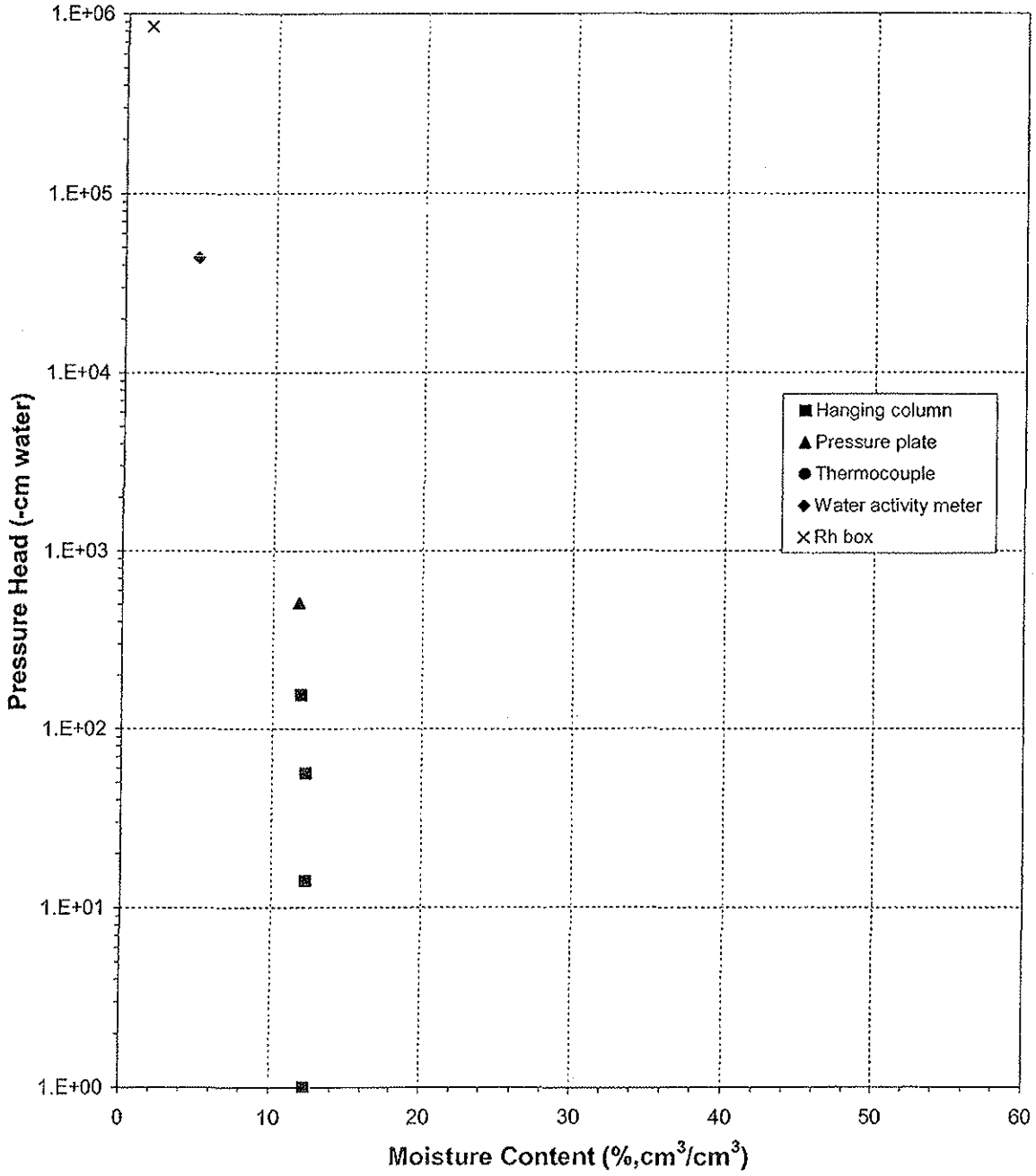

Predicted Water Retention Curve and Data Points

Sample Number: MW-23 74.3-74.6

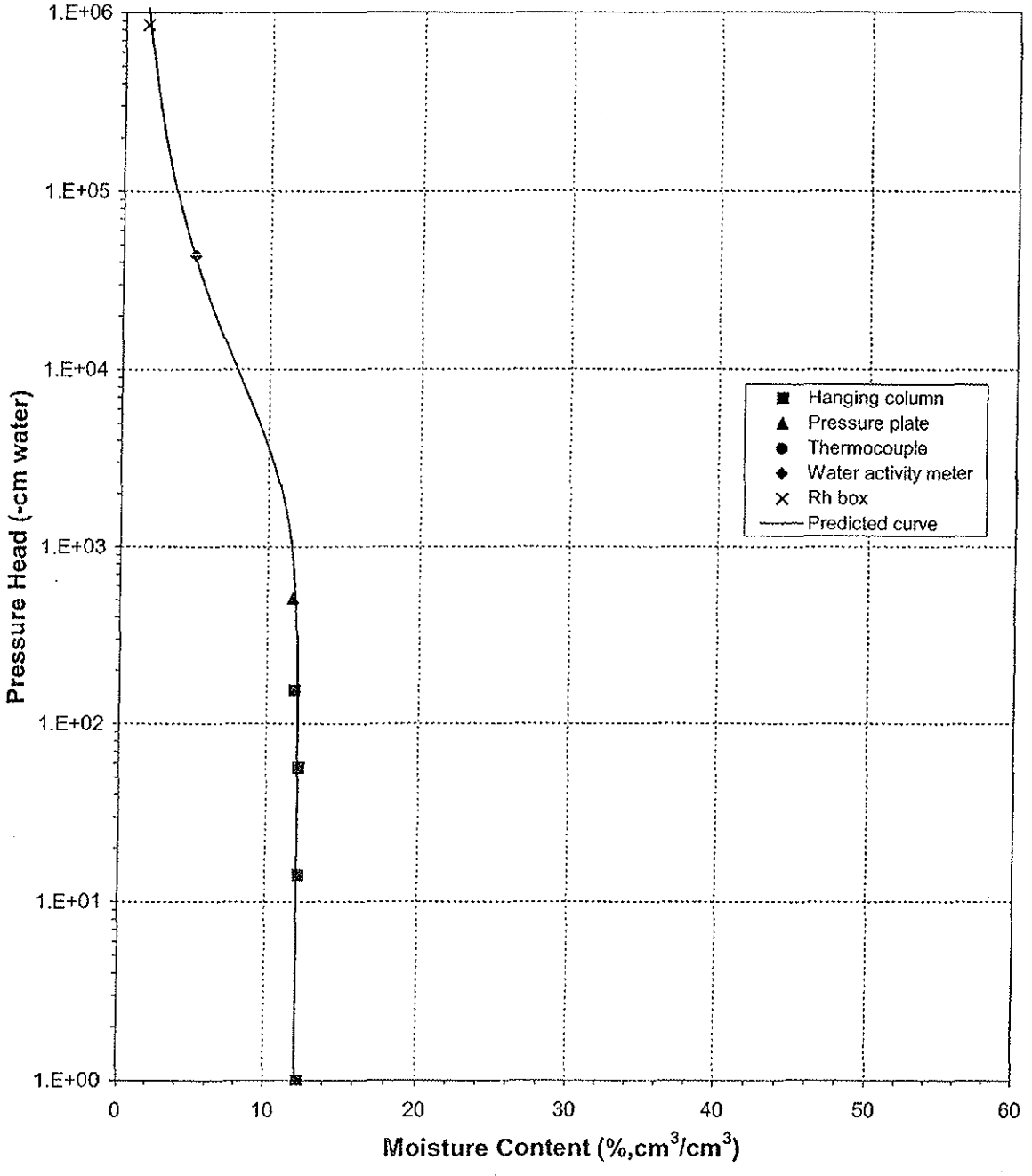

Plot of Relative Hydraulic Conductivity vs Moisture Content

Sample Number: MW-23 74.3-74.6

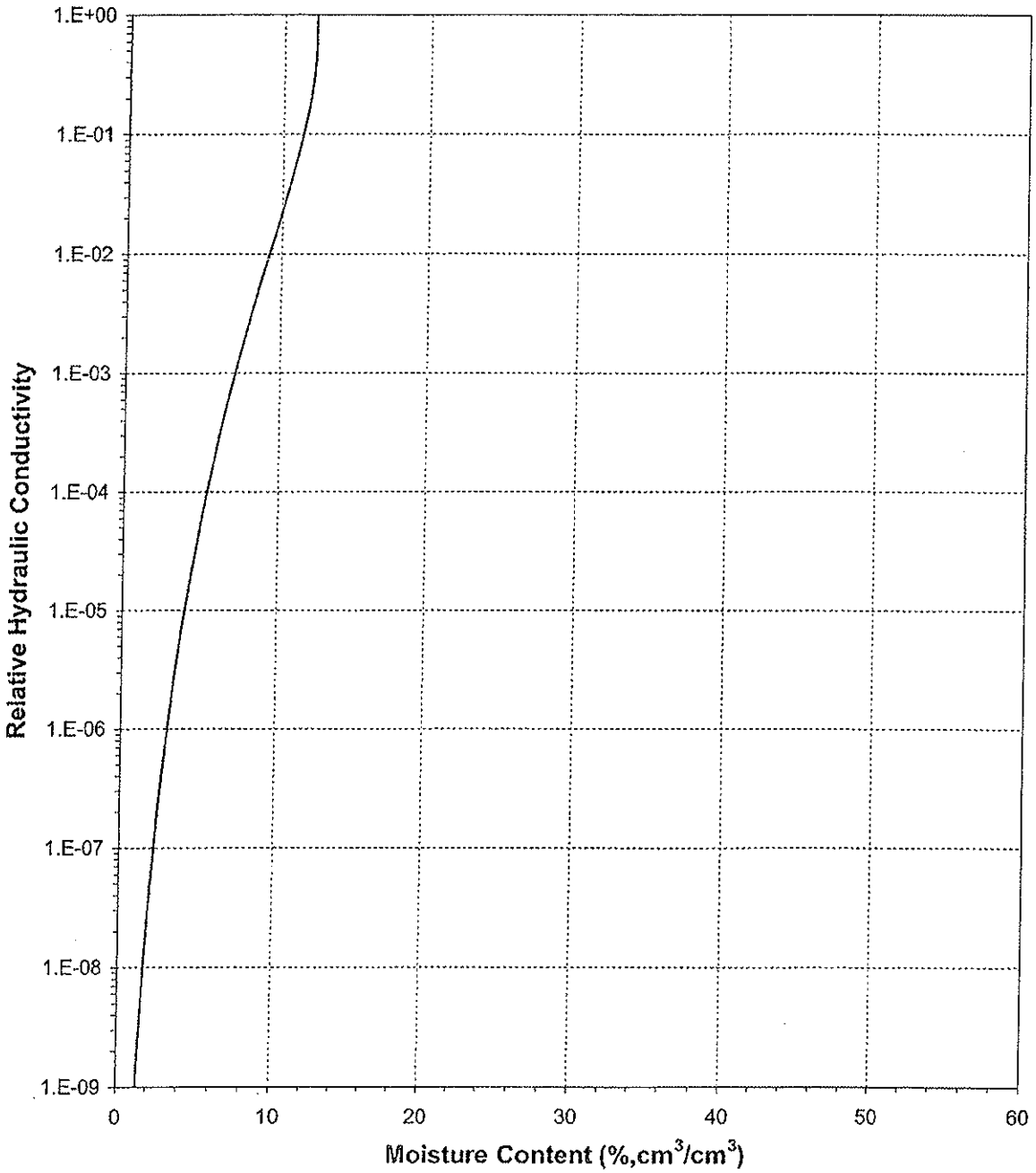

Plot of Hydraulic Conductivity vs Moisture Content

Sample Number: MW-23 74.3-74.6

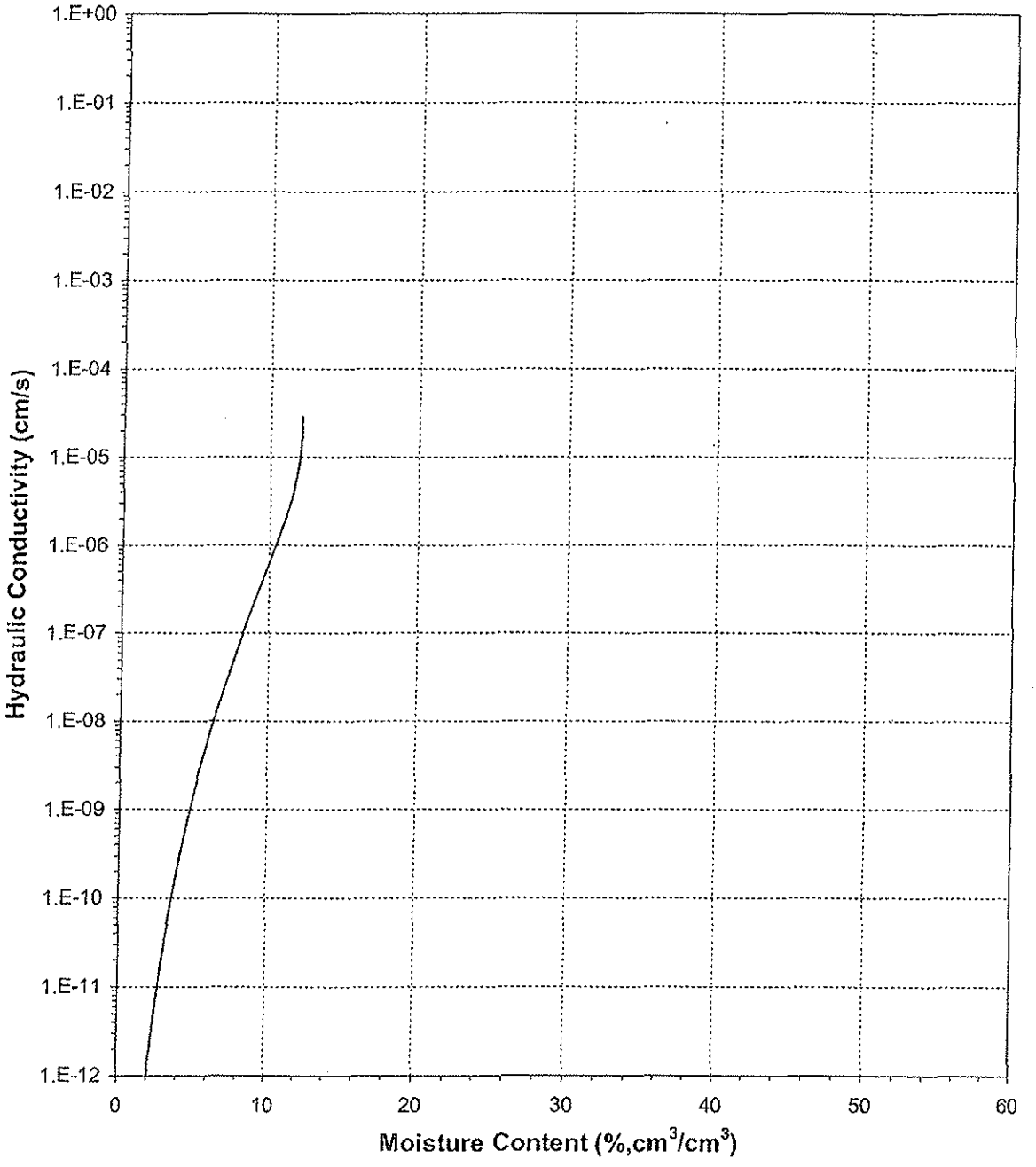

Plot of Relative Hydraulic Conductivity vs Pressure Head

Sample Number: MW-23 74.3-74.6

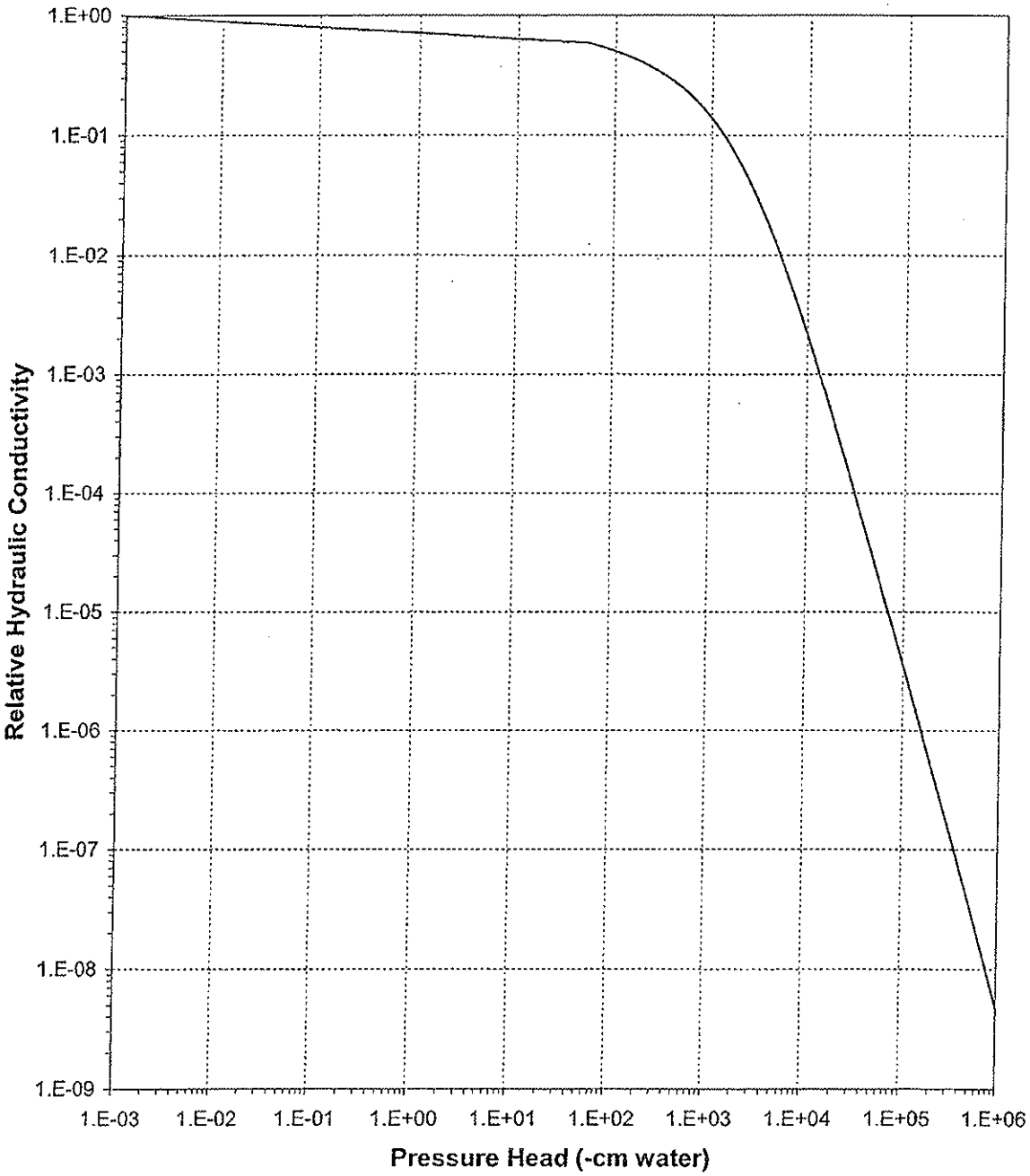

Plot of Hydraulic Conductivity vs Pressure Head

Sample Number: MW-23 74.3-74.6

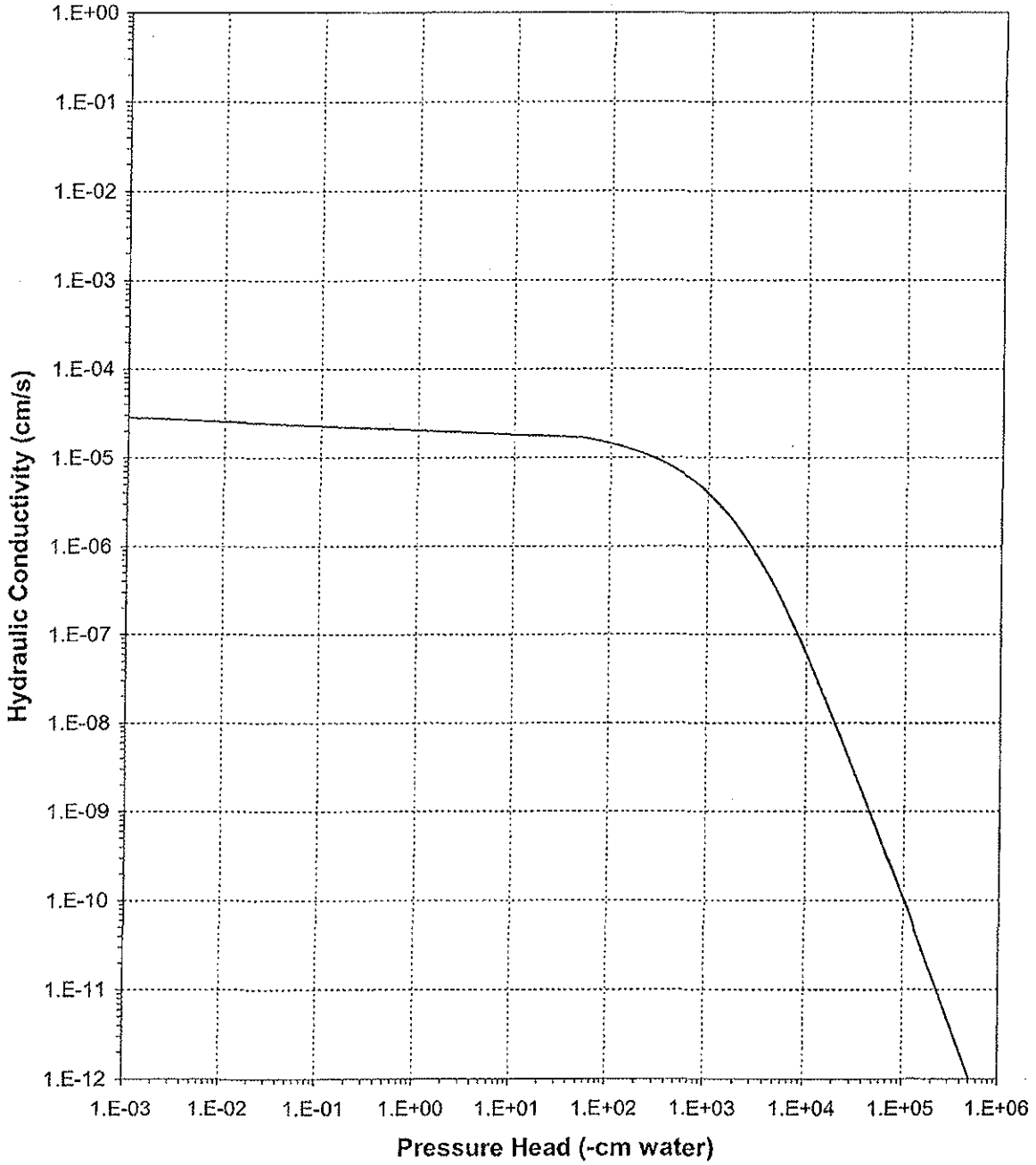

Daniel B. Stephens & Associates, Inc.

Moisture Retention Data

Hanging Column/Pressure Plate/Thermocouple

Job Name: MWH AMERICAS, INC.
Job Number: LB07.0048.00
Sample Number: MW-23 82.7-82.9
Ring Number: NA
Depth: 82.7-82.9

Dry wt. of sample (g): 151.98
Tare wt., ring (g): 0.00
Tare wt., screen & clamp (g): 0.00
Sample volume (cm^3): 72.35

Saturated weight at 0 cm tension* (g): 163.80
Volume of water† in saturated sample (cm^3): 11.82
Saturated moisture content (% vol): 16.34
Sample bulk density (g/cm^3): 2.10

	Date/Time	Weight* (g)	Matric Potential (-cm water)	Moisture Content† (% vol)
Hanging column:	19-Mar-07 / 15:30	163.80	0.00	16.34
	25-Mar-07 / 15:00	163.08	11.80	15.34
	31-Mar-07 / 08:15	163.02	38.00	15.26
	10-Apr-07 / 13:10	162.73	96.50	14.86
Pressure plate:	19-Apr-07 / 08:40	158.95	509.90	9.63

Comments:

* Weight including tares

† Assumed density of water is 1.0 g/cm^3

Laboratory analysis by: D. O'Dowd
Data entered by: T. Bowekaty
Checked by: J. Hines

Moisture Retention Data

Water Activity Meter/Relative Humidity Box

Job Name: MWH AMERICAS, INC.
Job Number: LB07.0048.00
Sample Number: MW-23 82.7-82.9
Ring Number: NA
Depth: 82.7-82.9

Dry weight of water activity meter sample* (g): 240.86
Tare weight, jar (g): 197.73
Sample bulk density (g/cm^3): 2.10

	Date/Time	Weight* (g)	Matric Potential (-cm water)	Moisture Content† (% vol)
Water Activity Meter:	16-Apr-07 / 11:13	241.56	23557.4	3.41

Dry weight of relative humidity box sample* (g): 64.98
Tare weight (g): 41.87
Sample bulk density (g/cm^3): 2.10

	Date/Time	Weight* (g)	Matric Potential (-cm water)	Moisture Content† (% vol)
Relative humidity box:	22-Mar-07 / 12:00	65.02	851293	0.35

Comments:

* Weight including tares

† Assumed density of water is 1.0 g/cm^3

Laboratory analysis by: C. Krous/D. O'Dowd
Data entered by: T. Bowekaty
Checked by: J. Hines

Water Retention Data Points

Sample Number: MW-23 82.7-82.9

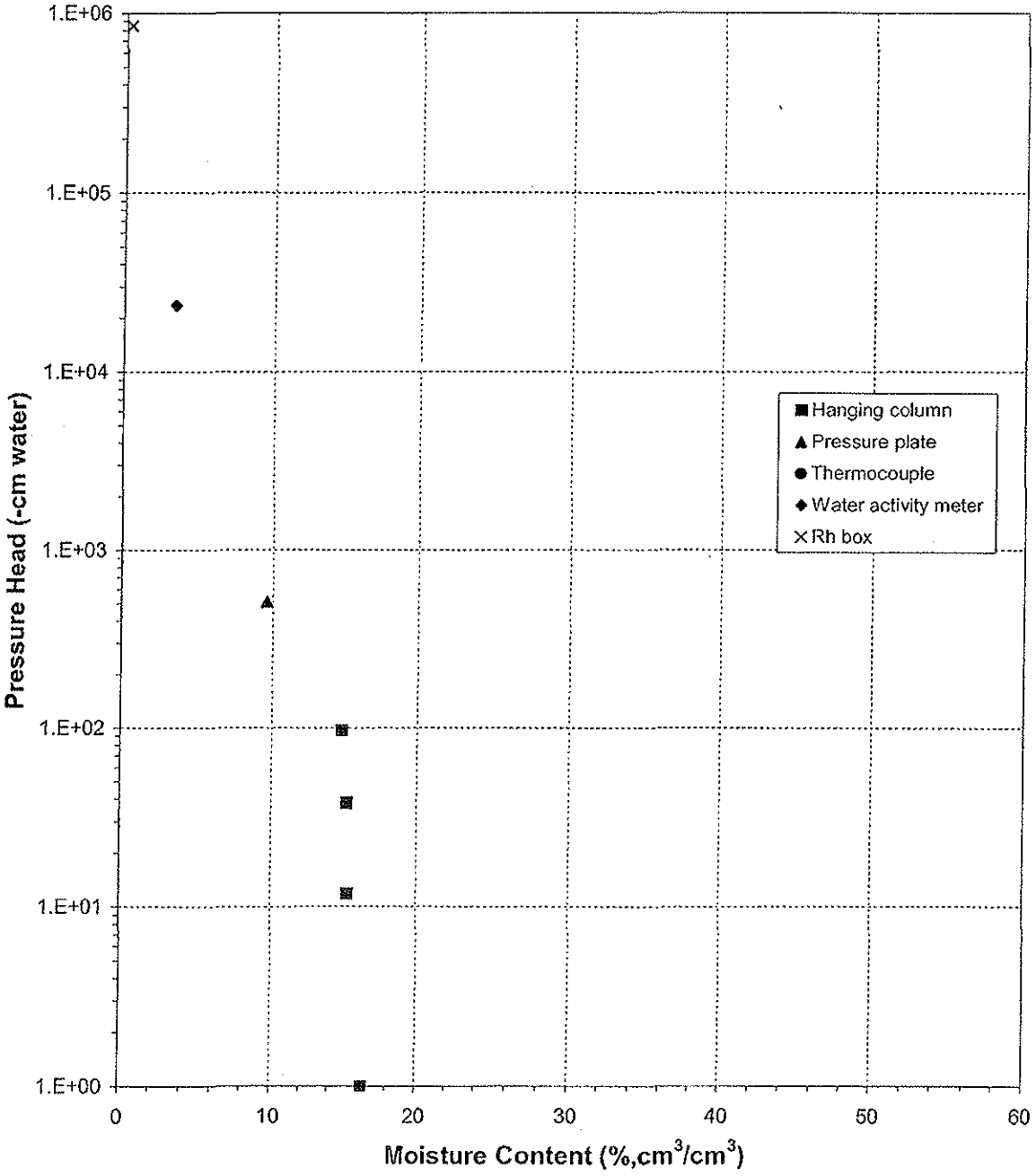

Predicted Water Retention Curve and Data Points

Sample Number: MW-23 82.7-82.9

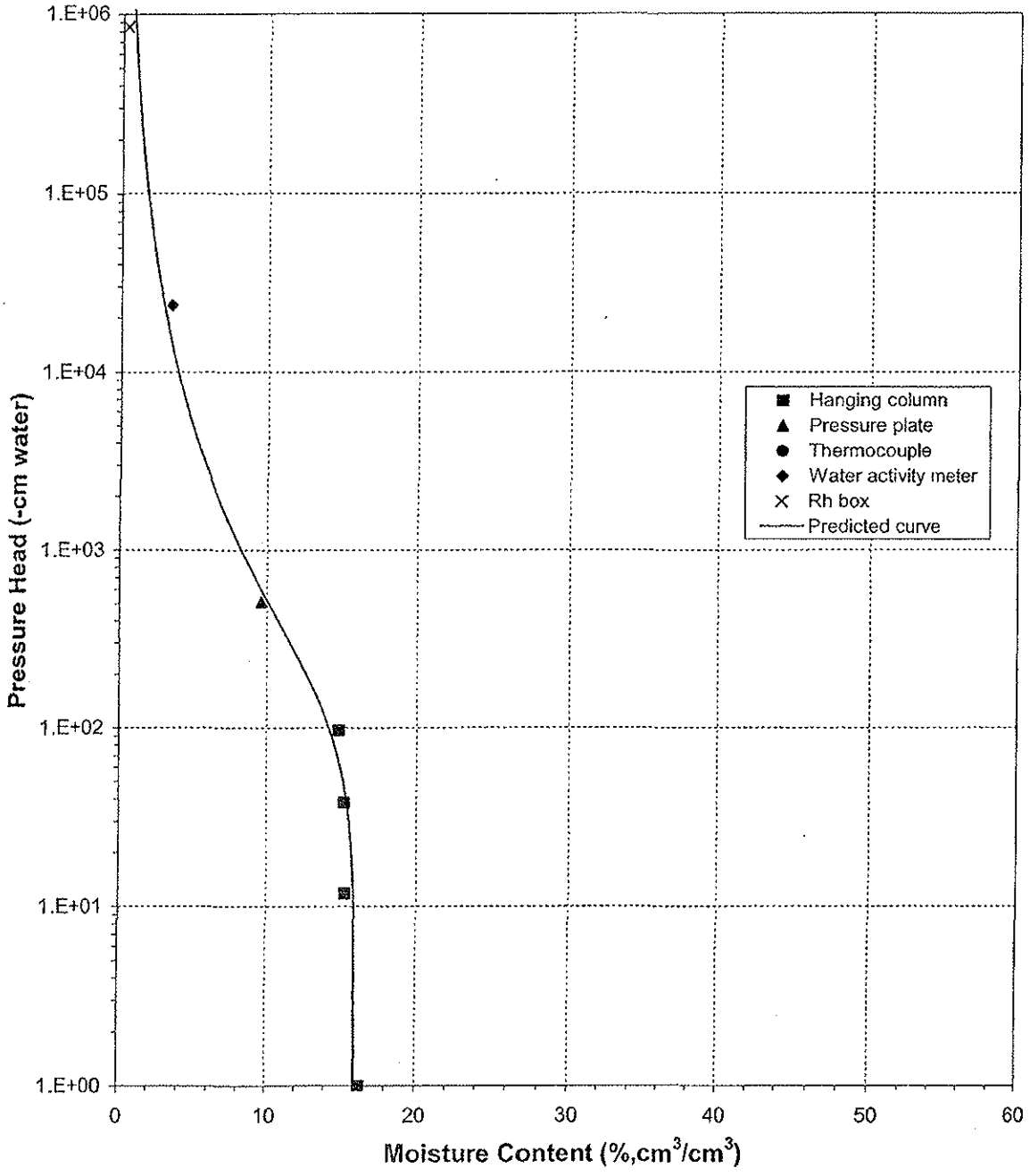

Plot of Relative Hydraulic Conductivity vs Moisture Content

Sample Number: MW-23 82.7-82.9

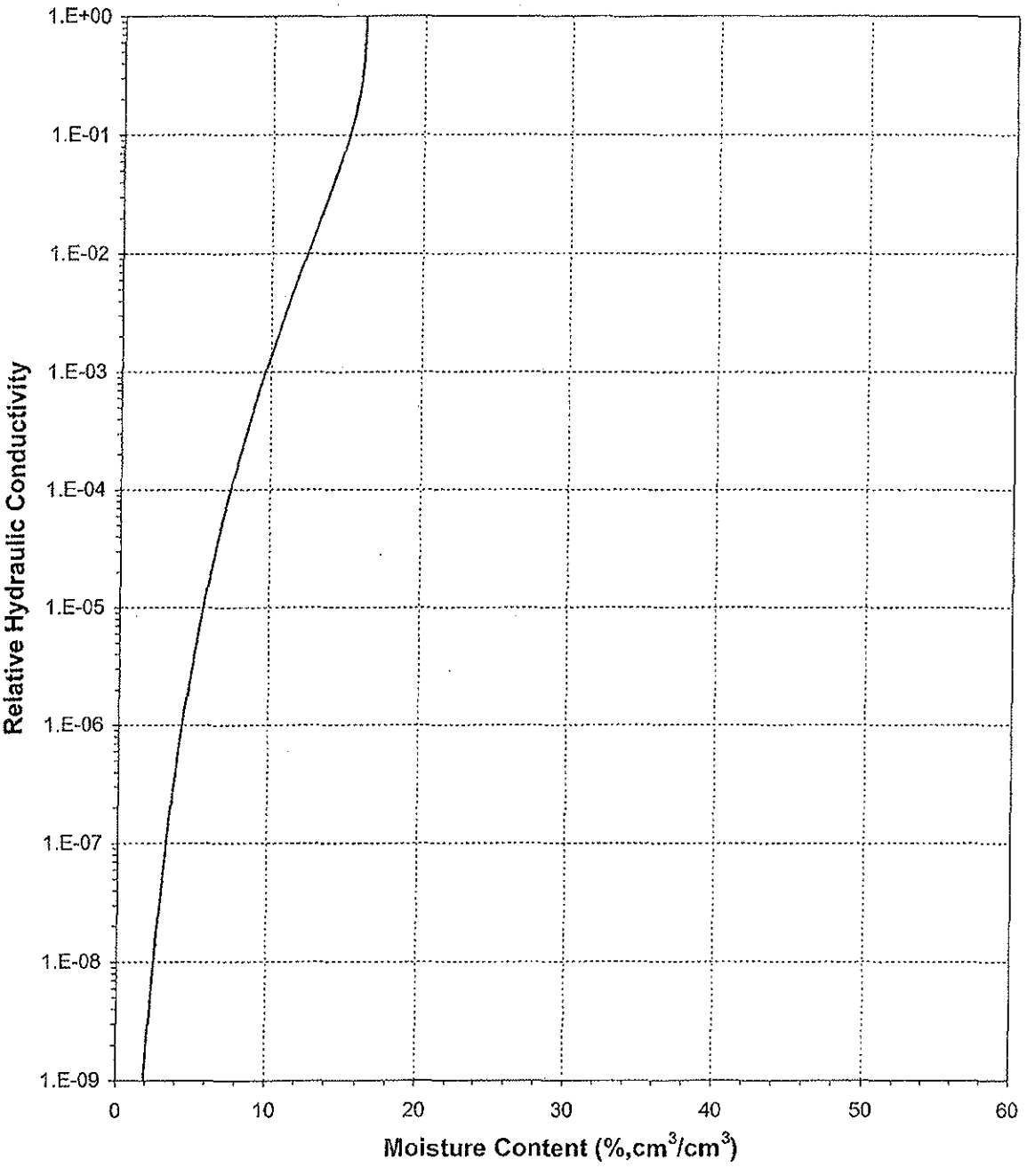

Plot of Hydraulic Conductivity vs Moisture Content

Sample Number: MW-23 82.7-82.9

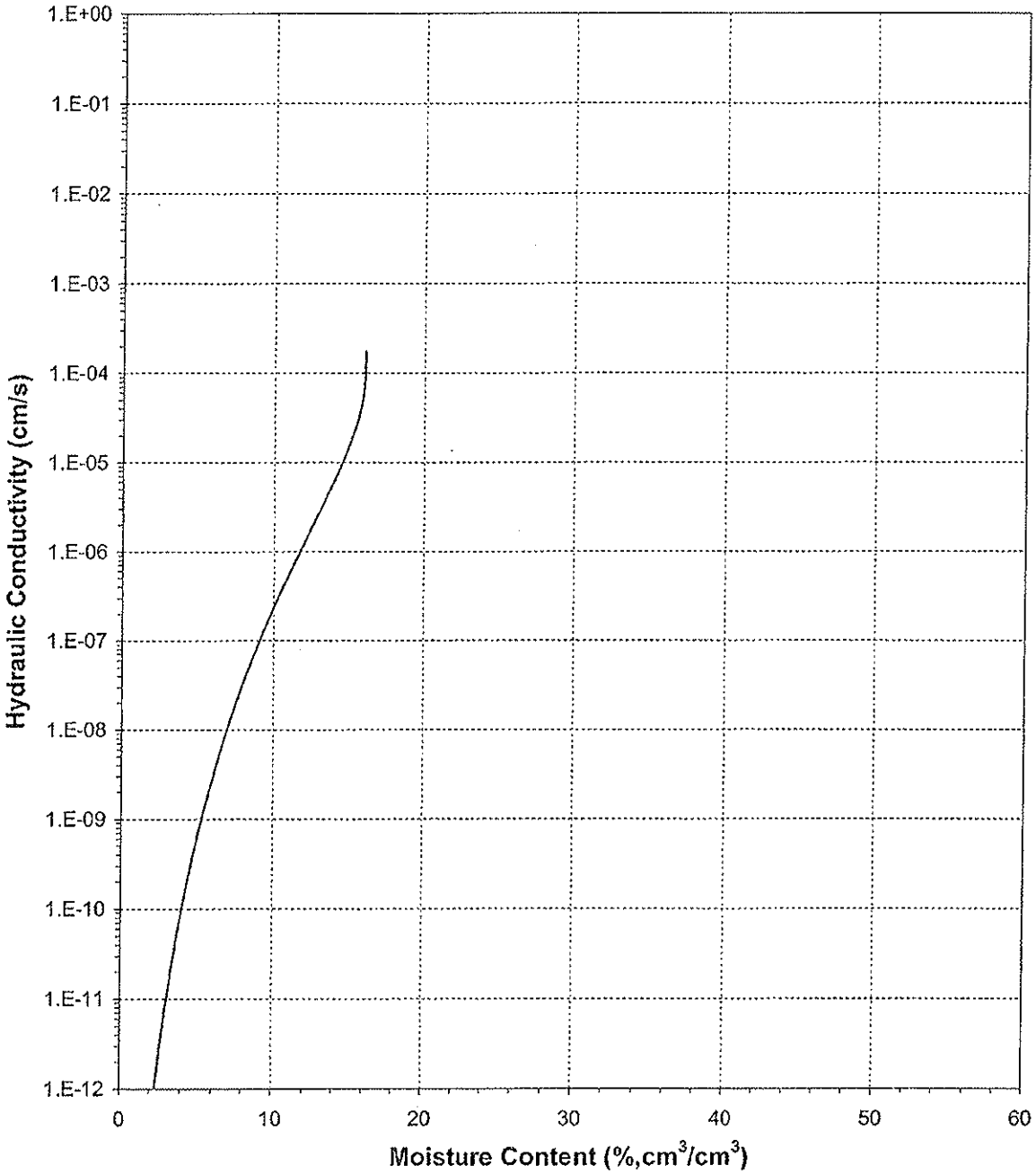

Plot of Relative Hydraulic Conductivity vs Pressure Head

Sample Number: MW-23 82.7-82.9

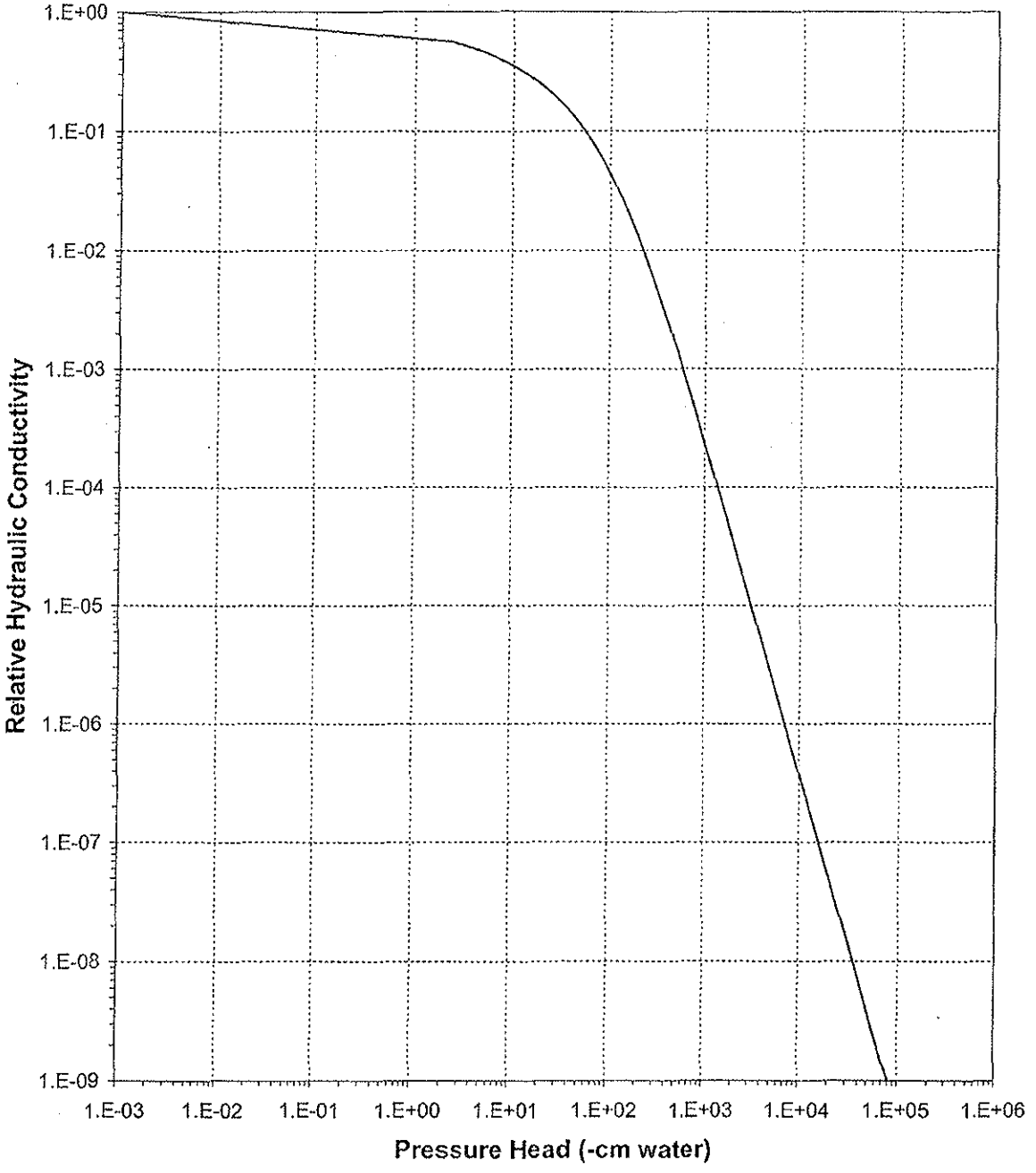

Plot of Hydraulic Conductivity vs Pressure Head

Sample Number: MW-23 82.7-82.9

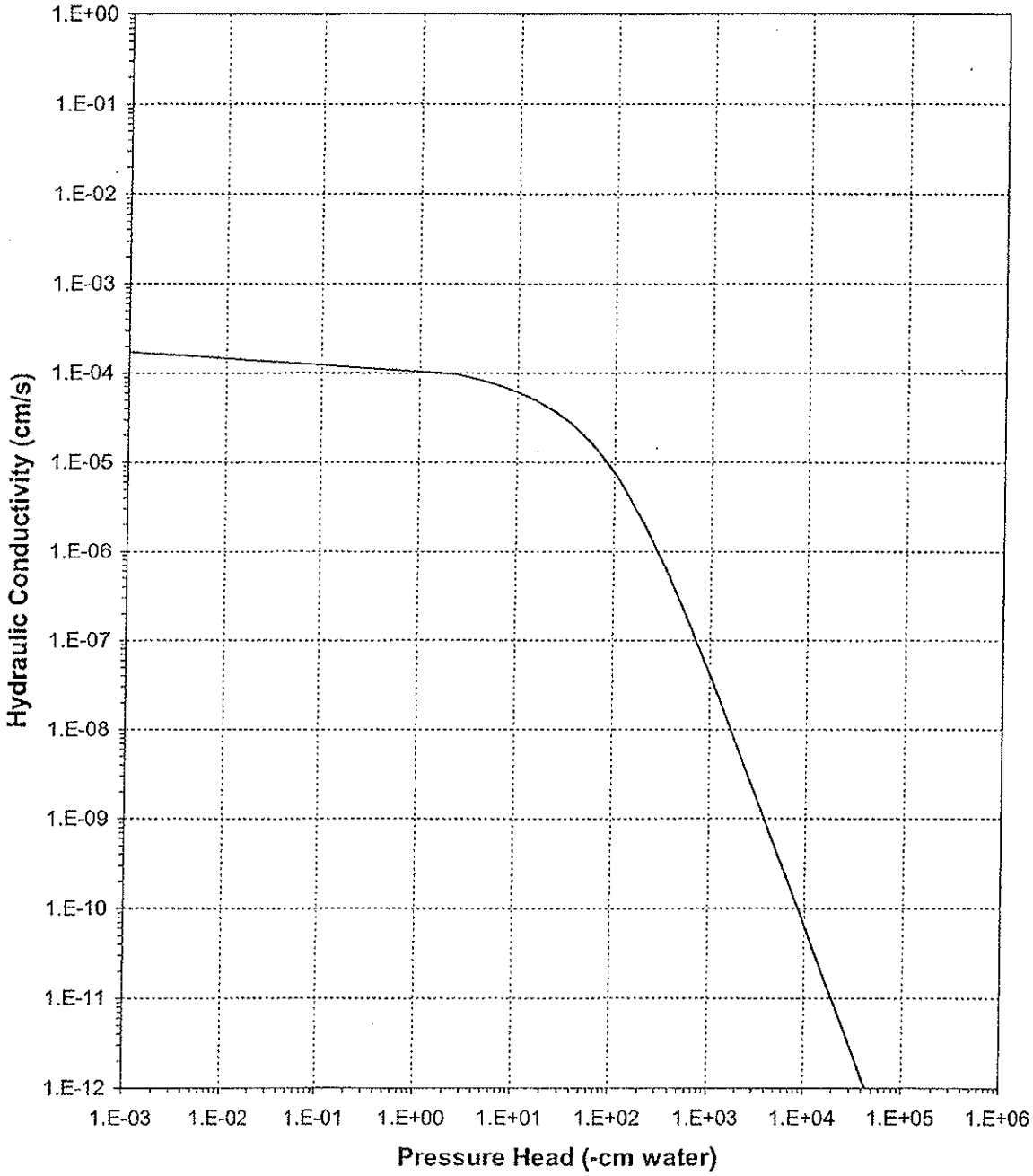

Moisture Retention Data

Hanging Column/Pressure Plate/Thermocouple

Job Name: MWH AMERICAS, INC.
Job Number: LB07.0048.00
Sample Number: MW-23 103.3-103.5
Ring Number: NA
Depth: 103.3-103.5

Dry wt. of sample (g): 126.16
Tare wt., ring (g): 0.00
Tare wt., screen & clamp (g): 0.00
Sample volume (cm^3): 68.67

Saturated weight at 0 cm tension* (g): 140.16
Volume of water† in saturated sample (cm^3): 14.00
Saturated moisture content (% vol): 20.39
Sample bulk density (g/cm^3): 1.84

	Date/Time	Weight* (g)	Matric Potential (-cm water)	Moisture Content† (% vol)
Hanging column:	19-Mar-07 / 15:30	140.16	0.00	20.39
	25-Mar-07 / 15:02	139.41	7.60	19.30
	31-Mar-07 / 08:15	139.36	23.50	19.22
	10-Apr-07 / 13:15	135.79	85.00	14.02
Pressure plate:	19-Apr-07 / 08:40	130.83	509.90	6.80

Comments:

* Weight including tares

† Assumed density of water is 1.0 g/cm^3

Laboratory analysis by: D. O'Dowd
Data entered by: T. Bowekaty
Checked by: J. Hines

Moisture Retention Data

Water Activity Meter/Relative Humidity Box

Job Name: MWH AMERICAS, INC.
Job Number: LB07.0048.00
Sample Number: MW-23 103.3-103.5
Ring Number: NA
Depth: 103.3-103.5

Dry weight of water activity meter sample* (g): 259.47
Tare weight, jar (g): 199.70
Sample bulk density (g/cm^3): 1.84

	Date/Time	Weight* (g)	Matric Potential (-cm water)	Moisture Content† (% vol)
Water Activity Meter:	13-Apr-07 / 16:56	260.54	16826.7	3.29
	12-Apr-07 / 16:29	260.28	32837.6	2.49

Dry weight of relative humidity box sample* (g): 87.89
Tare weight (g): 38.83
Sample bulk density (g/cm^3): 1.84

	Date/Time	Weight* (g)	Matric Potential (-cm water)	Moisture Content† (% vol)
Relative humidity box:	23-Mar-07 / 12:00	88.06	851293	0.63

Comments:

* Weight including tares
† Assumed density of water is 1.0 g/cm^3

Laboratory analysis by: C. Krous/D. O'Dowd
Data entered by: T. Bowekaty
Checked by: J. Hines

Water Retention Data Points

Sample Number: MW-23 103.3-103.5

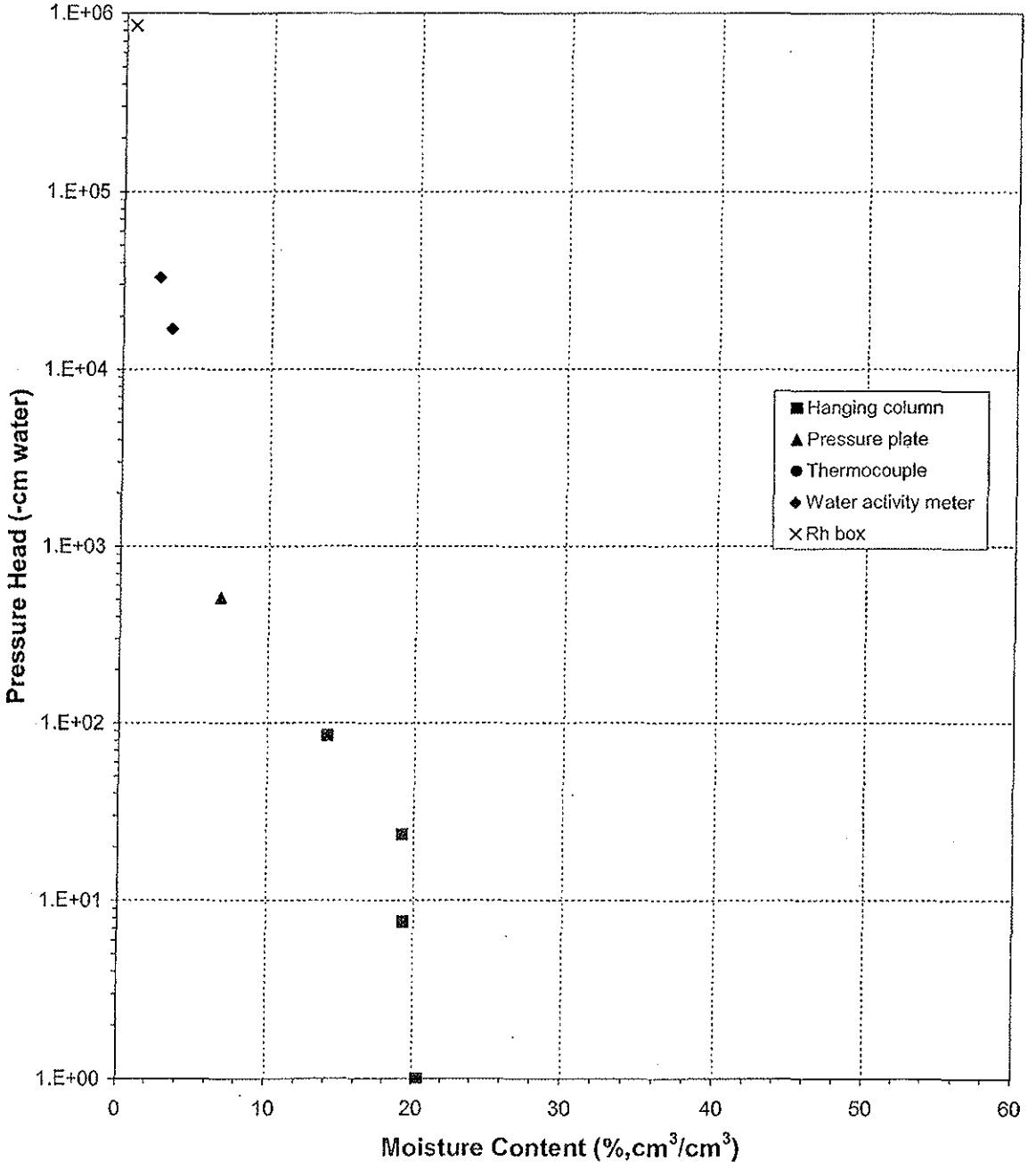

Predicted Water Retention Curve and Data Points

Sample Number: MW-23 103.3-103.5

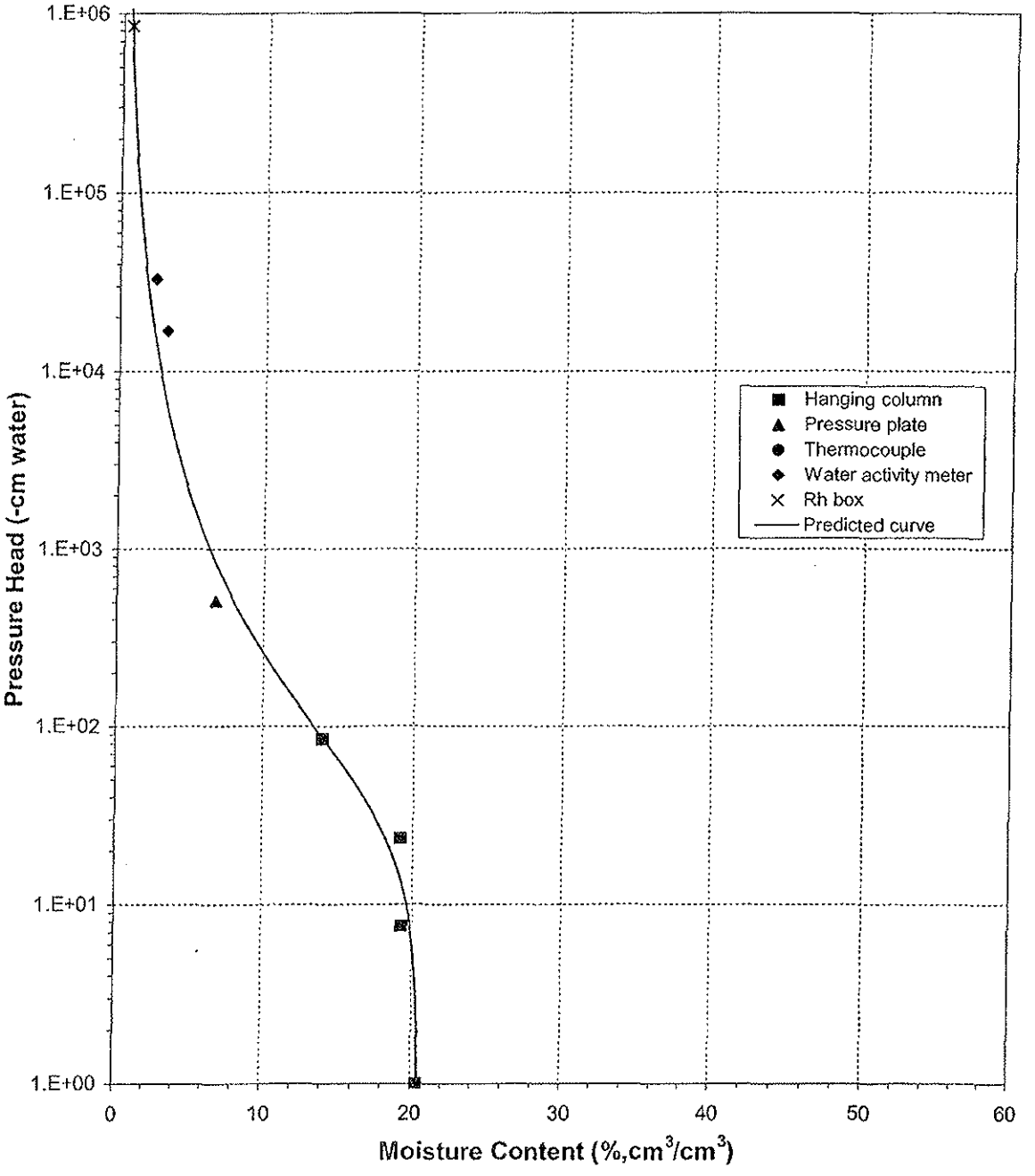

Plot of Relative Hydraulic Conductivity vs Moisture Content

Sample Number: MW-23 103.3-103.5

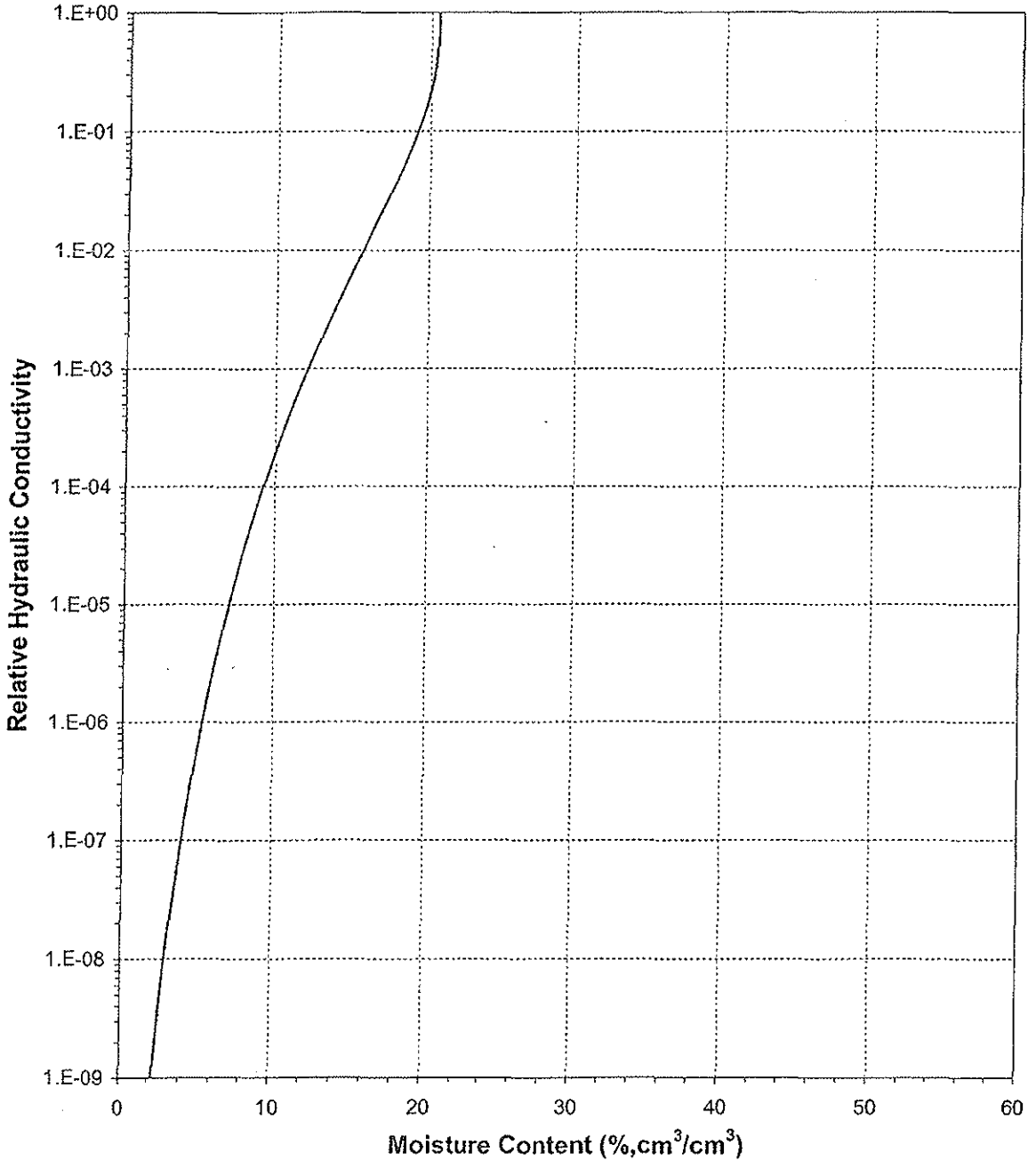

Plot of Hydraulic Conductivity vs Moisture Content

Sample Number: MW-23 103.3-103.5

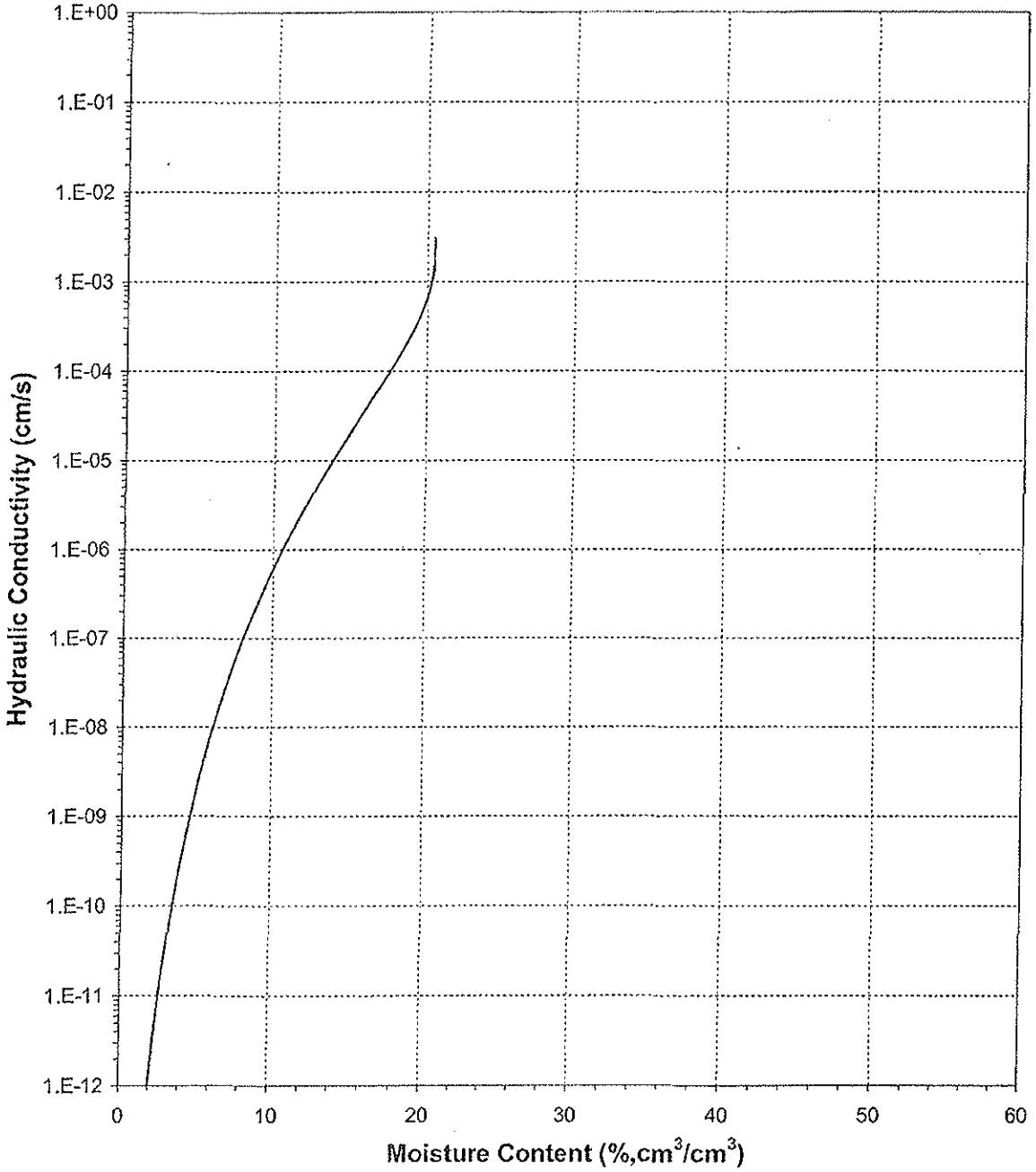

Plot of Relative Hydraulic Conductivity vs Pressure Head

Sample Number: MW-23 103.3-103.5

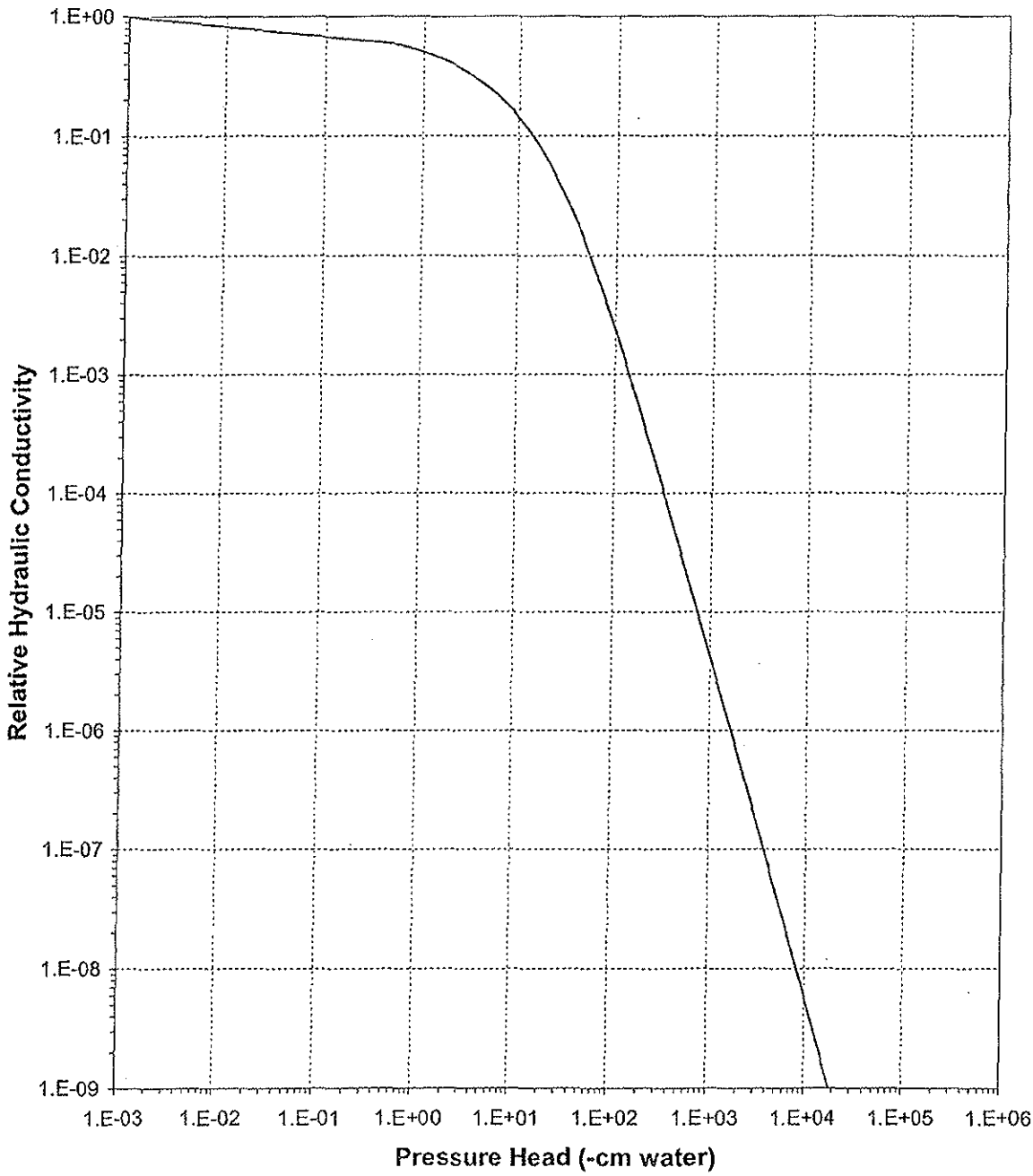

Plot of Hydraulic Conductivity vs Pressure Head

Sample Number: MW-23 103.3-103.5

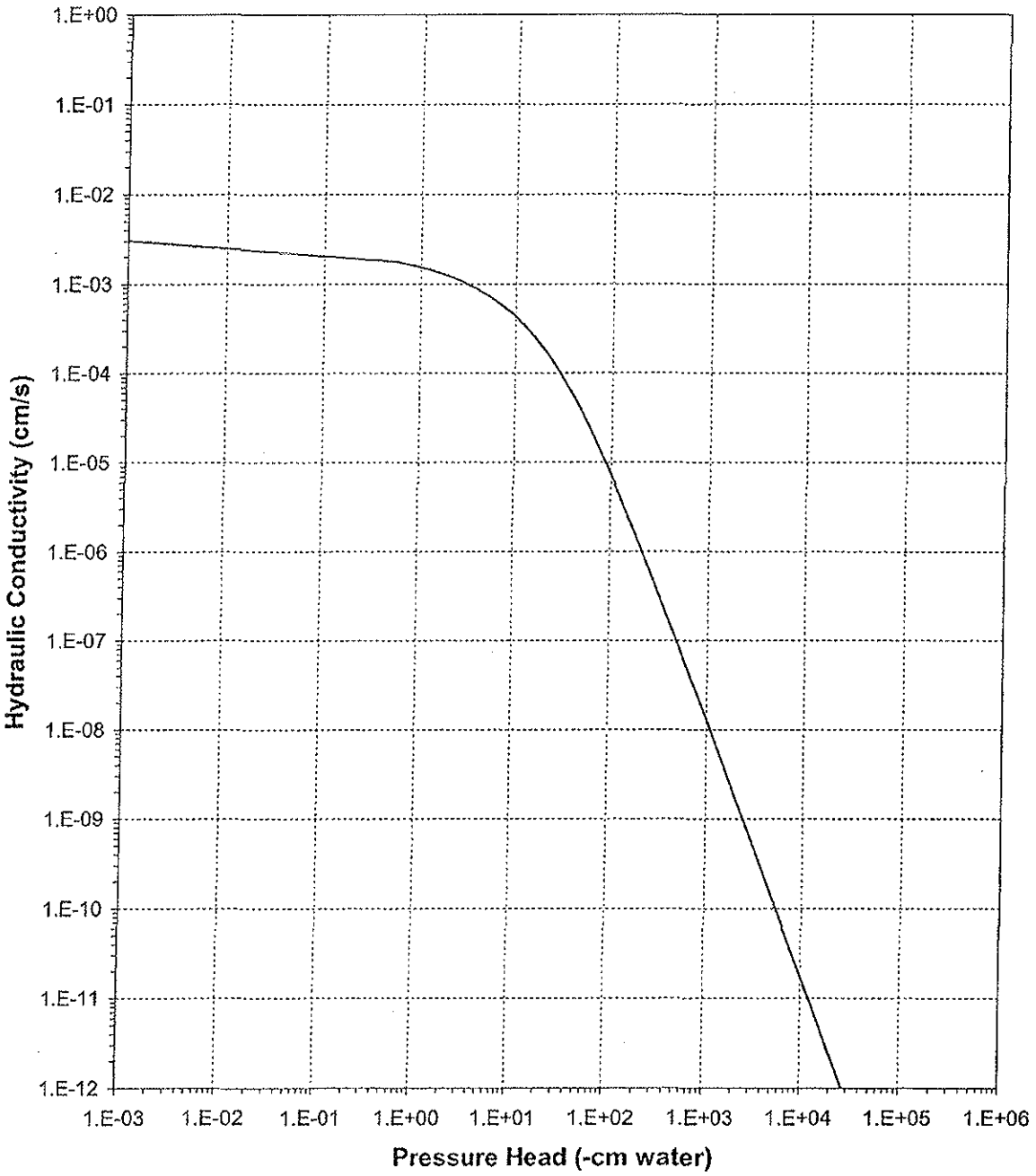

Moisture Retention Data

Hanging Column/Pressure Plate/Thermocouple

Job Name: MWH AMERICAS, INC.
Job Number: LB07.0048.00
Sample Number: MW-30 35.5-36.0
Ring Number: NA
Depth: 35.5'-36.0'

Dry wt. of sample (g): 169.77
Tare wt., ring (g): 0.00
Tare wt., screen & clamp (g): 0.00
Sample volume (cm^3): 85.85

Saturated weight at 0 cm tension* (g): 186.53
Volume of water† in saturated sample (cm^3): 16.76
Saturated moisture content (% vol): 19.52
Sample bulk density (g/cm^3): 1.98

	Date/Time	Weight* (g)	Matric Potential (-cm water)	Moisture Content† (% vol)
Hanging column:	21-Mar-07 / 10:45	186.53	0.00	19.52
	27-Mar-07 / 10:05	186.25	6.50	19.20
	02-Apr-07 / 08:45	186.06	19.80	18.98
	10-Apr-07 / 12:04	181.85	73.50	14.07
Pressure plate:	19-Apr-07 / 08:30	176.32	509.90	7.63

Comments:

* Weight including tares

† Assumed density of water is 1.0 g/cm^3

Laboratory analysis by: D. O'Dowd
Data entered by: T. Bowekaty
Checked by: J. Hines

Moisture Retention Data

Water Activity Meter/Relative Humidity Box

Job Name: MWH AMERICAS, INC.
Job Number: LB07.0048.00
Sample Number: MW-30 35.5-36.0
Ring Number: NA
Depth: 35.5'-36.0'

Dry weight of water activity meter sample* (g): 272.00
Tare weight, jar (g): 199.26
Sample bulk density (g/cm^3): 1.98

	Date/Time	Weight* (g)	Matric Potential (-cm water)	Moisture Content† (% vol)
Water Activity Meter:	13-Apr-07 / 09:56	272.96	23251.4	2.61
	12-Apr-07 / 16:53	272.76	35081.1	2.07

Dry weight of relative humidity box sample* (g): 57.87
Tare weight (g): 38.35
Sample bulk density (g/cm^3): 1.98

	Date/Time	Weight* (g)	Matric Potential (-cm water)	Moisture Content† (% vol)
Relative humidity box:	24-Mar-07 / 12:00	57.91	851293	0.37

Comments:

* Weight including tares
† Assumed density of water is 1.0 g/cm^3

Laboratory analysis by: C. Krous/D. O'Dowd
Data entered by: T. Bowekaty
Checked by: J. Hines

Water Retention Data Points

Sample Number: MW-30 35.5-36.0

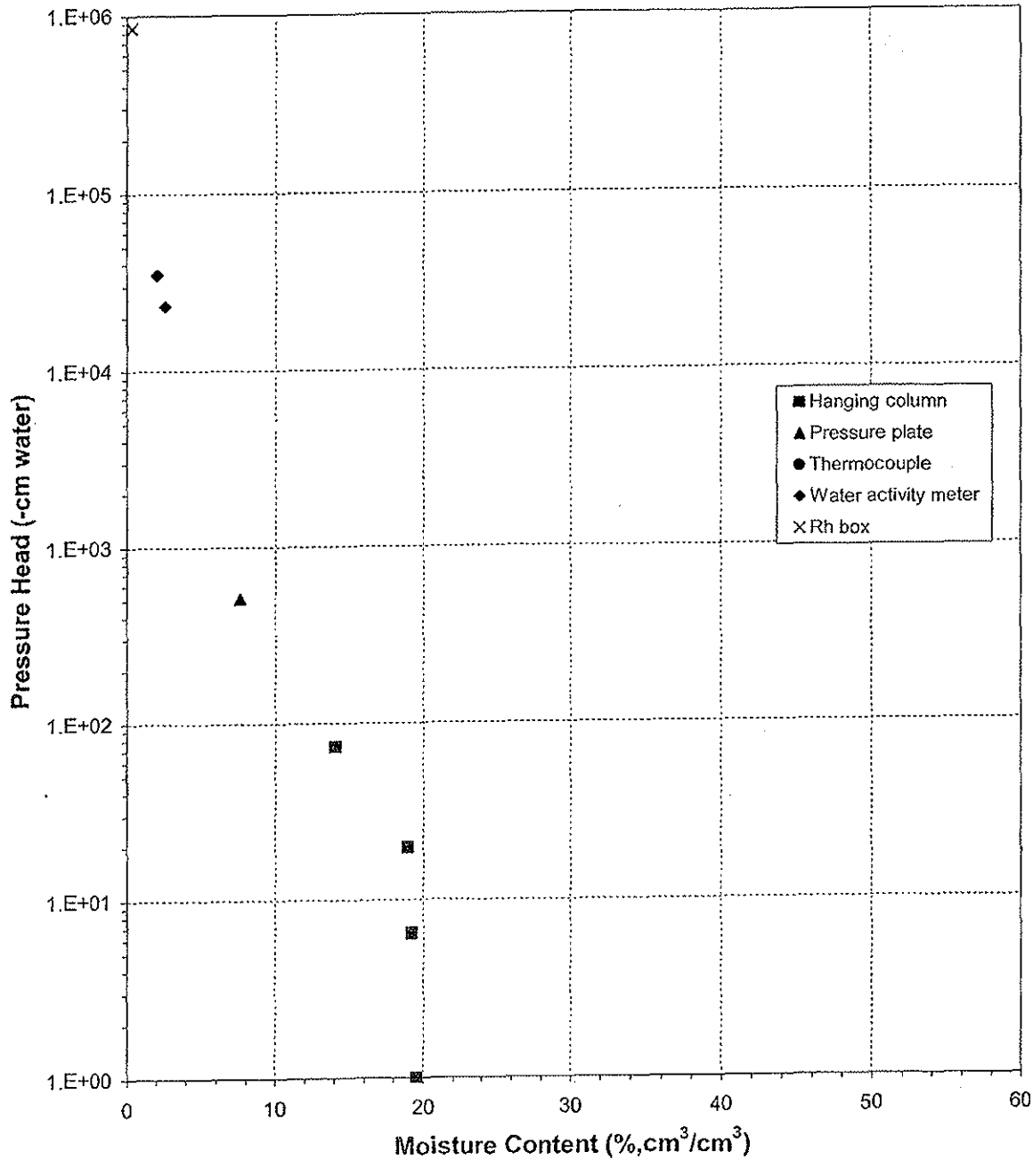

Predicted Water Retention Curve and Data Points

Sample Number: MW-30 35.5-36.0

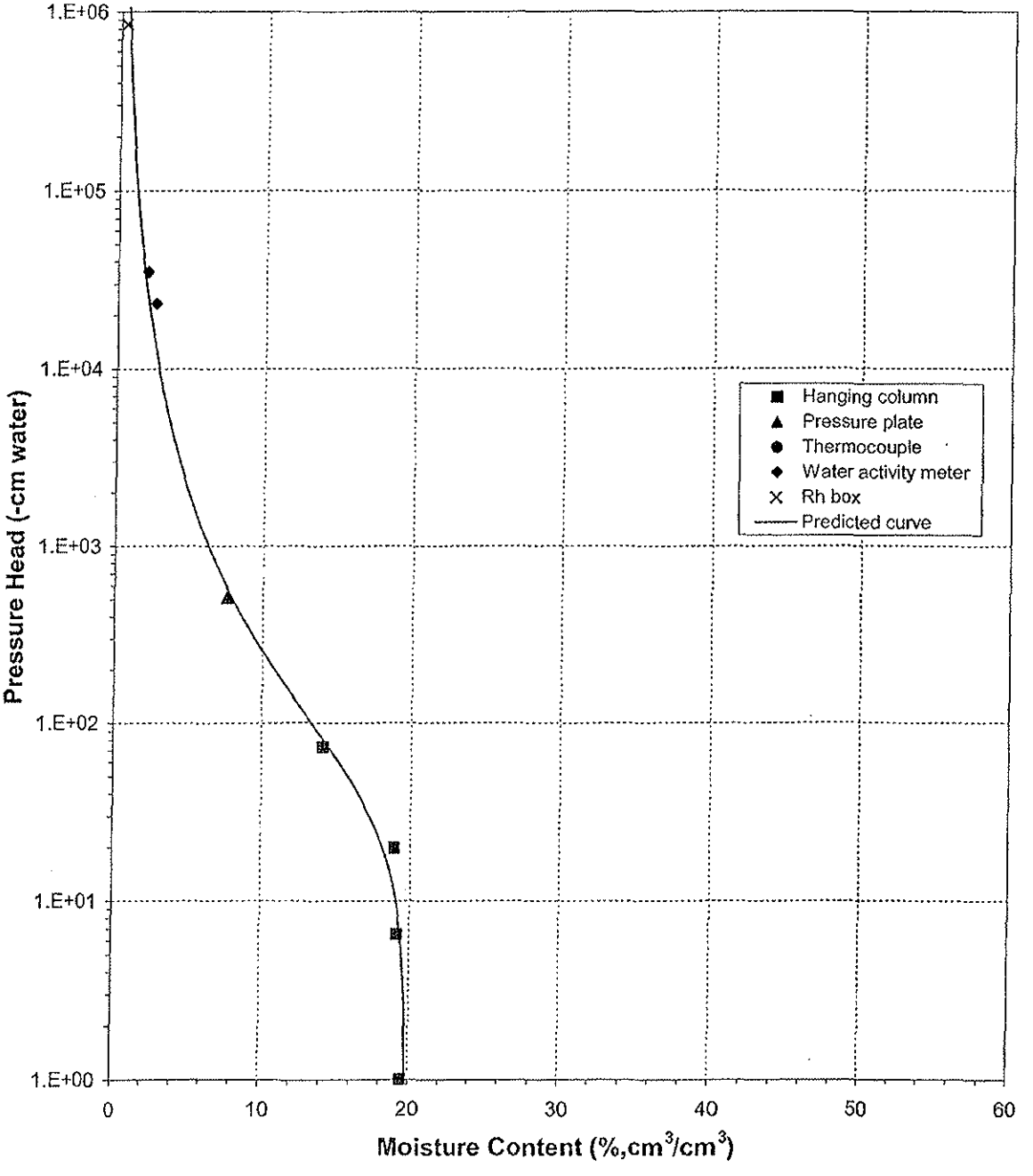

Plot of Relative Hydraulic Conductivity vs Moisture Content

Sample Number: MW-30 35.5-36.0

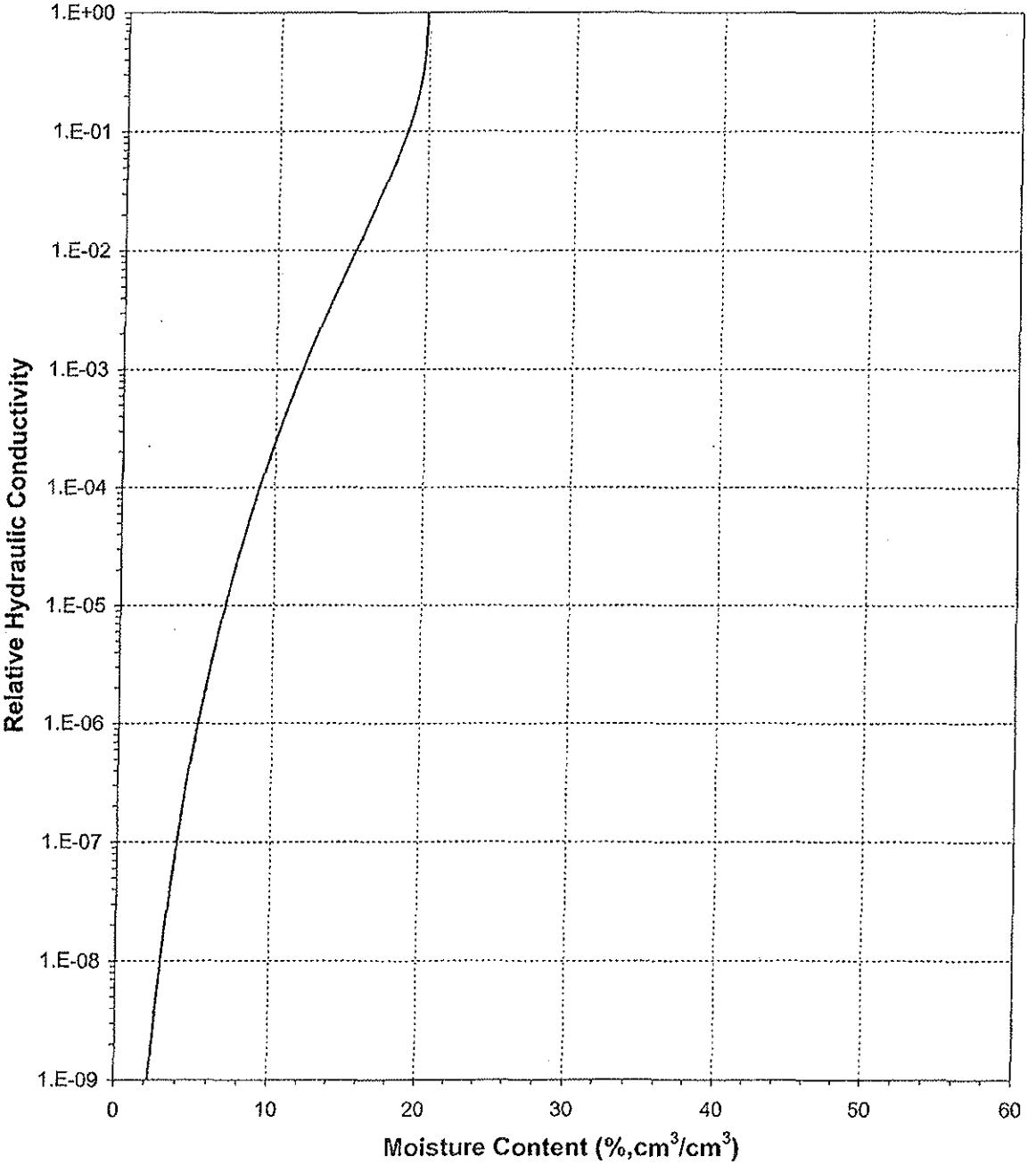

Plot of Hydraulic Conductivity vs Moisture Content

Sample Number: MW-30 35.5-36.0

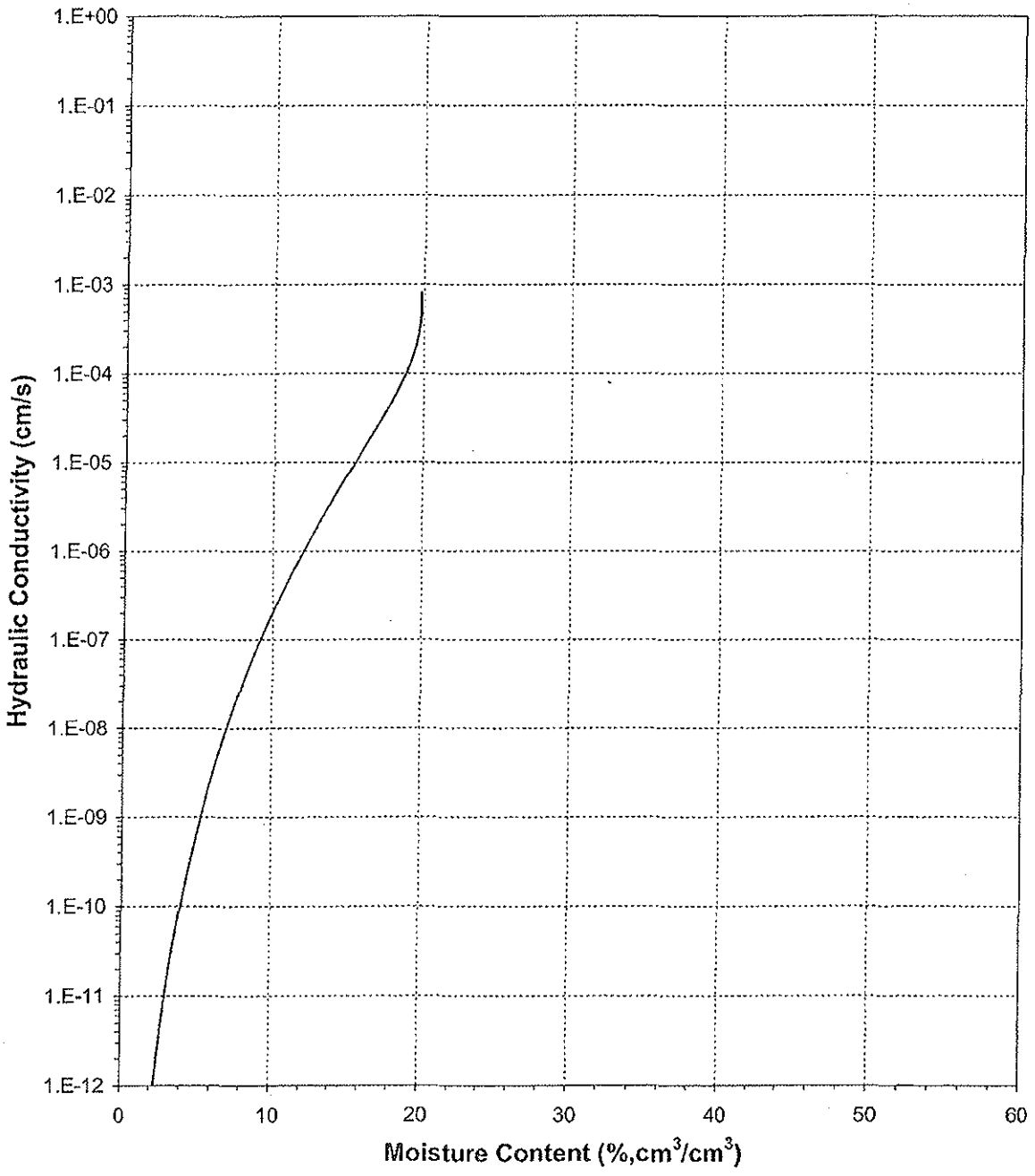

Plot of Relative Hydraulic Conductivity vs Pressure Head

Sample Number: MW-30 35.5-36.0

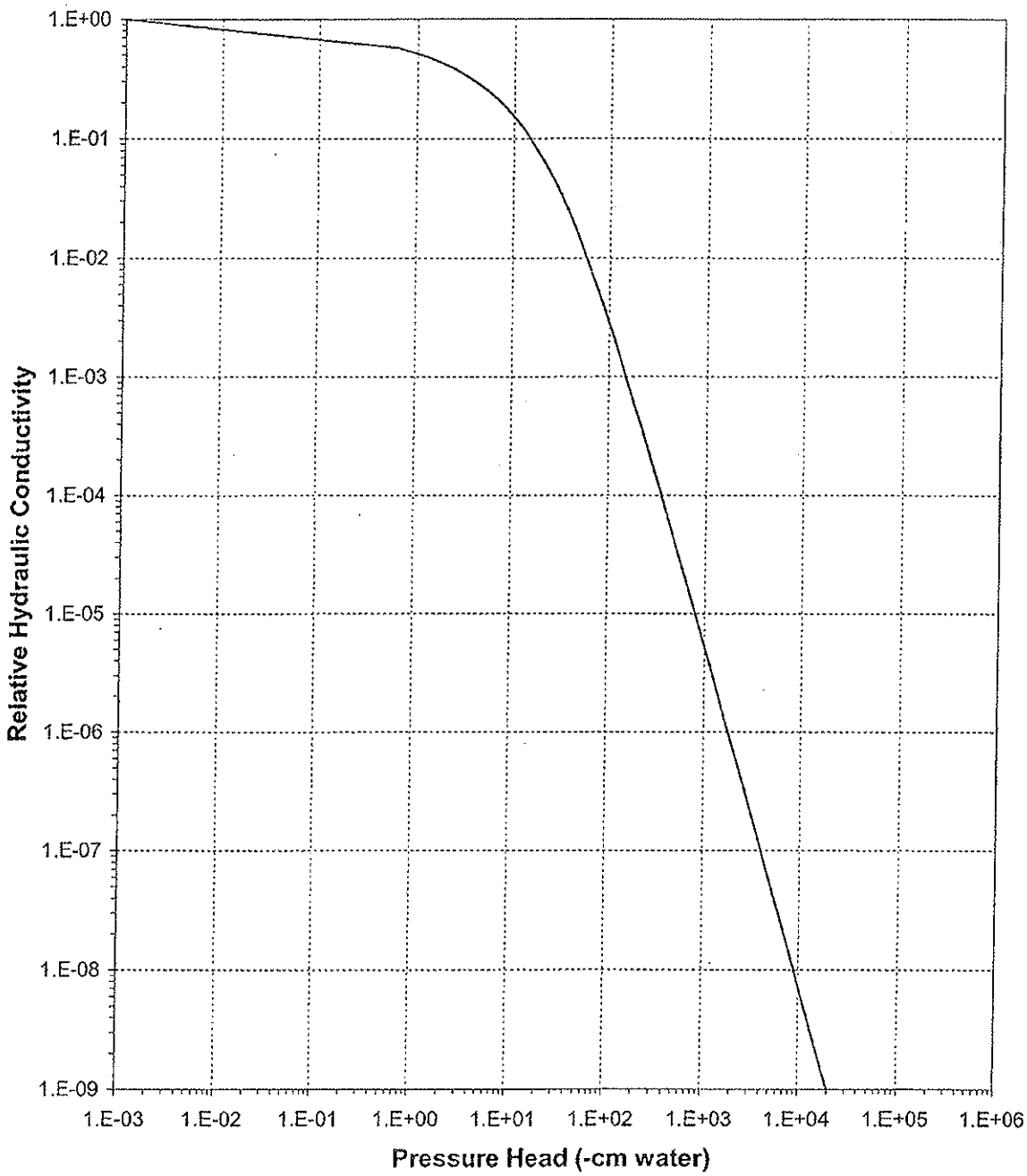

Plot of Hydraulic Conductivity vs Pressure Head

Sample Number: MW-30 35.5-36.0

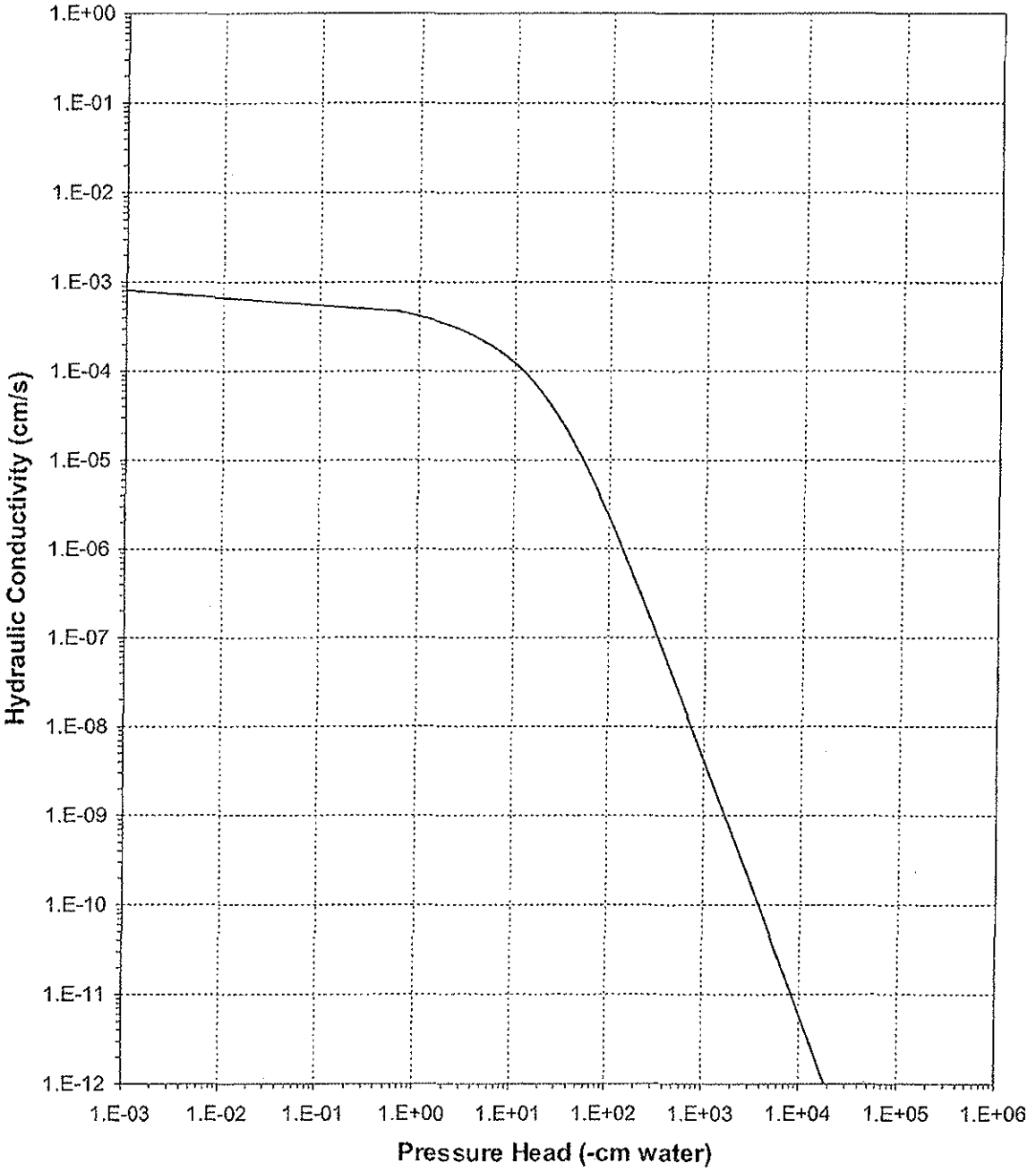

Moisture Retention Data

Hanging Column/Pressure Plate/Thermocouple

Job Name: MWH AMERICAS, INC.
Job Number: LB07.0048.00
Sample Number: MW-30 44.0-44.5
Ring Number: NA
Depth: 44.0-44.5

Dry wt. of sample (g): 193.77
Tare wt., ring (g): 0.00
Tare wt., screen & clamp (g): 0.00
Sample volume (cm^3): 86.88

Saturated weight at 0 cm tension* (g): 218.01
Volume of water† in saturated sample (cm^3): 24.24
Saturated moisture content (% vol): 27.90
Sample bulk density (g/cm^3): 2.23

	Date/Time	Weight* (g)	Matric Potential (-cm water)	Moisture Content† (% vol)
Hanging column:	30-Mar-07 / 08:55	218.01	0.00	27.90
	27-Mar-07 / 10:10	216.98	34.50	26.71
	05-Apr-07 / 11:40	215.27	100.50	24.75
	11-Apr-07 / 07:50	214.25	197.00	23.57
Pressure plate:	25-Apr-07 / 15:30	211.55	509.90	20.46

Comments:

* Weight including tares

† Assumed density of water is 1.0 g/cm^3

Laboratory analysis by: D. O'Dowd
Data entered by: T. Bowekaty
Checked by: J. Hines

Moisture Retention Data

Water Activity Meter/Relative Humidity Box

Job Name: MWH AMERICAS, INC.
Job Number: LB07.0048.00
Sample Number: MW-30 44.0-44.5
Ring Number: NA
Depth: 44.0-44.5

Dry weight of water activity meter sample* (g): 249.86
Tare weight, jar (g): 196.46
Sample bulk density (g/cm^3): 2.23

	Date/Time	Weight* (g)	Matric Potential (-cm water)	Moisture Content† (% vol)
Water Activity Meter:	12-Apr-07 / 15:17	252.48	23353.4	10.94

Dry weight of relative humidity box sample* (g): 90.08
Tare weight (g): 38.03
Sample bulk density (g/cm^3): 2.23

	Date/Time	Weight* (g)	Matric Potential (-cm water)	Moisture Content† (% vol)
Relative humidity box:	21-Mar-07 / 12:00	90.87	851293	3.38

Comments:

* Weight including tares

† Assumed density of water is 1.0 g/cm^3

Laboratory analysis by: C. Krous/D. O'Dowd
Data entered by: T. Bowekaty
Checked by: J. Hines

Water Retention Data Points

Sample Number: MW-30 44.0-44.5

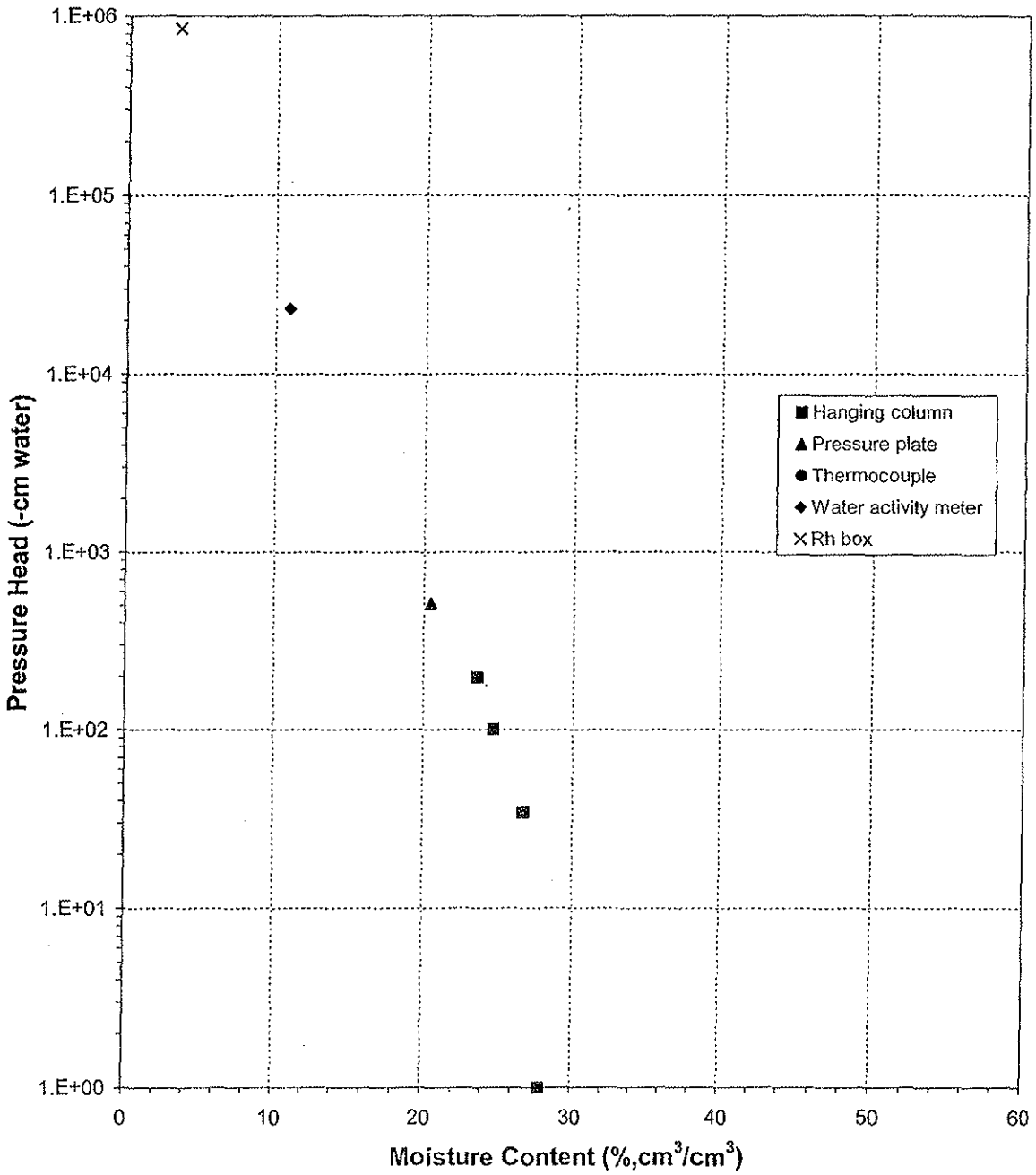

Predicted Water Retention Curve and Data Points

Sample Number: MW-30 44.0-44.5

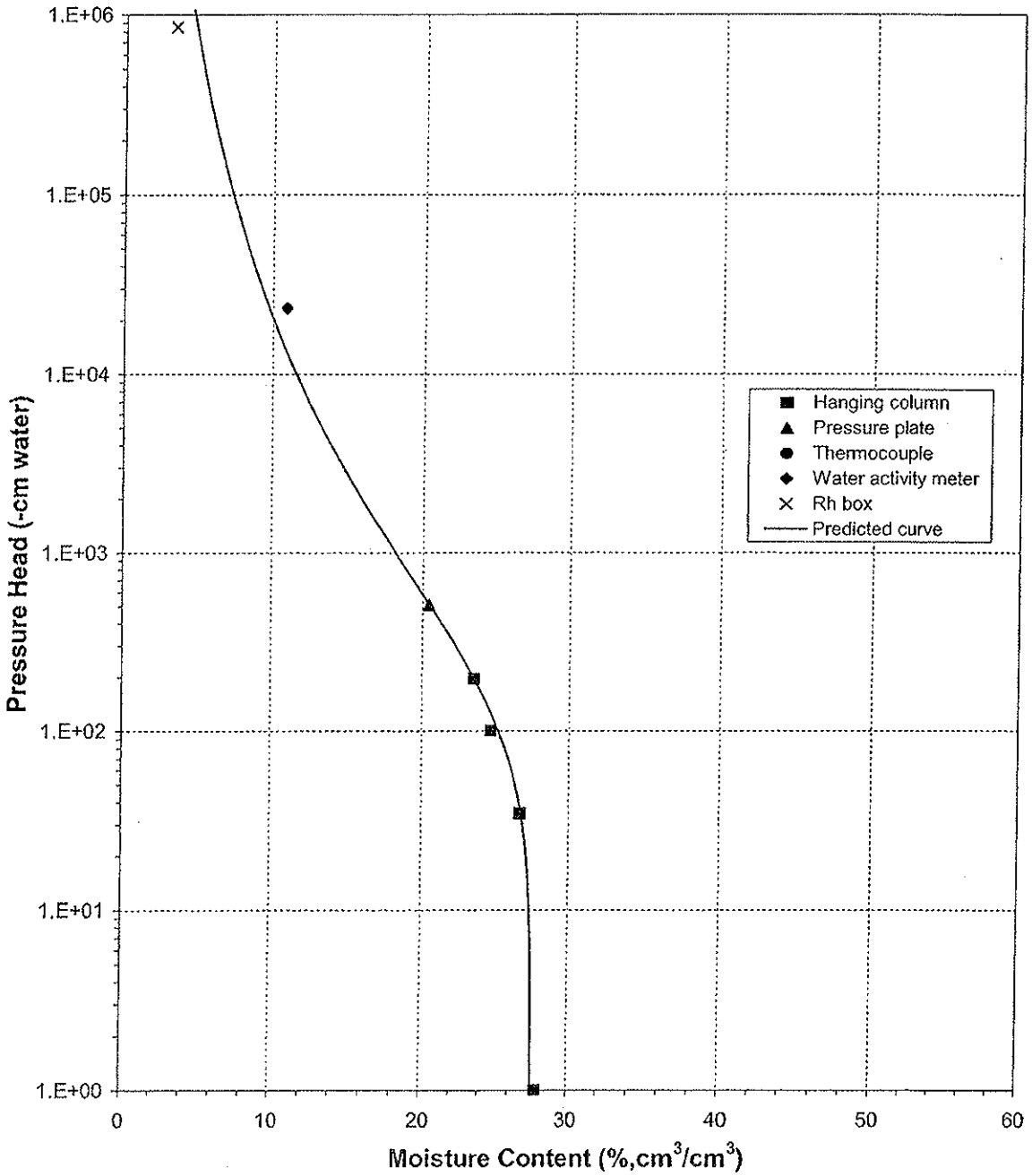

Predicted Water Retention Curve and Data Points

Sample Number: MW-30 44.0-44.5 (Volume Adjusted)

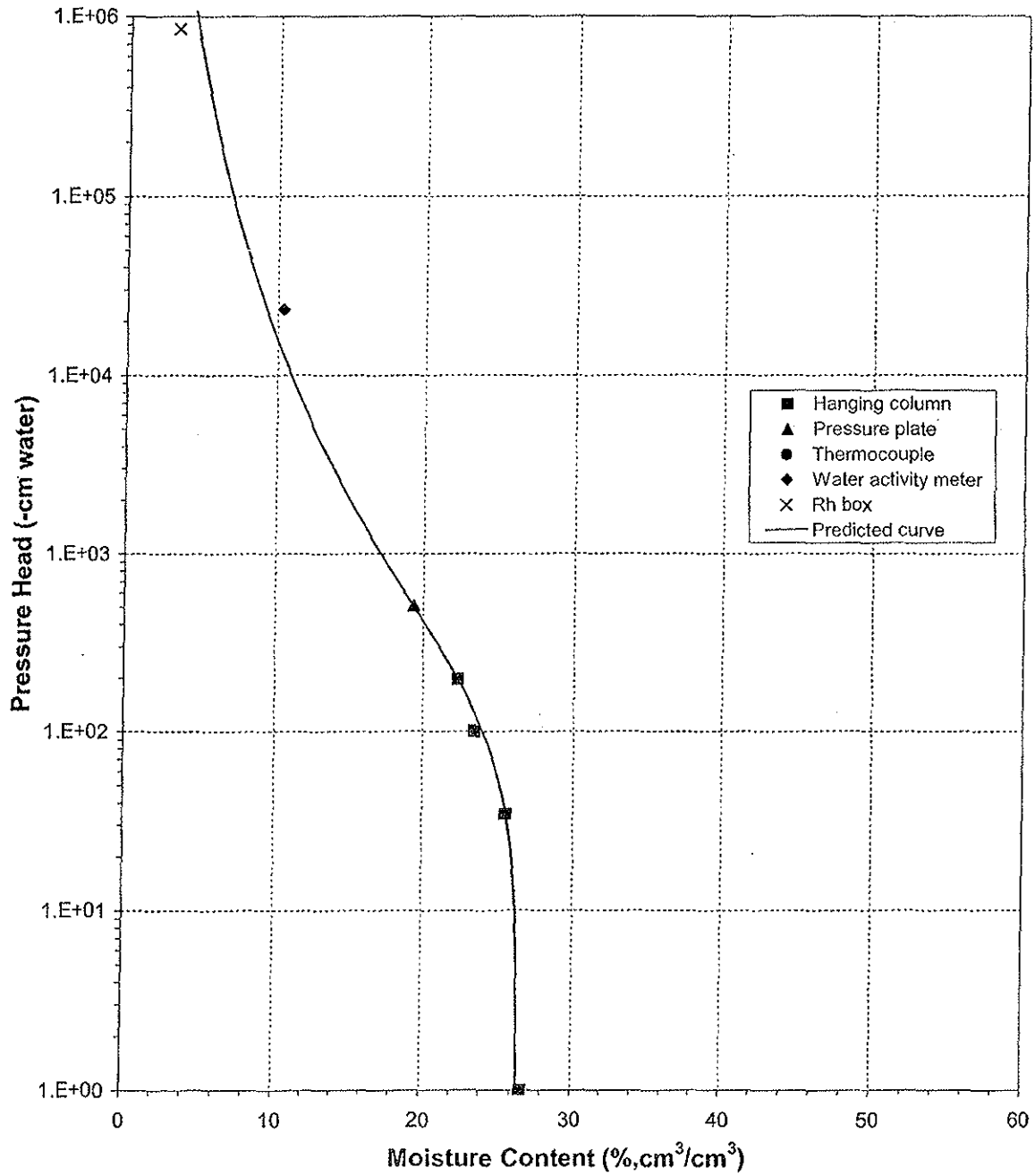

Plot of Relative Hydraulic Conductivity vs Moisture Content

Sample Number: MW-30 44.0-44.5

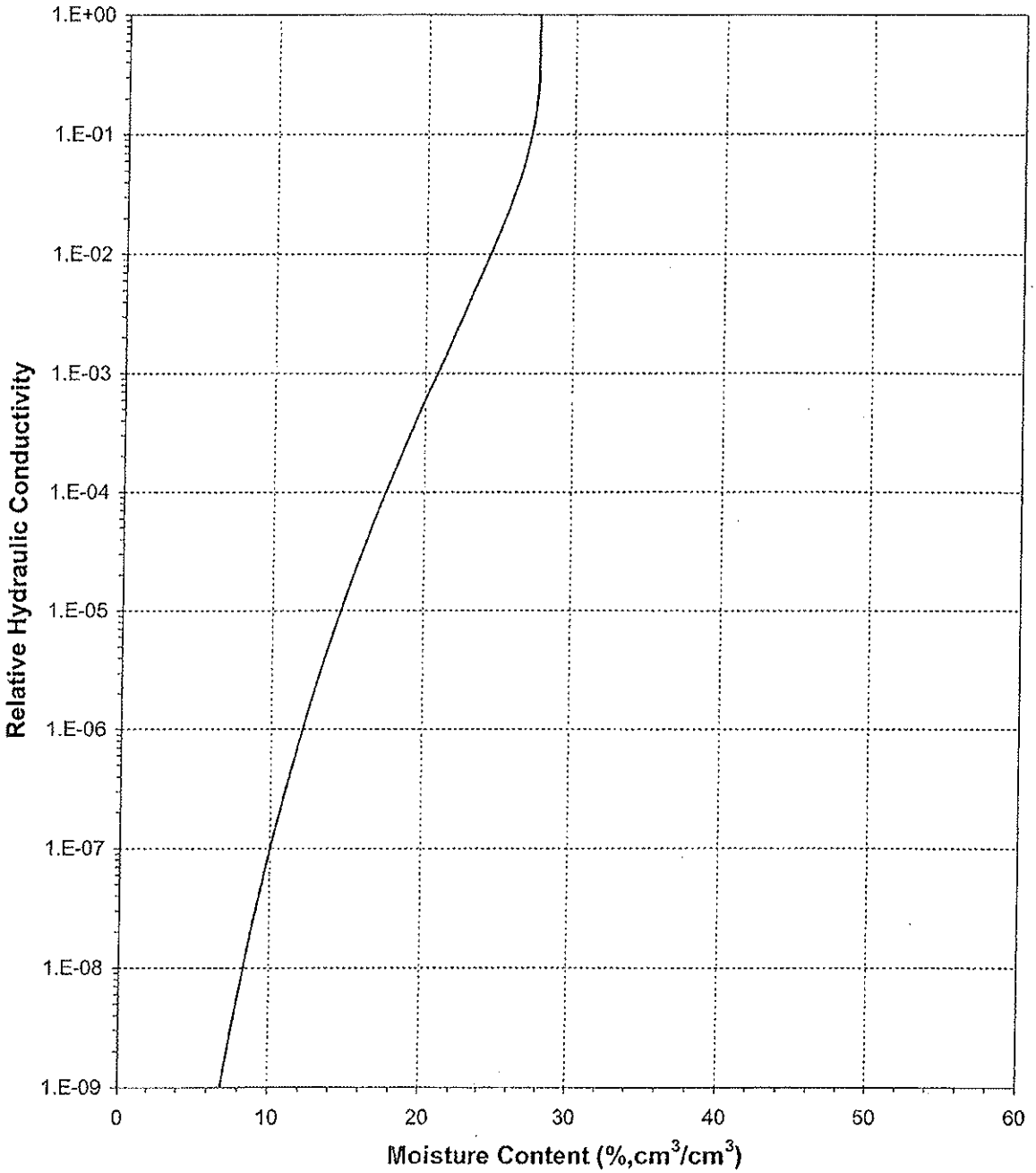

Plot of Hydraulic Conductivity vs Moisture Content

Sample Number: MW-30 44.0-44.5

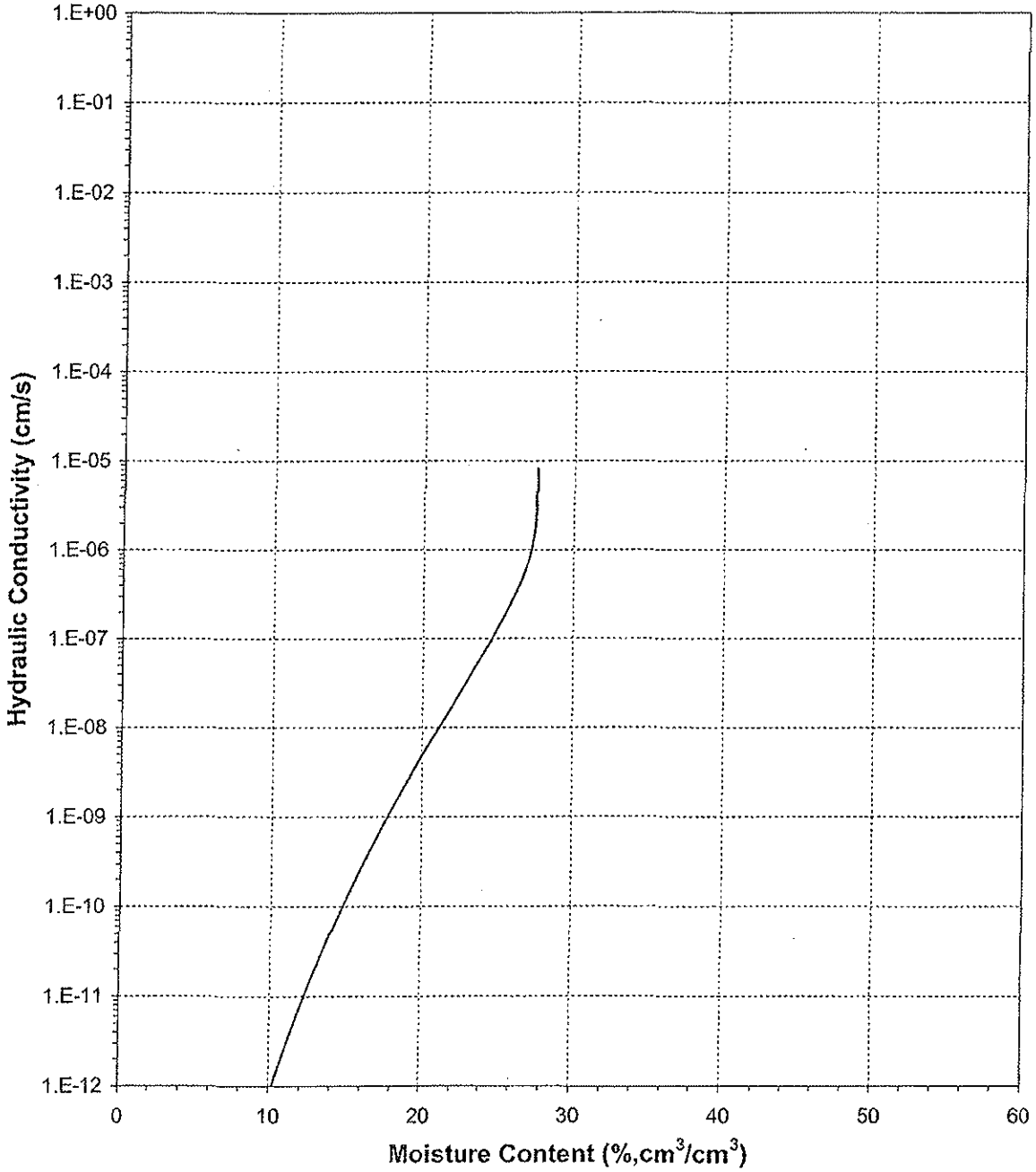

Plot of Relative Hydraulic Conductivity vs Pressure Head

Sample Number: MW-30 44.0-44.5

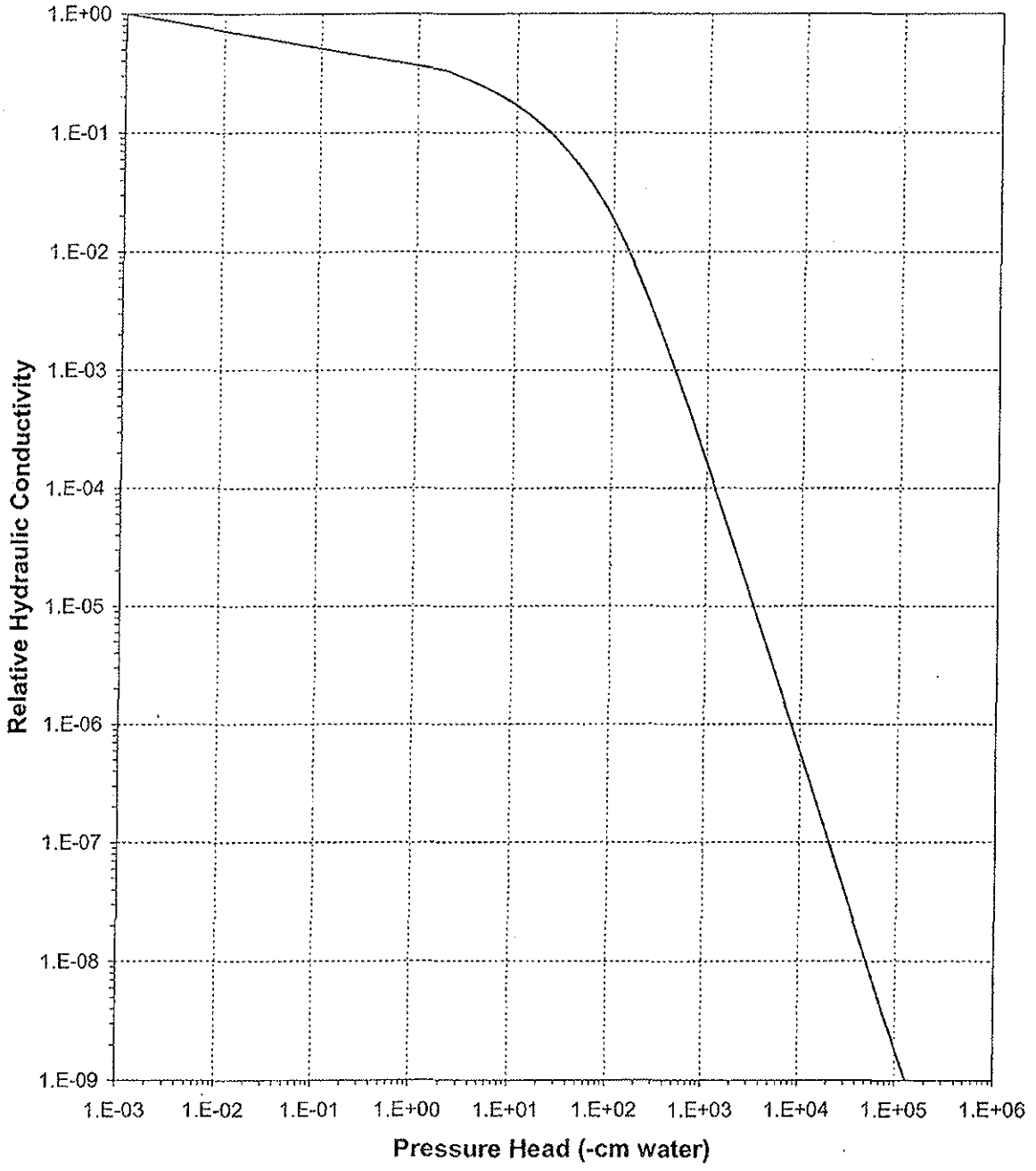

Plot of Hydraulic Conductivity vs Pressure Head

Sample Number: MW-30 44.0-44.5

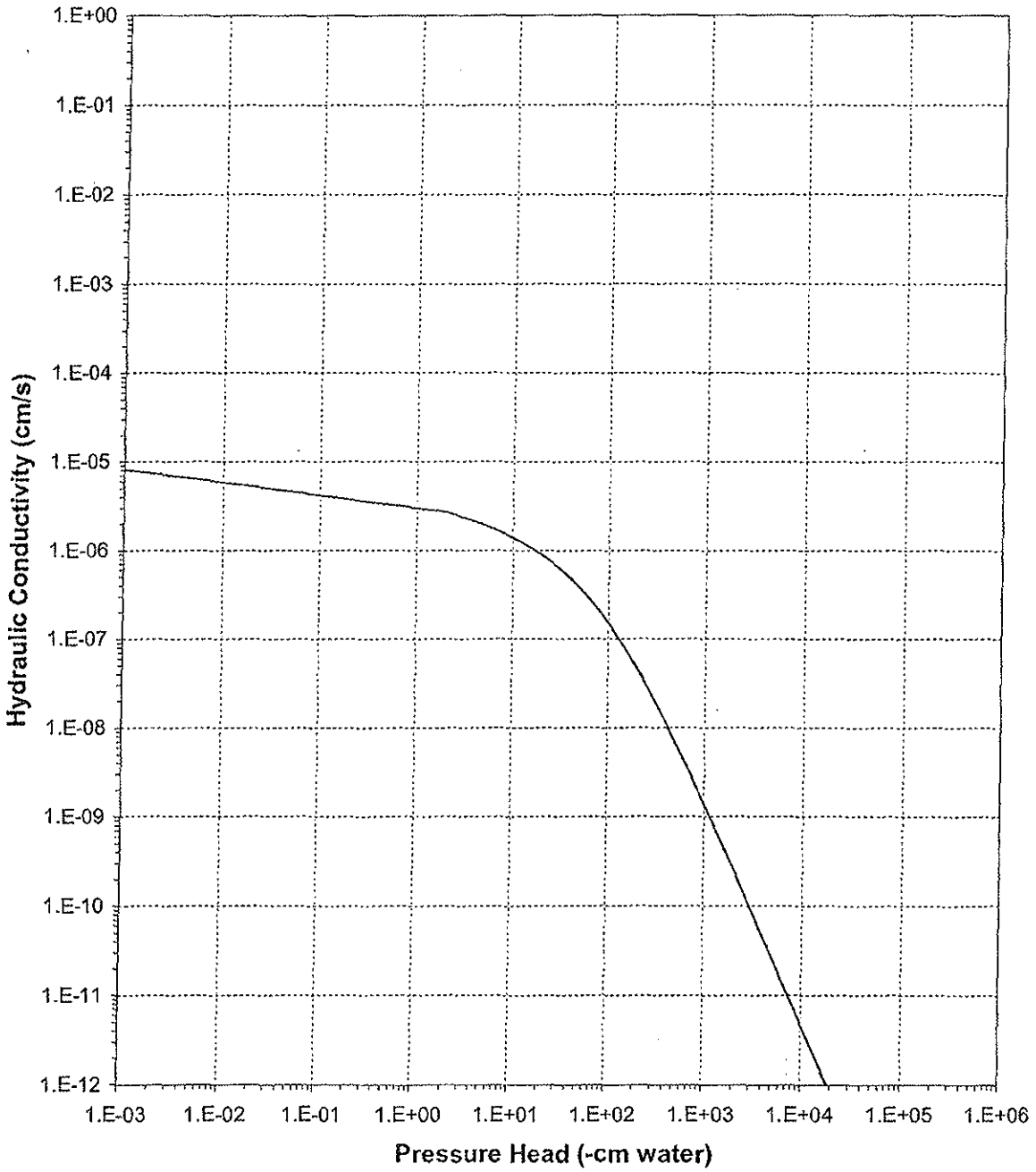

Laboratory Tests and Methods

Tests and Methods

Dry Bulk Density:	ASTM D4531; ASTM D6836
Moisture Content:	ASTM D2216; ASTM D6836
Calculated Porosity:	ASTM D2435; Klute, A. 1986. Porosity. Chp.18-2.1, pp. 444-445, in A. Klute (ed.), Methods of Soil Analysis, American Society of Agronomy, Madison, WI
Saturated Hydraulic Conductivity:	
Falling Head Rising Tail: (Flexible Wall)	ASTM D5084
Hanging Column Method:	ASTM D6836; Klute, A. 1986. Porosity. Chp.26, in A. Klute (ed.), Methods of Soil Analysis, American Society of Agronomy, Madison, WI
Pressure Plate Method:	ASTM D6836; ASTM D2325
Water Potential (Dewpoint Potentiometer) Method:	ASTM D6836; Rawlins, S.L. and G.S. Campbell, 1986. Water Potential: Thermocouple Psychrometry. Chp. 24, pp. 597-619, in A. Klute (ed.), Methods of Soil Analysis, Part 1. American Society of Agronomy, Madison, WI.
Relative Humidity (Box) Method:	Karathanasis & Hajek. 1982. Quantitative Evaluation of Water Adsorption on Soil Clays.SSA Journal 46:1321-1325; Campbell, G. and G. Gee. 1986. Water Potential: Miscellaneous Methods.Chp. 25, pp. 631-632, in A. Klute (ed.), Methods of Soil Analysis, American Society of Agronomy, Madison, WI
Moisture Retention Characteristics & Calculated Unsaturated Hydraulic Conductivity:	ASTM D6836; van Genuchten, M.T. 1980. A closed-form equation for predicting the hydraulic conductivity of unsaturated soils. SSSAJ 44:892-898; van Genuchten, M.T., F.J. Leij, and S.R. Yates. 1991. The RETC code for quantifying the hydraulic functions of unsaturated soils. Robert S. Kerr Environmental Research Laboratory, Office of Research and Development, U.S. Environmental Protection Agency, Ada, Oklahoma. EPA/600/2091/065. December 1991

APPENDIX B

SPECIATION AND SURFACE-COMPLEXATION MODELING OF TAILINGS POREWATER

APPENDIX B

SPECIATION AND SURFACE-COMPLEXATION MODELING OF TAILINGS POREWATER

PURPOSE

The purpose of this appendix is to describe the methodology utilized in modeling the speciation and adsorption of aqueous complexes to predict the fate and transport of dissolved uranium and other contaminants of concern (e.g., arsenic, beryllium, cadmium, etc.) through the vadose zone beneath the White Mesa Mill tailings-disposal facility. As part of this study, a comparative analysis between different geochemical databases was completed in order to produce a dataset comprised of aqueous-complex formation and adsorption coefficients based-on a state-of-the-art understanding of uranium geochemistry and thermodynamics. The geochemical modeling was used to calculate distribution coefficients (K_d) between infiltrating tailings porewater and the underlying bedrock, thereby addressing requirements specified in Part I.H.11 of the Ground Water Discharge Permit No. UGW370004.

BACKGROUND

Geochemistry of Uranium

In groundwater considered to represent reducing or low Eh conditions, uranium in its +4 oxidation state (U(IV)) as uranous ion (U^{+4}) and its aqueous complexes comprise the dominant forms of uranium (Figure B-1). Uranium in its +6 oxidation state (U(VI)) as the uranyl ion (UO_2^{+2}; U^{+6}; U(VI)) and its aqueous complexes predominate under oxidizing or high Eh conditions. Uranium in the mineral uraninite (UO_2 [crystalline]) is present mainly as U(IV), and is known to have a relatively low solubility. Consequently, uraninite is considered to be insoluble under reducing conditions and concentrations of dissolved uranium will be correspondingly low. The solid green line on Figure B-1 demarcates the solubility limit for uraninite at a concentration of 1 x 10^{-8} molar (M) or approximately 2 micrograms per liter (µg/l). The solid green line represents Eh and pH conditions for water in equilibrium with uraninite at a concentration of 2 µg/l. Thus,

water samples with pH values between 2 and 5.22 and Eh values lower than 0.174 Volts will have concentrations lower than 2 µg/l. Increasing the Eh will increase the dissolved uranium concentration. Under increasingly more oxidizing conditions the stability field of uraninite will increase, but with a correspondingly greater dissolved concentration. For example, Langmuir (1997, Figure 13.10) displays a diagram set at a concentration of 1×10^{-5} M total uranium. In Langmuir's (1997) diagram, the stability of UO_2 (crystalline) has "moved up" to approximately 0.25 Volts, but so has the concentration of uranium, which is now at a value of approximately 2 milligrams per liter (mg/l). In general, uranyl-bearing minerals tend to have higher solubilities and therefore uranyl is considered to be soluble or mobile in oxic groundwater environments. In that same figure, Schoepite (β-$UO_3 \cdot 2H_2O$ [crystalline]) shows stability between pH values of approximately 5 to 7 at a concentration of 1×10^{-5} M.

At pH values greater than approximately 5, uranyl forms strong complexes with carbonate species. An example of the distribution of uranyl complexes is shown on Figure B-2, which was constructed with the project-specific database described below. For simplicity, the figure does not include all of the aqueous complexes; it only shows the dominant species. These aqueous complexes influence the nature of the surface-complexation reactions that are used to define adsorption reactions and the subsequent estimation of sorption distribution coefficients (K_d's).

Generalized discussions regarding the geochemistry of additional solutes, including trace metals present in the tailings porewaters, is summarized in the Revised Background Groundwater Quality Report (INTERA, 2007), a partition coefficient document prepared by the U.S. EPA (1999), and textbooks on aqueous geochemistry (Langmuir, 1997).

Speciation of Aqueous Complexes

The distribution of elements among aqueous species and ionic states, and their proclivity for complexation, has a significant effect on solution chemistry and contaminant-transport mobility. The speciation of elements and formation of aqueous complexes is governed by thermodynamic constraints, which can be determined with a series of mass-

action and mass-balance equations solved simultaneously through the use of a geochemical-computer code (e.g., Parkhurst and Appelo, 1999). The code references a database containing mass-action equations and aqueous-complex formation (stability) constants. For example, the geochemical-computer code PHREEQC contains a suite of thermodynamic databases that the user may select as part of the modeling exercise. Two of the databases available with the PHREEQC-modeling package are identified as wateq4f.dat and minteqa.v4.dat. These particular databases include complexation reactions for uranium species and other trace metals. Unfortunately, databases distributed with the software are seldom updated on a regular basis. As a result, the user must update the database to reflect contemporary estimates of thermodynamic properties for the solutes of interest.

The results of the comparative analysis between geochemical databases for uranium are tabulated in Table B-1. Potential sources of error identified include the use of antiquated complex-formation constants and an incomplete dataset of uranium-aqueous species. The following uranium (VI) complexes identified in Grenthe et al. (1992); Davis and Curtis (2003); Guillaumont et al. (2003) were not included in the wateq4f and minteqa.v4 databases:

- $UO_2(OH)_{2,aq}$
- $(UO_2)_2CO_3(OH)_3^-$
- $(UO_2)_3CO_3(OH)_3^+$
- $(UO_2)_{11}(CO_3)_6(OH)_{12}^{2-}$
- $CaUO_2(CO_3)_3^{3-}$
- $Ca_2UO_2(CO_3)_{3,aq}$
- $UO_2(H_2PO_4)(H_3PO_4)^+$
- $UO_2SiO(OH)_3^+$
- $UO_2(SO_4)_3^{4-}$
- UO_2HAsO_4

- $UO_2H_2AsO_4^+$
- $UO_2(H_2AsO_4)_2$

For this study, these aqueous species were added to the dataset of uranyl complexes.

Although site-specific geochemical conditions will dictate uranium speciation among its complexes and ionic states, incorporation of a comprehensive thermodynamic database will serve to minimize the effect of excluding potentially salient species. For example, speciation calculations presented in the work of Davis et al. (2004) indicated that two calcium-uranyl-carbonate species accounted for 96.3 to 98.8% of dissolved uranium(VI). Exclusion of these calcium-uranyl-carbonate complexes from the thermodynamic database could significantly increase the total amount of uranyl available to participate in surface-complexation reactions. Therefore, because a greater proportion of uranyl will be stabilized in solution by the formation of uranyl-bearing aqueous complexes, the amount of uranyl available for surface complexation is lowered, which will therefore lower the total amount of uranium sorbed onto surfaces and ultimately lower the K_d. A complete listing of uranium aqueous-complex-formation constants and reactions incorporated as part of this study is included in Table B-1.

Adsorption of Aqueous Complexes

Chemical reactions between dissolved constituents in groundwater (e.g., metals and radionuclides) and the aquifer matrix often dictate spatiotemporal variations in contaminant-plume transport and mobility in the subsurface by controlling the degree of adsorption-desorption of aqueous complexes to surface assemblages. Surface-complexation models (SCM) apply principles of chemical equilibrium to reactions between dissolved species and potential sorption sites. A series of heterogeneous mass-action equations, mass-balance equations for surface sites, and charge-potential relations for each surface are coupled with aqueous-speciation equilibria to determine sorbate-sorbent interactions, commonly using a geochemical-computer code (e.g., Parkhurst and Appelo, 1999). In geochemical model PHREEQC, surface-complexation reactions are reproduced after the Dzombak and Morel (1990) diffuse-layer model with the option to

include effects from electrostatic potentials (Parkhurst and Appelo, 1999). The generalized, two-layer model quantifies the adsorption of speciated-aqueous complexes onto amorphous hydrous-ferric oxide (HFO) surface sites (Dzombak and Morel, 1990).

Since the publication of Dzombak and Morel's 1990 compilation, additional surface-complexation models that focus solely on uranium(VI) adsorption have been established. The different assumptions implicit with each surface-complexation model has the potential to significantly affect the quantity of uranyl (UO_2^{+2}) and uranium(VI) adsorbed. Potential differences between the various surface-complexation models include the absolute number and relative partitioning between strong-site and weak-site densities, coordination structure between uranyl and HFO surface sites, competitive sorption between uranyl and other dissolved species (mainly metals), and the methodology used to compute adsorption coefficients. The relative assumptions, advantages, and disadvantages between the various surface-complexation models are summarized in Table B-2.

METHODOLOGY

Measurement of HFO and Neutralization Potential

The mass of hydrous-ferric oxide present in bedrock underlying the White Mesa Mill tailings-disposal facility was determined via chemical extraction with hydroxylamine-hydrochloride (HH) solution. Chemical extractions with HH are expected to completely dissolve amorphous-mineral phases (e.g., ferrihydrite) and partially dissolve some crystalline minerals (e.g., goethite). Bedrock-core samples collected from MW-23 and MW-30 were air dried at 34°C and crushed (<3 mm). To represent the vadose zone beneath the tailings cells, these core samples were collected from the Dakota Sandstone and Burro Canyon Formation at similar depths to the samples collected for hydraulic testing performed by Daniel B. Stephens & Associates (2007). The HH solution (100 mL) was added to 10 grams of crushed rock in a 250 mL bottle and placed in a shaking-water bath at 50°C. Aliquots of extracted solution were withdrawn after 96 hours and filtered (<0.45 μm) prior to analysis. The extracted solution was analyzed

for dissolved aluminum, calcium, iron, magnesium, manganese, and uranium. The HH procedure was similar to the methodology incorporated by Davis and Curtis (2003, p. 34.). The acid-neutralization potential of the bedrock was measured directly using the methodology outlined in the U.S. EPA method M600/2-78-054. Sample preparation, laboratory experiments, and water-quality analyses were performed by ACZ Laboratories, Inc., Steamboat Springs, Colorado (original data included as Attachment 1 of this Appendix).

Geochemical Modeling

Water-quality data for the White Mesa Mill tailings porewaters and leach-extraction data for the underlying bedrock was examined to calculate adsorption of dissolved species under varying geochemical conditions. Neutralization of the infiltrating tailings porewaters and sorption of solutes onto HFO was determined using the geochemical code PHREEQC (version 2.13.2) (Parkhurst and Appelo, 1999). Distribution coefficients were calculated with the following equation (Langmuir, 1997, Equation 10.15):

$$K_d = \left(\frac{C_i - C_f}{C_f}\right) * \left(\frac{V}{M}\right) \qquad (1)$$

Where: K_d is the distribution coefficient [L^3M^{-1}]

C_i is the initial concentration [ML^{-3}]

C_f is the final concentration [ML^{-3}]

V is the volume of solution [L^3]

M is the mass of rock [M].

For each batch reaction, distribution coefficients were calculated using the initial concentration of the dissolved species present in the tailings porewaters at the surface (i.e., prior to neutralization and equilibration except for manganese, fluoride, and sulfate as explained below), the final concentration of the dissolved species subsequent to adsorption onto HFO, the mass of rock, and the calculated volume of solution. The initial concentration of a dissolved species present at the surface was used during the

distribution-coefficient calculations, rather than an iterative or pseudo-reactive-transport approach, in order to maintain conservative assumptions. An iterative approach would have used the previous solution as an initial condition in the geochemical model and for calculating adsorption for each subsequent hydrostratigraphic unit. The initial concentration of manganese, fluoride, and sulfate were determined for each hydrostratigraphic unit to account for mineral-precipitation reactions.

Assumptions implicit with modeling adsorption of dissolved species with the partition-coefficient approach include establishment of local equilibrium and completely-reversible geochemical reactions. Furthermore, conditions simulated in the geochemical model were assumed to be representative of expected hydrogeochemical conditions in the vadose zone beneath the White Mesa Mill.

As part of this study, we calculated K_d's with the Dzombak and Morel (1990) surface-complexation model. The number of strong and weak sites and surface-complexes considered for their surface-complexation model is listed in Table B-3. Electrostatic effects were explicitly accounted for during the calculations. Most surface-complexation coefficients for the Dzombak and Morel (1990) model were taken directly from the wateq4f-thermodyanic database distributed with PHREEQC (version 2.13.2); with the exception of a few trace metal surface-complexation coefficients which were taken from the minteq.v2-thermodynamic database (Table B-3). For the Dzombak and Morel (1990) model, the surface-complexation coefficients for uranyl and uranyl-carbonate were optimized against the Payne (1999) and Hsi (1981) datasets, as explained below. Surface-complexation reactions and coefficients are summarized in Table B-4.

Verification of Surface-Complexation Model

The surface-complexation model described in the Payne (1999) dissertation has some unique characteristics that complicate its actualization in PHREEQC. Payne set up the models using MINTEQA2 (Allison et al., 1991), which has a more flexible system to define reactions on surfaces. PHREEQC has similar capabilities but requires the inclusion of keywords that limit stoichiometric checks on the surface-complexation

equations. To verify that the assumptions and setup in PHREEQC were correct, a comparison between Payne's data (1999, Appendix 1) and the PHREEQC model-generated output produced as part of this study was performed. The Payne (1999) experimental conditions included ΣU of 1 x 10^{-6} M in a 0.1 M $NaNO_3$ solution with 0.089 g of HFO. The solutions were equilibrated in air ($10^{-0.7}$ atmospheres oxygen and $10^{-3.5}$ atmospheres carbon dioxide) and the pH was fixed in PHREEQC by addition of NaOH.

Figure B-3 shows the comparison between the Payne (1999) dataset of laboratory-measured uranium sorption values and values calculated with PHREEQC using the surface-complexation models of Payne (1999) and Dzombak and Morel (1990). The model-predicted uranium sorption values using the Payne (1999) surface-complexation model closely match the laboraotory-measured values. The comparison demonstrates that assumptions and details of the Payne (1999) surface-complexation model can be replicated using PHREEQC. The other model uses surface-complexation parameters identified by Dzombak and Morel (1990). Despite differences between adsorption predicted with the Dzombak and Morel (1990) surface-complexation model and Payne's laboratory measurements (Figure B-3), there is a general agreement between the two datasets. However, to improve the fit between measured and model-predicted adsorption of uranium with the Dzombak and Morel (1990) model, the strong-site and weak-site surface-complexation coefficients for uranyl were optimized to fit the Payne (1999) and Hsi (1981) datasets. During optimization, inclusion of a uranyl-carbonate surface complex, allowing adsorption onto weak sites only, was necessary to decrease residuals and improve the model fit; the uranyl-carbonate surface complex was only compared to the Payne (1999) dataset. The Hsi (1981) experimental conditions included ΣU of 1 x 10^{-5} M in a 0.1 M $NaNO_3$ solution with 1 g of HFO. The solution pH was fixed in PHREEQC by addition of NaOH.

Figure B-4 shows the comparison between the Payne (1999) dataset and two different model representations: the model using the Payne (1999) surface-complexation parameters and the model using the optimized Dzombak and Morel (1990) surface-complexation parameters. The model using the optimized-parameter set is clearly

excellent, with a reduction of the root mean square error from 23.5% to 5.0%. Figure B-5 shows the comparison between the Hsi (1981) dataset and the optimized Dzombak and Morel (1990) surface-complexation parameters, and illustrates an excellent fit between the measured and predicted values. The two outliers at elevated pH conditions may be attributed to laboratory error. These comparisons demonstrate that the model setup with the optimized-parameter set for the Dzombak and Morel (1990) surface-complexation model is appropriate and can be considered to compute uranium adsorption onto HFO.

Retardation Factor

Adsorption coefficients are generally incorporated into a solute-transport model by multiplying the advective- and diffusive-transport terms by a retardation factor, which can be calculated with the following equation (Freeze and Cherry, 1979):

$$R_f = 1 + \left(\frac{\rho_b * K_d}{\theta} \right) \qquad (2)$$

where R_f is the retardation factor [dimensionless]

ρ_b is the dry-bulk density of the porous media [ML^{-3}]

K_d is the distribution coefficient [L^3M^{-1}]

θ is the volumetric-water content of the porous media [L^3L^{-3}].

The retardation factor is commonly used to determine the transport of a contaminant plume undergoing adsorption, and is measured relative to the advective transport of groundwater (Freeze and Cherry, 1979). A retardation factor of 1.0 indicates that the contaminant plume migrates at the same rate as the advective velocity, as is typically the case for chloride.

Initial-Solute Concentrations

The average-solute concentrations measured between September 1980 and March 2003 for the tailings-wastewater (Utah Division of Radiation Control, 2004) were used as an

initial condition for calculating adsorption of solutes onto HFO (Table B-5). The initial solution was assumed to be in equilibrium with atmospheric oxygen (21% or $10^{-0.7}$ atmospheres) at the measured pH (1.83 s.u.). Initially the concentration of sulfate was allowed to be adjusted to achieve charge balance; however, establishment of electroneutrality resulted in a significant reduction in sulfate concentrations. Therefore, the solution chemistry was not balanced resulting in a final charge-balance error of ~ 30%, which is regarded to be reasonable considering the initial solution represents an average value. The occurrence of an imbalanced solution will not affect the calculations because the charge-balance equation is not used to determine a solution to the equilibrium problem. Solute concentrations originally reported in mg/l were converted to moles per kilogram of water (mol/kgw) to minimize differences between the initial and equilibrated solutions prior to reaction with the mass of calcite and hydrous-ferric oxide for each hydrostratigraphic unit. The pH was fixed at the measured value by addition of NaOH. Equilibration of the initial solution with atmospheric oxygen was necessary to ensure oxidized conditions that would prohibit saturation of uranium-bearing phases and speciation of non-uranium(VI) aqueous complexes. The wateq4f-thermodynamic database distributed with PHREEQC (version 2.13.2) was edited to remove uranium(VI) aqueous complexes and the input files were modified accordingly to incorporate aqueous complexes listed in Table B-1; incorporation of the speciation database as part of the model-input files ensured complete control of the uranium-aqueous complexes used in the calculations. In addition, aqueous complexes and surface complexes incorporated from the minteq.v4.dat-file (Table B-3) were added to the modified database.

Uranium-Adsorption Calculations

During batch-reaction calculations performed with PHREEQC, the initial-solute concentrations were equilibrated with:

1. quartz, gypsum, calcite, barite, rhodochrosite, pyrolusite, and fluorite,
2. the calculated mass of calcite for each vadose-zone hydrostratigraphic unit determined from the acid-neutralization tests, and
3. carbon dioxide concentrations measured for a typical soil ($10^{-2.0}$ atmospheres) (Sposito, 1989).

Additionally, the initial iron dissolved in the tailings porewaters was allowed to equilibrate with amorphous-iron hydroxide (i.e., HFO), the phases identified above, and the mass of calcite for each hydrostratigraphic unit; the resultant mass of HFO was added to the mass determined from the leach-extraction tests. Following partial neutralization of the tailings porewaters, the resultant solution underwent speciation and surface complexation with the mass of HFO (total extracted and precipitated). For each batch reaction, distribution coefficients were calculated according to Equation 1 (see above) using the initial dissolved uranium(VI) concentration (~ 94 mg/l or 3.91×10^{-4} molal), the final dissolved uranium(VI) concentration, the mass of rock, and the calculated volume of solution.

In addition to uranium, distribution coefficients of other metals in addition to sulfate, selenium and fluoride were also calculated for each stratigraphic unit similar to the approach described above. Sorption of nitrogen species was not considered since the Dzombak and Morel (1990) database does not include this element. The results are described below.

RESULTS

HFO and Acid-Neutralization Potential

The mass of hydrous-ferric oxide leached from the crushed-bedrock samples, and acid neutralization-potential, is presented in Table B-6. With the exception of two elevated values, there was little variation in dissolved iron (and inferred mass of HFO) for the bedrock. The absolute number of surface sites and relative partitioning between strong-site and weak-site densities were calculated from the moles of HFO and the site densities listed in Table B-3.

Geochemical Modeling

Selected output computed with PHREEQC for the vadose zone hydrostratigraphic units is summarized in Table B-7. The average ionic strength of the initial and equilibrated

solutions for the Dzombak and Morel (1990) model was 1.32 molal, which approaches the limits imposed by the ion-association model (i.e., Davies Equation) used to calculate activity coefficients. Therefore, aqueous- and surface-complexation calculations should be considered in a semi-quantitative framework.

Water-quality data of the infiltrating tailings porewaters indicates that sufficient buffering minerals would be present to neutralize the low-pH waters to circumneutral conditions. Model simulations predicting neutralization of the low-pH fluids in the vadose zone beneath the White Mesa Mill agree with investigations at a large number of uranium-tailings facilities in the western United States, which have demonstrated neutralization of low-pH fluids within a few hundred feet in any transport direction (INTERA, 2007).

Differences in equilibrated-solution pH resulted from the variability in the mass of calcite for each hydrostratigraphic unit. The low-pH solution chemistry predicted for the third hydrostratigraphic unit results from the low acid-neutralization potential measured from the bedrock sample and the conservative assumptions used to construct the geochemical model. In actuality, water moving through the third unit would represent the integrated effects of water-rock reactions that occurred during transport through the overlying hydrostratigraphic units (i.e., vadose-zone water in this unit would likely be at circumneutral conditions).

Speciation of the equilibrated waters for the Dzombak and Morel (1990) surface-complexation model is presented in Table B-8. Variability of total carbon resulted from different final solution pH's and complexation with uranium(VI).

Adsorption of Uranium

At the equilibrated-solution compositions (Tables B-7 and B-8), the calculated K_d values and retardation factors for uranium transport in the vadose zone hydrostratigraphic units are summarized in Table B-9. Retardation factors are only presented for the base-case scenario for Cells 2 and 3. The calculated K_d values are considered conservative since only iron-oxyhydroxide phases were considered as minerals that could participate in

surface-complexation reactions (e.g., adsorption of uranium onto goethite, montmorillonite, and quartz were not included in the model; Davis et al. 2004). Inclusion of additional HFO precipitated during equilibration of the tailings porewaters did not significantly affect the K_d values. An additional 1.70 and 3.54 grams of HFO was added to the first and second batch reactions.

Most uranium-bearing phases were undersaturated except for carnotite and tyuyamunite which were supersaturated in the first vadose zone hydrostratigraphic unit; however, these uranium-vandadium-bearing phases were not allowed to precipitate, which is consistent with a more conservative approach. Iron, aluminum, and manganese-oxyhydroxide phases (except for the third hydrostratigraphic unit) were at conditions that could lead to precipitation.

Adsorption of Additional Solutes

Sorption coefficients and retardation factors were calculated for additional contaminants of concern to assess their potential transport through the bedrock vadose zone (see Table B-10). The Dzombak and Morel (1990) surface-complexation model considers competitive adsorption between a large number of dissolved species (Table B-3). Retardation factors are only presented for the base-case scenario for Cells 2 and 3.

DISCUSSION AND CONCLUSIONS

The fate-and-transport potential of contaminants through the vadose zone to the underlying perched water table beneath the White Mesa Mill is summarized in order to draw some general conclusions regarding processes that may control a solutes ability to reach the perched aquifer. Two geochemical processes are hypothesized to control solute-transport mobility in the vadose zone: adsorption of solutes onto HFO and precipitation of minerals.

The results presented in Table B-10 demonstrate a high-sorption potential for uranium and most trace metals, especially for the middle vadose zone hydrostratigraphic unit which contains sufficient buffering minerals capable of neutralizing the low-pH fluids present in the tailings. The distribution coefficients have been subdivided into three categories: high, intermediate, and low. Solutes predicted to have a high K_d include arsenic, beryllium, chromium, copper, lead, uranium, vanadium, and zinc. Solutes predicted to have an intermediate K_d include cadmium, cobalt, manganese, molybdenum, and nickel. Solutes predicted to have a low K_d include selenium and sulfate; while iron, fluoride, mercury, silver and thallium were predicted to have a K_d of approximately zero. Distribution coefficients predicted with the geochemical model generally agree with published estimates, with the exception of cadmium, cobalt, iron, manganese, mercury, nickel, selenium, silver, and thallium. Based on values reported by Sheppard and Thibault (1990), U.S. EPA (1996), and U.S. EPA (1999), distribution coefficients for these solutes are likely to be significantly larger than model predictions presented in Table B-10.

As described in Section 4.0 of the Infiltration and Contaminant Transport Modeling Report, uranium, as a result of the solute's strong capacitance for sorption and resultant high-retardation coefficients, is predicted to migrate a limited distance below the liner system in 200 years; uranium is not predicted to reach the perched aquifer within 200 years. Similarly to uranium, the metal species with high to intermediate distribution coefficients discussed above are also expected to be transported a limited distance beneath the liner system in 200 years. Sorption of selenium, iron, mercury, and thallium are expected to be larger than the model predictions, and these solutes are not expected to impact water quality in the perched aquifer within 200 years.

Mineral-saturation indices presented in Table B-11 demonstrate that dissolved concentrations of sulfate and manganese, and to a lesser extent fluoride, in vadose-zone porewater will be predominately controlled by mineral-precipitation reactions. The initial concentration of sulfate in the tailings porewater was reduced from 64,330 to 44,248 mg/l, primarily from the precipitation of gypsum and to a lesser extent barite. The concentration of fluoride was reduced from 1,679 to 1,175 mg/l through the precipitation

of fluorite; and manganese was reduced from 145 to 0 mg/l through the precipitation of pyrolusite. Additionally, concentrations of iron and aluminum in vadose-zone porewater are expected to be controlled by precipitation of iron and aluminum oxyhydroxides, and are not expected to impact water quality in the perched aquifer within 200 years. Equilibrium calculations also indicate that two uranium-vanadium-bearing phases (carnotite and tyuyamunite) are expected to precipitate in the vadose zone, which would act as a sink for these two solutes.

Given the high-pe conditions of the tailings porewater following equilibration with atmospheric oxygen, most of the total nitrogen was present as N(5+) and speciated as nitrate (NO_3^-). The average concentration of dissolved nitrate for the initial conditions and three hydrostratigraphic units was 10,127 mg/l; concentrations of nitrite and ammonia were approximately zero. Adsorption of nitrogen species was not determined since the Dzombak and Morel (1990) surface-complexation model does not contain any nitrogen species. As a result, nitrate is expected to be conservatively transported through the vadose zone, similar to chloride. Considering the low water fluxes through the vadose zone and reduced diffusion coefficient of nitrate as compared to chloride, nitrate is not expected to impact water quality in the perched aquifer within 200 years.

In summary, adsorption of contaminants onto HFO and precipitation of minerals in the vadose zone should limit the mobility of most trace metals in addition to uranium and sulfate. Furthermore, the calculated K_d values and retardation factors are considered conservative because:

1. only a single iron-oxyhydroxide phase was considered to participate in surface-complexation reactions (e.g., adsorption of metals onto aluminum-oxyhydroxides, goethite, montmorillonite, illite, and quartz were not included in the model);
2. coprecipitation of uranium (Abdelouas et al., 1998) and metals onto the surfaces of precipitating phases (e.g., hydrous-ferric oxide, sulfates, carbonates) was ignored, which could also serve as a sink for metals; and
3. neutralization of infiltrating tailings porewaters was calculated for each individual bedrock unit and not with an iterative (pseudo-reactive transport)

approach, which would serve to increase sorption for the third hydrostratigraphic unit.

REFERENCES

Abdelouas, A., W. Lutze, and E. Nuttall, 1998. Chemical reactions of uranium in ground water at a mill tailings site, *Journal of Contaminant Hydrology*, 34, 343–361.

Allison, J.D., D.S. Brown, and K.J. Novo-Gradac, 1991. *MINTEQA2/PRODEFA2*, a geochemical assessment model for environmental systems, Version 3.0 User's Manual: U.S. Environmental Protection Agency Report EPA/600/3-91/021, 106 p.

Bernhard, G., G. Geipel, T. Reich, V. Brendler, S. Amayri, and H. Nitsche, 1992. Uranyl(VI) carbonate complex formation: Validation of the Ca2UO2(CO3)3 (aq) species, *Radiochim. Acta*, 89, 8, 511-518.

Daniel B. Stephens & Associates, 2007. Laboratory Report Prepared for MWH Americas, Inc., April 27, 2007.

Davis, J.A. and G.P. Curtis, 2003. Application of Surface Complexation Modeling to Describe Uranium(VI) Adsorption and Retardation at the Uranium Mill Tailings Site at Naturita, Colorado, Report NUREG CR-6820, U. S. Nuclear Regulatory Commission, Rockville, MD., pp. 223. Available at http://www.nrc.gov/readingrm/doc-collections/nuregs/contract/cr6820/cr6820.pdf.

Davis, J.A., D.E. Meece, M. Kohler, and G.P. Curtis, 2004. Approaches to surface complexation modeling of Uranium(VI) adsorption on aquifer sediments, *Geochimica et Cosmochimica Acta*, 68, 18, 3621-3641.

Dzombak D. A. and F.M. Morel, 1990. *Surface complexation modeling: hydrous ferric oxide*, John Wiley & Sons, New York, NY, pp. 416.

Freeze, R.A. and J.A. Cherry, 1979. *Groundwater*, Prentice-Hall, Inc., Englewood Cliffs, N.J, pp. 604.

Grenthe, I. et al., 1992. *Chemical Thermodynamics of Uranium*, Elsevier, Amsterdam, The Netherlands, pp. 716.

Guillaumont, R. et al., 2003. *Update on the chemical thermodynamics of Uranium, Neptunium, Plutonium, Americium and Technetium*, Elsevier, Amsterdam, The Netherlands, pp. 919.

Hsi, Ching-Duo Daniel, 1981. Sorption of uranium (VI) by iron oxides, Ph.D. Dissertation, Colorado School of Mines, pp. 154.

INTERA, 2007. Revised Background Groundwater Quality Report: Existing Wells for Denison Mines (USA) Corp.'s White Mesa Uranium Mill Site, San Juan County, Utah. Prepared for Denison Mines (USA) Corp. October 2007.

Langmuir, D., 1997. *Aqueous Environmental Geochemistry*, Prentice-Hall, Inc., Englewood Cliffs, N.J., pp. 600.

Moll, H., 1997. Zur Wechselwirkung von Uran mit Silicat in wässrigen Systemen, Ph.D. Dissertation, Technische Universität Dresden.

Parkhurst, D.L and C.A.J. Appelo, 1999. User's guide to PHREEQC User's Guide to PHREEQC (Version 2)--A Computer Program for Speciation, Batch-Reaction, One-Dimensional Transport, and Inverse Geochemical Calculations, U.S. Geological Survey Water-Resources Investigations Report 99-4259, pp. 312.

Payne, T.E., 1999. Uranium(VI) interactions with mineral surfaces: controlling factors and surface complexation modeling, Ph.D. Dissertation, University of New South Wales, pp. 332.

Sandino, A. and J. Bruno, 1992. The Solubility of (UO2)3(PO4)2•4H2O(s) and the Formation of U(VI) Phosphate Complexes: Their Influence in Uranium Speciation in Natural Waters, *Geochimica et Cosmochimica Acta*, 56, 4135-4145.

Sheppard, M.I. and D.H. Thibault, 1990. Default soil solid/liquid partition coefficients, K_ds, for four major soil types: a compendium, *Health Physics*, 59(4), 471-482.

Silva, R.J., 1992. Mechanisms for the Retardation of Uranium(VI) Migration, Mat. Res. Soc. Symp. Proc., 257, 323-330.

Silva, R.J. et al., 1995. *Thermodynamics 2; Chemical Thermodynamics of Americium*, with an appendix on Chemical Thermodynamics of Uranium, Nuclear Energy Agency, OECD, North-Holland, Elsevier.

Sposito, G., 1989. *The chemistry of soils*, Oxford University Press, Inc., New York, NY, pp. 277

U.S. EPA, 1996. Soil Screening Guidance: Technical Background Document, Publication 9355.4-17A, 2nd ed., Office of Solid Waste and Emergency Response, U.S. Environmental Protection Agency, published May 1996.

U.S. EPA, 1999. Understanding variation in partition coefficient, K_d, values: Review of Geochemistry and Available K_d Values for Cadmium, Cesium, Chromium, Lead, Plutonium, Radon, Strontium, Thorium, Tritium (3H), and Uranium, Volume II, Publication 402-R-99-004B, Office of Air and Radiation, U.S. Environmental Protection Agency, published August 1999.

Utah Division of Radiation Control, 2004. Draft Ground Water Discharge Permit, Statement of Basis for a Uranium Milling Facility at White Mesa, South of Blanding, December 2004.

Waite, T.D., J.A. Davis, T.E. Payne, G.A. Waychunas, and N. Xu, 1994. Uranium(VI) adsorption to ferrihydrite: application of a surface complexation model, *Geochimica et Cosmochimica Acta*, 58, 24, 5465-5478.

Wazne, M., G.P. Korfiatis, and X. Meng, 2003. Carbonate effects on hexavalent uranium adsorption by iron oxyhydroxide, *Environmental Science & Technology*, 37, 3619-3624.

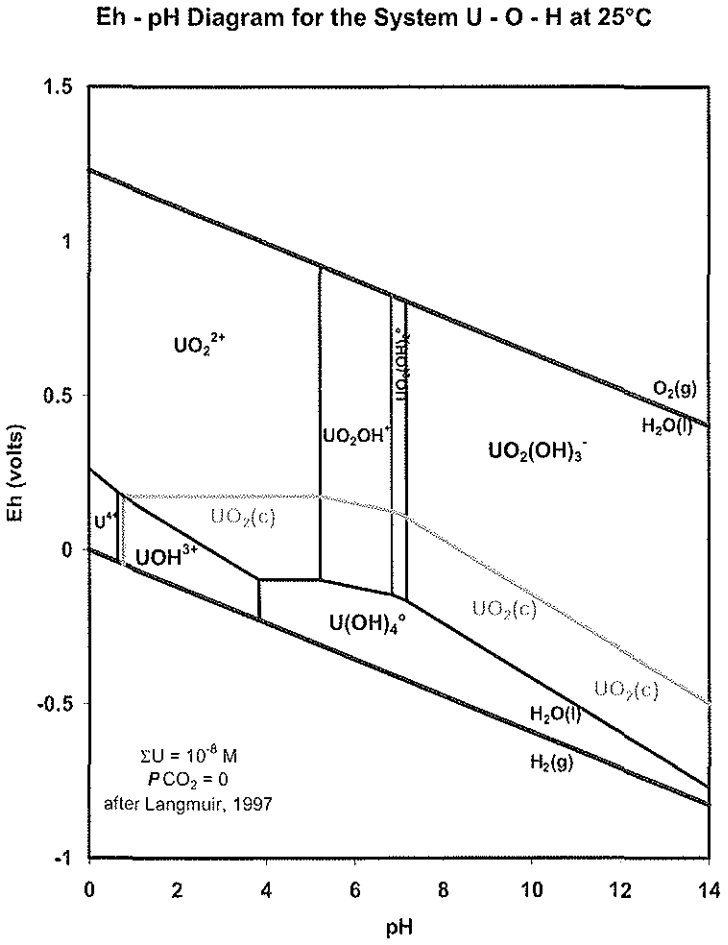

Figure B-1. Eh pH diagram for the system U – O_2 – H_2O in pure water for $\Sigma U = 1x10^{-8}$ M. The $UO_2(c)$ solid/solution boundary is represented by the green line, (after Langmuir, 1997).

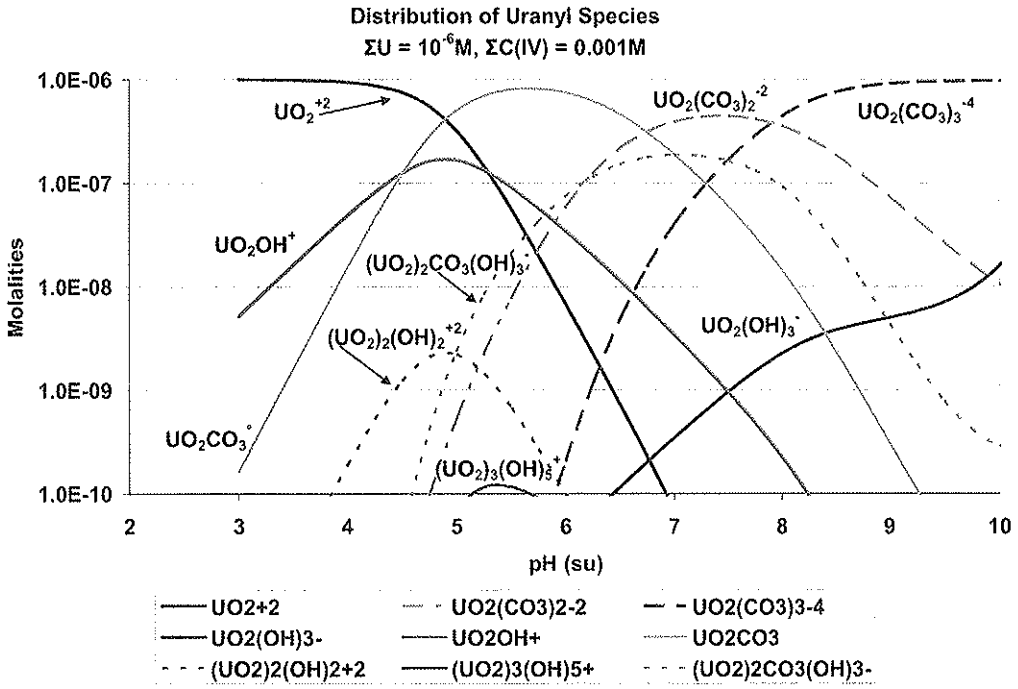

Figure B-2. Distribution of Uranyl Complexes as Function of pH for ΣU = 1.0×10^{-6} M and ΣC(IV) = 0.001 M calculated with the project-specific thermodynamic database.

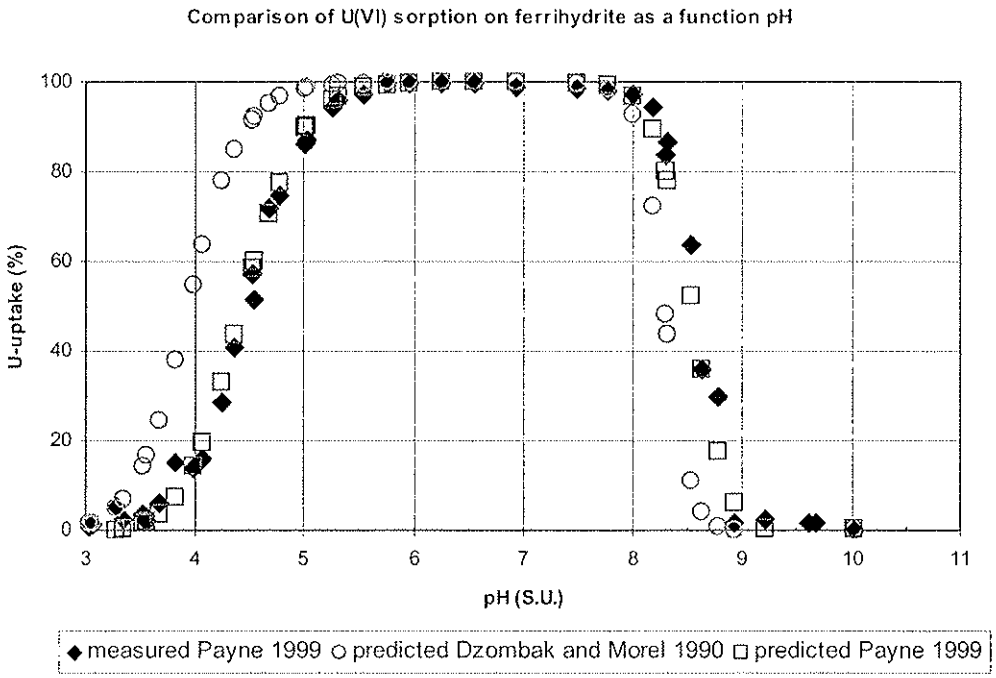

Figure B-3. Comparison of Payne (1999) laboratory-generated data (filled diamonds) and model-generated fits for uranium (uranyl adsorption) calculated with PHREEQC using the (i) Payne (1999) surface-complexation model (open squares) and (ii) Dzombak and Morel (1990) surface-complexation model (open circles).

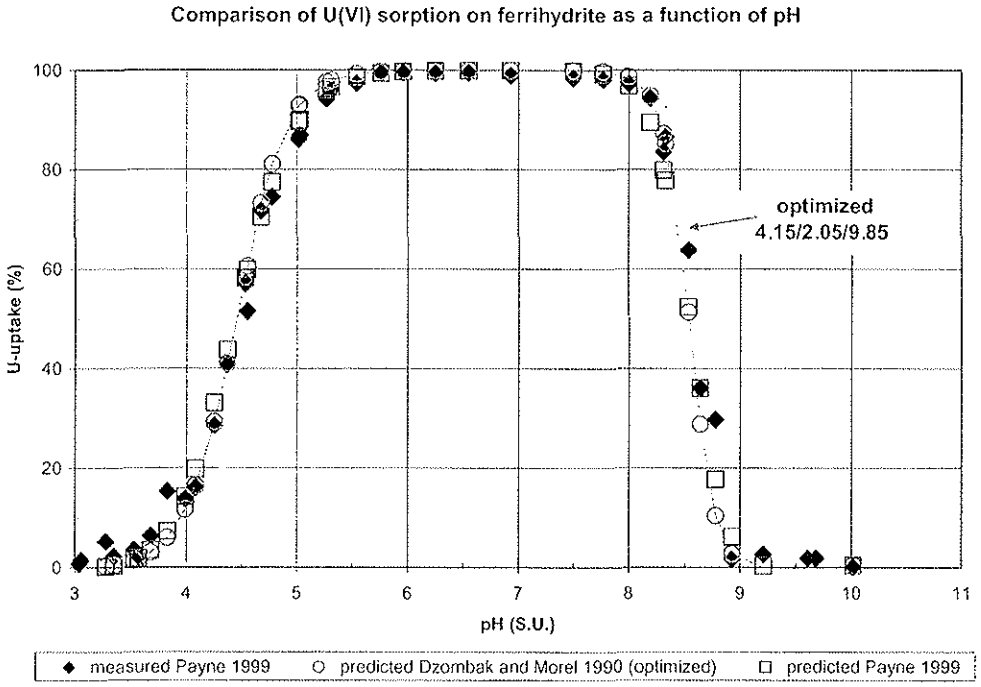

Figure B-4. Comparison of Payne (1999) laboratory-generated data (filled diamonds) and model-generated fits for uranium (uranyl adsorption) calculated with PHREEQC using the (i) Payne (1999) surface-complexation model (open squares) and (ii) Dzombak and Morel (1990) surface-complexation model after optimizing the uranyl and uranyl-carbonate surface-complexation coefficients (open circles with solid connecting line).

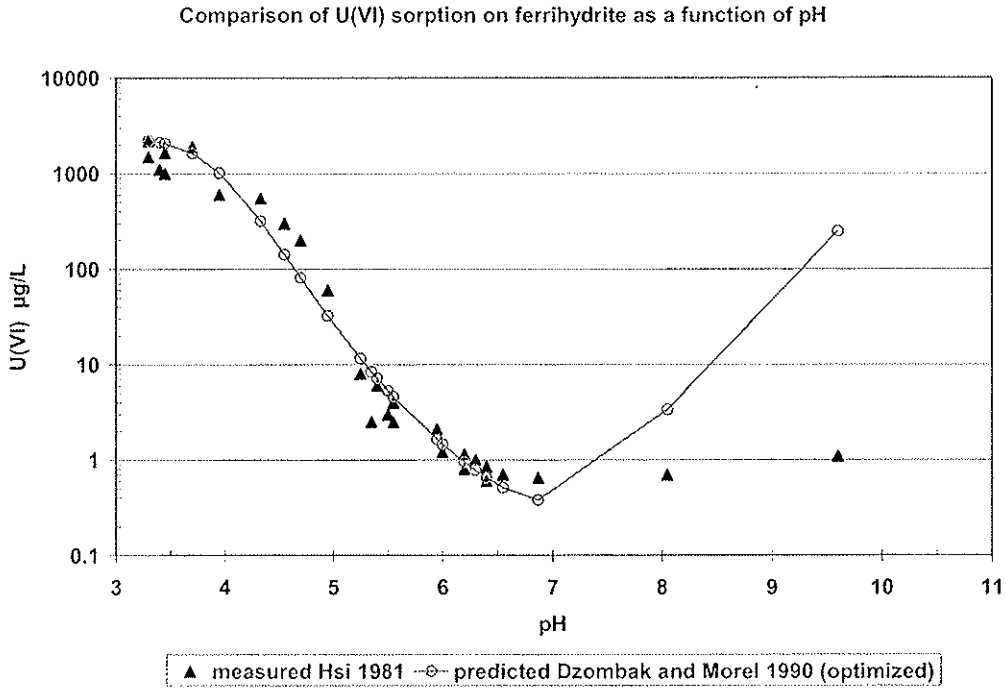

Figure B-5. Comparison of Hsi (1981) laboratory-generated data (filled triangles) and model-generated fits for uranium (uranyl adsorption) calculated with PHREEQC using the Dzombak and Morel (1990) surface-complexation model after optimizing the uranyl and uranyl-carbonate surface-complexation coefficients (open circles with solid connecting line).

Table B-1. Comparison of aqueous-complex formation (stability) coefficients between thermodynamic databases. All data were calculated at a standard temperature of 25 °C and a pressure of 0.1 MPa at infinite dilution (zero ionic strength).

number	complex	reaction	This Study log K (--)	This Study reference	Davis and Curtis (2003) log K (--)	Davis and Curtis (2003) reference	Payne (1999) log K (--)	Payne (1999) reference	Guillaumont et al. (2003) log K (--)	Guillaumont et al. (2003) reference	MINTEQ.V4 (2007) log K (--)	MINTEQ.V4 (2007) reference	WATEQ4F (2007) log K (--)	WATEQ4F (2007) reference
	UO_2-OH-complexes	equation												
1	$UO_2(OH)^+$	$H_2O + UO_2^{2+} = H^+ + UO_2OH^+$	-5.25	a	-5.2	d	-5.2	i	-5.250	a	-5.897	j	-5.2	k
2	$UO_2(OH)_{2,aq}$	$2H_2O + UO_2^{2+} = 2H^+ + UO_2(OH)_{2,aq}$	-12.15	a,b	≤ -11.5	b	-12	i	-12.15	a				k
3	$UO_2(OH)_3^-$	$3H_2O + UO_2^{2+} = 3H^+ + UO_2(OH)_3^-$	-20.25	a,c	-20	c	-20	i	-20.25	a			-19.2	k
4	$UO_2(OH)_4^{2-}$	$4H_2O + UO_2^{2+} = 4H^+ + UO_2(OH)_4^{2-}$	-32.4	a,d	-33	d	-33	i	-32.4	a			-33	k
5	$(UO_2)_2(OH)^{3+}$	$H_2O + 2UO_2^{2+} = H^+ + (UO_2)_2OH^{3+}$	-2.7	a,d	-2.7	d	-2.8	i	-2.7	a			-2.7	k
6	$(UO_2)_2(OH)_2^{2+}$	$2H_2O + 2UO_2^{2+} = 2H^+ + (UO_2)_2(OH)_2^{2+}$	-5.62	a,d	-5.62	d	-5.63	i	-5.62	a	-5.574	j	-5.62	k
7	$(UO_2)_3(OH)_4^{2+}$	$4H_2O + 3UO_2^{2+} = 4H^+ + (UO_2)_3(OH)_4^{2+}$	-11.9	a,d	-11.9	d	-11.9	i	-11.9	a			-11.9	k
8	$(UO_2)_3(OH)_5^+$	$5H_2O + 3UO_2^{2+} = 5H^+ + (UO_2)_3(OH)_5^+$	-15.55	a,d	-15.55	d	-15.56	i	-15.55	a	-15.585	j	-15.55	k
9	$(UO_2)_3(OH)_7^-$	$7H_2O + 3UO_2^{2+} = 7H^+ + (UO_2)_3(OH)_7^-$	-32.2	a	-31	d	-31	i	-32.2	a			-31	k
10	$(UO_2)_4(OH)_7^+$	$7H_2O + 4UO_2^{2+} = 7H^+ + (UO_2)_4(OH)_7^+$	-21.9	a,d	-21.9	d			-21.9	a			-21.9	k
number	UO_2-CO_3-complexes	equation	log K (--)	reference	log K (--)	reference	log K (--)	reference	log K (--)	reference	log K (--)	reference	log K (--)	reference
1	$UO_2CO_{3,aq}$	$CO_3^{2-} + UO_2^{2+} = UO_2CO_{3,aq}$	9.94	a	9.67	g	9.7	i	9.94	a	9.6	j	9.63	k
	$UO_2CO_{3,aq}$	$HCO_3^- + UO_2^{2+} = UO_2CO_{3,aq} + 1H^+$												
2	$UO_2(CO_3)_2^{2-}$	$2CO_3^{2-} + UO_2^{2+} = UO_2(CO_3)_2^{2-}$	16.61	a	16.94	d	17	i	16.61	a	16.9	j	17	k
	$UO_2(CO_3)_2^{2-}$	$2HCO_3^- + UO_2^{2+} = UO_2(CO_3)_2^{2-} + 2H^2$												
3	$UO_2(CO_3)_3^{4-}$	$3CO_3^{2-} + UO_2^{2+} = UO_2(CO_3)_3^{4-}$	21.84	a	21.6	d	21.63	i	21.84	a	21.6	j	21.63	k
	$UO_2(CO_3)_3^{4-}$	$3HCO_3^- + UO_2^{2+} = UO_2(CO_3)_3^{4-} + 3H^+$												
4	$UO_2(CO_3)_3^{5-}$	$3CO_3^{2-} + UO_2^{2+} = UO_2(CO_3)_3^{5-}$	6.95	a					6.95	a			7.43	k
	$UO_2(CO_3)_3^{5-}$	$3HCO_3^- + UO_2^{2+} = UO_2(CO_3)_3^{5-} + 3H^+$												
5	$(UO_2)_3(CO_3)_6^{6-}$	$6CO_3^{2-} + 3UO_2^{2+} = (UO_2)_3(CO_3)_6^{6-}$	54	a,d	54	d			54	a			54	k
number	UO_2-CO_3-OH-complexes	equation	log K (--)	reference	log K (--)	reference	log K (--)	reference	log K (--)	reference	log K (--)	reference	log K (--)	reference
1	$(UO_2)_2CO_3(OH)_3^-$	$CO_3^{2-} + 2UO_2^{2+} + 3H_2O = (UO_2)_2CO_3(OH)_3^- + 3H^+$	-0.86	d	-0.86	d	-1.18	i	reaction w/ $CO_{2,g}$	a				
2	$(UO_2)_3CO_3(OH)_3^+$	$CO_3^{2-} + 3UO_2^{2+} + 3H_2O = (UO_2)_3CO_3(OH)_3^+ + 3H^+$	0.66	d	0.66	d			reaction w/ $CO_{2,g}$	a				
3	$(UO_2)_{11}(CO_3)_6(OH)_{12}^{2-}$	$6CO_3^{2-} + 11UO_2^{2+} + 12H_2O = (UO_2)_{11}(CO_3)_6(OH)_{12}^{2-} + 12H^+$	36.43	d	36.43	d			reaction w/ $CO_{2,g}$	a				
number	UO_2-Ca-CO_3-complexes	equation	log K (--)	reference	log K (--)	reference	log K (--)	reference	log K (--)	reference	log K (--)	reference	log K (--)	reference
1	$CaUO_2(CO_3)_3^{2-}$	$3CO_3^{2-} + Ca^{2+} + UO_2^{2+} = CaUO_2(CO_3)_3^{2-}$	25.4	e	25.4	e								
2	$Ca_2UO_2(CO_3)_{3,aq}$	$3CO_3^{2-} + 2Ca^{2+} + UO_2^{2+} = CaUO_2(CO_3)_{3,aq}$	30.55	e	30.55	e								
number	UO_2-F-CO_3-complexes	equation	log K (--)	reference	log K (--)	reference	log K (--)	reference	log K (--)	reference	log K (--)	reference	log K (--)	reference
1	$UO_2CO_3F^-$	$CO_3^{2-} + F^- + UO_2^{2+} = UO_2CO_3F^-$	13.75	a					13.75	a				
2	$UO_2CO_3F_2^{2-}$	$CO_3^{2-} + 2F^- + UO_2^{2+} = UO_2CO_3F_2^{2-}$	15.57	a					15.57	a				
3	$UO_2CO_3F_3^{3-}$	$CO_3^{2-} + 3F^- + UO_2^{2+} = UO_2CO_3F_3^{3-}$	16.38	a					16.38	a				
number	UO_2-Halogen-complexes	equation	log K (--)	reference	log K (--)	reference	log K (--)	reference	log K (--)	reference	log K (--)	reference	log K (--)	reference
1	UO_2F^+	$F^- + UO_2^{2+} = UO_2F^+$	5.16	a					5.16	a	5.14	j	5.09	k
2	$UO_2F_{2,aq}$	$2F^- + UO_2^{2+} = UO_2F_{2,aq}$	8.83	a					8.83	a	8.6	j	8.62	k
3	$UO_2F_3^-$	$3F^- + UO_2^{2+} = UO_2F_3^-$	10.9	a					10.9	a	11	j	10.9	k
4	$UO_2F_4^{2-}$	$4F^- + UO_2^{2+} = UO_2F_4^{2-}$	11.84	a					11.84	a	11.9	j	11.7	k
5	UO_2Cl^+	$Cl^- + UO_2^{2+} = UO_2Cl^+$	0.17	a,d	0.17	d			0.17	a	0.21	j	0.17	k
6	$UO_2Cl_{2,aq}$	$2Cl^- + UO_2^{2+} = UO_2Cl_{2,aq}$	-1.1	a,d	-1.1	d			-1.1	a			-1.1	k

number	UO_2-SO_4-complexes	equation	This Study log K (--)	This Study reference	Davis and Curtis (2003) log K (--)	Davis and Curtis (2003) reference	Payne (1999) log K (--)	Payne (1999) reference	Guillaumont et al. (2003) log K (--)	Guillaumont et al. (2003) reference	MINTEQ.V4 (2007) log K (--)	MINTEQ.V4 (2007) reference	WATEQ4F (2007) log K (--)	WATEQ4F (2007) reference
1	$UO_2SO_{4,aq}$	$SO_4^{2-} + UO_2^{2+} = UO_2SO_{4,aq}$	3.15	a,d	3.15	d	3.15	i	3.15	a	3.18	j	3.15	k
2	$UO_2(SO_4)_2^{2-}$	$2SO_4^{2-} + UO_2^{2+} = UO_2(SO_4)_2^{2-}$	4.14	a,d	4.14	d	4.14	i	4.14	a	4.3	j	4.14	k
3	$UO_2(SO_4)_3^{4-}$	$3SO_4^{2-} + UO_2^{2+} = UO_2(SO_4)_3^{4-}$	3.02	a					3.02	a				
number	**UO_2-PO_4-complexes**	**equation**	**log K (--)**	**reference**	**log K (--)**	**reference**	**log K (--)**	**reference**	**log K (--)**	**reference**	**log K (--)**	**reference**	**log K (--)**	**reference**
1	$UO_2PO_4^-$	$PO_4^{3-} + UO_2^{2+} = UO_2PO_4^-$	13.23	a,d	13.23	d	13.23	i	13.23	a	13.25	j	13.69	k
	$UO_2PO_4^-$	$HPO_4^{2-} + UO_2^{2+} = UO_2PO_4^- + H^+$												
2	$UO_2HPO_{4,aq}$	$PO_4^{3-} + UO_2^{2+} + H^+ = UO_2HPO_{4,aq}$	19.59	s	19.59	d	19.59	i			19.655	j	20.21	k
	$UO_2HPO_{4,aq}$	$HPO_4^{2-} + UO_2^{2+} = UO_2HPO_{4,aq}$							7.24	a				
3	$UO_2(HPO_4)_2^{2-}$	$2PO_4^{3-} + UO_2^{2+} + 2H^+ = UO_2(HPO_4)_2^{2-}$									42.986	j	43.441	k
4	$UO_2H_2PO_4^+$	$PO_4^{3-} + UO_2^{2+} + 2H^+ = UO_2H_2PO_4^+$	22.82	d	22.62	d	22.82	i			22.833	j	22.87	k
	$UO_2H_2PO_4^+$	$H_3PO_{4,aq} + UO_2^{2+} = H^+ + UO_2H_2PO_4^+$							1.12	a				
	$UO_2H_2PO_4^+$	$HPO_4^{2-} + UO_2^{2+} + H^+ = UO_2H_2PO_4^+$												
5	$UO_2(H_2PO_4)_3^-$	$3PO_4^{3-} + UO_2^{2+} + 6H^+ = UO_2(H_2PO_4)_3^-$									66.245	j	66.245	k
6	$UO_2H_3PO_4^{2+}$	$PO_4^{3-} + UO_2^{2+} + 3H^+ = UO_2H_3PO_4^{2+}$	22.46	d	22.46	d	22.46	i					22.813	k
	$UO_2H_3PO_4^{2+}$	$H_3PO_{4,aq} + UO_2^{2+} = UO_2H_3PO_4^{2+}$							0.76	a				
	$UO_2H_3PO_4^{2+}$	$HPO_4^{2-} + UO_2^{2+}\ 2H^+ = UO_2H_3PO_4^{2+}$												
7	$UO_2(H_2PO_4)_{2,aq}$	$2PO_4^{3-} + UO_2^{2+} + 4H^+ = UO_2(H_2PO_4)_{2,aq}$	44.04	d	44.04	d	44.04	i			44.7	j	44.36	k
	$UO_2(H_2PO_4)_{2,aq}$	$2H_3PO_{4,aq} + UO_2^{2+} = 2H^+ + UO_2(H_2PO_4)_{2,aq}$							0.64	a				
	$UO_2(H_2PO_4)_{2,aq}$	$2HPO_4^{2-} + UO_2^{2+} + 2H^+ = + UO_2(H_2PO_4)_{2,aq}$												
8	$UO_2(H_2PO_4)(H_3PO_4)^+$	$2PO_4^{3-} + UO_2^{2+} + 5H^+ = UO_2(H_2PO_4)(H_3PO_4)^+$	45.05	d	45.05	d	45.05	i						
	$UO_2(H_2PO_4)(H_3PO_4)^+$	$2H_3PO_{4,aq} + UO_2^{2+} = H^+ + UO_2(H_2PO_4)(H_3PO_4)^+$							1.55	a				
	$UO_2(H_2PO_4)(H_3PO_4)^+$	$2HPO_4^{2-} + UO_2^{2+} + 3H^+ = UO_2(H_2PO_4)(H_3PO_4)^+$												
number	**PO_4-complex**	**equation**	**log K (--)**	**reference**	**log K (--)**	**reference**	**log K (--)**	**reference**	**log K (--)**	**reference**	**log K (--)**	**reference**	**log K (--)**	**reference**
1	H_3PO_4	$PO_4^{3-} + 3H^+ = H_3PO_4$	21.702	d	21.702	d								
number	**UO_2-NO_3-complexes**	**equation**	**log K (--)**	**reference**	**log K (--)**	**reference**	**log K (--)**	**reference**	**log K (--)**	**reference**	**log K (--)**	**reference**	**log K (--)**	**reference**
1	$UO_2NO_3^+$	$NO_3^- + UO_2^{2+} = UO_2NO_3^+$	0.3	a,d	0.3	d	0.3	i	0.3	a	0.3	j	0.3	k
number	**UO_2-SiO_2-complexes**	**equation**	**log K (--)**	**reference**	**log K (--)**	**reference**	**log K (--)**	**reference**	**log K (--)**	**reference**	**log K (--)**	**reference**	**log K (--)**	**reference**
1	$UO_2SiO(OH)_3^+$	$UO_2^{2+} + SiO_2(OH)_2^{2-} + H^+ = UO_2SiO(OH)_3^+$			21.54	h								
		$UO2^{2+} + H_4SiO_4 = UO_2SiO(OH)_3^+ + H^+$	-1.46	f										
2	$UO_2H_3SiO_4^+$	$UO_2^{2+} + H_4SiO_4 = UO_2H_3SiO_4^+ + H^+$									-1.9111	j		
number	**UO_2-AsO_4-complexes**	**equation**	**log K (--)**	**reference**	**log K (--)**	**reference**	**log K (--)**	**reference**	**log K (--)**	**reference**	**log K (--)**	**reference**	**log K (--)**	**reference**
1	$UO_2HAsO_{4,aq}$	$UO_2^{2+} + AsO_4^{3-} + H^+ = UO_2HAsO_{4,aq}$	18.76	a					18.76	a				
2	$UO_2H_2AsO_4^+$	$UO_2^{2+} + AsO_4^{3-} + 2H^+ = UO_2H_2AsO_4^+$	21.96	a					21.96	a				
3	$UO_2(H_2AsO_4)_{2,aq}$	$UO_2^{2+} + 2AsO_4^{3-} + 4H^+ = UO_2(H_2AsO_4)_{2,aq}$	41.53	a					41.53	a				

a = reported in Guillaumont et al. (2003)
b = reported in Davis and Curtis (2003), reproduced after Silva (1992)
c = reported in Davis and Curtis (2003), reproduced after Sandino and Bruno (1992)
d = reported in Davis and Curtis (2003), reproduced after Grenthe et al. (1992)
e = reported in Davis and Curtis (2003) and Davis et al. (2004), reproduced after Bernhard et al. (2001)
f = rewritten w/ H_4SiO_4, similar to Grenthe et al. (1992)
g = reported in Davis and Curtis (2003), reproduced after Silva et al. (1995)
h = reported in Davis and Curtis (2003), reproduced after Moll (1997)
i = reported in Payne (1999)
j = MINTEQ.V4 February 2007 release with PHREEQC (version 2.13.2)
k = WATEQ4F February 2007 release with PHREEQC (version 2.13.2)

Table B-2. Comparison between different surface-complexation models (SCM) of uranium(VI) adsorption onto ferrihydrite or hydrous ferric oxide (HFO).

SCM	COMPARISON CRITERIA		
Dzombak and Morel 1990	**Assumptions**	**Advantages**	**Disadvantages**
Diffuse-layer model with electrical double-layer corrections considering a two-site binding model.	Adsorption of inner-sphere complexes including uranyl onto ferrihydrite via uptake on monodentate surface sites. Total site density of 0.205 mol sites/mol Fe and 0.005 moles of strong sites determined from mean value of dataset. HFO surface area 600 m^2/g. There are 40-fold more weak sites than strong sites. Adsorption coefficients determined empirically.	Surface-complexation reactions are easily simulated with geochemical codes (e.g., PHREEQC and MINTEQA2) for a variety of common dissolved species including most metals. Dzombak and Morel's (1990) database does contain adsorption coefficients for most major cations/anions, which allows competitive sorption to be modeled.	Ion-adsorption coefficients determined independently based on simple electrolyte solutions; effects due to competitive sorption from other charged species ignored.
Waite et al. 1994	**Assumptions**	**Advantages**	**Disadvantages**
Diffuse-layer model with electrical double-layer corrections considering a two-site binding model.	Uranyl adsorption as an inner-sphere complex onto ferrihydrite via uptake on bidentate surface sites. Total site density set to 0.875 mol sites/mol Fe and the number of strong sites (equal to 0.00184	Model able to explain experimental dataset for a wide range of dissolved uranium(VI) and pH conditions and a limited range of ionic strength and pCO_2. Considers competitive sorption of carbonate onto ferrihydrite in	Sensitivity of Fe concentration (as HFO) not evaluated. Surface properties of HFO are assumed equal to values reported by Dzombak and Morel (1990). Ion-adsorption coefficients

	mol/mol Fe) was determined via optimization to the measured (laboratory) adsorption data. HFO surface area 600 m^2/g. There are 485-fold more weak sites than strong sites. As compared to Dzombak and Morel (1990), the number of weak sites increased 4.4-fold and strong sites decreased 2.7-fold. Adsorption constants determined through optimization with FITEQL.	presence of uranyl and varying pH. Model results suggest that only one postulated ternary uranyl-carbonate surface complex may be necessary to simulate uranium(VI) adsorption.	determined independently based on simple electrolyte solutions; effects due to competitive sorption from other charged species ignored (excluding carbonate).
Payne 1999	**Assumptions**	**Advantages**	**Disadvantages**
Diffuse-layer model with electrical double-layer corrections considering a two-site binding model.	Same as Waite et al. 1994.	Considers competitive sorption of carbonate, sulfate, and phosphate onto ferrihydrite in presence of uranyl and varying pH. Surface-complexation reactions were simulated with MINTEQA2 after altering mass-balance equations to accommodate bidentate nature of uranyl sorption onto ferrihydrite. Model able to explain	Surface properties of HFO are assumed equal to values reported by Dzombak and Morel (1990). Ion-adsorption coefficients determined independently based on simple electrolyte solutions; effects due to competitive sorption from other charged species ignored (excluding carbonate, phosphate, and sulfate). Results suggest the postulated

		experimental dataset for a wide range of dissolved uranium(VI) and pH conditions and a limited range of ionic strength, pCO_2, and amount of HFO.	occurrence of a ternary surface complex between uranyl and phosphate. Lacking spectroscopic verification, predicting uranium(VI) adsorption with this species should be exercised with caution.
Wazne et al. 2003	**Assumptions**	**Advantages**	**Disadvantages**
Diffuse-layer model with electrical double-layer considering a one-site binding model was used.	Monodentate adsorption of uranyl, uranyl-monocarbonate, and uranyl-dicarbonate as inner-sphere complexes onto ferrihydrite surface sites. Total site density set to 0.875 mol sites/mol Fe. The number of strong sites was not mentioned. HFO surface area 600 m^2/g. Adsorption constants determined through optimization by minimizing the root-mean-square error (RMSE).	SCM simulating monodentate surfaces-site coordination of uranyl and uranyl-carbonate species was able to predict adsorption under a wide range of pH and carbonate concentrations for experimental and contaminated-groundwater solutions. Surface-complexation reactions were simulated with MINTEQA2 *without* altering mass-balance equations due to monodentate surface-site assumption. Ion-adsorption coefficients determined for uranyl and uranyl-carbonate species simultaneously based on simple electrolyte solutions.	Number of strong and weak sites not mentioned. Surface properties of HFO are assumed equal to values reported by Dzombak and Morel (1990). SCM ignores competitive adsorption effects from phosphate and sulfate; unfortunately concentrations of contaminated groundwater are not presented to verify this assumption. SCM developed by Wazne et al. (2003) does not evaluate sensitivity of HFO concentration.

Davis et al. 2004	Assumptions	Advantages	Disadvantages
For component additivity approach, model set-up similar to Waite et al. (1994). However, natural sediments and synthetic groundwater solutions were used to conduct batch experiments. Also examined adsorption due to surface-complexation reactions with quartz, montmorillonite, and goethite for different laboratory conditions.	Same as Waite et al. (1994) but with increased level of complexity due to modeling adsorption with additional sorbing phases. Assumes all iron dissolved from grain coatings was present as ferrihydrite.	Demonstrated that SCM developed by Waite et al. (1994) can be used to predict uranium(VI) adsorption for natural sediments and synthetic contaminated-groundwater solutions under certain environmental conditions. Experimentally determined surface area was used in model simulations.	More complicated, site-specific model not easily implemented without experimental determination of HFO and surface area. Results indicate that other sorbing phases should be considered as part of the surface-complexation modeling exercise which necessitates a more complex conceptual model for natural systems. As presented in Davis et al. (2004, Fig. 9), the Waite et al. (1994) SCM significantly underpredicted uranium(VI) sorption at elevated pCO_2's.

Table B-3. Absolute number and relative partitioning between strong- and weak-site densities in addition to aqueous species considered for the two surface-complexation models.

Surface-complexation model	total surface-site density	strong sites	weak sites	HFO surface area[a]
Dzombak and Morel (1990)	0.205 mol sites/mol Fe	0.005 mol sites/mol Fe	0.200 mol sites/mol Fe	600 m^2/g
Payne (1999)	0.875 mol sites/mol Fe	0.00184 mol sites/mol Fe	0.8732 mol sites/mol Fe	600 m^2/g

Surface-complexation model	Surface complexes considered for adsorption onto HFO
Dzombak and Morel (1990)[b,c,d]	Protonation, Deprotonation, Calcium, Strontium, Barium, Silver, Nickel, Cadmium, Zinc, Copper, Lead, Magnesium, Manganese, Uranyl, Uranyl-carbonate, Iron, Beryllium, Cobalt, Chromium, Chromate, Mercury, Thallium, Phosphate, Arsenate, Arsenite, Borate, Sulfate, Molybdate, Vanadate, Selenate, Selenite, and Fluoride
Payne (1999)	Protonation, Deprotonation, Uranyl, Uranyl-carbonate, Carbonate, Phosphate, and Sulfate

[a] Value taken from Dzombak and Morel (1990).

[b] Sorption coefficients taken from Dzombak and Morel (1990) as distributed with PHREEQC Version 2.13.2 (wateq4f.dat) except those noted below.

[c] Strong-site and weak-site sorption coefficients for uranyl and the weak-site sorption coefficient for uranyl-carbonate were optimized to fit the Payne (1999) and Hsi (1981) datasets.

[d] Sorption coefficients for Beryllium, Cobalt, Chromium, Chromate, Mercury, Molybdate, Thallium, and Vanadate taken from Dzombak and Morel (1990) as distributed with PHREEQC Version 2.13.2 (minteq.v2.dat).

Table B-4. Comparison between surface-complexation reactions and coefficients for the Payne (1999) and Dzombak and Morel (1990) surface-complexation models.

				Payne 1999		Dzombak and Morel 1990	
number	adsorbate	site bond	equation	log K (--)	reference	log K (--)	reference
1	protonation	strong	$SOH + H^+ = SOH_2^+$	6.62	a	7.29	d
2	protonation	weak	$WOH + H^+ = WOH_2^+$	6.62	a	7.29	d
3	deprotonation	strong	$SOH = SO^- + H^+$	-9.24	a	-8.93	d
4	deprotonation	weak	$WOH = WO^- + H^+$	-9.24	a	-8.93	d
number	adsorbate	site bond	equation	log K (--)	reference	log K (--)	reference
5	UO_2^{2+}	strong	$S(OH)_2 + UO_2^{2+} = SO_2UO_2 + 2H^+$	-2.35	a		
6	UO_2^{2+}	weak	$W(OH)_2 + UO_2^{2+} = WO_2UO_2 + 2H^+$	-6.06	a		
7	UO_2^{2+}	strong	$SOH + UO_2^{2+} = SOUO_2^+ + H^+$			4.15	e
8	UO_2^{2+}	weak	$WOH + UO_2^{2+} = WOUO_2^+ + H^+$			2.05	f
9	UO_2^{2+}-CO_3^{2-}	strong	$S(OH)_2 + UO_2^{2+} + CO_3^{2-} = SO_2UO_2CO_3^{2-} + 2H^+$	4.33	a		
10	UO_2^{2+}-CO_3^{2-}	weak	$W(OH)_2 + UO_2^{2+} + CO_3^{2-} = WO_2UO_2CO_3^{2-} + 2H^+$	0.24	a		
11	UO_2^{2+}-CO_3^{2-}	weak	$WOH + UO_2^{2+} + CO_3^{2-} = WOUO_2CO_3^- + H^+$			9.85	g
number	adsorbate	site bond	equation	log K (--)	reference	log K (--)	reference
12	CO_3^{2-}	strong	$SOH + H^+ + CO_3^{2-} = SOCO_2^-, H_2O$	11.48	a		
13	CO_3^{2-}	weak	$WOH + H^+ + CO_3^{2-} = WOCO_2^-, H_2O$	11.48	a		
14	CO_3^{2-}	strong	$SOH + 2H^+ + CO_3^{2-} = SOCO_2H + H_2O$	19.58	a		
15	CO_3^{2-}	weak	$WOH + 2H^+ + CO_3^{2-} = WOCO_2H + H_2O$	19.58	a		
16	PO_4^{3-}	strong	$SOH + PO_4^{3-} + H^+ = SPO_4^{2-} + H_2O$	18.05	b		
17	PO_4^{3-}	weak	$WOH + PO_4^{3-} + H^+ = WPO_4^{2-} + H_2O$	18.05	b	17.72	d
18	SO_4^{2-}	strong	$SOH + SO_4^{2-} = SOHSO_4^{2-}$	0.24	c		
19	SO_4^{2-}	weak	$WOH + SO_4^{2-} = WOHSO_4^{2-}$	0.24	c	0.79	d

Note 1: Additional surface-complexation reactions and coefficients included as part of the Dzombak and Morel (1990) model are included with PHREEQC (version 2.13.2).

Note 2: Two separate uranyl surface-complexation reactions and coefficients are necessary to account for the Payne (1999) and Dzombak and Morel (1990) assumption of bidentate and monodentate adsorption of uranyl, respectively.

a = from Payne (1999), Tables 11.1 and 11.2.
b = from Payne (1999), text and equations 13.5 and 13.6.
c = from Payne (1999), text and equation 11.11.
d = from Dzombak and Morel (1990), reproduced as part of PHREEQC (version 2.13.2).
e = original value (5.2) from Dzombak and Morel (1990), optimized against Payne (1999) and Hsi (1981) datasets.
f = original value (2.8) from Dzombak and Morel (1990), optimized against Payne (1999) and Hsi (1981) datasets.
g = parameter included to improve the fit at elevated pH conditions, optimized against Payne (1999) dataset.

Table B-5. Initial-solute concentrations for the tailings wastewater measured at the White Mesa Mill prior to equilibration with oxygen[a].

Analyte	Value	Units
Aluminum	1827	mg/l
Ammonia	3131	mg/l
Arsenic	149	mg/l
Barium	0.048	mg/l
Beryllium	0.5	mg/l
Boron	6.9	mg/l
Cadmium	3.4	mg/l
Calcium	368	mg/l
Chloride	4608	mg/l
Chromium	6.2	mg/l
Cobalt	60.7	mg/l
Copper	234.4	mg/l
Fluoride	1695	mg/l
Iron	2212	mg/l
Lead	3	mg/l
Magnesium	4774	mg/l
Manganese	146	mg/l
Mercury	3.5	mg/l
Molbdenum	52.8	mg/l
Nickel	82.6	mg/l
Nitrate	24	mg/l
Phosphorus	273	mg/l
Potassium	433	mg/l
Selenium	1.4	mg/l
Silicon	210	mg/l
Silver	0.1	mg/l
Sodium	5809	mg/l
Strontium	7	mg/l
Sulfate	64914	mg/l
Thallium	16	mg/l
Total Organic Carbon	78.5	mg/l
Uranium	94	mg/l
Vanadium	263.1	mg/l
Zinc	641	mg/l
pH	1.83	s.u.
pe[b]	20.2	-
temperature[c]	9.9	°C

[a] PHREEQC adjusts the initial concentrations according to the total mass of solutes; as a result, all input values were converted from mg/l to mol/kgw (moles per kg of water).

[b] Value allowed to adjust until redox equilibrium is established.

[c] Value not measured but assumed equal to the average daily air temperature between 1932 and 1988.

Table B-6. Selected results from chemical extractions of crushed bedrock in addition to measurements of acid-neutrilization potential.

Well ID and core depth (ft)	Vadose Zone Hydrostratigraphic Unit[a]	ANALYTE	leachate (mg/L)	solution (L)	rock (kg)	dry-bulk density[b] (kg / m^3)	porosity[b] (-)	HFO extracted[c] (mg rock / kg rock)	HFO extracted (g / kg solution)	HFO precipitated (g / kg solution)	HFO total (moles / kg solution)	ANP[d] (g $CaCO_3$ / kg rock)	ANP (moles / kg solution)
MW-30 37.5-38.0	top	Iron, dissolved	295	0.1	0.01	1978	0.199	4701.41	46.73	1.70	0.544	1	0.099
MW-30 43.0-43.2	top	Iron, dissolved	38.3	0.1	0.01	2023	0.264	610.39	4.68	1.70	0.072	1	0.077
MW-30 43.2-43.5	top	Iron, dissolved	25.3	0.1	0.01	2023	0.264	403.21	3.09	1.70	0.054	0	0.000
MW-23 53.0-53.5	middle	Iron, dissolved	304	0.1	0.01	2026	0.184	4844.84	53.35	3.54	0.639	4	0.440
MW-23 74.0-74.3	bottom	Iron, dissolved	19.1	0.1	0.01	2329	0.122	304.40	5.81	0.00	0.065	0	0.000

[a] Due to there spatial proximity, model output for the three "top" vadose zone hydrostratigraphic units were averaged into one value.

[b] Dry-bulk density (ρ_b) and porosity (n) data taken from Daniel B. Stephens & Associates (2007). Value of ρ_b and n for MW-30 43.0-43.2 and 43.2-43.5 represent corrected value after volume change.

[c] For conversion from mass of Fe to mass of HFO the assumed stoichiometry of ferrihydrite was Fe_2O_3:H2O with a molecular weight of 89 g/mol (Dzombak and Morel 1990).

[d] Acid-neutralization potential (ANP) value of 1 g $CaCO_3$ per kg of rock measured at the level of detection and a value of 0 indicates the analyte was not detected.

Table B-7. Selected water-quality from geochemical modeling of tailings-pore waters during neutralization with underlying bedrock and surface-complexation with HFO.

Surface-complexation model	PHREEQC Iteration	Vadose Zone Hydrostratigraphic Unit	Ionic strength (-)	$CO_2(g)$ partial pressure	pH (s.u.)	pe (-)	calcium (molal)	sulfate (molal)	total carbon (molal)	total uranium (mg/L)	uranium(VI) (molal)	uranyl (molal)
-	IC	IC	1.37	$10^{-0.764}$	1.83	20.15	9.09E-03	6.70E-01	6.48E-03	3.91E-04	3.91E-04	7.32E-06
Dzombak and Morel	Reaction 1	top	1.42	$10^{-2.0}$	5.39	15.51	5.55E-03	5.97E-01	4.86E-04	5.44E-06	5.44E-06	8.48E-08
Dzombak and Morel	Reaction 2	middle	1.14	$10^{-2.0}$	7.50	12.92	6.12E-03	4.45E-01	1.17E-02	3.37E-06	3.37E-06	2.54E-14
Dzombak and Morel	Reaction 3	bottom	1.35	$10^{-2.0}$	1.92	19.75	6.12E-03	6.65E-01	3.96E-04	3.91E-04	3.91E-04	7.43E-06

Table B-8. Speciation of tailings-pore waters after equilibration with calcite and complexation with HFO for the Dzombak and Morel (1990) model[a].

Surface-complexation model	PHREEQC Iteration	Vadose Zone Hydrostratigraphic Unit	$Ca_2UO_2(CO_3)_3$ (%)	$CaUO_2(CO3)_3^{-2}$ (%)	$UO2(CO_3)_2^{-2}$ (%)	$UO_2(CO_3)_3^{-4}$ (%)	UO_2CO_3 (%)	UO_2^{+2} (%)
Dzombak and Morel	Reaction 1	top	--	--	--	--	2.04	1.56
Dzombak and Morel	Reaction 2	middle	84.00	2.64	1.10	12.22	0.01	7.53×10^{-7}
Dzombak and Morel	Reaction 3	bottom	--	--	--	--	--	1.90

Surface-complexation model	PHREEQC Iteration	Vadose Zone Hydrostratigraphic Unit	UO_2SO_4 (%)	$UO_2(SO_4)_2^{-2}$ (%)	$UO_2(SO_4)_3^{-4}$ (%)	$UO_2NO_3^+$ (%)	UO_2F^+ (%)	UO_2HAsO_4 (%)
Dzombak and Morel	Reaction 1	top	42.37	45.29	0.8	0.29	1.64	2.49
Dzombak and Morel	Reaction 2	middle	--	--	--	--	--	--
Dzombak and Morel	Reaction 3	bottom	46.01	48.44	0.98	0.35	1.78	0.01

[a] Subset of speciation results presented. Blank values represent values less than 0.01%

Table B-9. Calculated distribution (K_d) coefficients and retardation factors of uranium for the Dzombak and Morel (1990) surface-complexation model.

Surface-complexation model	PHREEQC Iteration	Vadose Zone Hydrostratigraphic Unit	total uranium (molal)	$(C_i-C_f)/C_f$ (-)	mass of rock (mg)	volume of H_2O[a] (mL)	ρ_b[b] (mg/cm^3)	θ[c] (-)	K_d (mL/mg)	R (-)
-	IC	IC	3.91E-04	-	--	1009	-	-	-	-
Dzombak and Morel	Reaction 1	top	5.44E-06	7.09E+01	8.424E+06	1007	1980	0.067	0.00847	251
Dzombak and Morel	Reaction 2	middle	3.37E-06	1.15E+02	1.101E+07	1000	2030	0.089	0.0104	239
Dzombak and Morel	Reaction 3	bottom	3.91E-04	2.56E-04	1.909E+07	1010	2330	0.121	0	1

[a] For conversion 1 L assumed equal to 1 kg.

[b] Dry-bulk density (ρ_b) taken from Daniel B. Stephens & Associates (2007).

[c] Average volumetric-water content of the underlying vadose zone units were predicted with the HYDRUS-1D base-case scenario for Cells 2 and 3.

Table B-10. White Mesa Mill vadose zone distribution (K_d) coefficients and retardation factors (R) for selected contaminants present in the tailings-pore fluids[a,b].

Vadose Zone Hydrostratigraphic Unit	Arsenic K_d (l/kg)	Beryllium K_d (l/kg)	Cadmium K_d (l/kg)	Chromium K_d (l/kg)	Cobalt K_d (l/kg)	Copper K_d (l/kg)	Fluorine[c] K_d (l/kg)	Iron[c] K_d (l/kg)	Lead K_d (l/kg)	Manganese[c] K_d (l/kg)	Mercury K_d (l/kg)	Molybdenum K_d (l/kg)	Nickel K_d (l/kg)	Selenium K_d (l/kg)	Silver K_d (l/kg)	Sulfate[c] K_d (l/kg)	Thallium K_d (l/kg)	Uranium K_d (l/kg)	Vanadium K_d (l/kg)	Zinc K_d (l/kg)
top	7.19	82.1	0.001	0.557	0.000	4.13	0.000	0.000	9.48	0.001	0.000	0.014	0.005	0.015	0.000	0.002	0.000	8.47	0.000	0.009
middle	7094	72140	1.033	4.90	0.115	1220	0.0003	0.000	2197	0.901	0.000	0.663	1.380	0.015	0.000	0.003	0.000	10.4	559	11.3
bottom	0.119	0.000	0.000	0.000	0.000	0.000	0.000	0.000	0.000	0.000	0.000	0.000	0.000	0.001	0.000	0.000	0.000	0.000	0.000	0.000

Vadose Zone Hydrostratigraphic Unit	R (--)	R (--)	R (--)	R (--)	R (--)	R (--)	R (--)	R (--)	R (--)	R (--)	R (--)	R (--)	R (--)	R (--)	R (--)	R (--)	R (--)	R (--)	R (--)	R (--)
top	213	2428	1.02	17	1.00	123	1.00	1.00	281	1.02	1.00	1.41	1.14	1.46	1.00	1.07	1.00	251	1.00	1.26
middle	161804	1645434	25	113	3.63	27822	1.01	1.00	50105	22	1.00	16	32	1.34	1.00	1.07	1.00	239	12744	260
bottom	3.30	1.00	1.00	1.00	1.00	1.00	1.00	1.00	1.00	1.00	1.00	1.00	1.00	1.01	1.00	1.00	1.00	1.00	1.00	1.00

[a] Methodology and assumptions used to determine sorption coefficients are described in Appendix B.

[b] Average volumetric-water content of the underlying vadose zone units were predicted with the HYDRUS-1D base-case scenario for Cells 2 and 3.

[c] Sorption coefficients for fluorine, manganese, and sulfate were corrected to account for precipitation of fluorite, pyrolusite, and gypsum/barite, respectively.

Table B-11. Saturation indices (SI) for the tailings-pore waters and equilibrated solutions predicted for the White Mesa Mill vadose zone hydrostratigraphic units[a].

Vadose Zone Hydrostratigraphic Unit	Calcite $CaCO_3$	Barite $BaSO_4$	Gypsum $CaSO_4 \cdot 2H_2O$	Anhydrite $CaSO_4$	Amorphous HFO $Fe(OH)_{3(a)}$	Goethite $FeOOH$	Amorphous Al-hydroxide $Al(OH)_{3(a)}$	Gibbsite $Al(OH)_3$	Fluorite CaF_2	Pyrolusite MnO_2	Carnotite KUO_2VO_4	Tyuyamunite $Ca(UO_2)_2(VO_4)_2$
initial condition	-9.98	1.18	0.17	-0.06	-3.83	1.51	-10.56	-7.73	-2.21	0.29	-3.98	-10.85
top	-4.27	0	0	-0.23	5.11	10.45	0.09	2.92	-2.35	0	2.49	1.88
middle	0	0	0	-0.23	7.09	12.43	3.54	6.38	0	0	-1.72	-6.52
bottom	-11.19	0	0	-0.23	-3.49	1.84	-10.30	-7.47	-2.38	-0.18	-3.70	-10.48

[a] A SI > 0 indicates mineral precipitation; a SI < 0 indicates mineral dissolution; and a SI = 0 indicates equilibrium conditions.
HFO is equal to hydrous-ferric oxide

Attachment 1

Laboratory data for hydrous-ferric oxide chemical extraction and acid-neutralization tests on selected core samples of the White Mesa Mill bedrock vadose zone

ACZ Laboratories, Inc.
2773 Downhill Drive Steamboat Springs, CO 80487 (800) 334-5493

Analytical Report

April 27, 2007

Report to:
Doug Oliver
MWH America's Inc.
10619 S. Jordan Gateway Suite 100
Salt Lake City, UT 84095

Bill to:
Accounts Payable
MWH America's Inc.
P.O. Box 6610
Broomfield, CO 80021

cc: Ryan Jakubowski

Project ID: 1004-A0002-87430-OM/
ACZ Project ID: L62140

Doug Oliver:

Enclosed are the analytical results for sample(s) submitted to ACZ Laboratories, Inc. (ACZ) on April 20, 2007. This project has been assigned to ACZ's project number, L62140. Please reference this number in all future inquiries.

All analyses were performed according to ACZ's Quality Assurance Plan, version 11.0. The enclosed results relate only to the samples received under L62140. Each section of this report has been reviewed and approved by the appropriate Laboratory Supervisor, or a qualified substitute.

Except as noted, the test results for the methods and parameters listed on ACZ's current NELAC certificate letter (#ACZ) meet all requirements of NELAC.

This report shall be used or copied only in its entirety. ACZ is not responsible for the consequences arising from the use of a partial report.

All samples and sub-samples associated with this project will be disposed of after May 27, 2007. If the samples are determined to be hazardous, additional charges apply for disposal (typically less than $10/sample). If you would like the samples to be held longer than ACZ's stated policy or to be returned, please contact your Project Manager or Customer Service Representative for further details and associated costs. ACZ retains analytical reports for five years.

If you have any questions or other needs, please contact your Project Manager.

27/Apr/07

Tony Antalek, Project Manager, has reviewed and approved this report in its entirety.

ACZ Laboratories, Inc.
2773 Downhill Drive Steamboat Springs, CO 80487 (800) 334-5493

Inorganic Analytical Results

MWH America's Inc.
Project ID: 1004-A0002-87430-OM/
Sample ID: MW-30 37.5-38.0

ACZ Sample ID: ***L62140-01***
Date Sampled: *04/20/07 00:00*
Date Received: *04/20/07*
Sample Matrix: *Leachate*

Metals Analysis

Parameter	EPA Method	Result	Qual	XQ	Units	MDL	PQL	Date	Analyst
Aluminum, dissolved	M200.7 ICP	137		*	mg/L	0.03	0.2	04/25/07 21:09	djt
Calcium, dissolved	M200.7 ICP	53.5		*	mg/L	0.2	1	04/25/07 0:40	djt
Iron, dissolved	M200.7 ICP	295		*	mg/L	0.02	0.05	04/25/07 21:09	djt
Magnesium, dissolved	M200.7 ICP	59.6		*	mg/L	0.2	1	04/25/07 0:40	djt
Manganese, dissolved	M200.7 ICP	8.440		*	mg/L	0.005	0.03	04/25/07 0:40	djt
Uranium, dissolved	M200.8 ICP-MS	0.0156		*	mg/L	0.0001	0.0005	04/24/07 1:15	scp

** Please refer to Qualifier Reports for detail.*

ACZ Laboratories, Inc.
2773 Downhill Drive Steamboat Springs, CO 80487 (800) 334-5493

Inorganic Analytical Results

MWH America's Inc.
Project ID: 1004-A0002-87430-OM/
Sample ID: MW-30 43.0-43.2

ACZ Sample ID: ***L62140-02***
Date Sampled: *04/20/07 00:00*
Date Received: *04/20/07*
Sample Matrix: *Leachate*

Metals Analysis

Parameter	EPA Method	Result	Qual	XQ	Units	MDL	PQL	Date	Analyst
Aluminum, dissolved	M200.7 ICP	69.90		*	mg/L	0.03	0.2	04/25/07 21:13	djt
Calcium, dissolved	M200.7 ICP	68.4		*	mg/L	0.2	1	04/25/07 1:01	djt
Iron, dissolved	M200.7 ICP	38.30		*	mg/L	0.02	0.05	04/25/07 21:13	djt
Magnesium, dissolved	M200.7 ICP	32.5		*	mg/L	0.2	1	04/25/07 1:01	djt
Manganese, dissolved	M200.7 ICP	0.057		*	mg/L	0.005	0.03	04/25/07 1:01	djt
Uranium, dissolved	M200.8 ICP-MS	0.0109		*	mg/L	0.0001	0.0005	04/24/07 1:21	scp

** Please refer to Qualifier Reports for detail.*

ACZ Laboratories, Inc.
2773 Downhill Drive Steamboat Springs, CO 80487 (800) 334-5493

Inorganic Analytical Results

MWH America's Inc.
Project ID: 1004-A0002-87430-OM/
Sample ID: MW-30 43.2-43.5

ACZ Sample ID: ***L62140-03***
Date Sampled: *04/20/07 00:00*
Date Received: *04/20/07*
Sample Matrix: *Leachate*

Metals Analysis

Parameter	EPA Method	Result	Qual	XC	Units	MDL	PQL	Date	Analyst
Aluminum, dissolved	M200.7 ICP	58.30		*	mg/L	0.03	0.2	04/25/07 21:18	djt
Calcium, dissolved	M200.7 ICP	53.5		*	mg/L	0.2	1	04/25/07 1:05	djt
Iron, dissolved	M200.7 ICP	25.30		*	mg/L	0.02	0.05	04/25/07 21:18	djt
Magnesium, dissolved	M200.7 ICP	26.1		*	mg/L	0.2	1	04/25/07 1:05	djt
Manganese, dissolved	M200.7 ICP	0.070		*	mg/L	0.005	0.03	04/25/07 1:05	djt
Uranium, dissolved	M200.8 ICP-MS	0.0078		*	mg/L	0.0002	0.001	04/24/07 1:27	scp

** Please refer to Qualifier Reports for detail.*

ACZ Laboratories, Inc.
2773 Downhill Drive Steamboat Springs, CO 80487 (800) 334-5493

Inorganic Analytical Results

MWH America's Inc.
Project ID: 1004-A0002-87430-OM/
Sample ID: MW-23 53.0-53.5

ACZ Sample ID: ***L62140-04***
Date Sampled: *04/20/07 00:00*
Date Received: *04/20/07*
Sample Matrix: *Leachate*

Metals Analysis

Parameter	EPA Method	Result	Qual	XQ	Units	MDL	PQL	Date	Analyst
Aluminum, dissolved	M200.7 ICP	176		*	mg/L	0.03	0.2	04/25/07 21:30	djt
Calcium, dissolved	M200.7 ICP	76.5		*	mg/L	0.2	1	04/25/07 1:09	djt
Iron, dissolved	M200.7 ICP	304		*	mg/L	0.02	0.05	04/25/07 21:30	djt
Magnesium, dissolved	M200.7 ICP	106		*	mg/L	0.2	1	04/25/07 1:09	djt
Manganese, dissolved	M200.7 ICP	4.370		*	mg/L	0.005	0.03	04/25/07 1:09	djt
Uranium, dissolved	M200.8 ICP-MS	0.0156		*	mg/L	0.0001	0.0005	04/24/07 1:45	scp

** Please refer to Qualifier Reports for detail.*

ACZ Laboratories, Inc.
2773 Downhill Drive Steamboat Springs, CO 80487 (800) 334-5493

Inorganic Analytical Results

MWH America's Inc.
Project ID: 1004-A0002-87430-OM/
Sample ID: MW-23 74.0-74.3

ACZ Sample ID: ***L62140-05***
Date Sampled: *04/20/07 00:00*
Date Received: *04/20/07*
Sample Matrix: *Leachate*

Metals Analysis

Parameter	EPA Method	Result	Qual	XQ	Units	MDL	PQL	Date	Analyst
Aluminum, dissolved	M200.7 ICP	40.70		*	mg/L	0.03	0.2	04/25/07 21:43	djt
Calcium, dissolved	M200.7 ICP	24.7		*	mg/L	0.2	1	04/25/07 1:14	djt
Iron, dissolved	M200.7 ICP	19.10		*	mg/L	0.02	0.05	04/25/07 21:43	djt
Magnesium, dissolved	M200.7 ICP	28.4		*	mg/L	0.2	1	04/25/07 1:14	djt
Manganese, dissolved	M200.7 ICP	0.069		*	mg/L	0.005	0.03	04/25/07 1:14	djt
Uranium, dissolved	M200.8 ICP-MS	0.0112		*	mg/L	0.0001	0.0005	04/24/07 1:50	scp

ACZ Laboratories, Inc.
2773 Downhill Drive Steamboat Springs, CO 80487 (800) 334-5493

Inorganic Analytical Results

MWH America's Inc.
Project ID: 1004-A0002-87430-OM/
Sample ID: MW-23 82.5-82.7

ACZ Sample ID: ***L62140-06***
Date Sampled: *04/20/07 00:00*
Date Received: *04/20/07*
Sample Matrix: *Leachate*

Metals Analysis

Parameter	EPA Method	Result	Qual	XQ	Units	MDL	PQL	Date	Analyst
Aluminum, dissolved	M200.7 ICP	15.20		*	mg/L	0.03	0.2	04/25/07 21:48	djt
Calcium, dissolved	M200.7 ICP	11.3		*	mg/L	0.2	1	04/25/07 1:18	djt
Iron, dissolved	M200.7 ICP	14.50		*	mg/L	0.02	0.05	04/25/07 21:48	djt
Magnesium, dissolved	M200.7 ICP	12.7		*	mg/L	0.2	1	04/25/07 1:18	djt
Manganese, dissolved	M200.7 ICP	0.049		*	mg/L	0.005	0.03	04/25/07 1:18	djt
Uranium, dissolved	M200.8 ICP-MS	0.0122		*	mg/L	0.0001	0.0005	04/24/07 1:56	scp

** Please refer to Qualifier Reports for detail.*

ACZ Laboratories, Inc.
2773 Downhill Drive Steamboat Springs, CO 80487 (800) 334-5493

Inorganic Analytical Results

MWH America's Inc.
Project ID: 1004-A0002-87430-OM/
Sample ID: MW-23 99.8-100.0

ACZ Sample ID: ***L62140-07***
Date Sampled: *04/20/07 00:00*
Date Received: *04/20/07*
Sample Matrix: *Leachate*

Metals Analysis

Parameter	EPA Method	Result	Qual	XQ	Units	MDL	PQL	Date	Analyst
Aluminum, dissolved	M200.7 ICP	29.50	*		mg/L	0.03	0.2	04/25/07 21:52	djt
Calcium, dissolved	M200.7 ICP	19.1	*		mg/L	0.2	1	04/25/07 1:22	djt
Iron, dissolved	M200.7 ICP	74.60	*		mg/L	0.02	0.05	04/25/07 21:52	djt
Magnesium, dissolved	M200.7 ICP	9.0	*		mg/L	0.2	1	04/25/07 1:22	djt
Manganese, dissolved	M200.7 ICP	0.222	*		mg/L	0.005	0.03	04/25/07 1:22	djt
Uranium, dissolved	M200.8 ICP-MS	0.0147	*		mg/L	0.0001	0.0005	04/24/07 2:14	scp

ACZ Laboratories, Inc.
2773 Downhill Drive Steamboat Springs, CO 80487(800) 334-5493

Inorganic Analytical Results

MWH America's Inc.
Project ID: 1004-A0002-87430-OM/
Sample ID: MW-23 103.0-103.3

ACZ Sample ID: ***L62140-08***
Date Sampled: *04/20/07 00:00*
Date Received: *04/20/07*
Sample Matrix: *Leachate*

Metals Analysis

Parameter	EPA Method	Result	Qual	XQ	Units	MDL	PQL	Date	Analyst
Aluminum, dissolved	M200.7 ICP	24.50		*	mg/L	0.03	0.2	04/25/07 21:56	djt
Calcium, dissolved	M200.7 ICP	14.4		*	mg/L	0.2	1	04/25/07 1:26	djt
Iron, dissolved	M200.7 ICP	15.50		*	mg/L	0.02	0.05	04/25/07 21:56	djt
Magnesium, dissolved	M200.7 ICP	9.8		*	mg/L	0.2	1	04/25/07 1:26	djt
Manganese, dissolved	M200.7 ICP	0.229		*	mg/L	0.005	0.03	04/25/07 1:26	djt
Uranium, dissolved	M200.8 ICP-MS	0.0105		*	mg/L	0.0001	0.0005	04/24/07 2:19	scp

** Please refer to Qualifier Reports for detail.*

ACZ Laboratories, Inc.
2773 Downhill Drive Steamboat Springs, CO 80487 (800) 334-5493

Inorganic Analytical Results

MWH America's Inc.
Project ID: 1004-A0002-87430-OM/
Sample ID: MW-23 103.0-103.3DUP

ACZ Sample ID: ***L62140-09***
Date Sampled: *04/20/07 00:00*
Date Received: *04/20/07*
Sample Matrix: *Leachate*

Metals Analysis

Parameter	EPA Method	Result	Qual	XQ	Units	MDL	PQL	Date	Analyst
Aluminum, dissolved	M200.7 ICP	23.50		*	mg/L	0.03	0.2	04/26/07 6:12	djt
Calcium, dissolved	M200.7 ICP	12.7		*	mg/L	0.2	1	04/26/07 6:12	djt
Iron, dissolved	M200.7 ICP	15.20		*	mg/L	0.02	0.05	04/26/07 6:12	djt
Magnesium, dissolved	M200.7 ICP	9.4		*	mg/L	0.2	1	04/26/07 6:12	djt
Manganese, dissolved	M200.7 ICP	0.224		*	mg/L	0.005	0.03	04/26/07 6:12	djt
Uranium, dissolved	M200.8 ICP-MS	0.0105		*	mg/L	0.0001	0.0005	04/24/07 2:25	scp

ACZ Laboratories, Inc.
2773 Downhill Drive Steamboat Springs, CO 80487 (800) 334-5493

Inorganic Analytical Results

MWH America's Inc.
Project ID: 1004-A0002-87430-OM/
Sample ID: PBS

ACZ Sample ID: ***L62140-10***
Date Sampled: *04/20/07 00:00*
Date Received: *04/20/07*
Sample Matrix: *Leachate*

Metals Analysis

Parameter	EPA Method	Result	Qual	XQ	Units	MDL	PQL	Date	Analyst
Aluminum, dissolved	M200.7 ICP	0.15	B	*	mg/L	0.03	0.2	04/26/07 6:16	djt
Calcium, dissolved	M200.7 ICP	0.2	B	*	mg/L	0.2	1	04/26/07 6:16	djt
Iron, dissolved	M200.7 ICP	0.04	B	*	mg/L	0.02	0.05	04/26/07 6:16	djt
Magnesium, dissolved	M200.7 ICP		U	*	mg/L	0.2	1	04/26/07 6:16	djt
Manganese, dissolved	M200.7 ICP		U	*	mg/L	0.005	0.03	04/26/07 6:16	djt
Uranium, dissolved	M200.8 ICP-MS		U	*	mg/L	0.0001	0.0005	04/24/07 2:31	scp

Report Header Explanations

Batch	A distinct set of samples analyzed at a specific time
Found	Value of the QC Type of interest
Limit	Upper limit for RPD, in %.
Lower	Lower Recovery Limit, in % (except for LCSS, mg/Kg)
MDL	Method Detection Limit. Same as Minimum Reporting Limit. Allows for instrument and annual fluctuations.
PCN/SCN	A number assigned to reagents/standards to trace to the manufacturer's certificate of analysis
PQL	Practical Quantitation Limit, typically 5 times the MDL.
QC	True Value of the Control Sample or the amount added to the Spike
Rec	Amount of the true value or spike added recovered, in % (except for LCSS, mg/Kg)
RPD	Relative Percent Difference, calculation used for Duplicate QC Types
Upper	Upper Recovery Limit, in % (except for LCSS, mg/Kg)
Sample	Value of the Sample of interest

QC Sample Types

AS	Analytical Spike (Post Digestion)	*LCSWD*	Laboratory Control Sample - Water Duplicate
ASD	Analytical Spike (Post Digestion) Duplicate	*LFB*	Laboratory Fortified Blank
CCB	Continuing Calibration Blank	*LFM*	Laboratory Fortified Matrix
CCV	Continuing Calivation Verification standard	*LFMD*	Laboratory Fortified Matrix Duplicate
DUP	Sample Duplicate	*LRB*	Laboratory Reagent Blank
ICB	Initial Calibration Blank	*MS*	Matrix Spike
ICV	Initial Calibration Verification standard	*MSD*	Matrix Spike Duplicate
ICSAB	Inter-element Correction Standard - A plus B solutions	*PBS*	Prep Blank - Soil
LCSS	Laboratory Control Sample - Soil	*PBW*	Prep Blank - Water
LCSSD	Laboratory Control Sample - Soil Duplicate	*PQV*	Practical Quantitation Verification standard
LCSW	Laboratory Control Sample - Water	*SDL*	Serial Dilution

QC Sample Type Explanations

Blanks	Verifies that there is no or minimal contamination in the prep method or calibration procedure.
Control Samples	Verifies the accuracy of the method, including the prep procedure.
Duplicates	Verifies the precision of the instrument and/or method.
Spikes/Fortified Matrix	Determines sample matrix interferences, if any.
Standard	Verifies the validity of the calibration.

ACZ Qualifiers (Cont'd)

B	Analyte concentration detected at a value between MDL and PQL.
H	Analysis exceeded method hold time. pH is a field test with an immediate hold time.
U	Analyte was analyzed for but not detected at the indicated MDL

Method References

(1)	EPA 600/4-83-020. Methods for Chemical Analysis of Water and Wastes, March 1983.
(2)	EPA 600/R-93-100. Methods for the Determination of Inorganic Substances in Environmental Samples, August 1993.
(3)	EPA 600/R-94-111. Methods for the Determination of Metals in Environmental Samples - Supplement I, May 1994.
(5)	EPA SW-846. Test Methods for Evaluating Solid Waste, Third Edition with Update III, December 1996.
(6)	Standard Methods for the Examination of Water and Wastewater, 19th edition, 1995.

Comments

(1)	QC results calculated from raw data. Results may vary slightly if the rounded values are used in the calculations.
(2)	Soil, Sludge, and Plant matrices for Inorganic analyses are reported on a dry weight basis.
(3)	Animal matrices for Inorganic analyses are reported on an "as received" basis.

ACZ Laboratories, Inc.
2773 Downhill Drive Steamboat Springs, CO 80487 (800) 334-5493

Inorganic Extended Qualifier Report

MWH America's Inc.

ACZ Project ID: ***L62140***

ACZ ID	WORKUNIT	PARAMETER	METHOD	QUAL	DESCRIPTION
L62140-01	WG223614	Manganese, dissolved	M200.7 ICP	M3	The accuracy of the spike recovery does not apply because analyte concentration in the sample is disproportionate to the spike level. The recovery of the method control sample was acceptable.
L62140-02	WG223614	Manganese, dissolved	M200.7 ICP	M3	The accuracy of the spike recovery does not apply because analyte concentration in the sample is disproportionate to the spike level. The recovery of the method control sample was acceptable.
L62140-03	WG223639	Aluminum, dissolved	M200.7 ICP	M3	The accuracy of the spike recovery does not apply because analyte concentration in the sample is disproportionate to the spike level. The recovery of the method control sample was acceptable.
		Iron, dissolved	M200.7 ICP	M3	The accuracy of the spike recovery does not apply because analyte concentration in the sample is disproportionate to the spike level. The recovery of the method control sample was acceptable.
	WG223614	Manganese, dissolved	M200.7 ICP	M3	The accuracy of the spike recovery does not apply because analyte concentration in the sample is disproportionate to the spike level. The recovery of the method control sample was acceptable.
L62140-04	WG223639	Aluminum, dissolved	M200.7 ICP	M3	The accuracy of the spike recovery does not apply because analyte concentration in the sample is disproportionate to the spike level. The recovery of the method control sample was acceptable.
		Iron, dissolved	M200.7 ICP	M3	The accuracy of the spike recovery does not apply because analyte concentration in the sample is disproportionate to the spike level. The recovery of the method control sample was acceptable.
	WG223614	Manganese, dissolved	M200.7 ICP	M3	The accuracy of the spike recovery does not apply because analyte concentration in the sample is disproportionate to the spike level. The recovery of the method control sample was acceptable.
L62140-05	WG223639	Aluminum, dissolved	M200.7 ICP	M3	The accuracy of the spike recovery does not apply because analyte concentration in the sample is disproportionate to the spike level. The recovery of the method control sample was acceptable.
		Iron, dissolved	M200.7 ICP	M3	The accuracy of the spike recovery does not apply because analyte concentration in the sample is disproportionate to the spike level. The recovery of the method control sample was acceptable.
	WG223614	Manganese, dissolved	M200.7 ICP	M3	The accuracy of the spike recovery does not apply because analyte concentration in the sample is disproportionate to the spike level. The recovery of the method control sample was acceptable.
L62140-06	WG223639	Aluminum, dissolved	M200.7 ICP	M3	The accuracy of the spike recovery does not apply because analyte concentration in the sample is disproportionate to the spike level. The recovery of the method control sample was acceptable.
		Iron, dissolved	M200.7 ICP	M3	The accuracy of the spike recovery does not apply because analyte concentration in the sample is disproportionate to the spike level. The recovery of the method control sample was acceptable.
	WG223614	Manganese, dissolved	M200.7 ICP	M3	The accuracy of the spike recovery does not apply because analyte concentration in the sample is disproportionate to the spike level. The recovery of the method control sample was acceptable.

ACZ Laboratories, Inc.
2773 Downhill Drive Steamboat Springs, CO 80487 (800) 334-5493

Inorganic Extended Qualifier Report

MWH America's Inc.

ACZ Project ID: ***L62140***

ACZ ID	Workorder	Parameter	Method	Qual	Description
L62140-07	WG223639	Aluminum, dissolved	M200.7 ICP	M3	The accuracy of the spike recovery does not apply becau analyte concentration in the sample is disproportionate to the spike level. The recovery of the method control sampl was acceptable.
		Iron, dissolved	M200.7 ICP	M3	The accuracy of the spike recovery does not apply becau analyte concentration in the sample is disproportionate to the spike level. The recovery of the method control sampl was acceptable.
	WG223614	Manganese, dissolved	M200.7 ICP	M3	The accuracy of the spike recovery does not apply becau analyte concentration in the sample is disproportionate to the spike level. The recovery of the method control sampl was acceptable.
L62140-08	WG223639	Aluminum, dissolved	M200.7 ICP	M3	The accuracy of the spike recovery does not apply becau analyte concentration in the sample is disproportionate to the spike level. The recovery of the method control sampl was acceptable.
		Iron, dissolved	M200.7 ICP	M3	The accuracy of the spike recovery does not apply becau analyte concentration in the sample is disproportionate to the spike level. The recovery of the method control sampl was acceptable.
	WG223614	Manganese, dissolved	M200.7 ICP	M3	The accuracy of the spike recovery does not apply becau analyte concentration in the sample is disproportionate to the spike level. The recovery of the method control sampl was acceptable.

MWH America's Inc. ACZ Project ID: ***L62140***

Metals Analysis

The following parameters are not covered by certification or are not covered by NELAC certificate #A02

Aluminum, dissolved	M200.7 ICP
Calcium, dissolved	M200.7 ICP
Iron, dissolved	M200.7 ICP
Magnesium, dissolved	M200.7 ICP
Manganese, dissolved	M200.7 ICP
Uranium, dissolved	M200.8 ICP-MS

~~L61917~~ L62140
L064.2007

Core Samples from White Mesa near Blanding UT shipped to ACZ for Leach Testing
Contact Info: Doug Oliver - MWH (801-617-3224) or Ryan Jakubowski in Steamboat (970-879-6260)
Subcontract Number: 1004-A0002-87430-OM/MSA CO1

Loc ID	Depth (feet bgs)
MW-30	37.5-38.0
MW-30	43.0-43.2
MW-30	43.2-43.5
MW-23	53.0-53.5
MW-23	74.0-74.3
MW-23	82.5-82.7
MW-23	99.8-100.0
MW-23	103.0-103.3

Please contact Ryan if you need any assistance with Sample prep. Also contact Ryan to pick up any unused samples

Thanks,
Doug

LGB 4-9-07 11:20

ACZ Laboratories, Inc.
2773 Downhill Drive Steamboat Springs, CO 80487 (800) 334-5493

Analytical Quote

Doug Oliver
MWH America's Inc.
10619 S. Jordan Gateway Suite 100
Salt Lake City, UT 84095

4/20/2007

Project Number: BH LEACHATE

Matrix: Leachate 96 Hour HH Extraction Leachates for metals

Parameter	Method	Detection Limit	Cost/Sample
Metals Analysis			
Aluminum, dissolved	M200.7 ICP	0.03 mg/L	$8.00
Calcium, dissolved	M200.7 ICP	0.2 mg/L	$8.00
Iron, dissolved	M200.7 ICP	0.02 mg/L	$8.00
Magnesium, dissolved	M200.7 ICP	0.2 mg/L	$8.00
Manganese, dissolved	M200.7 ICP	0.005 mg/L	$8.00
Uranium, dissolved	M200.8 ICP-MS	0.0001 mg/L	$38.00
		Cost/Sample:	**$78.00**

REPAD.09.06.05.01 D/ P/

Analytical Method: ________ **WG** ________

ACZ Laboratories, Inc.

Analyst: SRS

Start Date: ________

End Date: ________

ACZ ID	10g Sample	100 mL SHH Soln.	Start time/date 9am/Tues	Water temp tues		Wed		Thurs		Fri		Leachate Log in #'s	
PBS				50°C	50°C	50°C	50°C	50°C	50°C	50°	50°	62140-00	
L61917-1												-1	
-2												-2	
-3												-3	
-4												-4	
-5												-5	
-6												-6	
-7												-7	
-8												-8	
-8D												-9	

Comments: * all sample rotated @ 9am daily.
RPM's 30±2 filtered with a 0.45µm filter syringe, HH solution
SI070416-1, pcn 26729

Page ____ of ____

Bench Sheet Form.XLS, 08/15/2003

ACZ Laboratories, Inc.
2773 Downhill Drive Steamboat Springs, CO 80487 (800) 334-5493

Analytical Report

August 10, 2007

Report to:
John Mahoney
MWH America's Inc.
1801California Street Suite 2600
Denver, CO 80202

Bill to:
Accounts Payable
MWH America's Inc.
PO Box 6610
Broomfield, CO 80021

cc: Ryan Jakubowski

Project ID:
ACZ Project ID: L64240

John Mahoney:

Enclosed are the analytical results for sample(s) submitted to ACZ Laboratories, Inc. (ACZ) on August 03, 2007. This project has been assigned to ACZ's project number, L64240. Please reference this number in all future inquiries.

All analyses were performed according to ACZ's Quality Assurance Plan, version 11.0. The enclosed results relate only to the samples received under L64240. Each section of this report has been reviewed and approved by the appropriate Laboratory Supervisor, or a qualified substitute.

Except as noted, the test results for the methods and parameters listed on ACZ's current NELAC certificate letter (#ACZ) meet all requirements of NELAC.

This report shall be used or copied only in its entirety. ACZ is not responsible for the consequences arising from the use of a partial report.

All samples and sub-samples associated with this project will be disposed of after September 10, 2007. If the samples are determined to be hazardous, additional charges apply for disposal (typically less than $10/sample). If you would like the samples to be held longer than ACZ's stated policy or to be returned, please contact your Project Manager or Customer Service Representative for further details and associated costs. ACZ retains analytical reports for five years.

If you have any questions or other needs, please contact your Project Manager.

S. Haberman 27/Apr/07

Tony Antalek, Project Manager, has reviewed and approved this report in its entirety.

ACCREDITED IN ACCORDANCE WITH nelac

ACIL

ACZ Laboratories, Inc.
2773 Downhill Drive Steamboat Springs, CO 80487 (800) 334-5493

Inorganic Analytical Results

MWH America's Inc.
Project ID:
Sample ID: L61917-01

ACZ Sample ID: ***L64240-01***
Date Sampled: *08/03/07 09:55*
Date Received: *08/03/07*
Sample Matrix: *Soil*

Soil Analysis

Parameter	EPA Method	Result	Qual	Xq	Units	MDL	PQL	Date	Analyst
Acid Neutralization Potential (calc)	M600/2-78-054 1.3	1			t CaCO3/Kt	1	5	08/08/07 16:22	calc
Neutralization Potential as CaCO3	M600/2-78-054 3.2.3	0.1	B	*	%	0.1	0.5	08/04/07 9:35	lwt

Soil Preparation

Parameter	EPA Method	Result	Qual	Xq	Units	MDL	PQL	Date	Analyst
Crush and Pulverize	USDA No. 1, 1972							08/03/07 14:00	lwt

ACZ Laboratories, Inc.
2773 Downhill Drive Steamboat Springs, CO 80487(800) 334-5493

Inorganic Analytical Results

MWH America's Inc.
Project ID:
Sample ID: L61917-02

ACZ Sample ID: ***L64240-02***
Date Sampled: *08/03/07 09:55*
Date Received: *08/03/07*
Sample Matrix: *Soil*

Soil Analysis

Parameter	EPA Method	Result	Qual	XQ	Units	MDL	PQL	Date	Analyst
Acid Neutralization Potential (calc)	M600/2-78-054 1.3	1			t CaCO3/Kt	1	5	08/08/07 16:22	calc
Neutralization Potential as CaCO3	M600/2-78-054 3.2.3	0.1	B	*	%	0.1	0.5	08/04/07 10:07	lwt

Soil Preparation

Parameter	EPA Method	Result	Qual	XQ	Units	MDL	PQL	Date	Analyst
Crush and Pulverize	USDA No. 1, 1972							08/03/07 14:03	lwt

ACZ Laboratories, Inc.
2773 Downhill Drive Steamboat Springs, CO 80487 (800) 334-5493

Inorganic Analytical Results

MWH America's Inc.
Project ID:
Sample ID: L61917-03

ACZ Sample ID: ***L64240-03***
Date Sampled: *08/03/07 09:55*
Date Received: *08/03/07*
Sample Matrix: *Soil*

Soil Analysis

Parameter	EPA Method	Result	Qual	XQ	Units	MDL	PQL	Date	Analyst
Acid Neutralization Potential (calc)	M600/2-78-054 1.3	0			t CaCO3/Kt	1	5	08/08/07 16:22	calc
Neutralization Potential as CaCO3	M600/2-78-054 3.2.3		U	*	%	0.1	0.5	08/04/07 10:39	lwt

Soil Preparation

Parameter	EPA Method	Result	Qual	XQ	Units	MDL	PQL	Date	Analyst
Crush and Pulverize	USDA No. 1, 1972							08/03/07 14:07	lwt

MWH America's Inc.
Project ID:
Sample ID: L61917-04

ACZ Sample ID: *L64240-04*
Date Sampled: *08/03/07 09:55*
Date Received: *08/03/07*
Sample Matrix: *Soil*

Soil Analysis

Parameter	EPA Method	Result	Qual	XQ	Units	MDL	PQL	Date	Analyst
Acid Neutralization Potential (calc)	M600/2-78-054 1.3	4			t CaCO3/Kt	1	5	08/08/07 16:23	calc
Neutralization Potential as CaCO3	M600/2-78-054 3.2.3	0.4	B	*	%	0.1	0.5	08/04/07 11:11	lwt

Soil Preparation

Parameter	EPA Method	Result	Qual	XQ	Units	MDL	PQL	Date	Analyst
Crush and Pulverize	USDA No. 1, 1972							08/03/07 14:11	lwt

MWH America's Inc.
Project ID:
Sample ID: L61917-05

ACZ Sample ID: ***L64240-05***
Date Sampled: *08/03/07 09:55*
Date Received: *08/03/07*
Sample Matrix: *Soil*

Soil Analysis

Parameter	EPA Method	Result	Qual	XQ	Units	MDL	PQL	Date	Analyst
Acid Neutralization Potential (calc)	M600/2-78-054 1.3	0			t CaCO3/Kt	1	5	08/08/07 16:23	calc
Neutralization Potential as CaCO3	M600/2-78-054 3.2.3		U	*	%	0.1	0.5	08/04/07 11:43	lwt

Soil Preparation

Parameter	EPA Method	Result	Qual	XQ	Units	MDL	PQL	Date	Analyst
Crush and Pulverize	USDA No. 1, 1972							08/03/07 14:15	lwt

Report Header Explanations

Batch	A distinct set of samples analyzed at a specific time
Found	Value of the QC Type of interest
Limit	Upper limit for RPD, in %.
Lower	Lower Recovery Limit, in % (except for LCSS, mg/Kg)
MDL	Method Detection Limit. Same as Minimum Reporting Limit. Allows for instrument and annual fluctuations.
PCN/SCN	A number assigned to reagents/standards to trace to the manufacturer's certificate of analysis
PQL	Practical Quantitation Limit, typically 5 times the MDL.
QC	True Value of the Control Sample or the amount added to the Spike
Rec	Amount of the true value or spike added recovered, in % (except for LCSS, mg/Kg)
RPD	Relative Percent Difference, calculation used for Duplicate QC Types
Upper	Upper Recovery Limit, in % (except for LCSS, mg/Kg)
Sample	Value of the Sample of interest

QC Sample Types

AS	Analytical Spike (Post Digestion)	*LCSWD*	Laboratory Control Sample - Water Duplicate
ASD	Analytical Spike (Post Digestion) Duplicate	*LFB*	Laboratory Fortified Blank
CCB	Continuing Calibration Blank	*LFM*	Laboratory Fortified Matrix
CCV	Continuing Calivation Verification standard	*LFMD*	Laboratory Fortified Matrix Duplicate
DUP	Sample Duplicate	*LRB*	Laboratory Reagent Blank
ICB	Initial Calibration Blank	*MS*	Matrix Spike
ICV	Initial Calibration Verification standard	*MSD*	Matrix Spike Duplicate
ICSAB	Inter-element Correction Standard - A plus B solutions	*PBS*	Prep Blank - Soil
LCSS	Laboratory Control Sample - Soil	*PBW*	Prep Blank - Water
LCSSD	Laboratory Control Sample - Soil Duplicate	*PQV*	Practical Quantitation Verification standard
LCSW	Laboratory Control Sample - Water	*SDL*	Serial Dilution

QC Sample Type Explanations

Blanks	Verifies that there is no or minimal contamination in the prep method or calibration procedure.
Control Samples	Verifies the accuracy of the method, including the prep procedure.
Duplicates	Verifies the precision of the instrument and/or method.
Spikes/Fortified Matrix	Determines sample matrix interferences, if any.
Standard	Verifies the validity of the calibration.

ACZ Qualifiers (Qual)

B	Analyte concentration detected at a value between MDL and PQL.
H	Analysis exceeded method hold time. pH is a field test with an immediate hold time.
U	Analyte was analyzed for but not detected at the indicated MDL

Method References

(1) EPA 600/4-83-020. Methods for Chemical Analysis of Water and Wastes, March 1983.
(2) EPA 600/R-93-100. Methods for the Determination of Inorganic Substances in Environmental Samples, August 1993.
(3) EPA 600/R-94-111. Methods for the Determination of Metals in Environmental Samples - Supplement I, May 1994.
(5) EPA SW-846. Test Methods for Evaluating Solid Waste, Third Edition with Update III, December 1996.
(6) Standard Methods for the Examination of Water and Wastewater, 19th edition, 1995.

Comments

(1) QC results calculated from raw data. Results may vary slightly if the rounded values are used in the calculations.
(2) Soil, Sludge, and Plant matrices for inorganic analyses are reported on a dry weight basis.
(3) Animal matrices for inorganic analyses are reported on an "as received" basis.

ACZ Laboratories, Inc.
2773 Downhill Drive Steamboat Springs, CO 80487 (800) 334-5493

Inorganic Extended Qualifier Report

MWH America's Inc.

ACZ Project ID: ***L64240***

ACZ ID	WORKNUM	PARAMETER	METHOD	QUAL	DESCRIPTION
L64240-01	WG229660	Neutralization Potential as CaCO3	M600/2-78-054 3.2.3	RA	Relative Percent Difference (RPD) was not used for data validation because the sample concentration is too low for accurate evaluation (< 10x MDL).
L64240-02	WG229660	Neutralization Potential as CaCO3	M600/2-78-054 3.2.3	RA	Relative Percent Difference (RPD) was not used for data validation because the sample concentration is too low for accurate evaluation (< 10x MDL).
L64240-03	WG229660	Neutralization Potential as CaCO3	M600/2-78-054 3.2.3	RA	Relative Percent Difference (RPD) was not used for data validation because the sample concentration is too low for accurate evaluation (< 10x MDL).
L64240-04	WG229660	Neutralization Potential as CaCO3	M600/2-78-054 3.2.3	RA	Relative Percent Difference (RPD) was not used for data validation because the sample concentration is too low for accurate evaluation (< 10x MDL).
L64240-05	WG229660	Neutralization Potential as CaCO3	M600/2-78-054 3.2.3	RA	Relative Percent Difference (RPD) was not used for data validation because the sample concentration is too low for accurate evaluation (< 10x MDL).

Soil Analysis

The following parameters are not offered for certification or are not covered by NELAC certificate #ACZ

Neutralization Potential as CaCO3	M600/2-78-054 3.2.3

ACZ Laboratories, Inc.

2773 Downhill Drive Steamboat Springs, CO 80487 (800) 334-5493

Sample Receipt

MWH America's Inc.

ACZ Project ID: L64240
Date Received: 8/3/2007
Received By:
Date Printed: 8/3/2007

Receipt Verification

	YES	NO	NA
1) Does this project require special handling procedures such as CLP protocol?			X
2) Are the custody seals on the cooler intact?			X
3) Are the custody seals on the sample containers intact?			X
4) Is there a Chain of Custody or other directive shipping papers present?	X		
5) Is the Chain of Custody complete?	X		
6) Is the Chain of Custody in agreement with the samples received?	X		
7) Is there enough sample for all requested analyses?	X		
8) Are all samples within holding times for requested analyses?	X		
9) Were all sample containers received intact?	X		
10) Are the temperature blanks present?			X
11) Are the trip blanks (VOA and/or Cyanide) present?			X
12) Are samples requiring no headspace, headspace free?			X
13) Do the samples that require a Foreign Soils Permit have one?			X

Exceptions (If not answered "Yes" to the above questions, please describe)

N/A

Contact (For any discrepancies, the client must be contacted)

N/A

Shipping Containers

Cooler Id		Temp (°C)	Rad (µR/hr)
NA4111		22.3	15

Client must contact ACZ Project Manager if analysis should not proceed for samples received outside of thermal preservation acceptance criteria.

Notes

ACZ Laboratories, Inc.
2773 Downhill Drive Steamboat Springs, CO 80487 (800) 334-5493

Sample Receipt

MWH America's Inc.

ACZ Project ID: L64240
Date Received: 8/3/2007
Received By:

Sample Container Preservation

SAMPLE	CLIENT ID	R < 2	G < 2	BK < 2	Y< 2	YG< 2	B< 2	O < 2	T >12	N/A	RAD	ID
L64240-01	L61917-01									X		
L64240-02	L61917-02									X		
L64240-03	L61917-03									X		
L64240-04	L61917-04									X		
L64240-05	L61917-05									X		

Sample Container Preservation Legend

Abbreviation	Description	Container Type	Preservative/Limits
R	Raw/Nitric	RED	pH must be < 2
B	Filtered/Sulfuric	BLUE	pH must be < 2
BK	Filtered/Nitric	BLACK	pH must be < 2
G	Filtered/Nitric	GREEN	pH must be < 2
O	Raw/Sulfuric	ORANGE	pH must be < 2
P	Raw/NaOH	PURPLE	pH must be > 12 *
T	Raw/NaOH-Zinc Acetate	TAN	pH must be > 12
Y	Raw/Sulfuric	YELLOW	pH must be < 2
YG	Raw/Sulfuric	YELLOW GLASS	pH must be < 2
N/A	No preservative needed	Not applicable	
RAD	Gamma/Beta dose rate	Not applicable	must be < 250 µR/hr

* pH check performed by analyst prior to sample preparation

Sample IDs Reviewed By: _____

ACZ Laboratories, Inc. L62140

2773 Downhill Drive Steamboat Springs, CO 80487 (800) 334-5493

CHAIN of CUSTODY

Report to:

Name: Ryan Jakubowski	Address:
Company: MWH	
E-mail: ryan.jakubowski@mwhglobal.com	Telephone: 970-879-6260

Copy of Report to:

Name:	E-mail:
Company:	Telephone:

Invoice to:

Name: Doug Oliver	Address:
Company:	
E-mail:	Telephone:

If sample(s) received past holding time (HT), or if insufficient HT remains to complete analysis before expiration, shall ACZ proceed with requested short HT analyses? YES ☐ NO ☐

If "NO" then ACZ will contact client for further instruction. If neither "YES" nor "NO" is indicated, ACZ will proceed with the requested analyses, even if HT is expired, and data will be qualified.

PROJECT INFORMATION

Quote #:

Project/PO #:

Reporting state for compliance testing:

Sampler's Name:

Are any samples NRC licensable material?

ANALYSES REQUESTED *(attach list or use quote number)*

SAMPLE IDENTIFICATION	DATE:TIME	Matrix	# of Containers	Alkalinity, Bicarbonate, Carbonate as CaCO3	ANP testing
L61917-01	8/3/07 9:55		1		✓
-02	↓		↓		↓
-03					
-04					
-05	↓		↓		↓

Matrix: SW (Surface Water) · GW (Ground Water) · WW (Waste Water) · DW (Drinking Water) · SL (Sludge) · SO (Soil) · OL (Oil) · Other

REMARKS/ SAMPLE DISCLOSURES

REF L61917

PAGE of

Please refer to ACZ's terms & conditions located on the reverse side of this COC.

RELINQUISHED BY:	DATE:TIME	RECEIVED BY:	DATE:TIME
Ryan Jakubowski	8/3/07 9:55		08/03/07 0955hrs

FRMAD050.03.05.02 White - Return with sample. Yellow - Retain for your records.